Supporting Information

Iron-Catalyzed Vinylsilane Dimerization and Cross-Cycloadditions with 1,3-Dienes: Probing the Origins of Chemo- and Regioselectivity

C. Rose Kennedy,‡ Matthew V. Joannou,‡ Janelle A. Steves, Jordan M. Hoyt, Carli B. Kovel, and Paul J. Chirik*

Department of Chemistry, Princeton University

Princeton, New Jersey 08544, United States

* pchirik@princeton.edu

Table of Contents for the Supporting Information

1. Procedures, Materials, and Instrumentation S4
   - 1.1 General Considerations S4
   - 1.2 Materials S4
   - 1.3 Instrumentation and Software S4
   - 1.4 Abbreviations S6
2. Synthesis of Iron Complexes S7
   - 2.1 Alternate Synthesis of $[(^{Me}PDI)Fe(N_2)]_2(\mu^2\text{-}N_2)$ S7
   - 2.2 Synthesis of $(^{Me}PDI)Fe(vinylsilane)_2$ S8
   - 2.3 Synthesis of $(^{Me}PDI)Fe(isoprene)$ and $(^{Me}PDI)Fe(myrcene)$ S10
3. Catalytic Procedures and Product Characterization S12
   - 3.1 General Procedure for *Head-to-Head* Vinylsilane Dimerization S12
   - 3.2 General Procedure for Cross-Cycloaddition Reactions S12
   - 3.3 Product Characterization Data S13
4. Independent Synthesis of **17bi** S122
5. Kinetic Analysis S126
   - 5.1 General Kinetic Procedure S126
   - 5.2 Test for Catalyst Death and/or Product Inhibition S129
   - 5.3 Determination of Order in Diene **9b** S134
   - 5.4 Determination of Order in Vinyl Silane **5b** S141
   - 5.5 Determination of Order in $[Fe]_{tot}$ S151
6. Supplemental Figures S159
   - 6.1 The α-Silicon Effect S159
   - 6.2 Lewis Acid Screen S160
7. Computational Analyses S161
   - 7.1 Sample Input File for Geometry Optimization & Mössbauer Parameter Calculation S161

7.2 Sample Input File for Natural Bond Order (NBO) Analysis S164

8. References S167

1. Procedures, Materials, and Instrumentation

1.1 General Considerations

All air- and moisture-sensitive manipulations were carried out using standard Schlenk techniques on a high vacuum line [1] or in an M. Braun glovebox containing an atmosphere of purified N_2. The M. Braun glovebox was equipped with a cold well designed for freezing samples in liquid N_2. Column chromatography was performed on SiliaFlash P60 (230–400 mesh) silica gel from SiliCycle using standard glass columns. Thin layer chromatography (TLC) was performed using aluminum-backed plates pre-coated with silica gel and a fluorescent indicator for visualization upon UV irradiation.

1.2 Materials

Reagents were purchased in reagent grade from commercial suppliers and used without further purification unless described otherwise. Pure (*E*)-piperylene and (*E/Z*)-piperylene were purchased from TCI, but crude (*E/Z*)-piperylene (also containing cyclopentene) was provided by Firmenich. Ethylene (**1e**), propylene (**1a**), and 3,3,3-trifluoropropylene (**1d**) were stored over activated 4 Å molecular sieves in a thick-walled glass pressure vessel for >24 hours prior to use, and *t*-butyl-ethylene (**1c**) was stored over calcium hydride in a thick-walled glass pressure vessel for >24 hours then degassed prior to use. Hydrogen (H_2) and deuterium (D_2) gas were passed through a column of activated molecular sieves and manganese oxide prior to use.[1] Allyltrimethylsilane (**1b**) and vinylsilanes (**6**) were stirred over lithium aluminum hydride for >48 hours, degassed, and distilled under high vacuum. Conjugated dienes (**13**) were stirred over calcium hydride for >48 hours, degassed, and distilled under high vacuum. The liquid reagents were then either passed through a plug of activated alumina and/or stored over activated 4 Å molecular sieves in the glovebox. Solvents (diethyl ether, dichloromethane, *n*-hexane, *n*-pentane, tetrahydrofuran, and toluene) used for air- and moisture-sensitive manipulations were dried and deoxygenated by passage through an activated alumina column.[2] Deuterated solvents for NMR spectroscopy of air- and moisture-sensitive species (C_6D_6 and C_6D_{12}) were distilled from sodium metal under an atmosphere of argon and stored over 4 Å molecular sieves. Deuterated chloroform ($CDCl_3$) was stored over anhydrous potassium carbonate. Dienes **13b–c**,[3] **13d**,[4] **13e**,[5] **13f**,[6] **13g**,[7] **13k–m**,[8] **13n–o**,[9] and **13p**[10] were prepared as reported previously. Iron complexes $[(^{Me}PDI)Fe(N_2)]_2(\mu^2\text{-}N_2)$,[11] $[(^{Me}(Et)PDI)Fe(N_2)]_2(\mu^2\text{-}N_2)$,[12] $[(^{Me}PDI)Fe(N_2)]_2(\eta^4\text{-}C_4H_6)$,[13] were prepared as reported previously. Magnesium butadiene ($Mg(C_4H_6)$•2THF),[14] was prepared according to a literature procedure.

1.3 Instrumentation and Software

Proton nuclear magnetic resonance (^{1}H NMR) spectra were recorded at 25 °C on a Bruker NanoBay 300 or Avance III 500 spectrometers operating at 300.13 MHz and 500.46 MHz, respectively. Proton-decoupled $^{13}C\{^1H\}$ APT NMR and quantitative $q^{13}C\{^1H\}$ NMR nuclear magnetic resonance spectra were recorded at 25 °C on a Bruker Avance III 500 instrument operating at 125.86 MHz. All experiments were performed at the Princeton University Nuclear Magnetic Resonance Facility. Chemical shifts are reported

in parts per million downfield from tetramethylsilane ($SiMe_4$) and are referenced in ppm relative to the NMR solvent according to literature values: [15,16] $\delta(^1H) = 7.26$, $\delta(^{13}C) = 77.0$ for $CDCl_3$, $\delta(^1H) = 7.16$, $\delta(^{13}C) = 128.1$ for C_6D_6.^{1}H NMR data for diamagnetic substances are reported as follows: chemical shift, (multiplicity, coupling constant in Hz, integration) where s = singlet, d = doublet, t = triplet, q = quartet, m = multiplet, and br = broad. ^{1}H NMR data for paramagnetic substances are reported as follows: chemical shift (integration, full-width at half-maximum height for broad signals). ^{13}C NMR data for diamagnetic substances are reported as a list of chemical shifts. NMR spectra were processed using the MestReNova software suite.[17]

Zero-field ^{57}Fe Mössbauer spectra were recorded on a SEE Co. Mössbauer spectrometer (MS4) at 80 K in constant acceleration mode. ^{57}Co/Rh was used as the radiation source. The temperature of the sample was controlled by a Janis Research Co. CC2-860 He/N_2 cryostat within an accuracy of 0.3 K. Isomer shifts were determined relative to α-iron at 298 K. WMOSS Spectral Analysis Software was used for the quantitative evaluation of the spectral parameters (least-squares fitting to Lorentzian peaks).[18]

Gas chromatographic analyses were performed using a Shimadzu GC-2010 gas chromatograph equipped with a Shimadzu AOC-20s autosampler. For samples analyzed on a Shimdzu SHRXI-5MS achiral stationary phase capillary column (15 m × 250 μm), the instrument was set to an injection volume of 1.0 μL, an inlet split ratio of 20:1, and inlet and detector temperatures of 250 °C and 275 °C, respectively. UHP-grade S3 helium was used as carrier gas with a flow rate of 1.96 mL/min. For samples analyzed on a Supelco BETA DEX 120 chiral stationary phase capillary column (30 m × 250 μm), the instrument was set to an injection volume of 1.0 μL, an inlet split ratio of 10:1, and inlet and detector temperatures of 250 °C. UHP-grade S3 helium was used as carrier gas with a flow rate of 1.00 mL/min.

High-resolution mass spectra were measured using an Agilent 5975C GC-MS or an Agilent 6210 TOF LC/MS at the Princeton University Mass Spectrometry Facility. In general, vinylsilane-derived substrates proved difficult to ionize and/or highly prone to fragmentation under standard conditions. Where mass spectral data are not reported, the parent ions for the indicated product were not readily detected. Infrared spectra were collected on a Thermo-Nicolet iS10 FT-IR spectrometer calibrated with a polystyrene standard. Elemental analyses were performed at Robertson Microlit Laboratories, Inc., in Ledgewood, NJ. Solid-state magnetic moments were determined at room temperature using a Johnson–Matthey magnetic susceptibility balance calibrated with $HgCO(SCN)_4$. Solution-state magnetic moments were determined in C_6D_6 at 25 °C using ferrocene as a standard according to the Evans procedure modified for use with an NMR spectrometer with a superconducting magnet.[19,20] Curve fitting and statistical analyses were carried out using the NumPy, SciPy, and MatPlotLib Python packages[21] in Jupyter Notebooks.[22,23] Kinetic simulations were performed with Copasi Software 4.24.197.[24]

All electronic structure calculations were performed on the Della computing cluster maintained by Princeton University Research Computing. Geometry optimizations and energy calculations for organic molecules only were performed using Gaussian[25] with the M06-2X level of density functional theory[26] with

the 6-311++g(d,p) basis set[27,28] and implicit solvent correction (CPCM, cyclohexane).[29,30,31] For iron complexes, geometry optimizations and single point calculations were carried out using ORCA[32,33] with the M06L[34,35] or B3LYP[35,36,37,38] level of DFT. The latter hybrid functional often outperforms pure gradient-corrected functionals in the accurate representation of transition metal complexes, especially those involving significant metal–ligand covalency.[39] Alrichs's all-electron Gaussian basis sets were employed for all calculations,[40,41] wherein the triple-ξ basis set def2-TZVP, which includes one set of polarization functions, was used to describe metal atoms and all atoms directly coordinated to a metal center. The double-ξ basis set def2-SV(P), which includes one set of polarizing d functionals on all non-hydrogen atoms, was used for all other atoms. Weigend's "universal" Coulomb fitting basis, which is suitable for all def2 type basis sets, was employed to generate auxiliary basis sets.[42,43,44] The RIJCOSX approximation was used to accelerate the calculations. [45,46,47,48] The ZORA relativistic correction was applied for the calculation of Mössbauer spectral parameters.[49,50] This correction has previously been demonstrated empirically to correct for systematic errors in these predictions.[10,51] Throughout this manuscript, computational results are described using the broken symmetry approach introduced by Ginsberg[52] and Noodleman et al.[53] Because several broken symmetry solutions to the spin-unrestricted Kohn–Sham equations may be obtained, the general notation for broken symmetry (*m*,*n*) has been adopted, where *m* (*n*) denotes the number of spin-up (spin-down) electrons at the two interacting fragments.[54,55] Computed structures were rendered using CYLview.[56] Representations of canonical orbitals and the corresponding spin density plots were generated with the program *Chimera*.[57]

1.4 Abbreviations

Bn = benzyl; DMAP = 4-dimethylaminopyridine; dme = 1,2-dimethoxyethane; dppe = 1,2-bis(diphenylphosphino)ethane; dvtms = 1,3-divinyltetramethyldisiloxane; EDC•HCl = *N*-(3-dimethylaminopropyl)-*N*′-ethylcarbodiimide hydrochloride; Im = imidazole; IR = infrared spectroscopy; NMR = nuclear magnetic resonance spectroscopy; ^{Me}PDI = 1,1'-(pyridine-2,6-diyl)bis(*N*-(2,6-dimethylphenyl)ethan-1-imine); ^{iPr}PDI = 1,1'-(pyridine-2,6-diyl)bis(*N*-(2,6-diisopropylphenyl)ethan-1-imine); $^{iPr(TB)}$PDI = 4,5-bis((2,6-diisopropylphenyl)-λ^4-azanylidene)-1,2,3,4,5,6,7,8-octahydroacridine; Piv = pivalate = 2,2-dimethylpropionyl; PTFE = polytetrafluoroethylene; Py = pyridine; TBDPS = *tert*-butyldiphenylsilyl; TBS = *tert*-butyldimethylsilyl; Tf = triflic = trifluoromethanesulfonyl; THF = tetrahydrofuran; TLC = thin-layer chromatography; TMS = trimethylsilyl; vtms = vinyltrimethylsilane

2. Synthesis of Iron Complexes

2.1 Alternate Synthesis of [(^{Me}PDI)Fe(N_2)]$_2$(μ^2-N_2)

A synthetic procedure for the preparation of iron precatalyst [(^{Me}PDI)Fe(N_2)]$_2$(μ^2-N_2) was reported previously by our group.[11] However, yields were found to be highly variable because [(^{Me}PDI)Fe(N_2)]$_2$(μ^2-N_2) is (a) highly moisture sensitive, (b) prone to over-reduction in the presence of excess sodium, and (c) unstable to prolonged vacuum due to loss of the dinitrogen ligands. To improve the reliability of the synthesis, the following modifications were made to the published procedure.

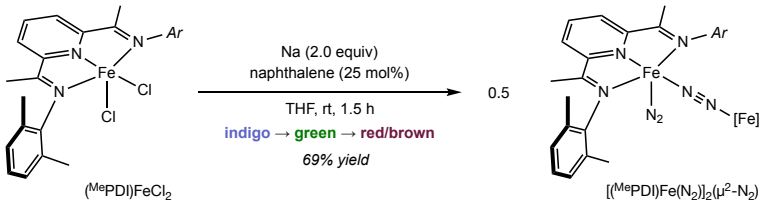

Figure S1. Modified procedure for the synthesis of [(^{Me}PDI)Fe(N_2)]$_2$(μ^2-N_2).

In a glovebox filled with an inert atmosphere of purified N_2, a 100-mL round-bottom flask was charged with finely chopped sodium (0.046 g, 2.0 mmol, 2.0 equiv), a PTFE-coated magnetic stir bar, and THF (~5 mL). The suspension was stirred for 3 minutes; then, the THF was removed with a pipette. Additional THF (16 mL) was added, the flask was sealed with a rubber septum, and the suspension was stirred at ambient temperature in the glovebox. After 2–8 hours, the sodium chunks were removed and freshly chopped sodium was added (0.046 g, 2.0 mmol, 2.0 equiv). Naphthalene (0.032 g, 0.25 mmol, 0.25 equiv) was added, and the suspension was stirred 5–10 minutes until a green color persisted. The iron dihalide complex (^{Me}PDI)$FeCl_2$ (0.496 g, 1.0 mmol, 1.0 equiv) was then added as a solid in a single portion. The flask was sealed with a rubber septum, and the suspension was stirred vigorously at ambient temperature in the glovebox. The purple hue of the iron dihalide complex gave way to green, then deep red. Upon formation of this red color (after 90 minutes) the reaction mixture was diluted with pentane (60 mL) and filtered through a pad of Celite on a medium porosity glass frit, rinsing with diethyl ether (20 mL). The filtrate was concentrated in vacuo for the minimum possible time to afford a brown residue. The residue was resuspended in a 1:1 mixture of diethyl ether and pentane, then filtered through a short plug of Celite in a monster pipette. The filtrate was concentrated in vacuo to half its initial volume and transferred to a –35 °C freezer overnight. After 12–24 hours, the supernatant was removed with a pipette and reserved. The remaining solid was rinsed twice with 2–3 mL portions of pentane, then dried briefly (5–10 minutes in vacuo). A second crop of clean material could also be obtained upon partial concentration and recrystallization of the supernatant to afford [(^{Me}PDI)Fe(N_2)]$_2$(μ^2-N_2) as a deep red solid (0.234 g + 0.055 g, 0.35 mmol, 69% yield). Spectroscopic data including ^{1}H NMR, ^{13}C NMR, and zero-field ^{57}Fe Mössbauer (solid-state, 80 K) spectra were consistent with the values reported previously.[11] The material was used without any further attempts to remove residual solvent.

2.2 Synthesis of (^{Me}PDI)Fe(vinylsilane)$_2$

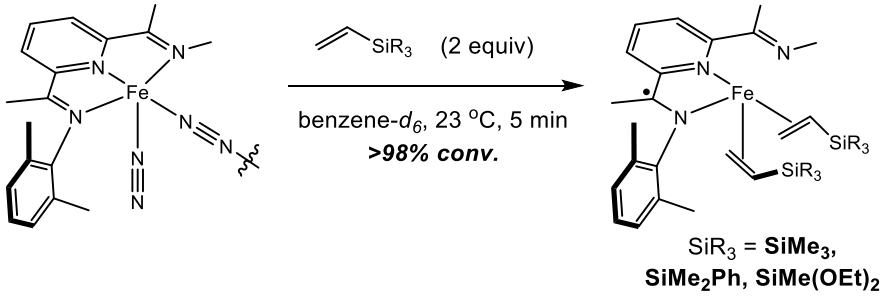

Figure S2. Procedure for the synthesis of (^{Me}PDI)Fe(**6a**)$_2$, (^{Me}PDI)Fe(**6b**)$_2$, and (^{Me}PDI)Fe(**6d**)$_2$.

Procedure: In an N_2-filled glovebox, a J. Young NMR tube was charged with [(^{Me}PDI)Fe(N_2)](μ-N_2) (20.0 mg, 0.0214 mmol) and 600 μL of benzene-d_6. The appropriate vinyl silane (**6**, 0.0856 mmol, 2 equivalents per iron center) was added via microliter syringe and the tube sealed and removed from the glovebox. After mixing at ambient temperature for 5 minutes, the reaction mixture was analyzed via ^{1}H NMR spectroscopy to reveal the title compounds formed in >98% conversion.

(^{Me}PDI)Fe(6a)$_2$: ^{1}H NMR (300 MHz, C_6D_6) δ 169.34 (s, 1H, 218 Hz, *p*-pyridine), 41.99 (s, 2H, 240 Hz, *m*-pyridine), 5.95 (s, 6H, Ar*H*), -0.01 (br s, 15H, *olefinic* and SiC*H*$_3$), -3.52 (s, 9H, SiC*H*$_3$), -16.33 & -17.77 (12H, ArC*H*$_3$), -117.20 (s, 6H, 1010 Hz, ArNCC*H*$_3$).

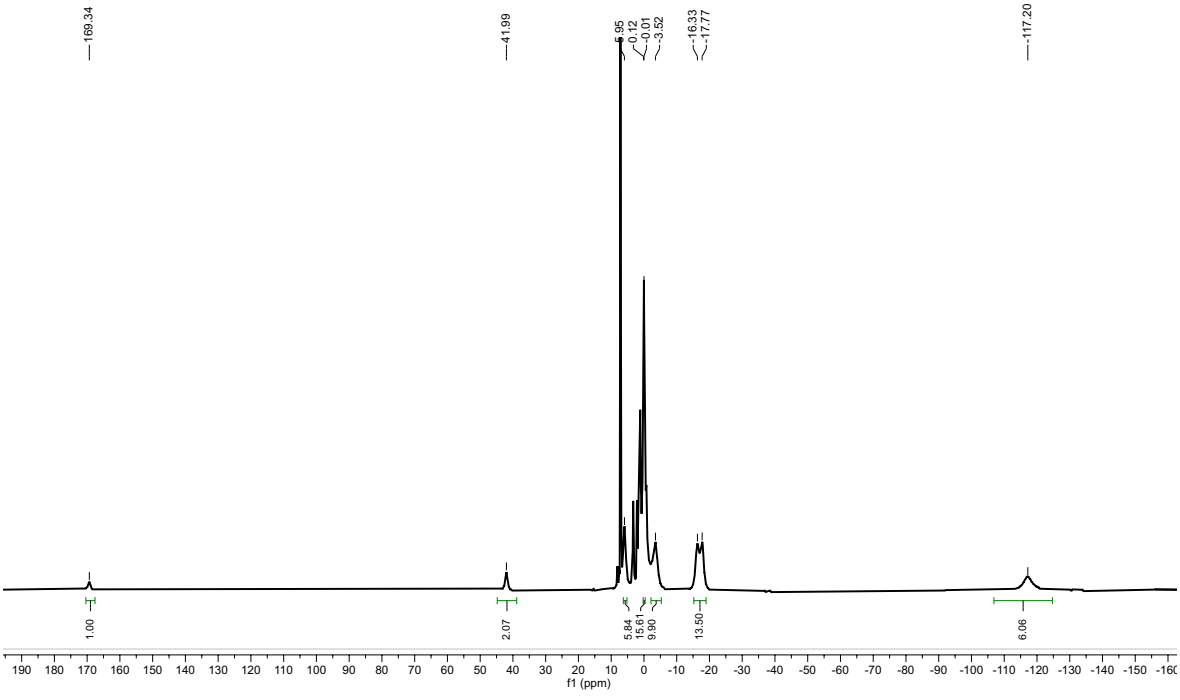

Figure S3. ^{1}H NMR (300Mz, C_6D_6) spectrum of (^{Me}PDI)Fe(**6a**)$_2$.

(MePDI)Fe(6b)$_2$: ^{1}H NMR (300 MHz, C_6D_6) δ 171.47 (1H, *p*-pyridine), 37.27 (2H, *m*-pyridine), 9.24 (2H, *olefinic*), 7.37 (6H, Ar*H*), 5.97(4H, *olefinic*), 3.26 (10H, Si*Ph*), 2.11 (3H, SiC*H*$_3$), 1.11 (3H, SiC*H*$_3$), 0.25 (3H, SiC*H*$_3$), -12.49 (3H, SiC*H*$_3$), -16.64 & -18.17 (12H, ArC*H*$_3$), -114.14 (6H, ArNCC*H*$_3$).

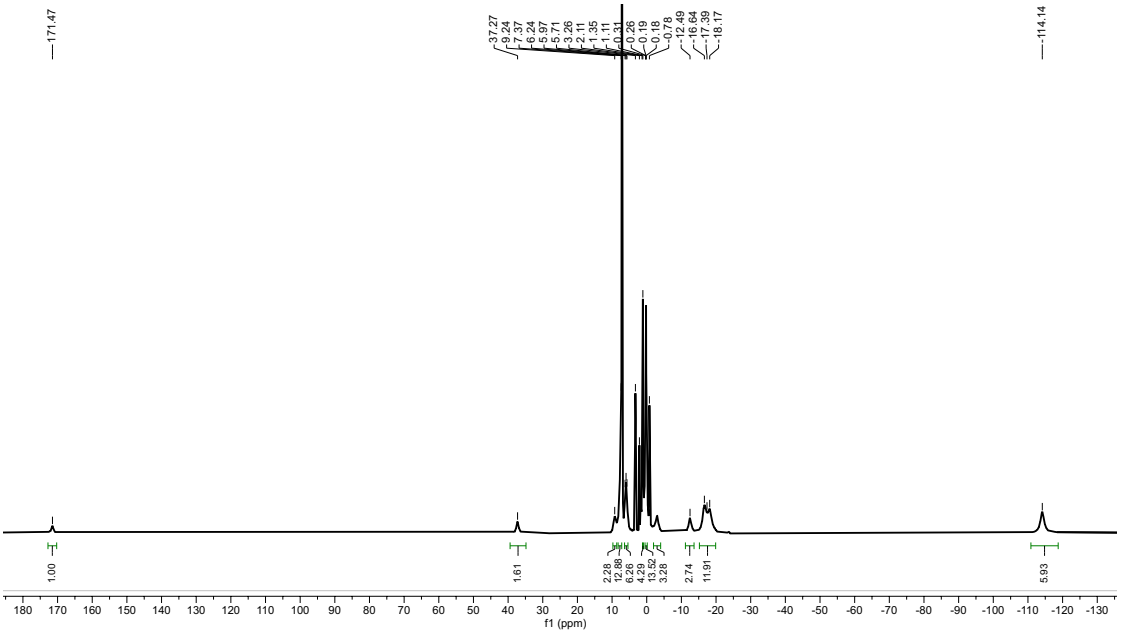

Figure S4. ^{1}H NMR (300Mz, C_6D_6) spectrum of (^{Me}PDI)Fe(**6b**)$_2$.

(MePDI)Fe(6d)$_2$: ^{1}H NMR (300 MHz, C_6D_6) δ 166.49 (1H, *p*-pyridine), 38.54 (2H, *m*-pyridine), 5.98 (6H, Ar*H*), 3.26 (4H, Si(OC*H*$_2$CH$_3$), 2.11-1.99 (m, 6H), 0.43- -0.18 (15H), -2.48 (6H, Si(OCH$_2$C*H*$_3$), -14.53 (3H, Si*CH*$_3$), -16.27 (6H, *Ar*C*H*$_3$), -21.45 (6H, *Ar*C*H*$_3$), -109.36 (6H, ArNCC*H*$_3$).

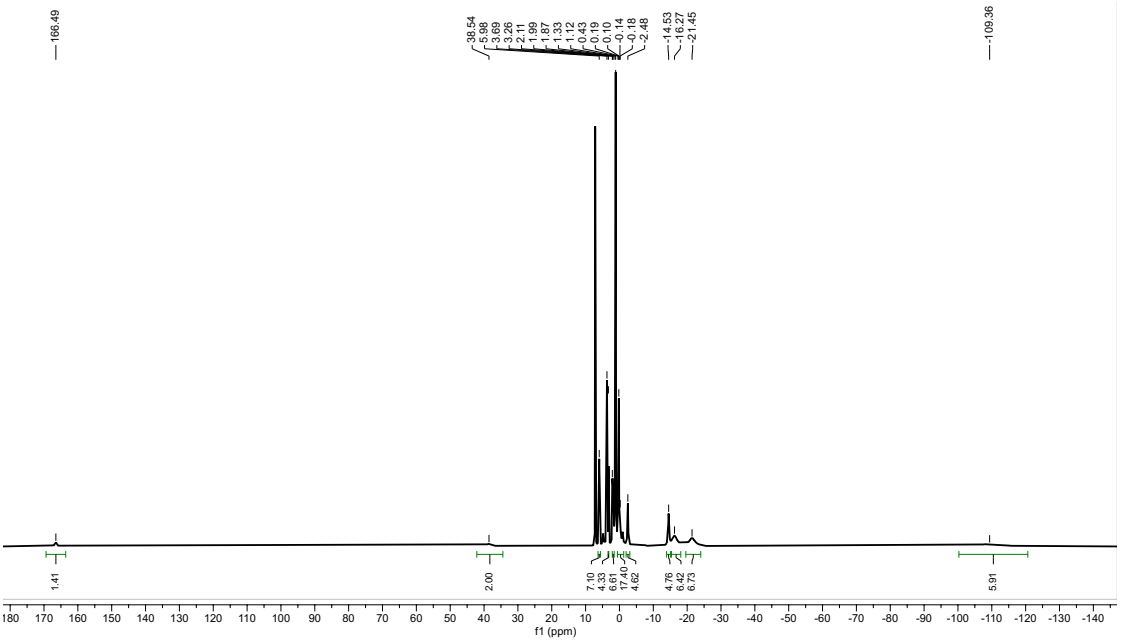

Figure S5. ^{1}H NMR (300Mz, C_6D_6) spectrum of (^{Me}PDI)Fe(**6d**)$_2$.

2.3 Synthesis of (^{Me}PDI)Fe(isoprene) and (^{Me}PDI)Fe(myrcene)

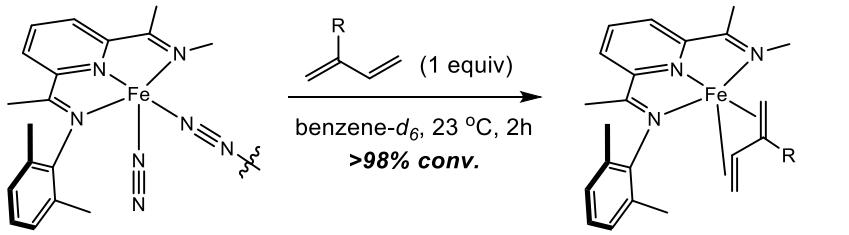

Figure S6. Procedure for the synthesis of (^{Me}PDI)Fe(**13i**) and (^{Me}PDI)Fe(**13j**).

In an N_2-filled glovebox, a J. Young NMR tube was charged with [(^{Me}PDI)Fe(N_2)](μ-N_2) (20.0 mg, 0.0214 mmol) and 600 μL of benzene-d_6. The appropriate 2-substituted diene (0.0428 mmol, 1 equivalents per iron center) was added via microliter syringe and the tube sealed and removed from the glovebox. After mixing at ambient temperature for 2 hours, the reaction mixture was analyzed via ^{1}H NMR spectroscopy to reveal the title compounds formed in >98% conversion. Half-life of the isoprene complex: 3 hours. Half-life of the myrcene complex: 9-12 hours. Spectroscopic data of (^{Me}PDI)Fe(isoprene) including ^{1}H NMR data were consistent with the previously reported complex.[58]

(^{Me}PDI)Fe(13j): ^{1}H NMR (300 MHz, C_6D_6) δ 7.95 (d, *J* = 29.0 Hz, 2H, *m*-pyridine), 7.38 (s, 1H *p*-pyridine), 6.91 (d, *J* = 12.9 Hz, 4H, *m-ArH*) 6.65-6.23 (m, 2H, *p-ArH*), 5.11 (m, 5H), 4.73 (d, *J* = 13.9, 1H, C*H*$_2$CH(C)CH$_2$), 4.62 (s, 1H, CH$_2$CH(C)C*H*$_2$), 4.16 (s, 1H, CH$_2$CH(C)C*H*$_2$), 3.51 (d. *J* = 8.7 Hz, 1H, C*H*$_2$CH(C)CH$_2$), 3.27 (s, 2H, allylicC*H*$_2$, alkene), 2.58-1.12 (m, 40H), 0.67 (s, 1H, myrcene (CH$_3$)$_2$C(C*H*)R), 0.04 (d, *J* = 6.2 Hz, 2H, allylicC*H*$_2$, diene).

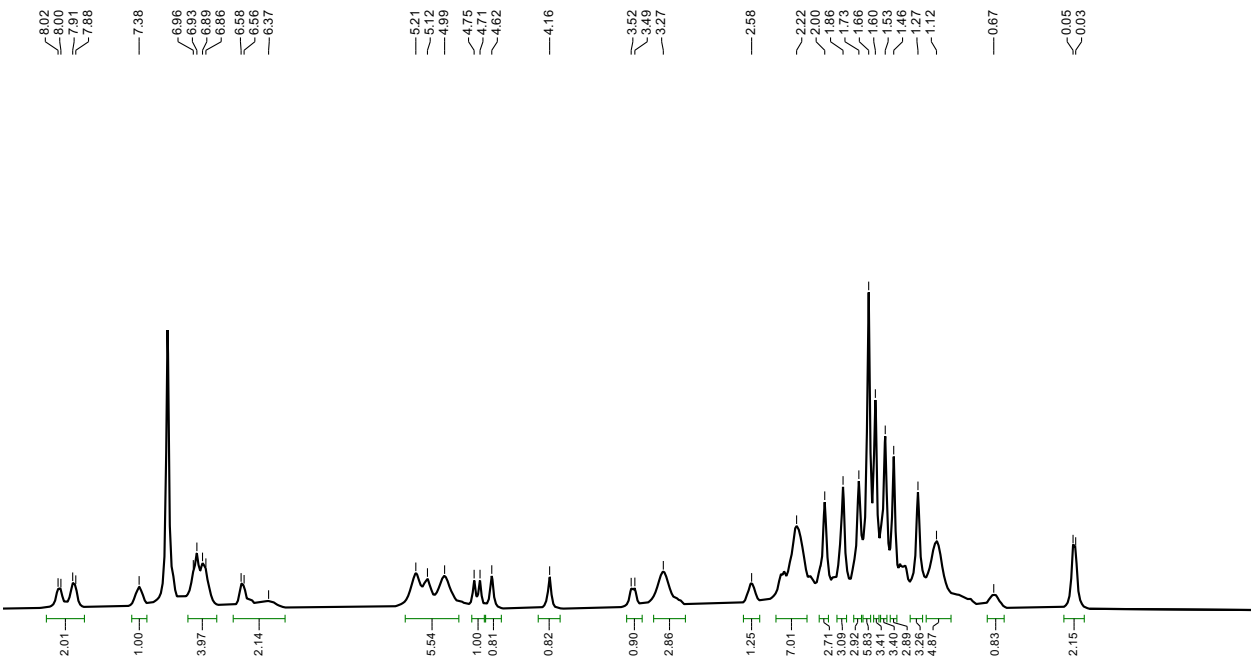

Figure S7. ^{1}H NMR (300Mz, C_6D_6)of Spectrum of **(^{Me}PDI)Fe(myrcene)**

3. Catalytic Procedures and Product Characterization

3.1 General Procedure for *Head-to-Head* Vinylsilane Dimerization

In a glovebox, a 1.5 mL vial was charged with [(^{Me}PDI)Fe(N_2)]$_2$(μ^2-N_2) (0.012 g, 0.0125 mmol, 2.5 mol% dimer, 5 mol% [Fe]). The vinylsilane substrate **6** (0.5 mmol, 1.0 equiv) was added by mass. A PTFE-coated magnetic stir bar was added, and the vial was sealed with a PTFE-lined screw cap. The reaction was maintained with stirring at ambient temperature (~23 °C) in the glovebox. After 48 hours, an aliquot was removed for gas chromatographic analysis to evaluate conversion (i.e. consumption of the starting material) and the selectivity of product formation. The reaction vial was then removed from the glovebox and opened to air. The reaction mixture was diluted with pentane and filtered through a plug of silica, rinsing with pentane until the product eluted completely, as judged by TLC. Where necessary, mixtures of pentane and benzene, diethyl ether, and/or ethyl acetate were employed. Fractions containing the major product, as judged by TLC (staining with $KMnO_4$) were combined and concentrated under reduced pressure prior to analysis by ^{1}H NMR and ^{13}C NMR spectroscopy and mass spectrometry. Yield was determined on the basis of the mass of product isolated.

3.2 Representative Procedure for Cross-Cycloaddition Reactions

In a glovebox, a 1.5 mL vial was charged with vinylsilane substrate **6** (1.0–1.2 mmol, 1.0–1.2 equiv) and diene substrate **13** (1.0–1.2 mmol, 1.0–1.2 equiv). The lower-boiling substrate was added in slight excess. Precatalyst [(^{Me}PDI)Fe(N_2)]$_2$(μ^2-N_2) (0.012 g, 0.0125 mmol, 1.25 mol% dimer, 2.5 mol% [Fe]) was added as a solid to initiate the reaction. A PTFE-coated magnetic stir bar was added, and the vial was sealed. The vial was maintained with stirring at ambient temperature (~23 °C). Reaction progress was monitored by GC analysis of aliquots removed from the reaction mixture. Upon consumption of the limiting substrate, the vial was removed from the glovebox. The reaction mixture was diluted with pentane and filtered through a plug of silica, rinsing with pentane until the product eluted completely, as judged by TLC. Where necessary, mixtures of pentane and benzene, diethyl ether, and/or ethyl acetate were employed. Fractions containing the major product, as judged by TLC (staining with $KMnO_4$) were combined and concentrated under reduced pressure prior to analysis by ^{1}H NMR and ^{13}C NMR spectroscopy and mass spectrometry (when compounds were suitable). Yield was determined on the basis of the mass of product isolated.

3.3 Product Characterization Data

A mixture of **1,2-dimethylcyclobutane (2a)** and **2,3-dimethylbut-1-ene (3a)** was afforded in 96% conversion (4% recovered **1a**, 40% **2a**, 56% **3a**) after 48 hours upon exposure of a solution of the iron precatalyst (2.5 mol% dimer, 5 mol% [Fe]) in benzene-d_6 to an excess of propylene.[59]

^{1}H NMR (300 MHz, C_6D_6) δ 4.78 (s, 1H, **3a**), 4.74 (s, 1H, **3a**), 2.43 – 2.28 (m, 2H, *cis*-**2a**), 2.15 (hept, *J* = 6.8 Hz, 1H, **3a**), 2.04 – 1.85 (m, 2H, *cis*-**2a** + *trans*-**2a**), 1.84 – 1.67 (m, 1H, *trans*-**2a**), 1.62 (s, 3H, **3a**), 1.66 – 1.47 (m, 2H, *cis*-**2a**), 1.45 – 1.26 (m, 2H, *trans*-**2a**), 0.98 (d, *J* = 6.2 Hz, 6H, *trans*-**2a**), 0.97 (d, *J* = 6.9 Hz, 6H, **3a**), obscured at ~0.94 (d, 6H, *cis*-**2a)**

^{13}C NMR (101 MHz, C_6D_6) δ 151.5 (**3a**), 108.2 (**3a**), 39.2 (*trans*-**2a**), 35.6 (**3a**), 27.0 (*trans*-**2a**), 21.6 (**3a**), 20.6 (**3a**), 20.2 (*trans*-**2a**)

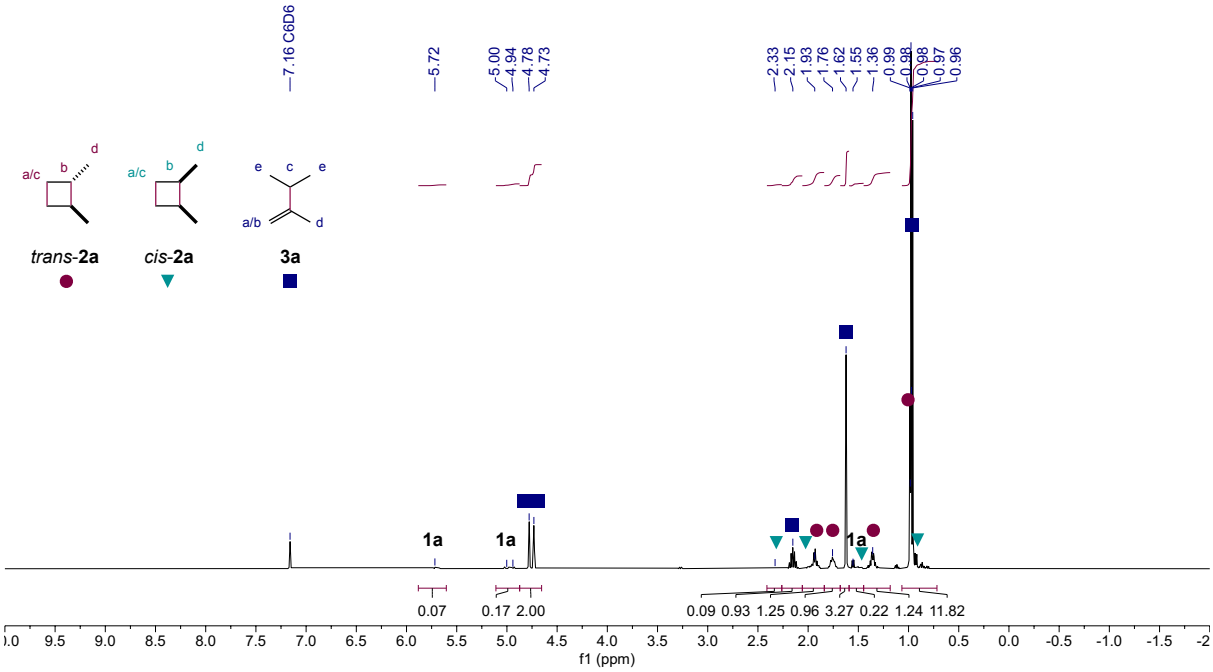

Figure S8. ^{1}H NMR (300 MHz, C_6D_6) spectrum of **2a** and **3a**.

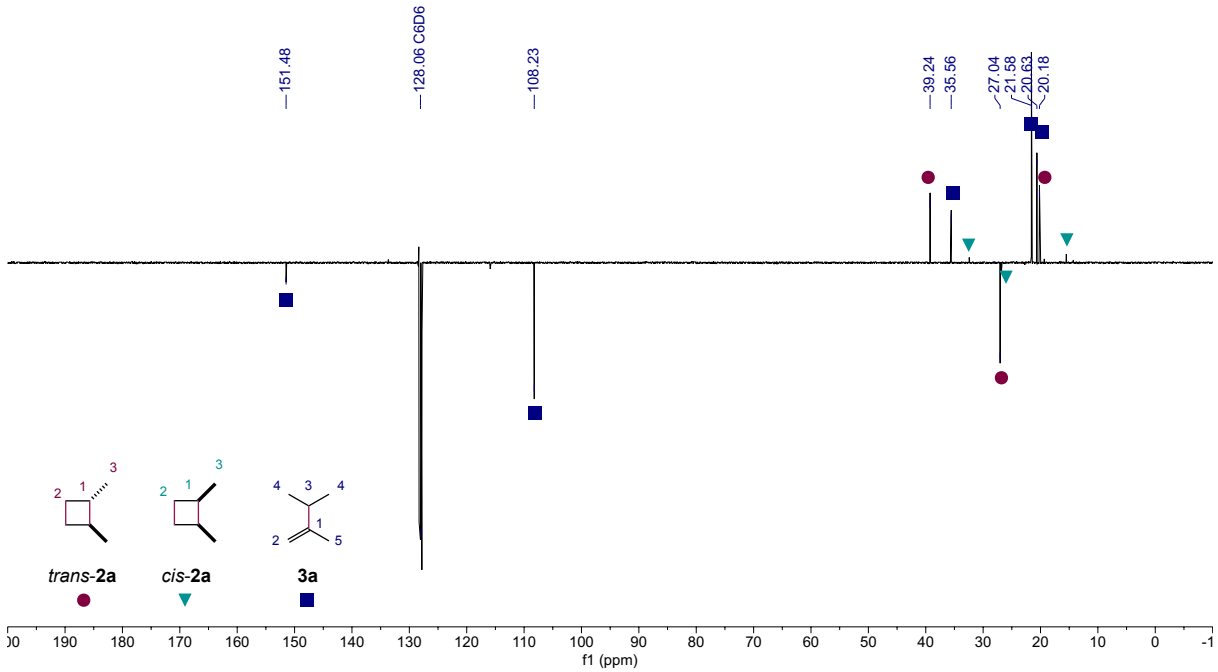

Figure S9. ^{13}C NMR (101 MHz, C_6D_6) spectrum of **2a** and **3a**.

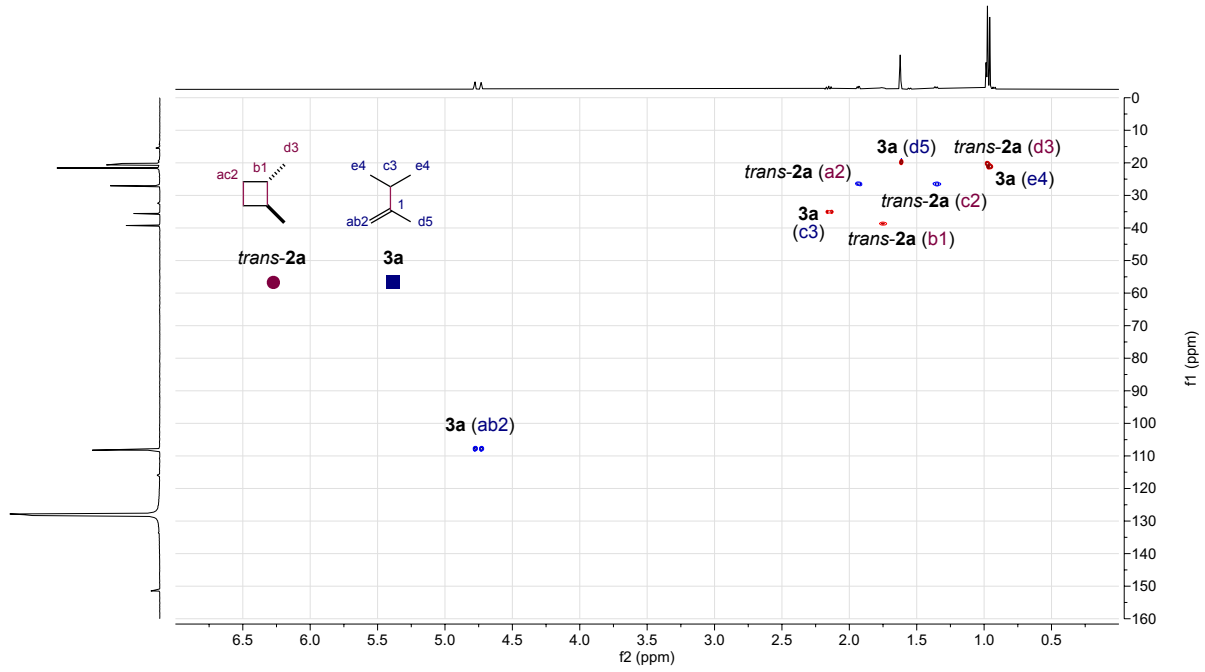

Figure S10. ^{1}H–^{13}C HSQC (300 MHz, C_6D_6) spectrum of **2a** and **3a**.

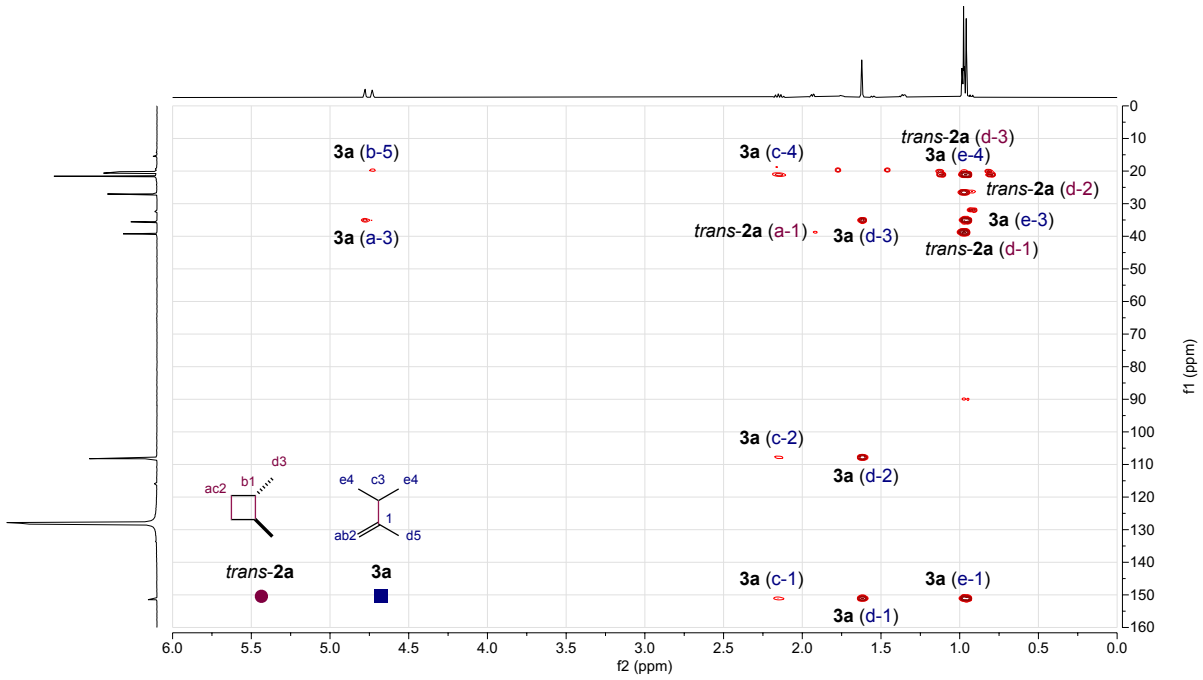

Figure S11. $^{1}H–^{13}C$ HMBC (300 MHz, C_6D_6) spectrum of **2a** and **3a**.

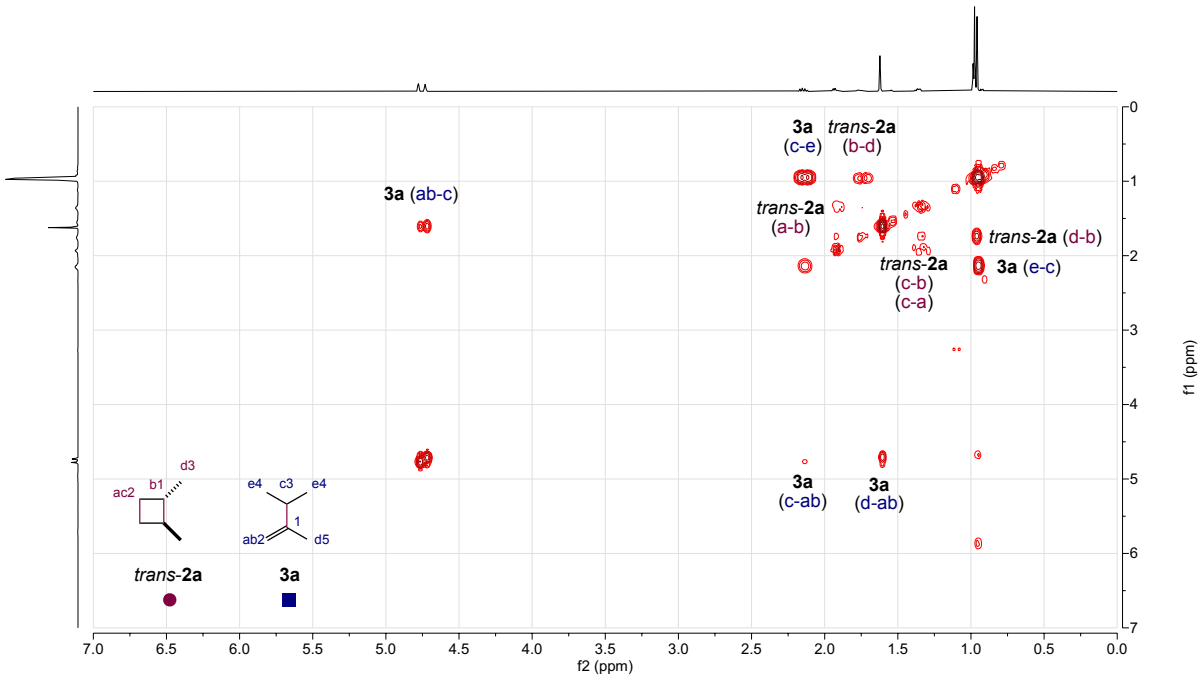

Figure S12. $^{1}H–^{1}H$ COSY (300 MHz, C_6D_6) spectrum of **2a** and **3a**.

(*E*)-but-1-ene-1,4-diylbis(trimethylsilane) (9a) was prepared in 32% yield, >98% purity, 98:2 *E*/*Z* after 48 hours as described in 3.1.

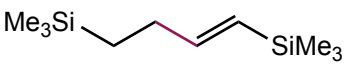

9a

^{1}H NMR (500 MHz, $CDCl_3$) δ 6.32 (dt, *J* = 13.9, 7.8 Hz, 1H, *Z*), 6.09 (dt, *J* = 18.4, 5.8 Hz, 1H, *E*), 5.61 (dt, *J* = 18.4, 1.6 Hz, 1H, *E*), 5.38 (d, *J* = 13.9 Hz, 1H, *Z*), 2.27 (t, *J* = 7.8 Hz, 1H, *Z*), 2.16 – 2.04 (m, 2H), 0.66 – 0.53 (m, 2H), 0.04 (s, 9H), -0.01 (s, 9H)

^{13}C NMR (126 MHz, $CDCl_3$) δ 150.04, 127.76, 30.94, 15.53, -1.00, -1.42

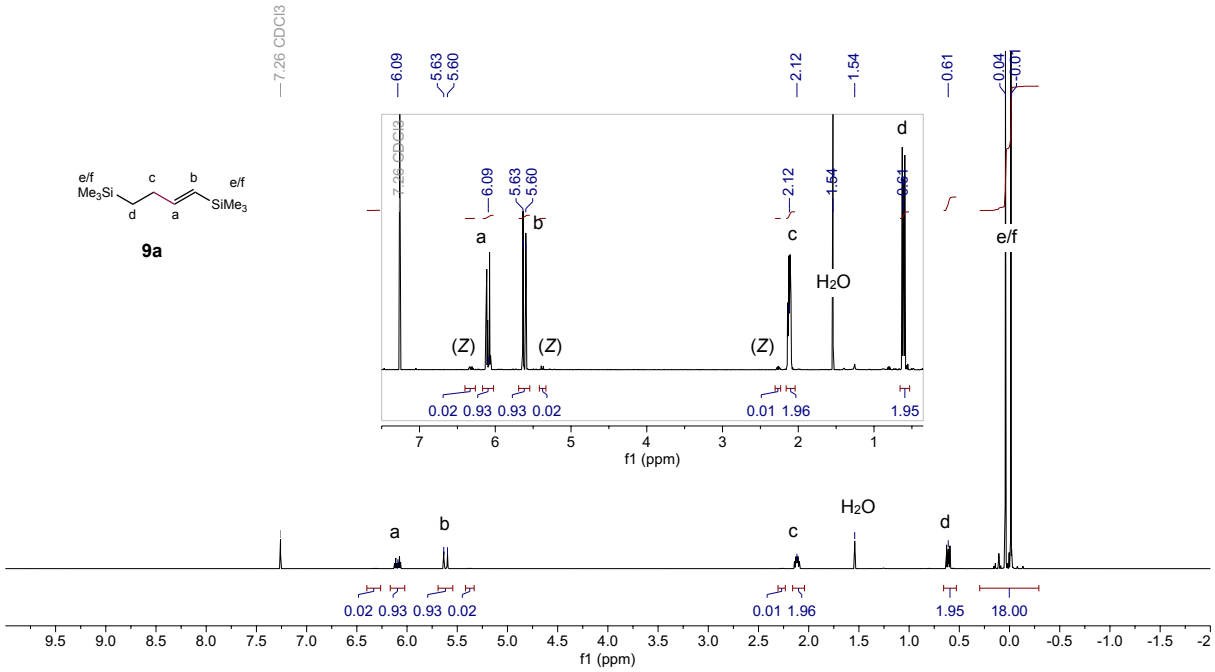

Figure S13. ^{1}H NMR (500 MHz, $CDCl_3$) spectrum of **9a**.

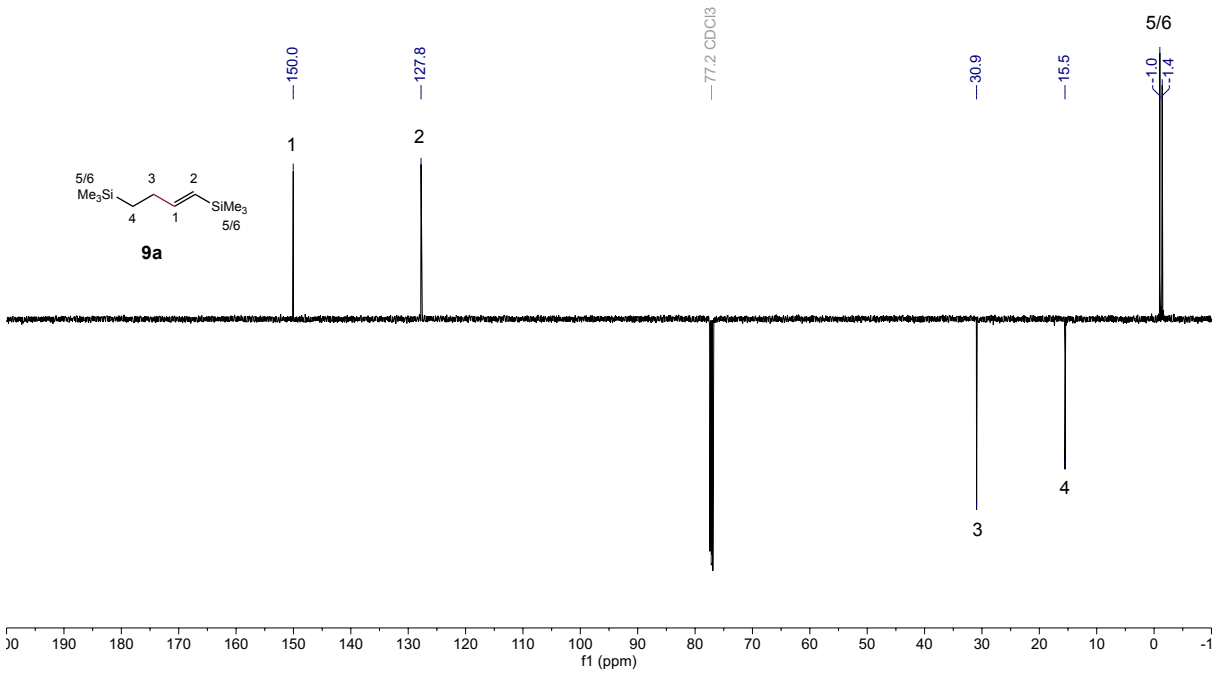

Figure S14. ^{13}C NMR (126 MHz, $CDCl_3$) spectrum of **9a**.

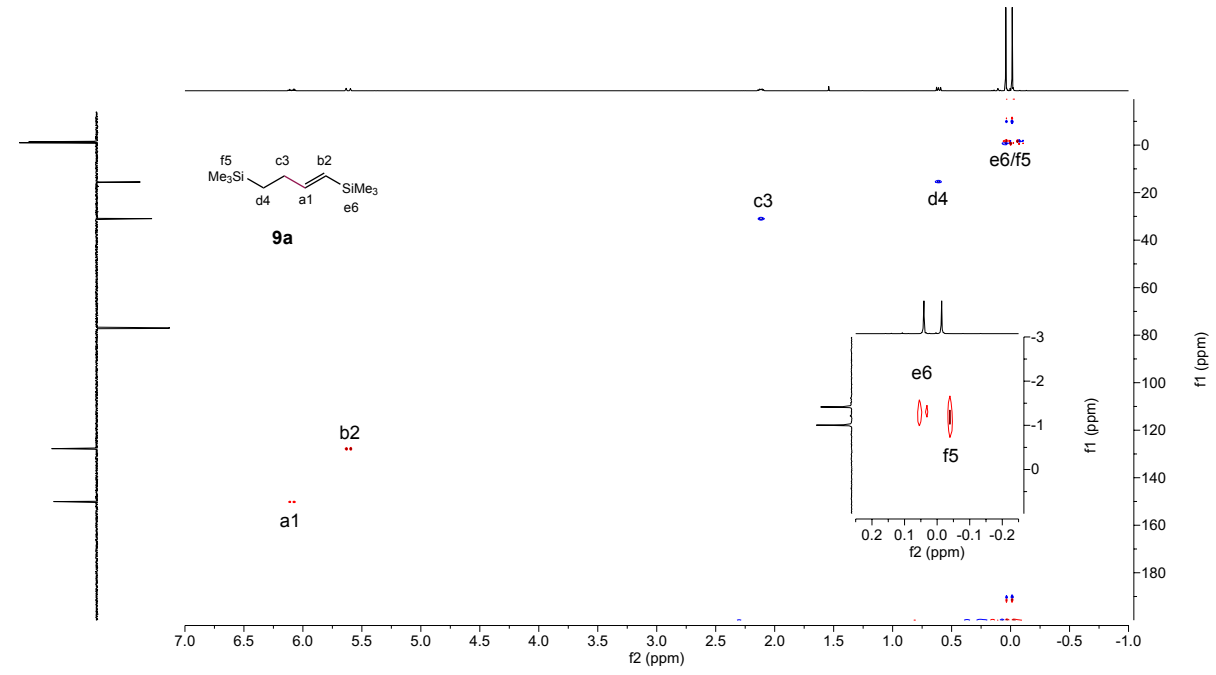

Figure S15. ^{1}H–^{13}C HSQC (500 MHz, $CDCl_3$) spectrum of **9a**.

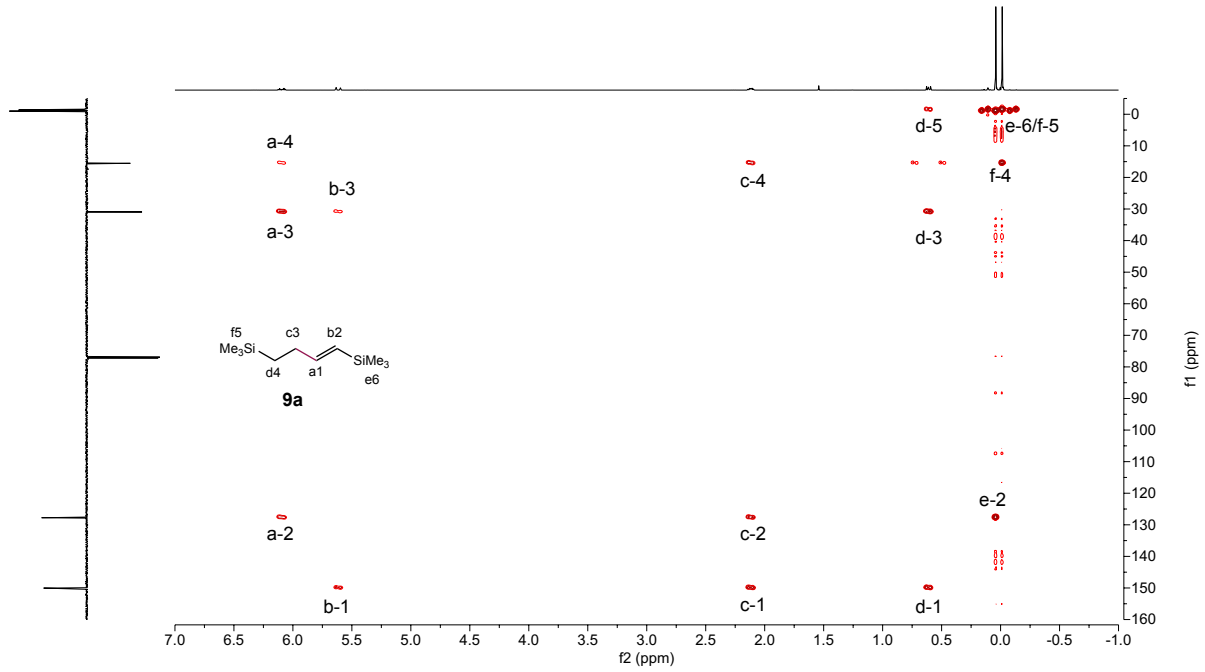

Figure S16. $^{1}H–^{13}C$ HMBC (500 MHz, $CDCl_3$) spectrum of **9a**.

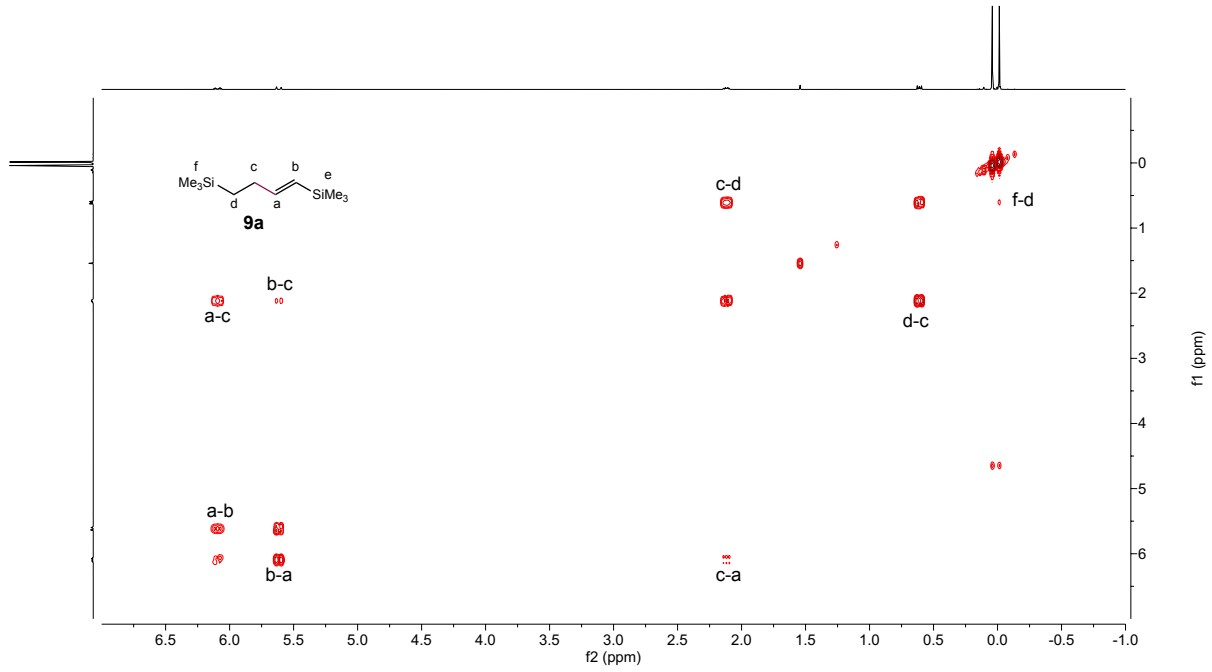

Figure S17. $^{1}H–^{1}H$ COSY (500 MHz, $CDCl_3$) spectrum of **9a**.

(*E*)-but-1-ene-1,4-diylbis(dimethyl(phenyl)silane) (9b) was prepared in 92% isolated yield, 96% purity, 97:3 *E*/*Z* after 48 hours as described in 3.1.

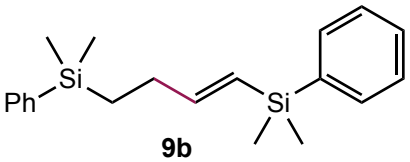

9b

^{1}H NMR (500 MHz, $CDCl_3$) δ 7.55 – 7.49 (m, 4H), 7.39 – 7.33 (m, 6H), 6.43 (dt, *J* = 14.0, 8.0 Hz, 1H, *Z*), 6.17 (dt, *J* = 18.3, 5.8 Hz, 1H, *E*), 5.75 (dd, *J* = 18.3, 2.3 Hz, 1H, *E*), 5.54 (d, *J* = 14.0 Hz, 1H, *Z*), 2.18 (q, *J* = 8.2, 5.8 Hz, 2H, *E*), 2.03 (q, *J* = 9.3, 8.4, 8.0 Hz, 2H, *Z*), 0.89 (t, *J* = 8.2 Hz, 2H, *E*), 0.75 (t, *J* = 9.3, 8.4 Hz, 2H, *Z*), 0.31 (d, *J* = 1.9 Hz, 6H), 0.28 (s, 6H)

^{13}C NMR (126 MHz, $CDCl_3$) δ 151.6, 139.5, 139.4, 134.0, 133.7, 129.0, 128.9, 127.9, 127.8, 125.7, 30.9, 14.6, -2.3, -2.8

GC-MS (EI): for $[M]^+ = C_{20}H_{28}Si_2$, calculated *m/z* = 324.17296, found *m/z* = 324.17207

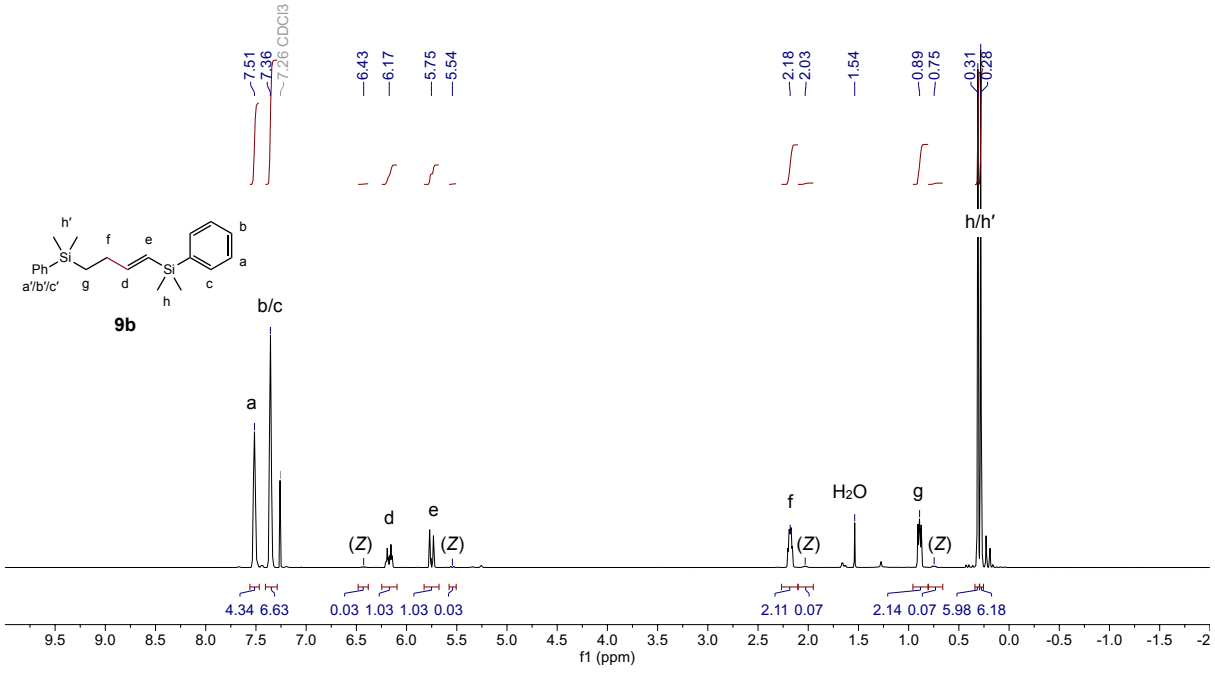

Figure S18. ^{1}H NMR (500 MHz, $CDCl_3$) spectrum of **9b**.

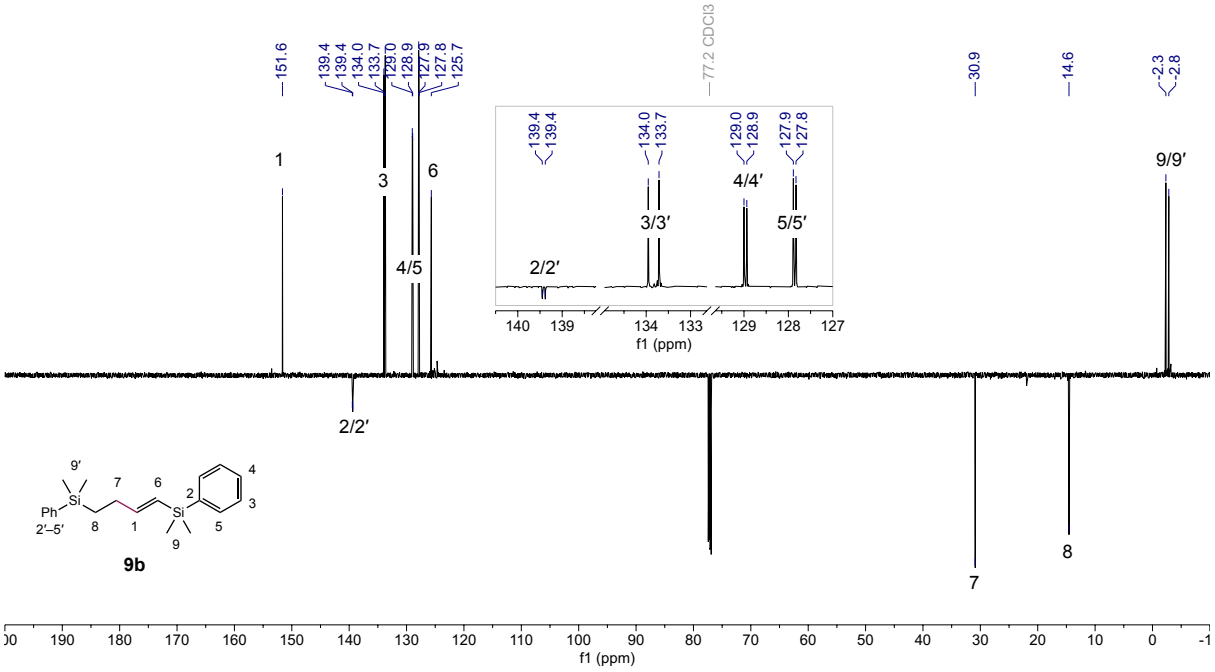

Figure S19. ^{13}C NMR (126 MHz, $CDCl_3$) spectrum of **9b**.

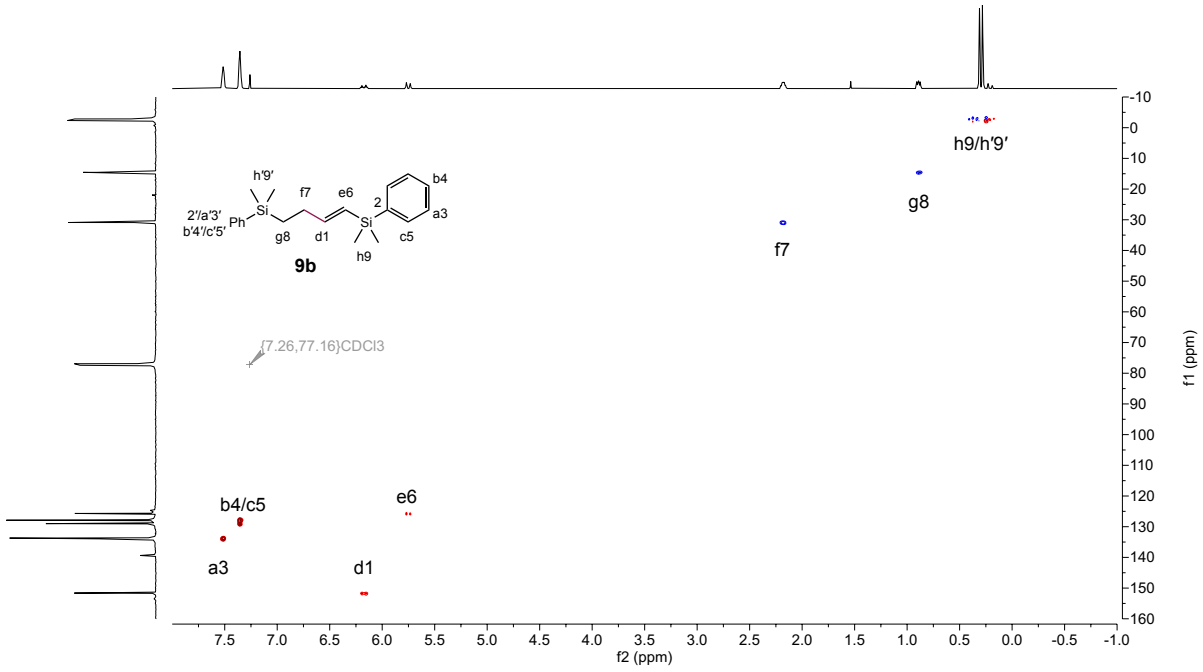

Figure S20. ^{1}H–^{13}C HSQC (500 MHz, $CDCl_3$) spectrum of **9b**.

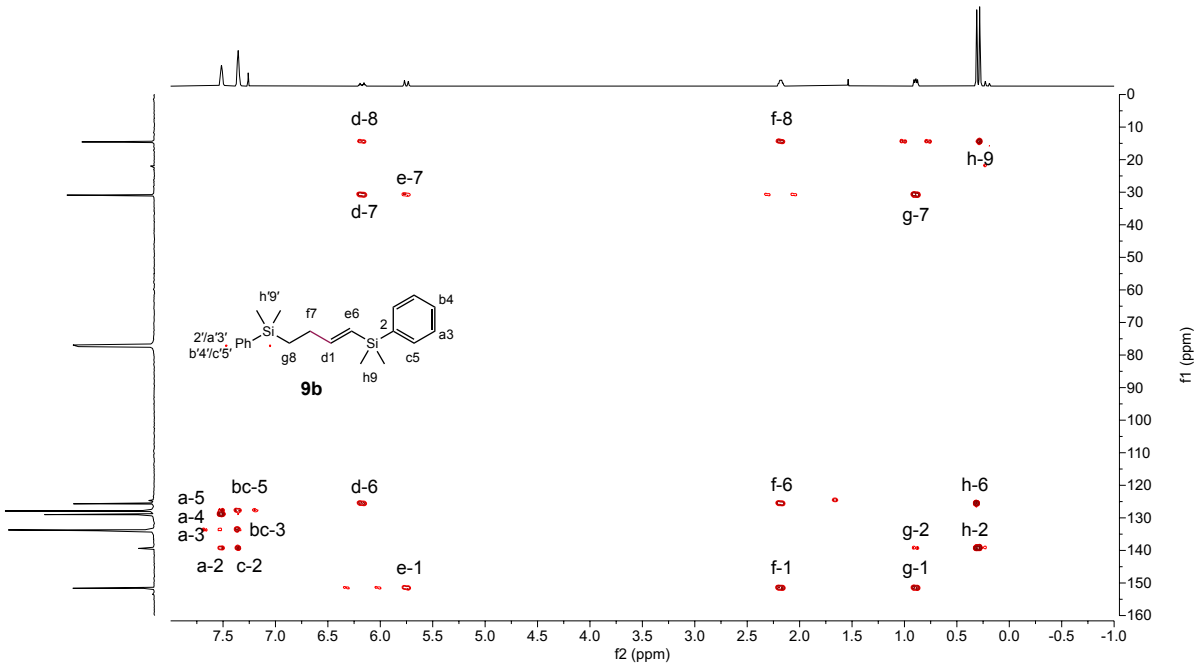

Figure S21. $^{1}H–^{13}C$ HMBC (500 MHz, $CDCl_3$) spectrum of **9b**.

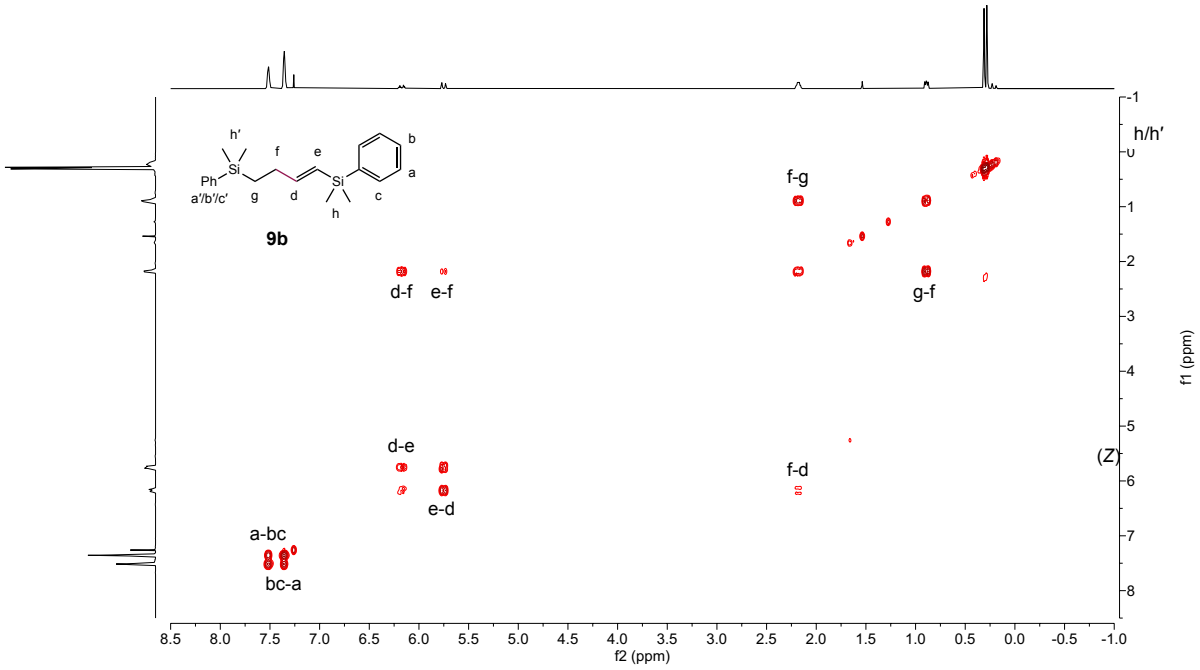

Figure S22. $^{1}H–^{1}H$ COSY (500 MHz, $CDCl_3$) spectrum of **9b**.

(*E*)-but-1-ene-1,4-diylbis(triphenylsilane) (9c) was prepared in 29% isolated yield, >98% purity, >98:2 *E*/*Z* after 48 hours as described in 3.1 but with added toluene (0.2 mL) as solvent. Due to precipitation of the product from solution, very poor mixing and low conversion was observed.

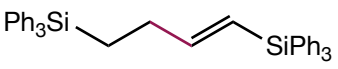

9c

^{1}H NMR (500 MHz, $CDCl_3$) δ 7.57 (d, *J* = 7.3 Hz, 6H), 7.55 (d, *J* = 7.3 Hz, 6H), 7.44 (t, *J* = 7.2 Hz, 6H), 7.39 (t, *J* = 7.3 Hz, 12H), 6.33 (dt, *J* = 18.5, 5.4 Hz, 1H), 6.24 (d, *J* = 18.5 Hz, 1H), 2.44 (q, *J* = 8.8, 5.4 Hz, 2H), 1.65 – 1.49 (m, 2H)

^{13}C NMR (126 MHz, $CDCl_3$) δ 155.37, 136.08, 135.78, 135.07, 134.96, 129.62, 129.52, 128.04, 127.92, 121.87, 31.16, 12.01

LC-MS (ESI): for $[M+Na]^+$ = $C_{40}H_{36}Si_2Na$, calculated *m*/*z* = 595.22533; found *m*/*z* = 595.22254; for $[M+K]^+$ = $C_{40}H_{36}Si_2K$, calculated *m*/*z* = 611.19927; found *m*/*z* = 611.19784

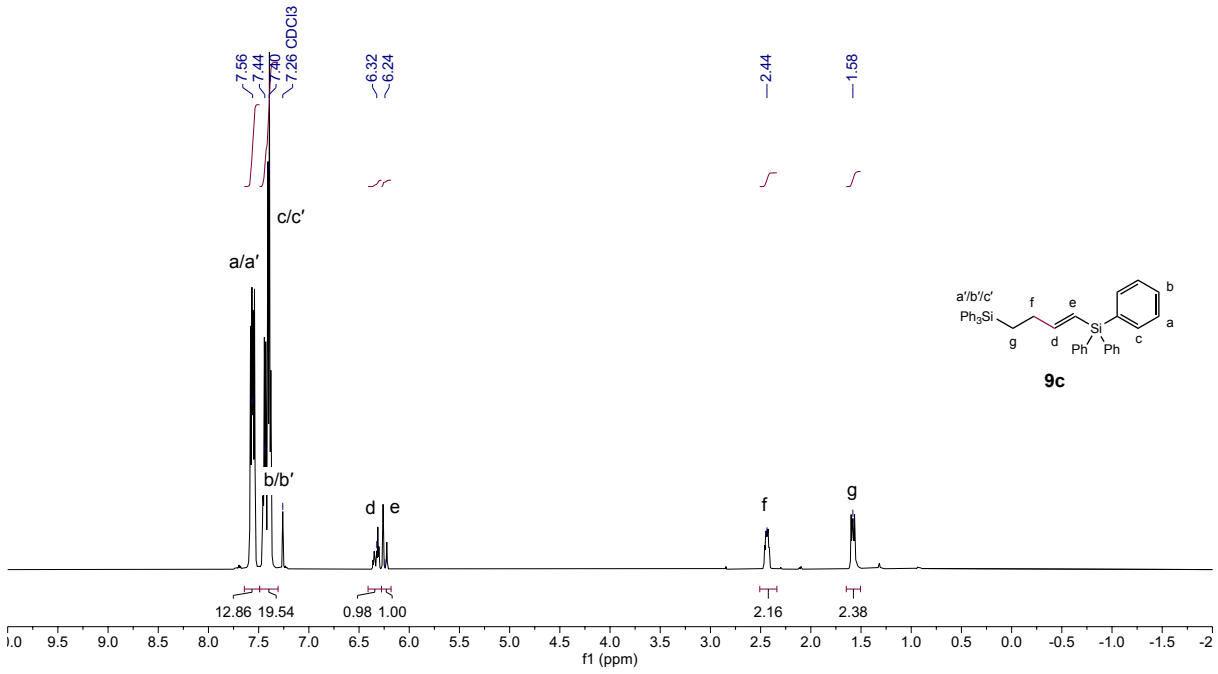

Figure S23. ^{1}H NMR (500 MHz, $CDCl_3$) spectrum of **9c**.

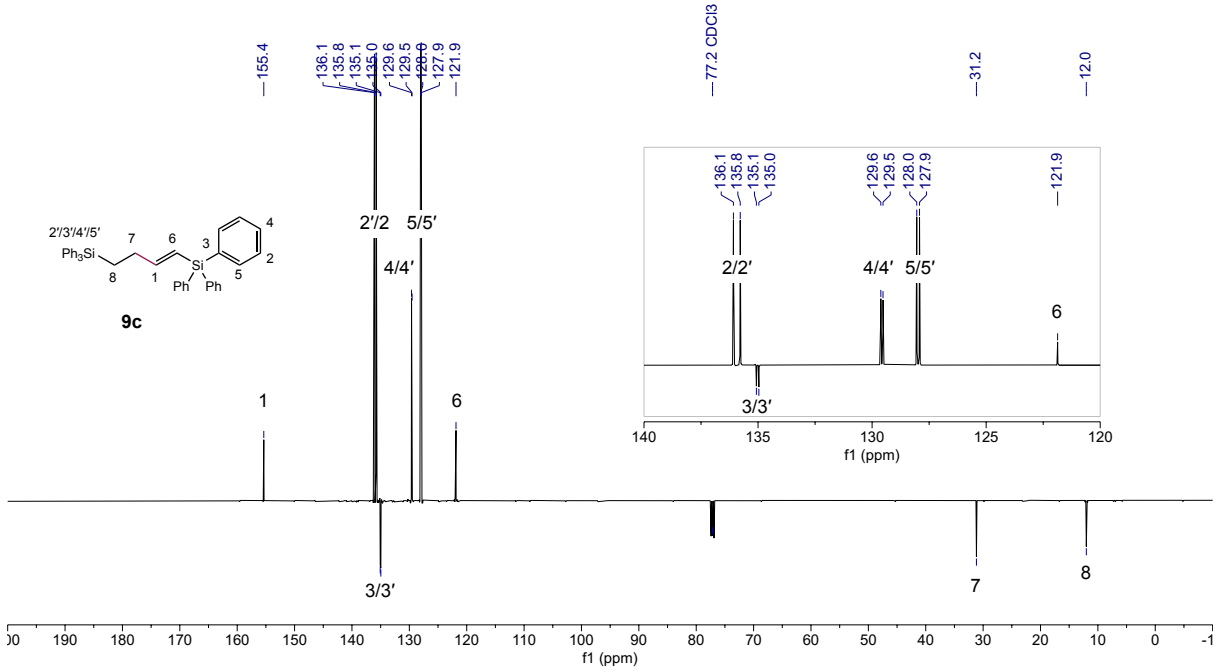

Figure S24. ^{13}C NMR (126 MHz, $CDCl_3$) spectrum of **9c**.

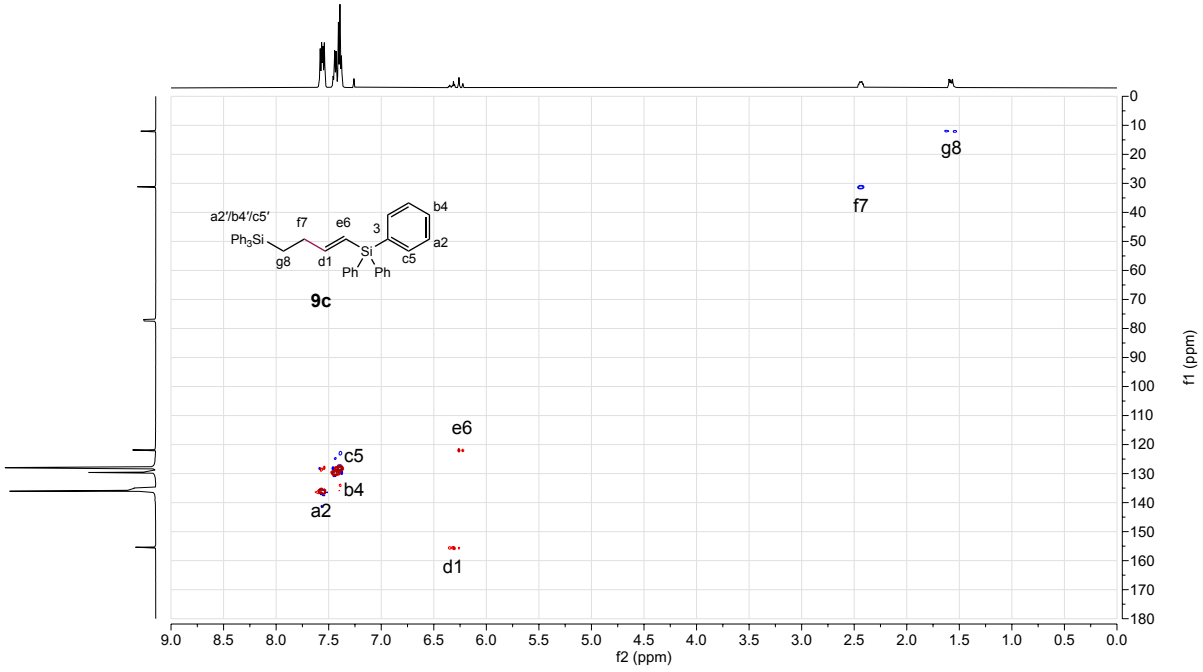

Figure S25. ^{1}H–^{13}C HSQC (500 MHz, $CDCl_3$) spectrum of **9c**.

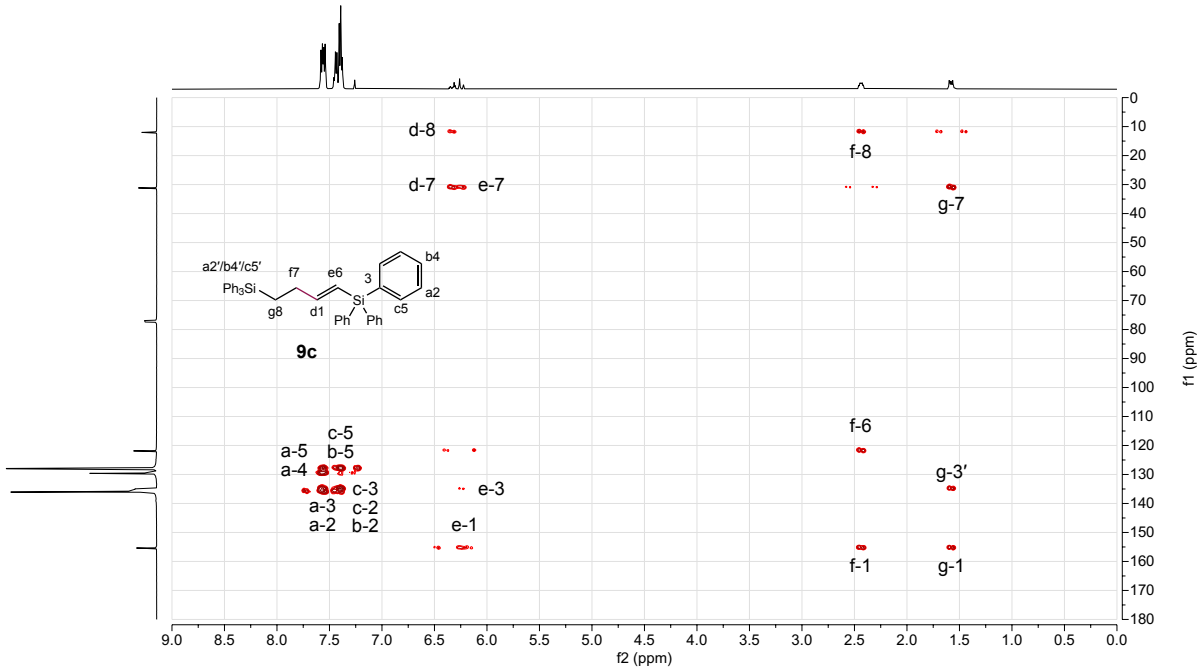

Figure S26. $^{1}H–^{13}C$ HMBC (500 MHz, $CDCl_3$) spectrum of **9c**.

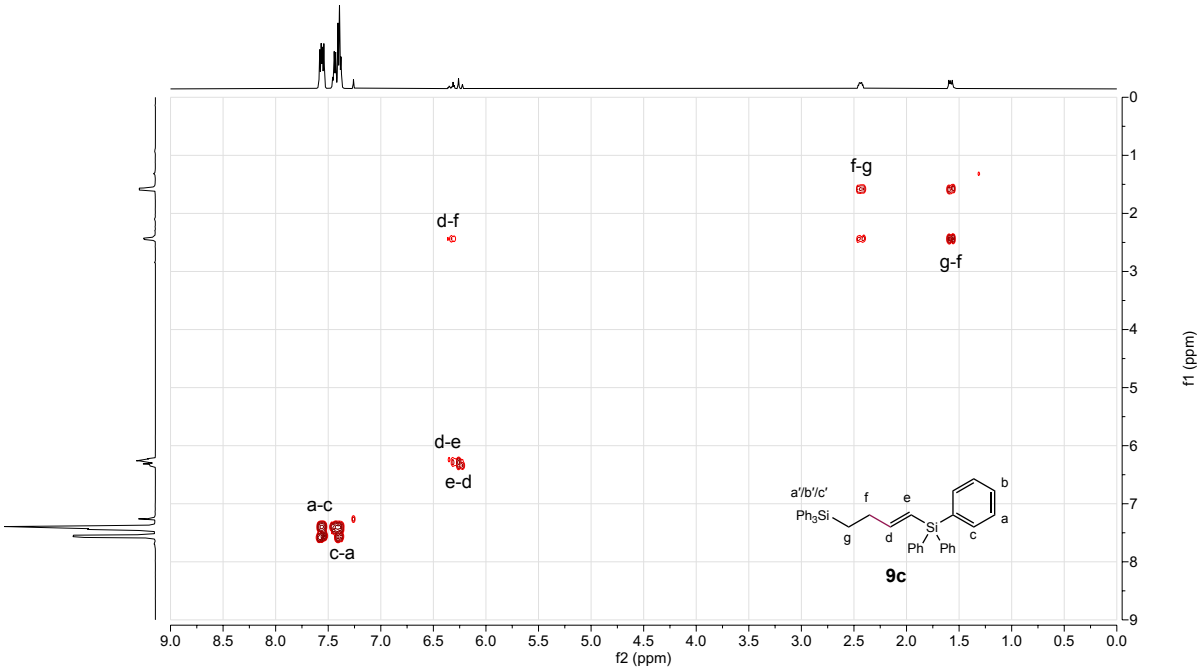

Figure S27. $^{1}H–^{1}H$ COSY (500 MHz, $CDCl_3$) spectrum of **9c**.

(*E*)-4,9-diethoxy-4,9-dimethyl-3,10-dioxa-4,9-disiladodec-5-ene (9d) was prepared in 75% isolated yield, 97% purity, 95:5 *E*/*Z* after 48 hours as described in 3.1.

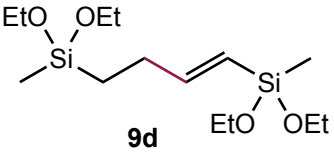

9d

^{1}H NMR (500 MHz, $CDCl_3$) δ 6.56 (dt, *J* = 18.7, 5.8 Hz, 1H), 5.75 (dt, *J* = 18.7, 1.7 Hz, 1H, *E*), 5.55 (d, *J* = 14.1 Hz, 1H, *Z*), 3.78 (q, *J* = 7.0 Hz, 4H), 3.65 (q, *J* = 7.0 Hz, 4H), 2.53 (q, *J* = 7.6 Hz, 2H, *Z*), 2.34 – 2.26 (m, 2H, *E*), 1.20 (t, *J* = 7.0 Hz, 6H), 1.14 (t, *J* = 7.0 Hz, 6H), 0.82 – 0.75 (m, 2H), 0.33 (s, 3H, *Z*), 0.29 (s, 3H, *E*), 0.17 (s, 3H, *Z*), 0.12 (s, 3H, *E*)

^{13}C NMR (126 MHz, $CDCl_3$) δ 153.65, 122.98, 58.30, 58.17, 30.13, 18.75, 18.71, 12.99, -3.74, -4.45

GC-MS (EI): for $[M]^+$ = $C_{14}H_{32}O_4Si_2$, calculated *m/z* = 320.18394, found *m/z* = 320.18283; for $[M - EtOH]^+$ = $C_{12}H_{26}O_3Si_2$, calculated *m/z* = 274.14207, found *m/z* = 274.14121

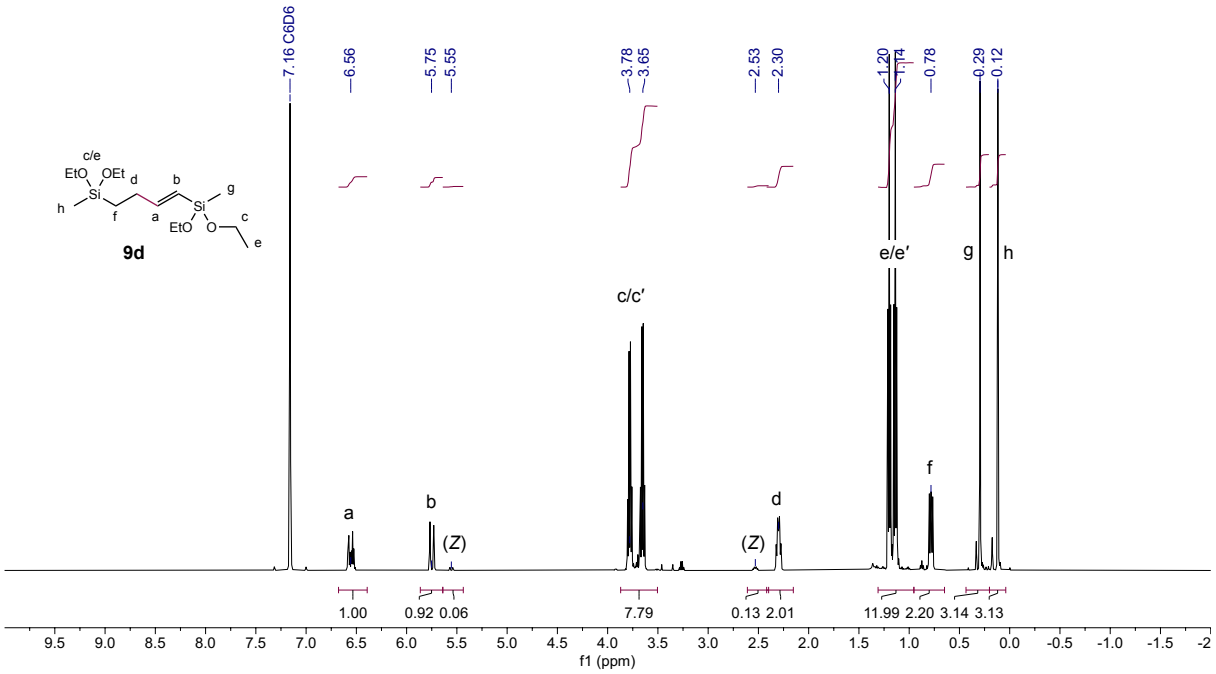

Figure S28. ^{1}H NMR (500 MHz, $CDCl_3$) spectrum of **9d**.

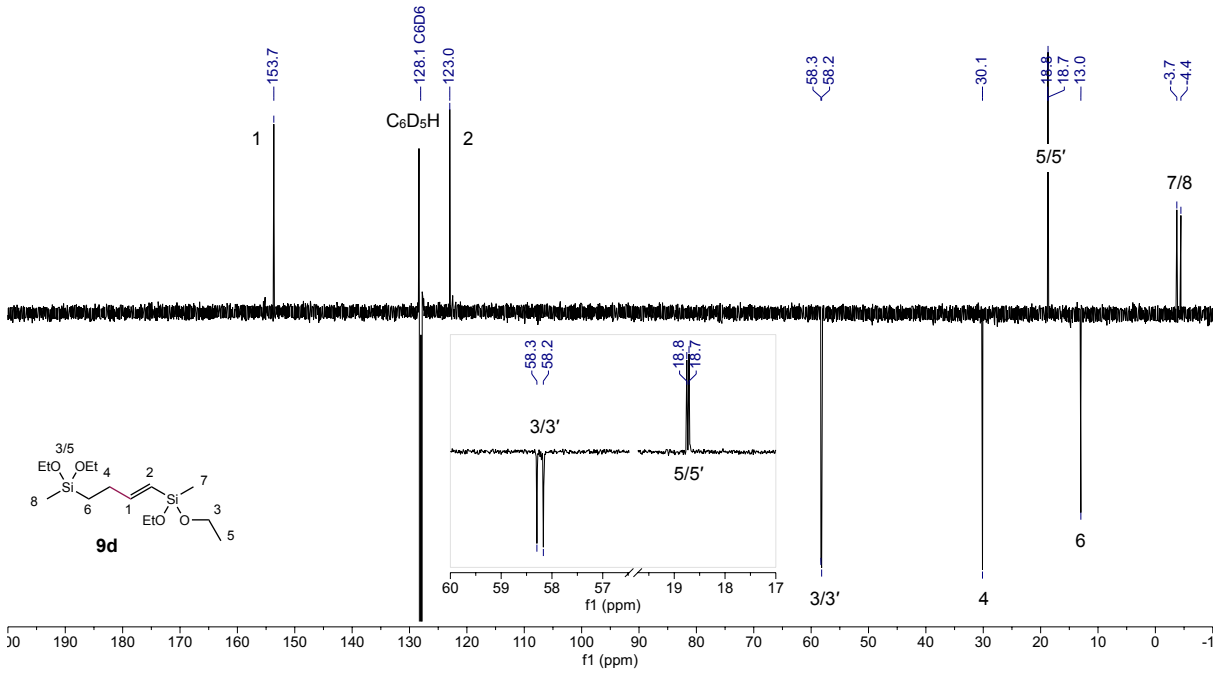

Figure S29. ^{13}C NMR (126 MHz, $CDCl_3$) spectrum of **9d**.

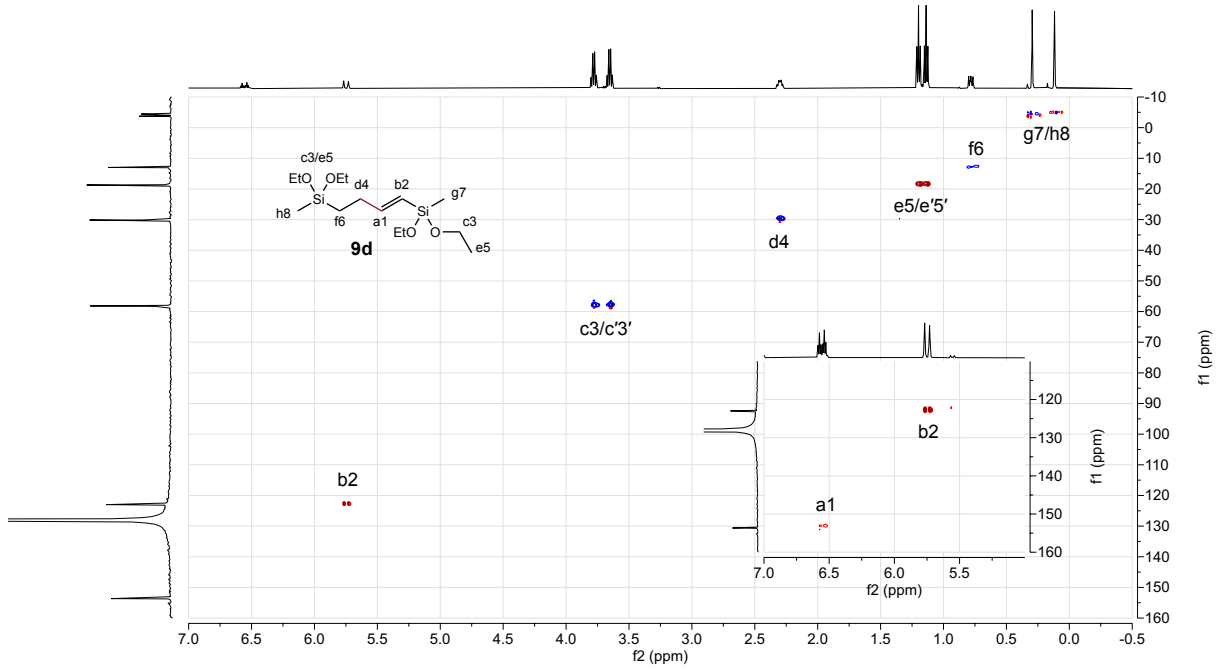

Figure S30. ^{1}H–^{13}C HSQC (500 MHz, $CDCl_3$) spectrum of **9d**.

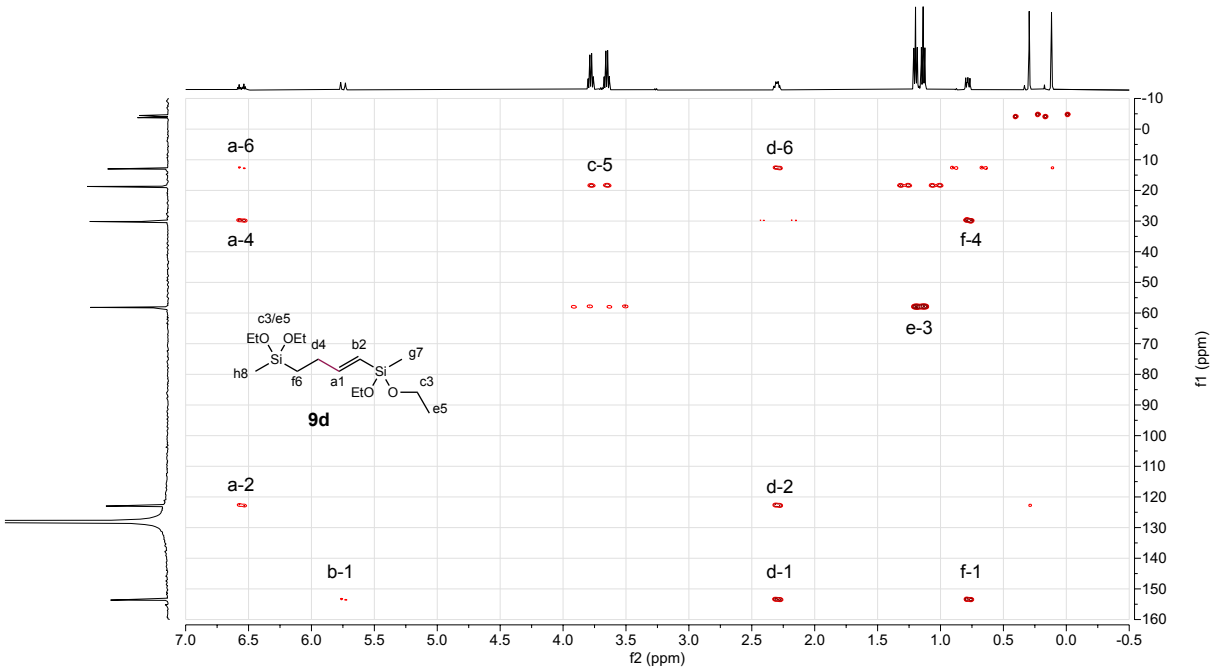

Figure S31. $^{1}H–^{13}C$ HMBC (500 MHz, $CDCl_3$) spectrum of **9d**.

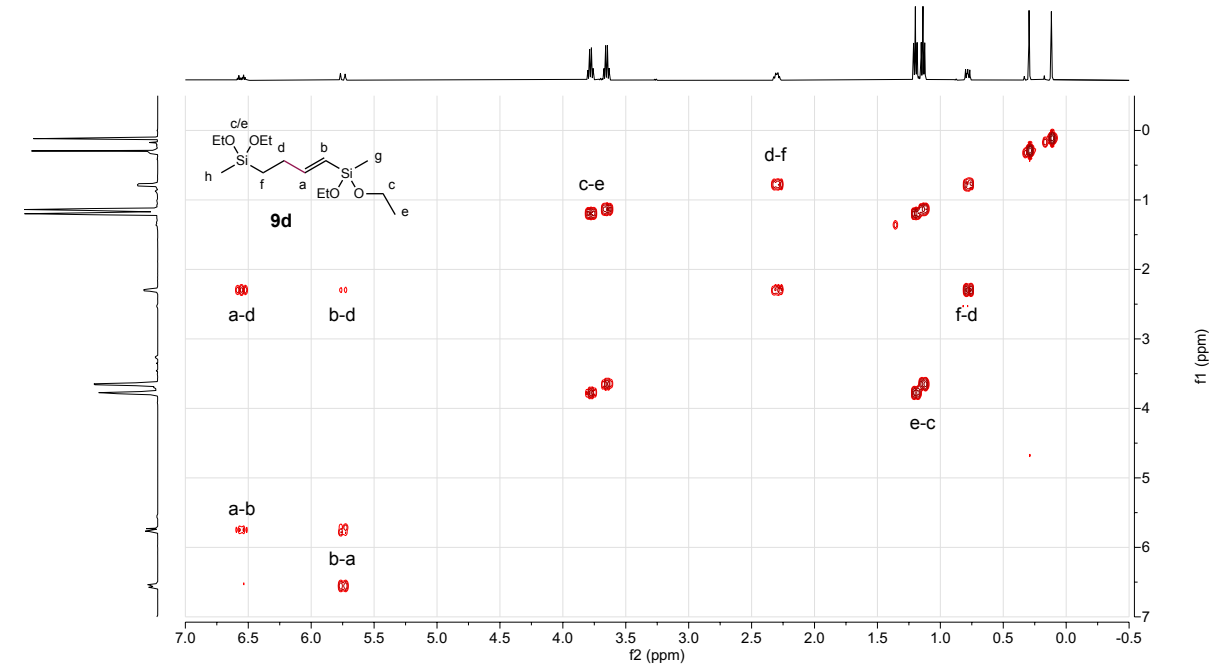

Figure S32. $^{1}H–^{1}H$ COSY (500 MHz, $CDCl_3$) spectrum of **9d**.

(*E*)-3,3'-(but-1-ene-1,4-diyl)bis(1,1,1,3,5,5,5-heptamethyltrisiloxane) (9e) was prepared in 87% isolated yield, 97% purity, 96:4 *E*/*Z* after 48 hours as described in 3.1.

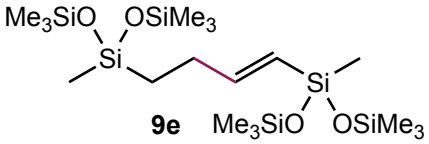

^{1}H NMR (500 MHz, $CDCl_3$) δ 6.28 (dt, *J* = 14.1, 7.3 Hz, 1H, *Z*), 6.20 (dt, *J* = 18.6, 5.8 Hz, 1H, *E*), 5.46 (dt, *J* = 18.6, 1.7 Hz, 1H, *E*), 5.26 (d, *J* = 14.1 Hz, 1H, *Z*), 2.19 (dt, *J* = 11.9, 7.3, 6.0 Hz, 2H, *Z*), 2.11 (tdd, *J* = 9.9, 7.0, 6.0, 1.2 Hz, 2H, *E*), 0.56 (dt, *J* = 8.5, 4.9 Hz, 2H), 0.09 (s, 36H), 0.08 (s, 3H), 0.02 (s, 3H)

^{13}C NMR (126 MHz, $CDCl_3$) δ 153.08 (*Z*), 151.50 (*E*), 125.78 (*E*), 125.71 (*Z*), 29.79 (*E*), 27.23 (*Z*), 18.02 (*Z*), 16.31 (*E*), 2.04, 2.01, 0.12, -0.03

LC-MS (ESI): for $[M+Na]^+$ = $C_{18}H_{48}O_4Si_6Na$, calculated *m/z* = 519.20663, found *m/z* = 519.20348

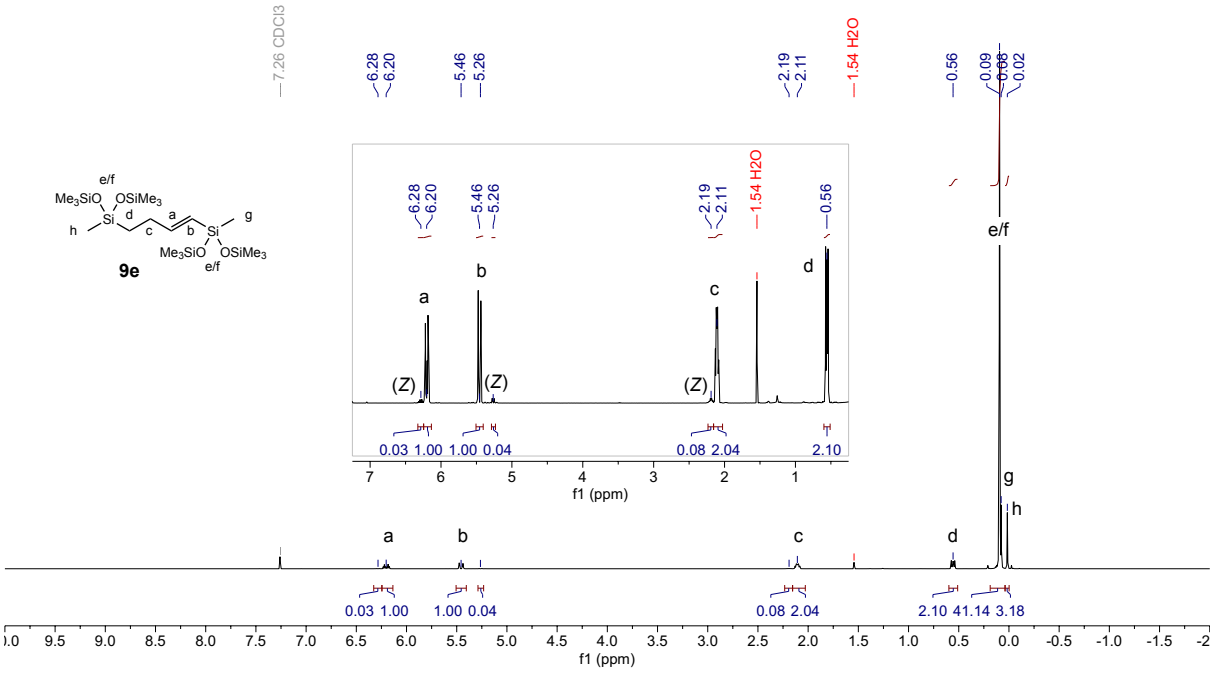

Figure S33. ^{1}H NMR (500 MHz, $CDCl_3$) spectrum of **9e**.

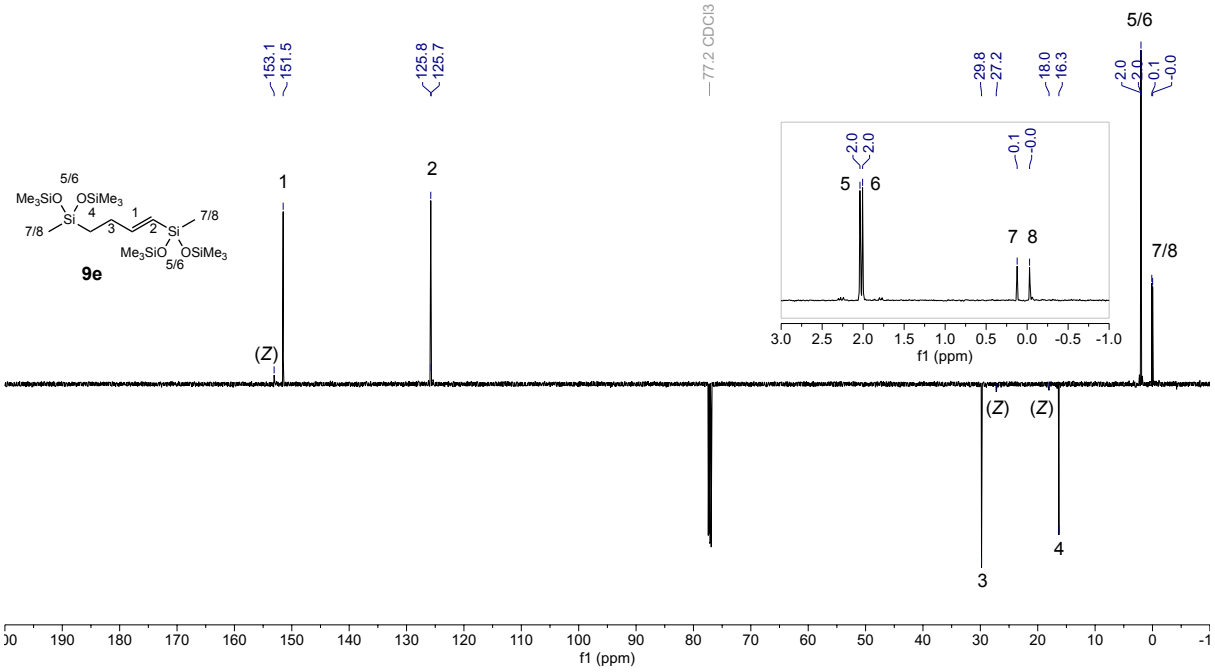

Figure S34. ^{13}C NMR (126 MHz, $CDCl_3$) spectrum of **9e**.

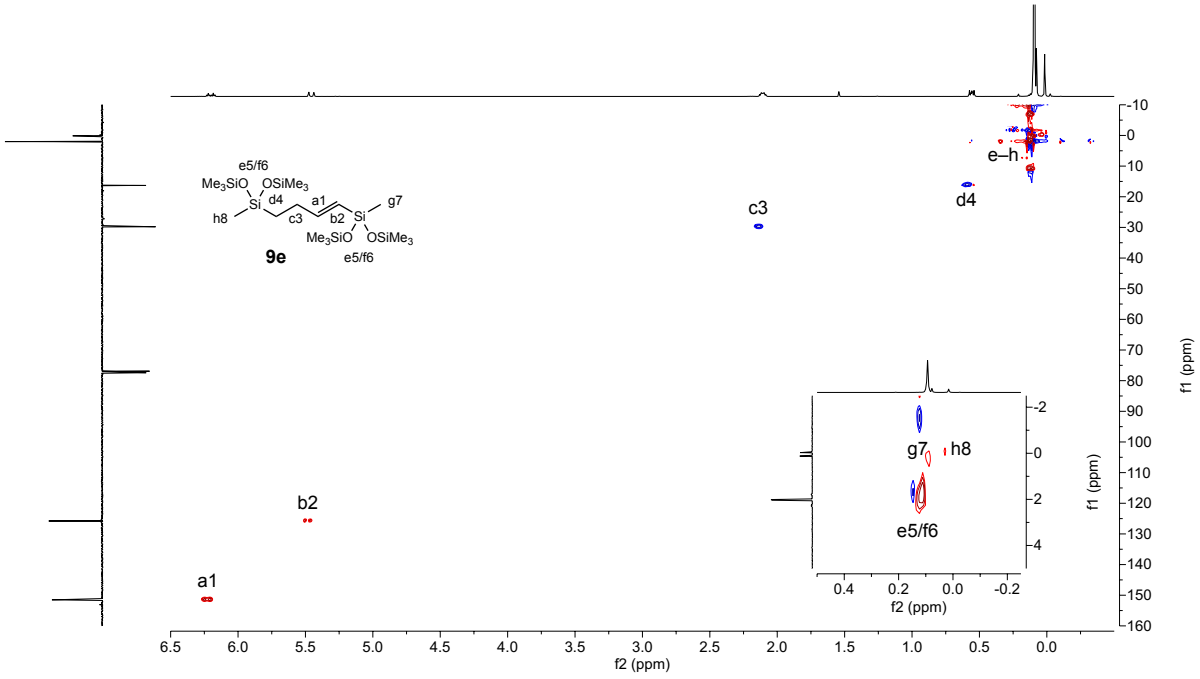

Figure S35. ^{1}H–^{13}C HSQC (500 MHz, $CDCl_3$) spectrum of **9e**.

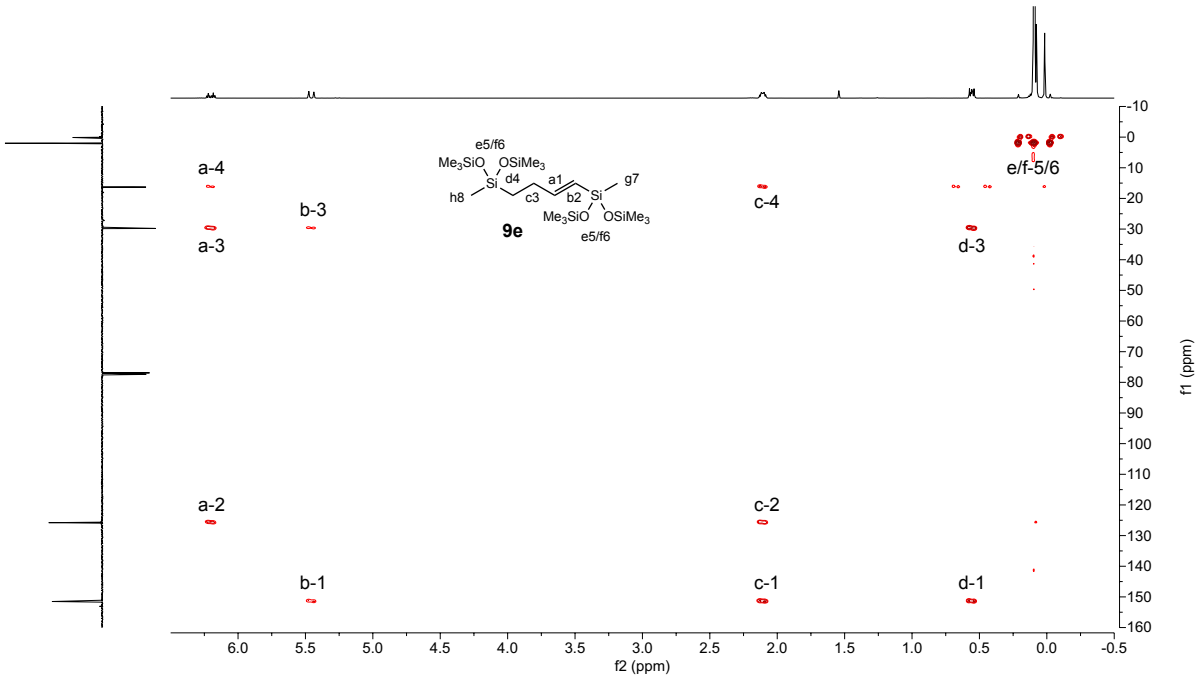

Figure S36. $^{1}H–^{13}C$ HMBC (500 MHz, $CDCl_3$) spectrum of **9e**.

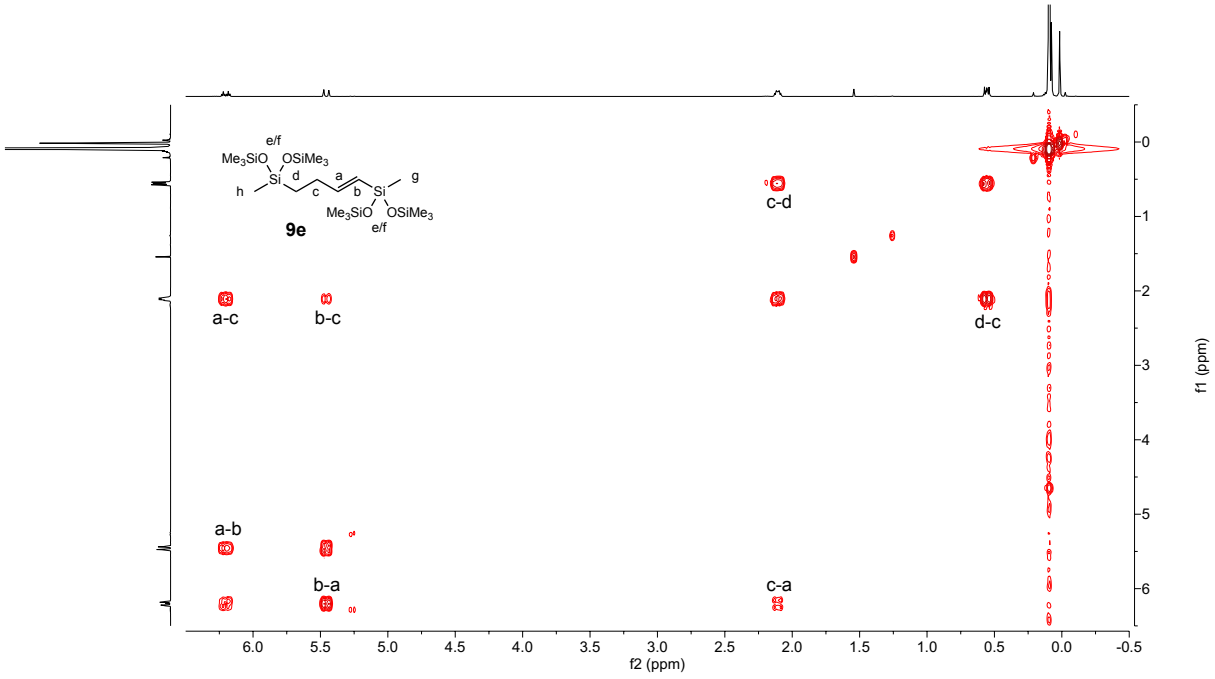

Figure S37. $^{1}H–^{1}H$ COSY (500 MHz, $CDCl_3$) spectrum of **9e**.

(*E*)-4,4,9,9-tetraethoxy-3,10-dioxa-4,9-disiladodec-5-ene (9f) was prepared in 68% isolated yield, 95% purity, 94:6 *E*/*Z* after 48 hours as described in 3.1.

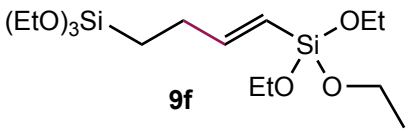

9f

^{1}H NMR (500 MHz, $CDCl_3$) δ 6.51 (dt, *J* = 18.7, 5.7 Hz, 1H), 5.42 (dt, *J* = 18.8, 1.8 Hz, 1H), 3.81 (q, *J* = 7.0 Hz, 12H), 2.31 – 2.20 (m, 2H), 1.22 (t, *J* = 7.0 Hz, 18H), 0.78 – 0.69 (m, 2H)

^{13}C NMR (126 MHz, $CDCl_3$) δ 155.69, 117.31, 58.56, 58.52, 29.54, 18.42, 18.37, 8.93

GC-MS (EI): for $[M - EtOH]^+ = C_{14}H_{30}O_5Si_2$, calculated *m/z* = 334.16321, found *m/z* = 334.16351

LC-MS (ESI): for $[M]^+ = C_{16}H_{37}O_6Si_2$, calculated *m/z* = 381.2129, found *m/z* = 381.21083; for $[M + Na]^+ = C_{16}H_{36}O_6Si_2Na$, calculated *m/z* = 403.19485, found *m/z* = 403.19432

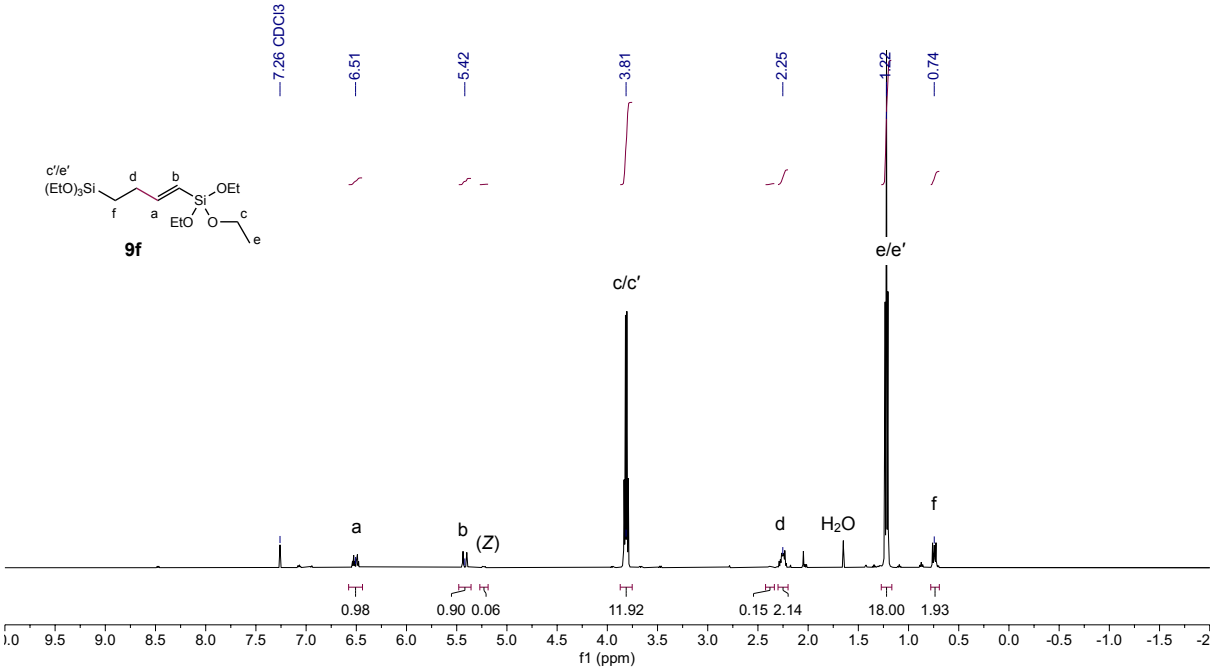

Figure S38. ^{1}H NMR (500 MHz, $CDCl_3$) spectrum of **9f**.

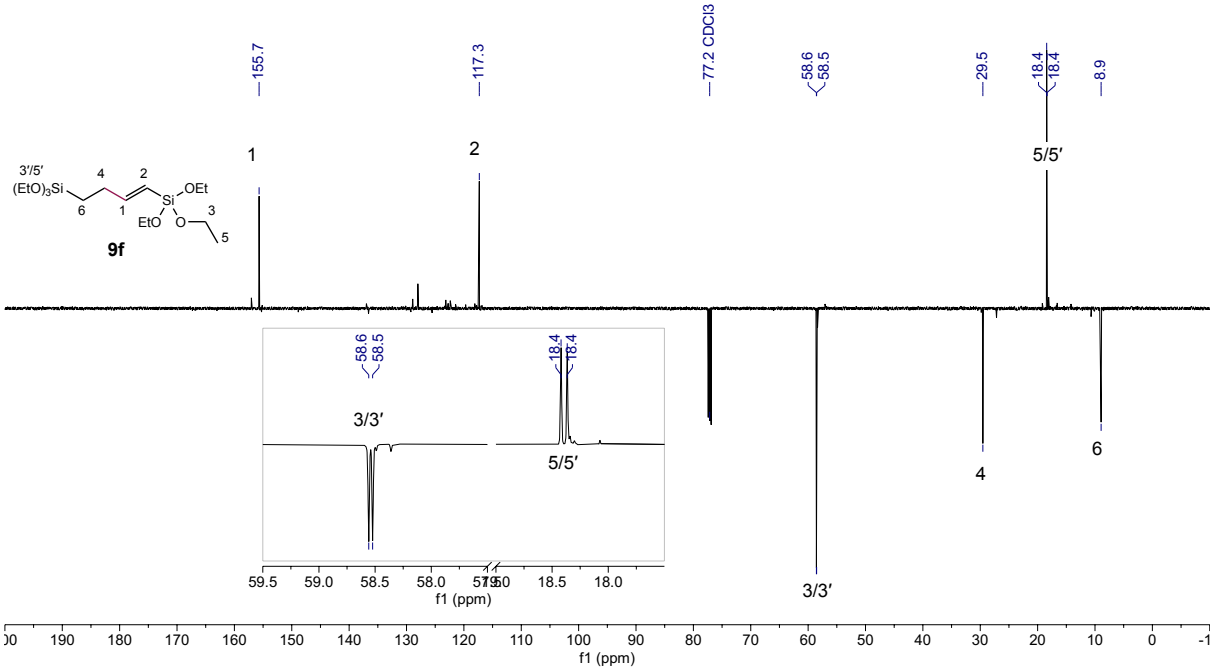

Figure S39. ^{13}C NMR (126 MHz, $CDCl_3$) spectrum of **9f**.

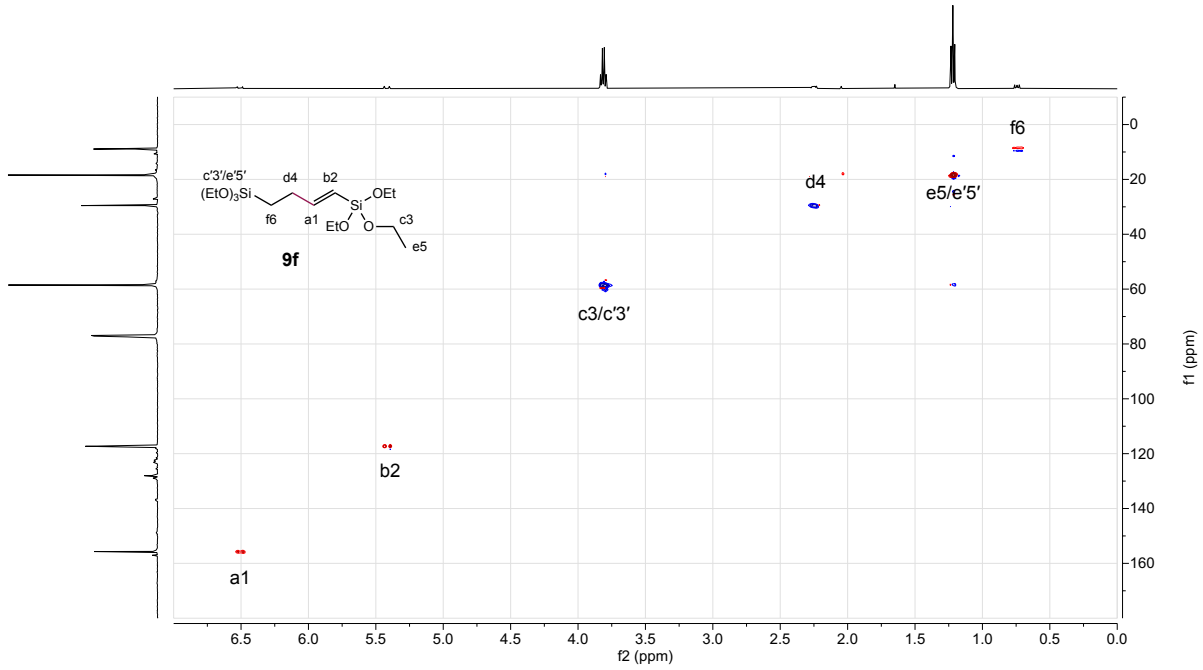

Figure S40. ^{1}H–^{13}C HSQC (500 MHz, $CDCl_3$) spectrum of **9f**.

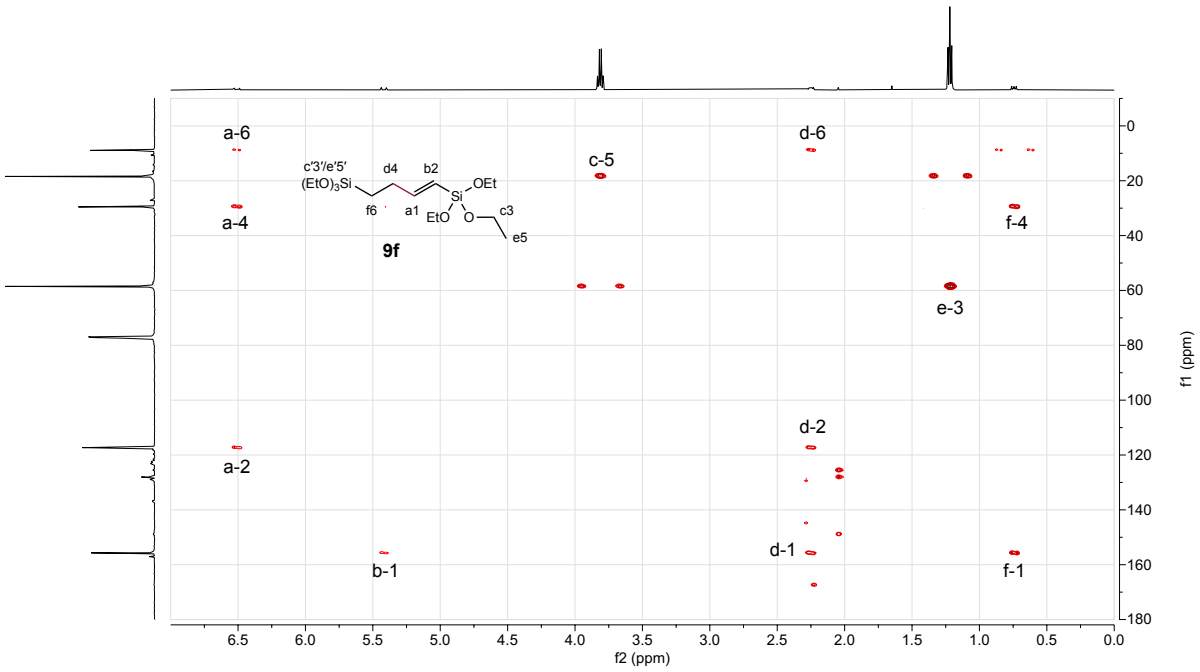

Figure S41. ^{1}H–^{13}C HMBC (500 MHz, $CDCl_3$) spectrum of **9f**.

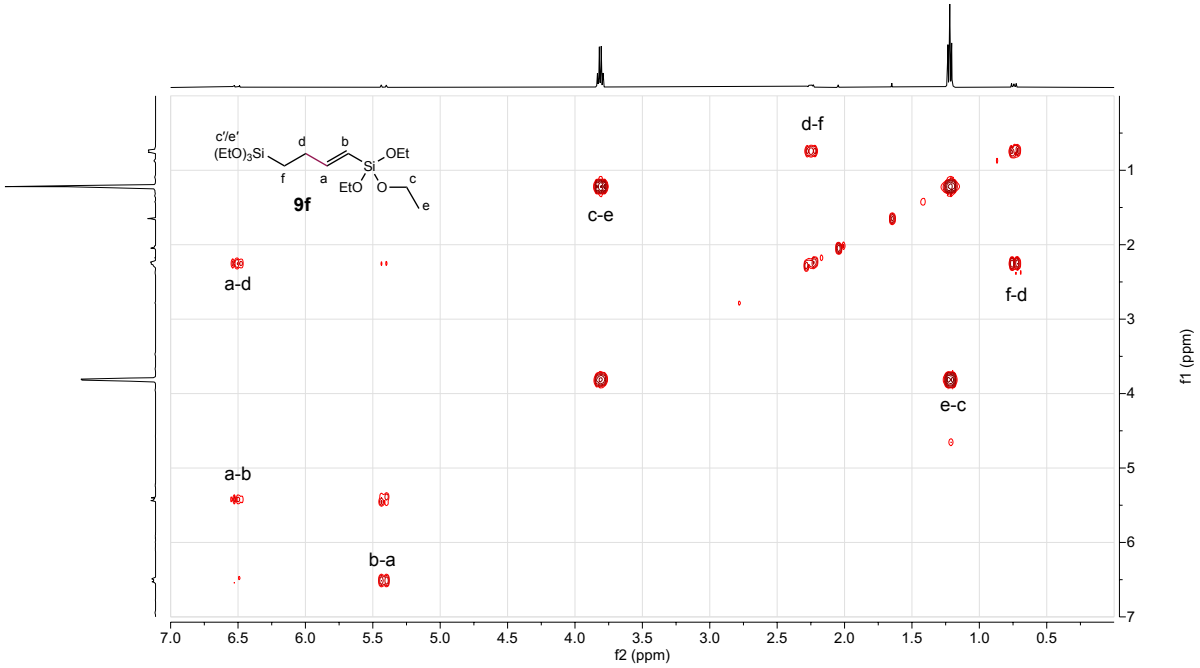

Figure S42. ^{1}H–^{1}H COSY (500 MHz, $CDCl_3$) spectrum of **9f**.

(3*E*,10*E*,17*E*)-2,2,7,7,9,9,14,14,16,16,21,21-dodecamethyl-1,8,15-trioxa-2,7,9,14,16,21-hexasilacyclohenicosa-3,10,17-triene and **(3*E*,12*E*,17*E*)-2,2,7,7,9,9,14,14,16,16,21,21-dodecamethyl-1,8,15-trioxa-2,7,9,14,16,21-hexasilacyclohenicosa-3,12,17-triene (9g)** was prepared in 97% isolated yield, ≥95% purity, 96:4 *E*/*Z* after 48 hours as described in 3.1. The product structure is proposed to be a cyclic trimer of dvtms on the basis of mass spectrometric data and observation of a single major set of peaks by Diffusion Ordered NMR Spectroscopy (DOSY).

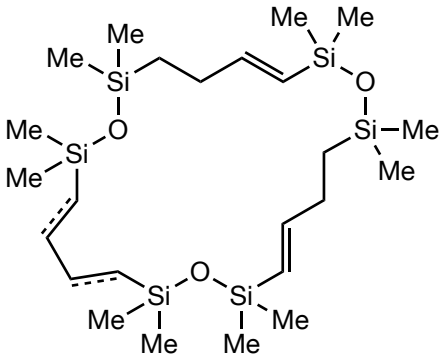

9g

^{1}H NMR (500 MHz, $CDCl_3$) δ 6.17 (dt, *J* = 18.7, 6.3 Hz, 1H), 5.60 (dd, *J* = 18.7, 2.5 Hz, 1H), 2.13 (p, *J* = 7.6, 6.3, 2.5 Hz, 2H), 0.64 (t, *J* = 7.6 Hz, 2H), 0.12 (s, 6H), 0.07 (s, 6H)

^{13}C NMR (126 MHz, $CDCl_3$) δ 150.7, 150.6, 150.6, 150.5, 127.7, 127.6, 127.5, 30.1, 30.1, 17.1, 17.1, 1.0, 1.0, 0.7, 0.7

LC-MS (ESI): for trimer $[M + Na]^+ = C_{24}H_{54}O_3Si_6Na$, calculated *m/z* = 581.25866, found *m/z* = 581.17408

LC-MS (APCI): for trimer $[M]^+ = C_{24}H_{54}O_3Si_6$, calculated *m/z* = 558.3, found *m/z* = 557.6

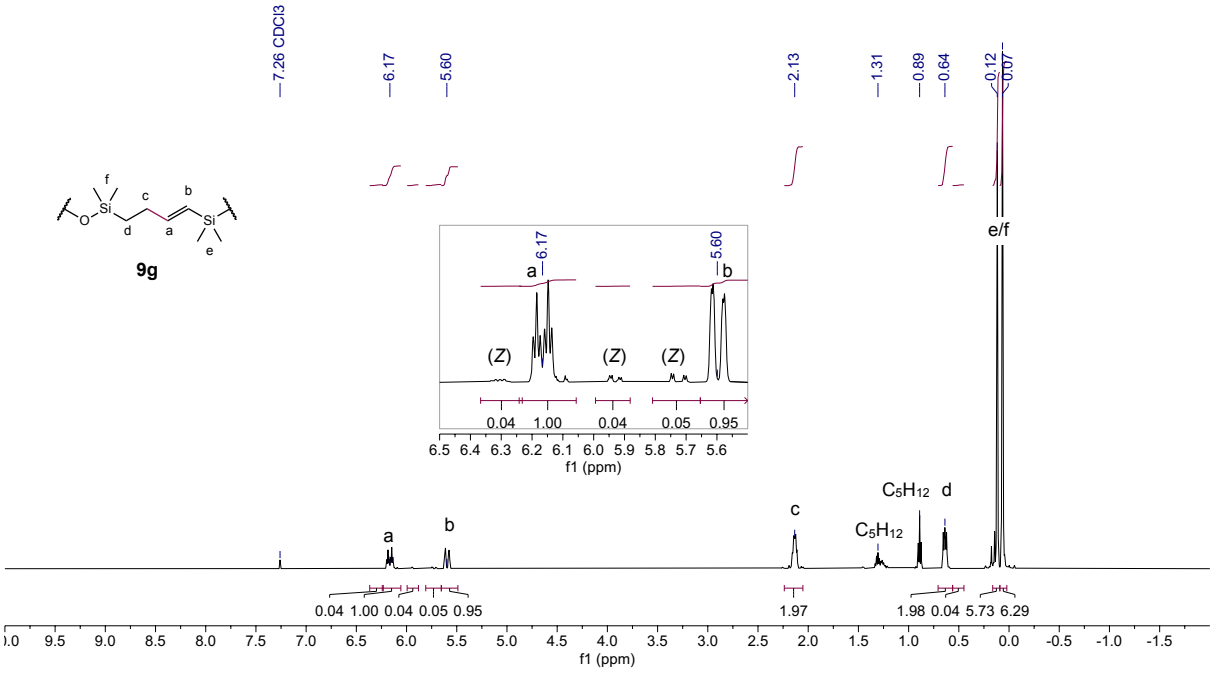

Figure S43. ^{1}H NMR (500 MHz, $CDCl_3$) spectrum of **9g**.

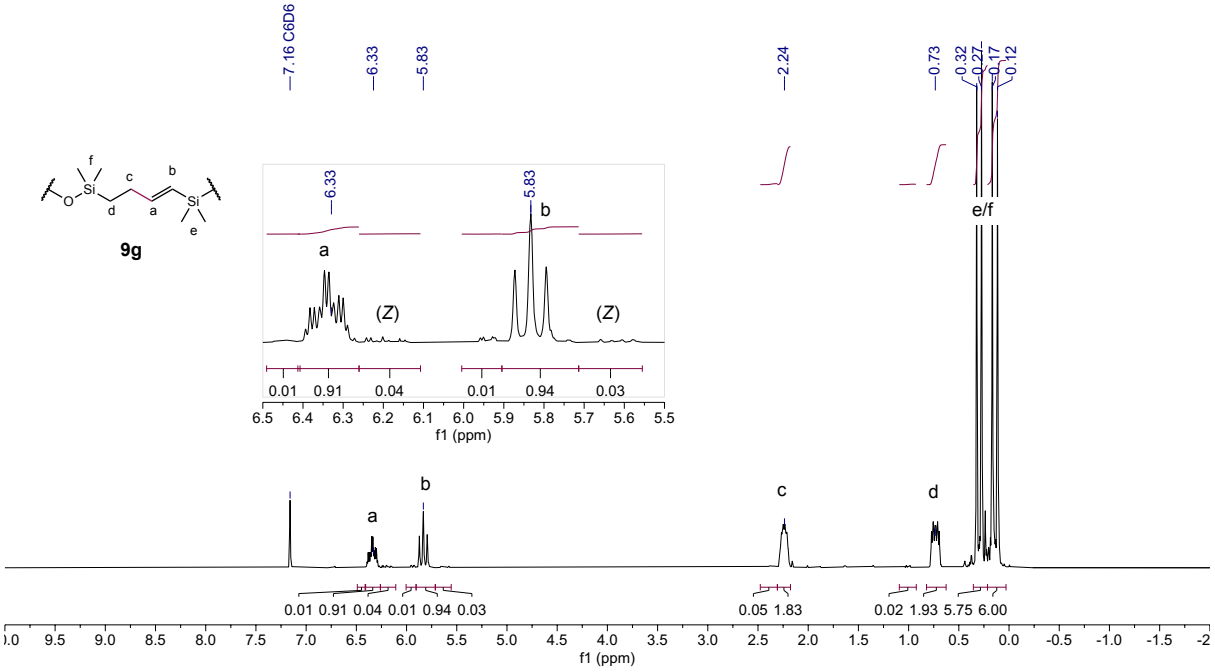

Figure S44. ^{1}H NMR (500 MHz, C_6D_6) spectrum of **9g**.

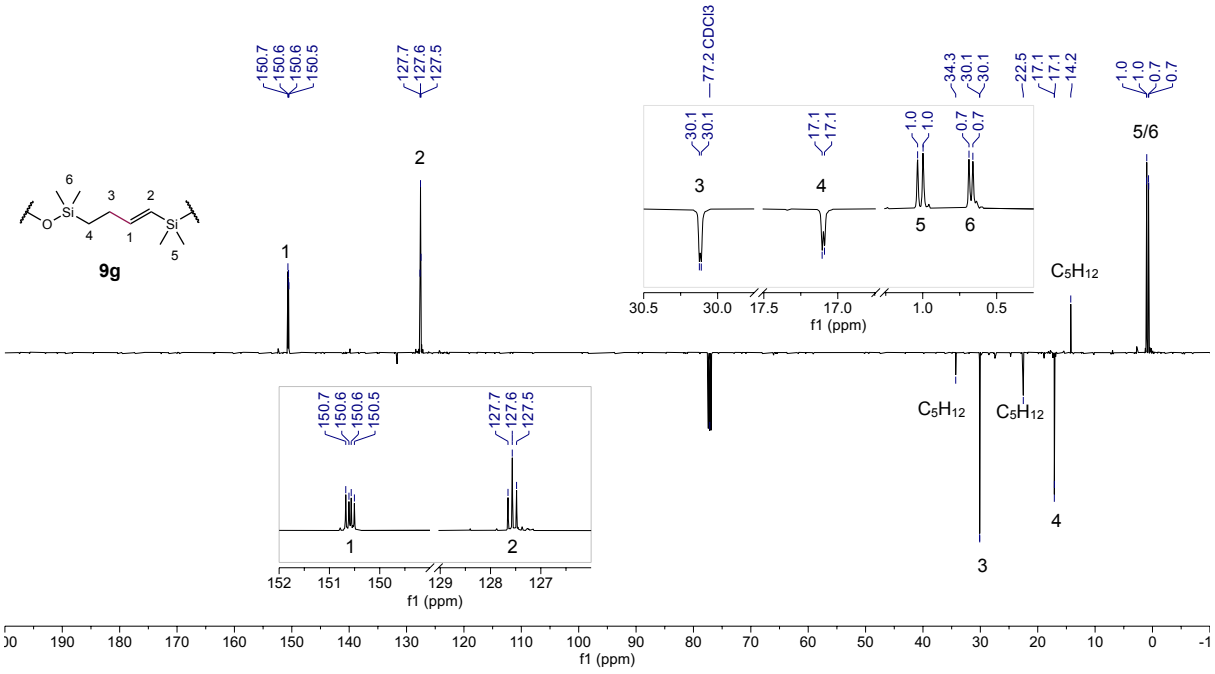

Figure S45. ^{13}C NMR (126 MHz, $CDCl_3$) spectrum of **9g**.

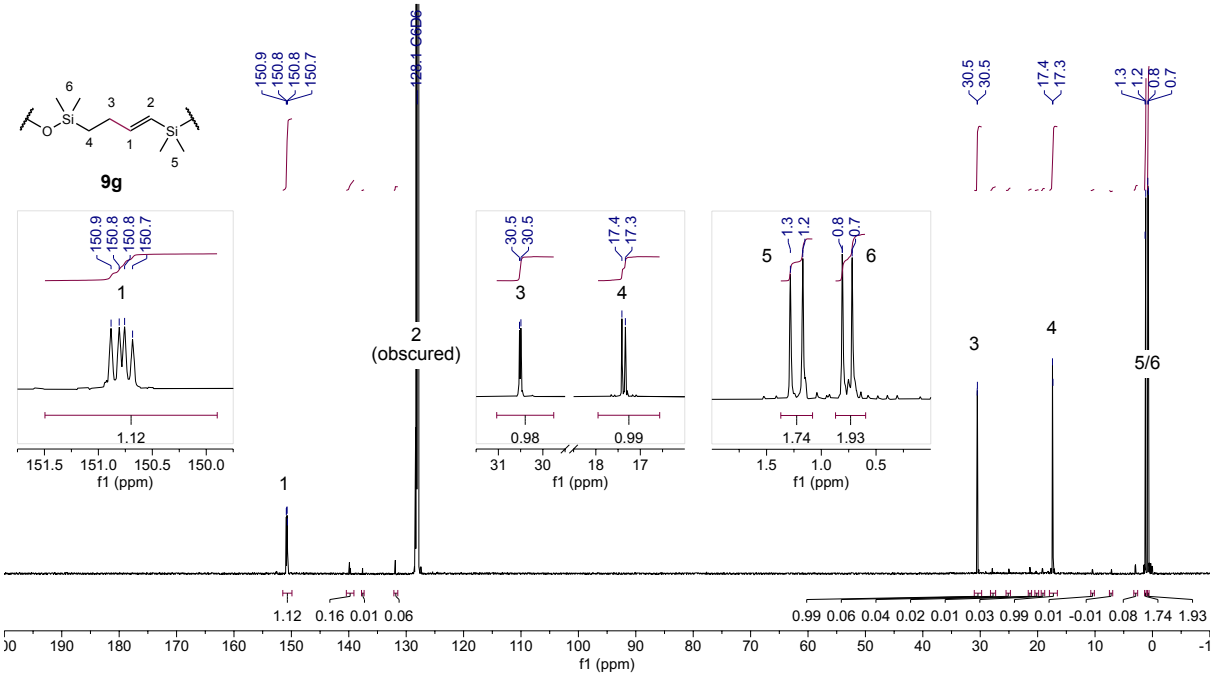

Figure S46. ^{13}C NMR (126 MHz, C_6D_6) spectrum of **9g**.

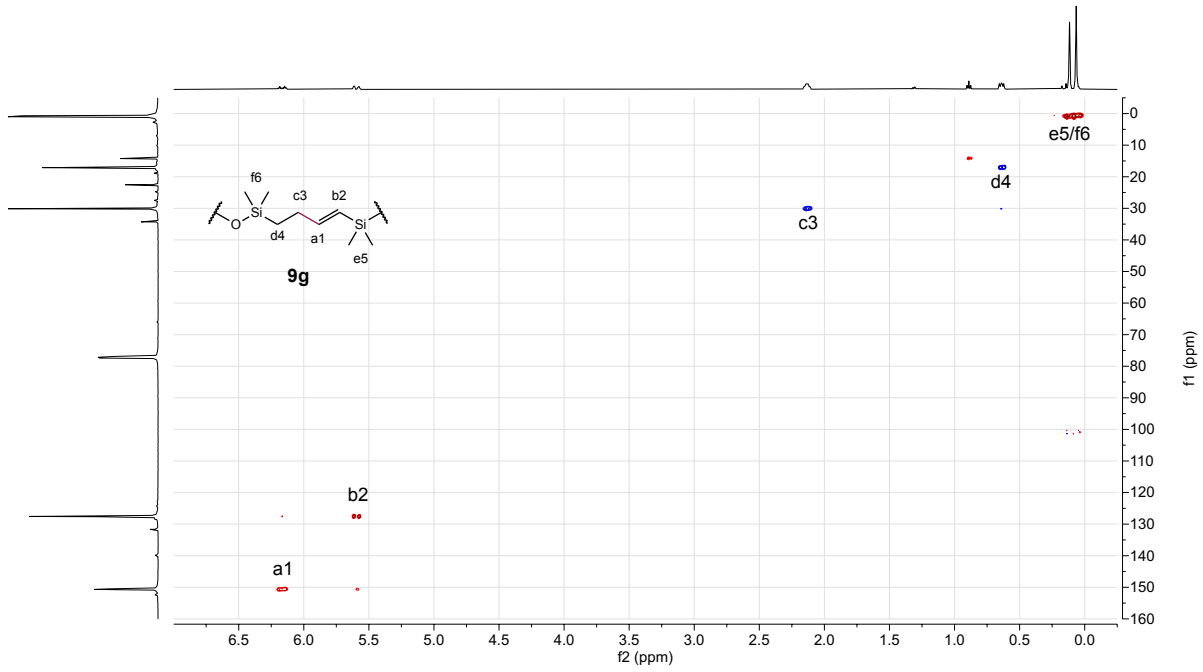

Figure S47. ^{1}H–^{13}C HSQC (500 MHz, $CDCl_3$) spectrum of **9g**.

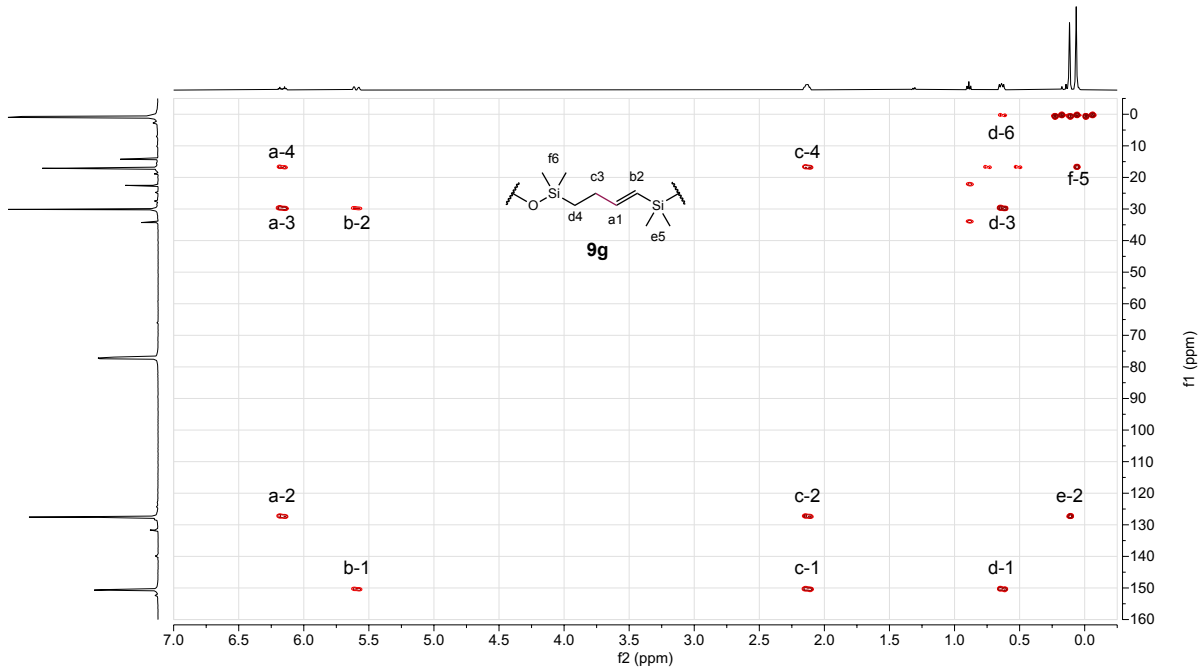

Figure S48. $^{1}H–^{13}C$ HMBC (500 MHz, $CDCl_3$) spectrum of **9g**.

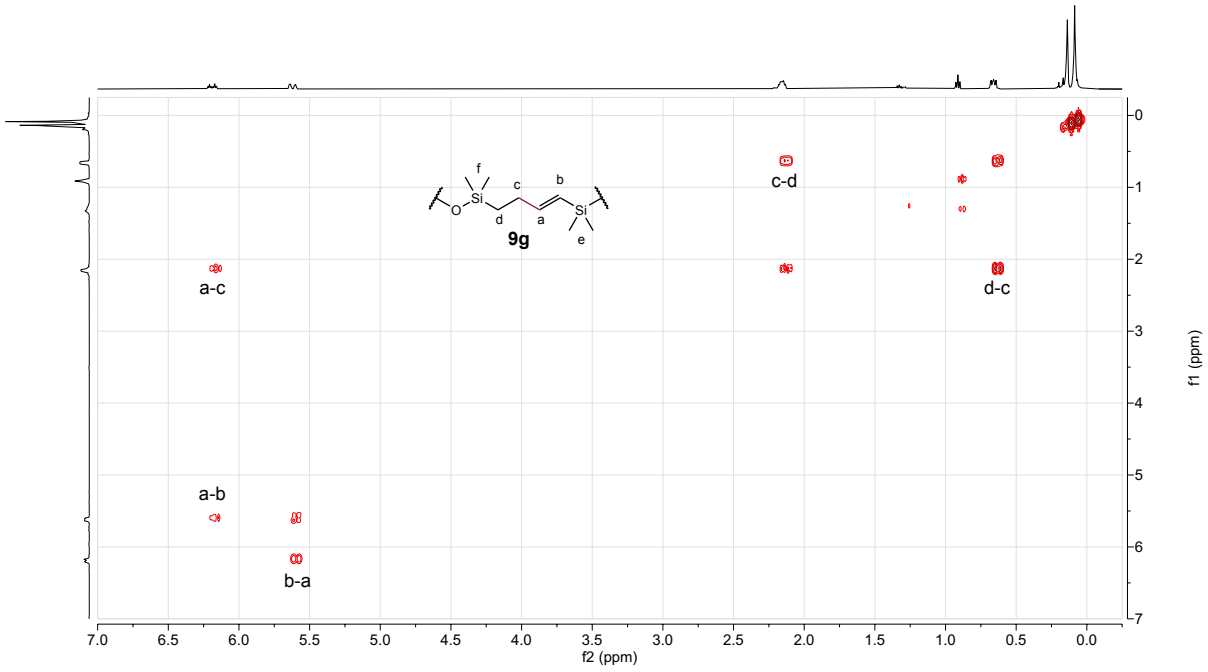

Figure S49. $^{1}H–^{1}H$ COSY (500 MHz, $CDCl_3$) spectrum of **9g**.

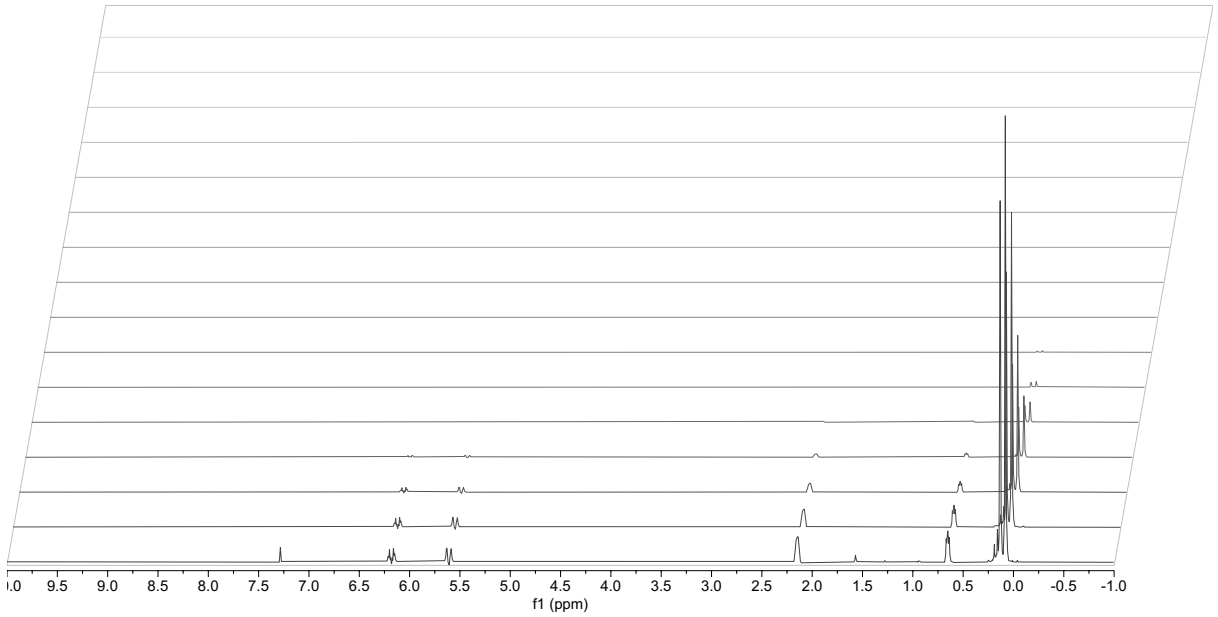

Figure S50. 1D ^{1}H DOSY (500 MHz, $CDCl_3$) spectrum of **9g**.

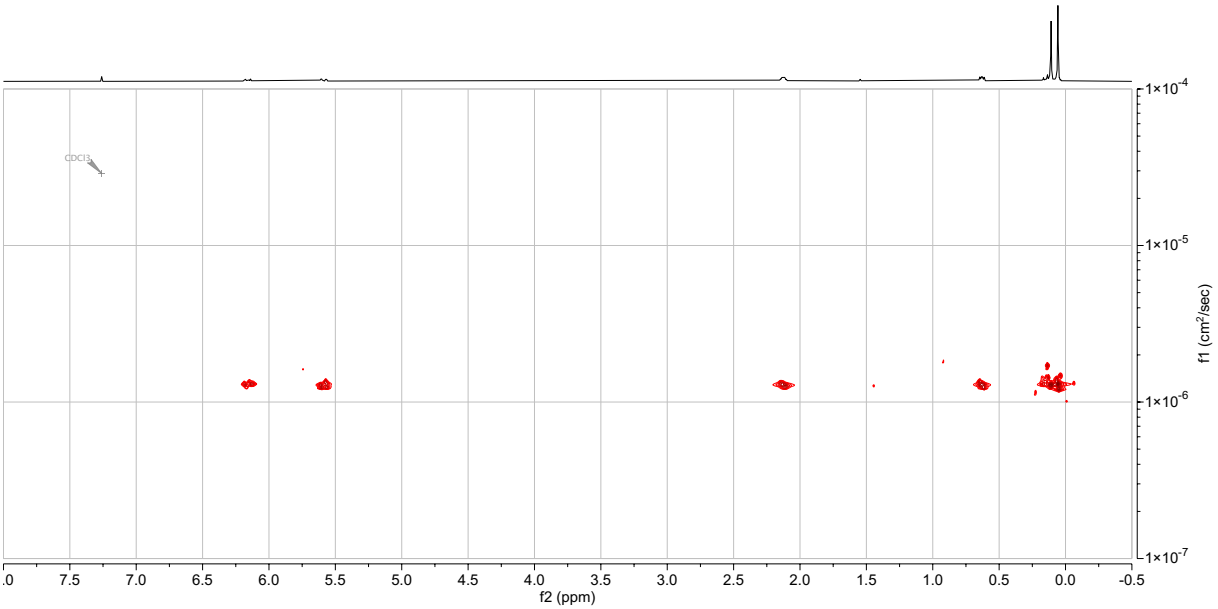

Figure S51. 2D ^{1}H DOSY (500 MHz, $CDCl_3$) spectrum of **9g**.

A mixture of **1-methyl-3-(6-methylhepta-1,5-dien-2-yl)cyclobutane (14aj)** and **(*E*)-2,5,9-trimethyldeca-1,4,8-triene (16aj)** was obtained in 65% combined yield (2:97 **14aj** : **16aj**) after 24 hours upon exposure of a solution of the iron precatalyst (1.25 mol% dimer, 2.5 mol% [Fe]) and myrcene to excess propylene.

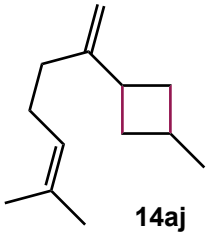

14aj

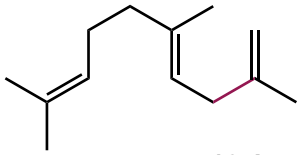

16aj

^{1}H NMR (500 MHz, Chloroform-*d*) δ 5.20 (td, *J* = 7.4, 1.5 Hz, 1H, **16aj**), 5.11 (tt, *J* = 7.0, 1.6 Hz, 1H, **16aj**), 4.71 (t, *J* = 1.7 Hz, 1H, **14aj**), 4.70 (s, 2H, **16aj**), 4.67 (d, *J* = 2.0 Hz, 1H, **14aj**), 2.70 (d, *J* = 7.4 Hz, 2H, **16aj**), 2.29 – 2.20 (m, 2H, **14aj**), 2.10 (t, *J* = 7.5 Hz, 2H, **16aj**), 2.04 (dd, *J* = 8.7, 6.4 Hz, 2H, **16aj**), 1.97 (dd, *J* = 9.3, 6.5 Hz, 2H, **14aj**), 1.72 (s, 3H, **16aj**), 1.69 (s, 3H, **16aj**), 1.62 (s, 3H, **16aj**), 1.61 (s, 3H, **16aj**), 1.45 (ddd, *J* = 11.4, 7.0, 2.4 Hz, 2H, **14aj**), 1.01 (d, *J* = 6.2 Hz, 3H, **14aj**)

^{13}C NMR (126 MHz, $CDCl_3$) δ 153.7 (**14aj**), 145.6, 136.7, 131.5, 124.5 (**14aj**), 124.5, 122.0, 109.8, 106.4 (**14aj**), 39.9, 36.9 (**14aj**), 36.6, 35.9 (**14aj**), 34.4, 26.8, 26.6 (**14aj**), 26.4 (**14aj**), 25.9, 25.8 (**14aj**), 22.7, 22.1 (**14aj**), 17.8, 16.0

GC-MS (EI): for $[M]^+ = C_{13}H_{22}$, calculated *m/z* = 178.17215, found *m/z* = 178.17111

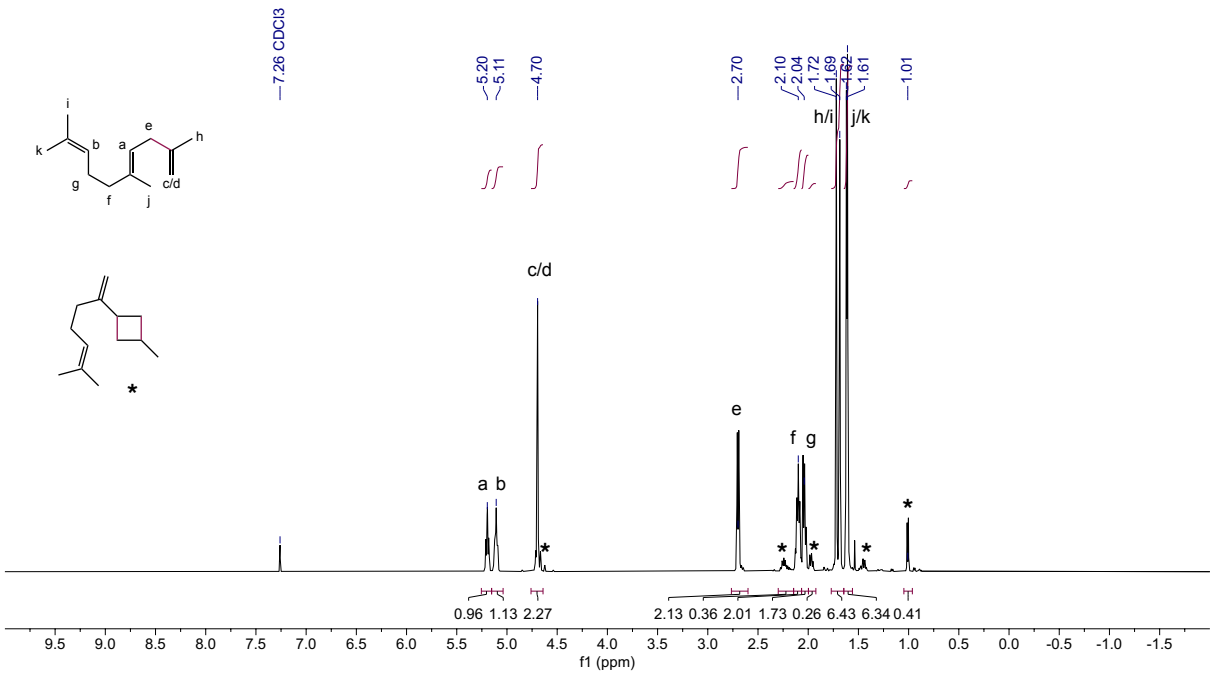

Figure S52. ^{1}H NMR (500 MHz, $CDCl_3$) spectrum of **14aj** and **16aj**.

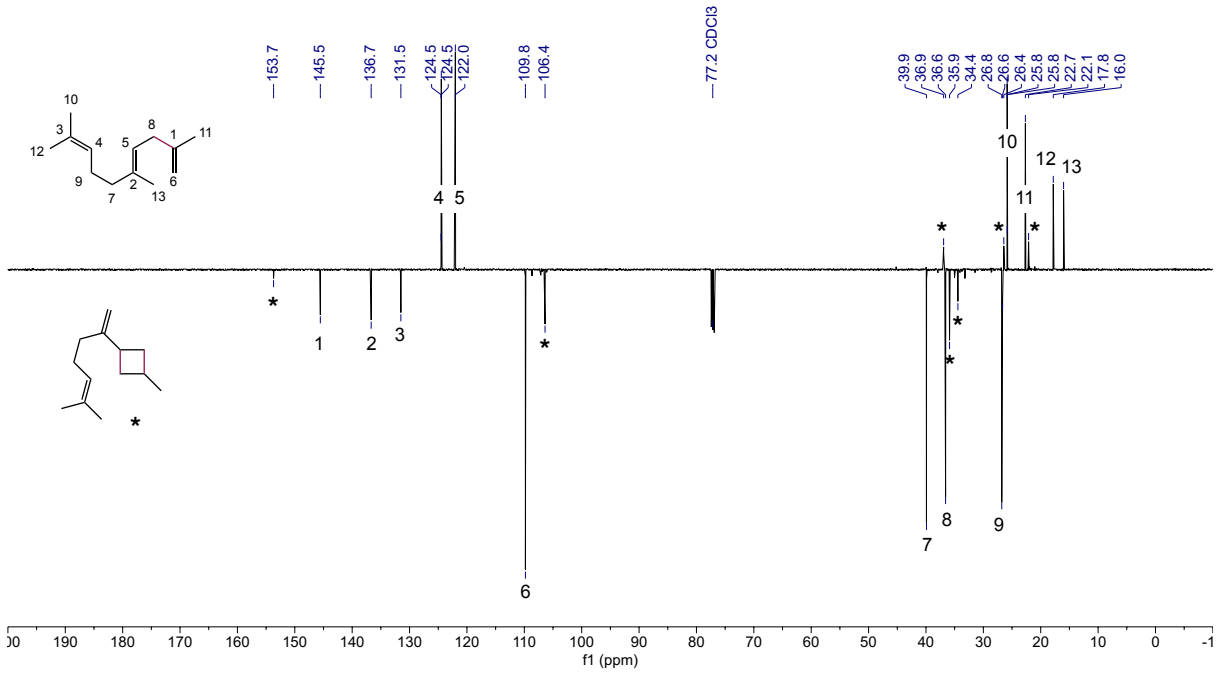

Figure S53. ^{13}C NMR (126 MHz, $CDCl_3$) spectrum of **14aj** and **16aj**.

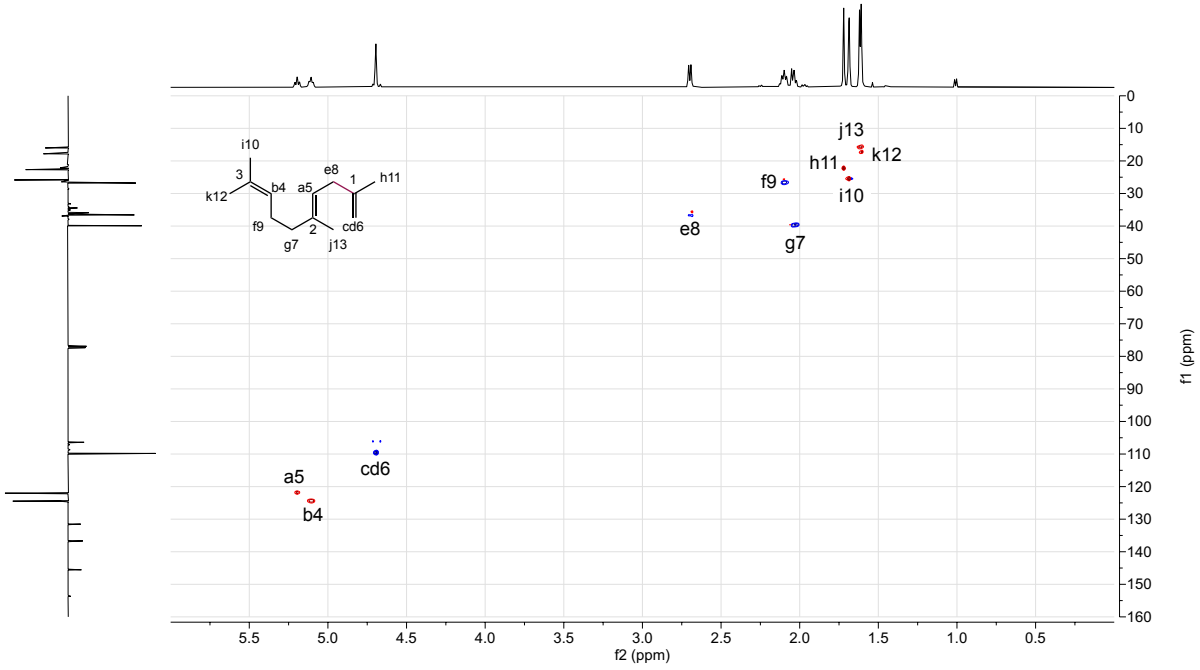

Figure S54. ^{1}H–^{13}C HSQC (500 MHz, $CDCl_3$) spectrum of **14aj** and **16aj**.

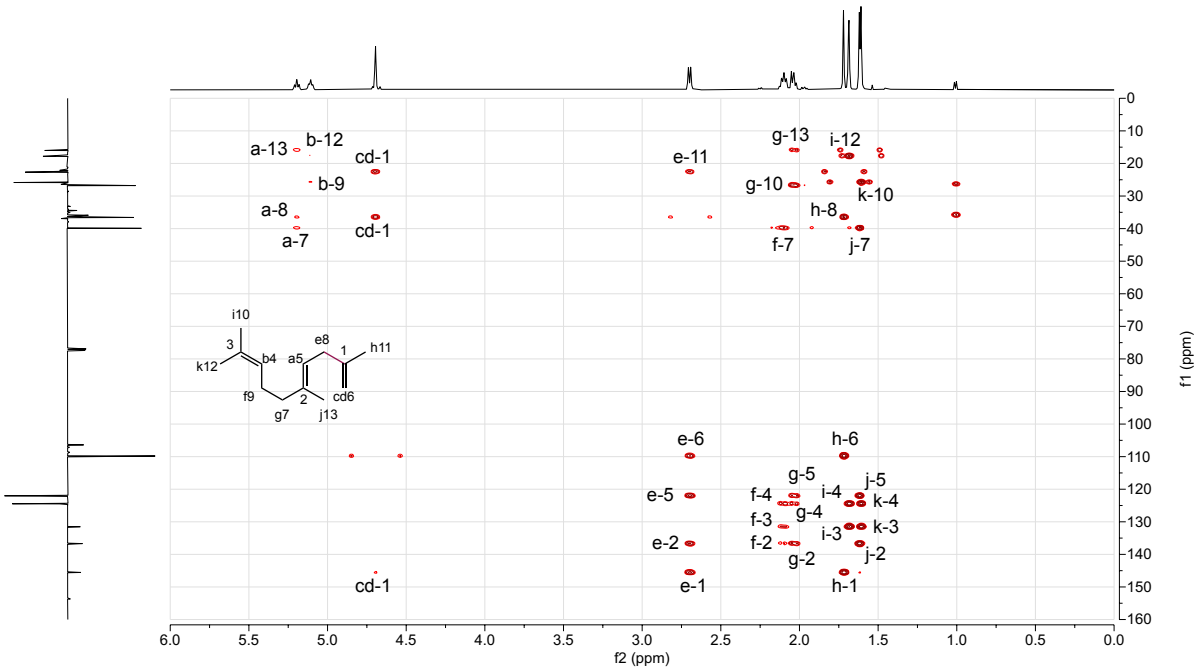

Figure S55. $^{1}H–^{13}C$ HMBC (500 MHz, $CDCl_3$) spectrum of **14aj** and **16aj**.

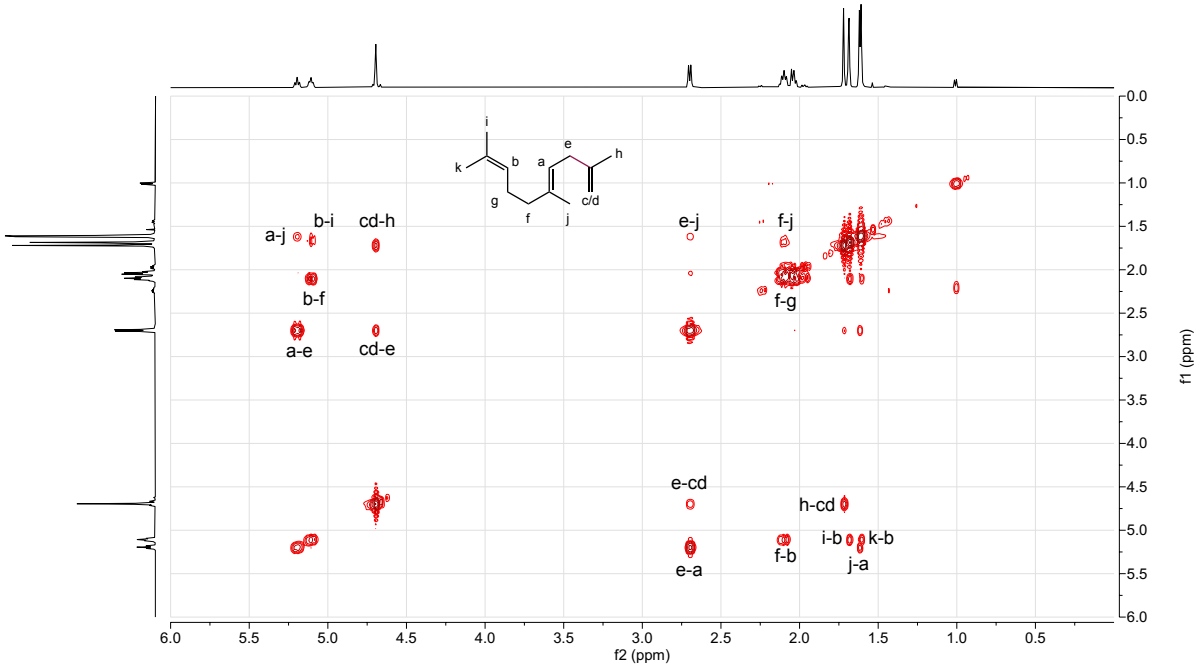

Figure S56. $^{1}H–^{1}H$ COSY (500 MHz, $CDCl_3$) spectrum of **14aj** and **16aj**.

A mixture of **trimethyl((3-(6-methylhepta-1,5-dien-2-yl)cyclobutyl)methyl)silane (14bj)** and **(*E*)- (*E*)- (5,9-dimethyl-2-methylenedeca-4,8-dien-1-yl)trimethylsilane (16bj)** was obtained in 45% combined yield (58:38 **14bj** : **16bj**) after 24 hours as described in 3.2.

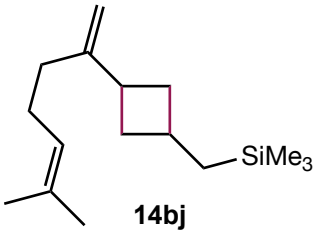

14bj

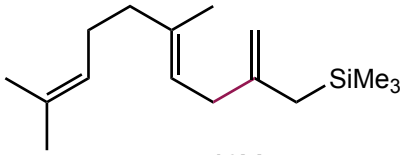

16bj

^{1}H NMR (500 MHz,$CDCl_3$) δ 5.19 (tq, *J* = 7.3, 1.3 Hz, 1H, **16bj**), 5.11 (t, *J* = 6.9 Hz, 1H, **14bj** & 1H, **16bj**), 4.70 (t, *J* = 1.6 Hz, 1H, **14bj**), 4.65 (s, 1H, **14bj**), 4.61 (q, *J* = 1.6 Hz, 1H, **16bj**), 4.51 (dt, *J* = 2.2, 1.1 Hz, 1H, **16bj**), 2.65 (d, *J* = 7.7 Hz, 2H, **16bj**), 2.69 – 2.59 (m, 1H, **14bj**), 2.29 (qd, *J* = 7.6, 2.6 Hz, 2H, **14bj**), 2.18 (tt, *J* = 16.6, 14.9, 9.2, 7.6 Hz, 1H, **16bj**), 2.13 – 2.02 (m, 2H, **14bj** & 2H, **16bj**), 1.96 (dd, *J* = 9.5, 6.3 Hz, 1H, 2H, **14bj** & 2H, **16bj**), 1.69 (s, 3H, **14bj** & 3H, **16bj**), 1.61 (s, 3H, **14bj** & 6H, **16bj**), 1.54 (d, *J* = 1.1 Hz, 2H, **16bj**), 1.45 (tdd, *J* = 10.2, 8.2, 2.6 Hz, 2H, **14bj**), 0.66 (d, *J* = 7.6 Hz, 2H, **14bj**), 0.04 (s, 9H, **16bj**), -0.03 (s, 9H, **16bj**).

^{13}C NMR (126 MHz, $CDCl_3$) δ 153.7 (**14bj**), 147.0 (**16bj**), 136.6 (**16bj**), 131.6 (**14bj**), 131.5 (**16bj**), 124.5 (**14bj** & **16bj**), 122.3 (**16bj**), 107.2 (**16bj**), 106.4 (**14bj**), 39.9 (**16bj**), 37.8 (**14bj**), 37.4 (**14bj**), 37.1 (**16bj**), 34.5 (**14bj**), 28.2 (**14bj**), 27.0 (**16bj**), 26.8 (**16bj**), 26.6 (**14bj**), 25.9 (**16bj**), 25.9 (**14bj**), 25.7 (**14bj**), 17.84 (**14bj** & **16bj**), 16.1 (**16bj**), –0.9 (**14bj**), –1.13 (**16bj**)

GC-MS (EI): for $[M]^+$ = C16H30Si, calculated *m/z* = 250.21168, found *m/z* = 250.2116

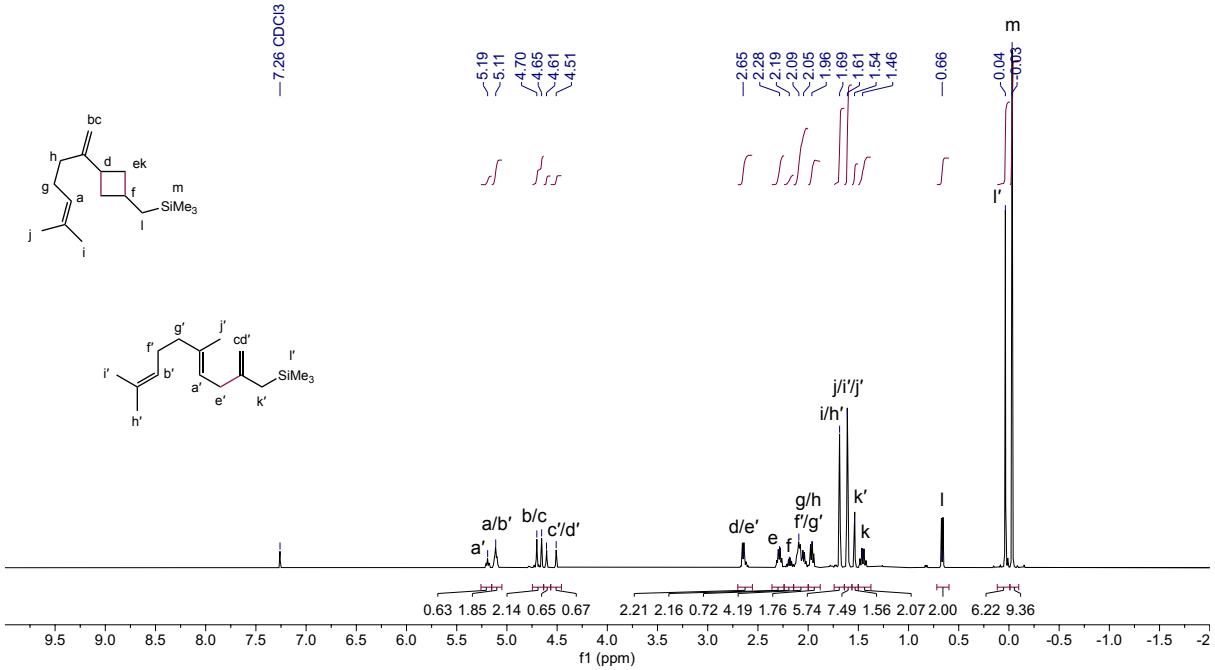

Figure S57. ^{1}H NMR (500 MHz, $CDCl_3$) spectrum of **14bj** and **16bj**.

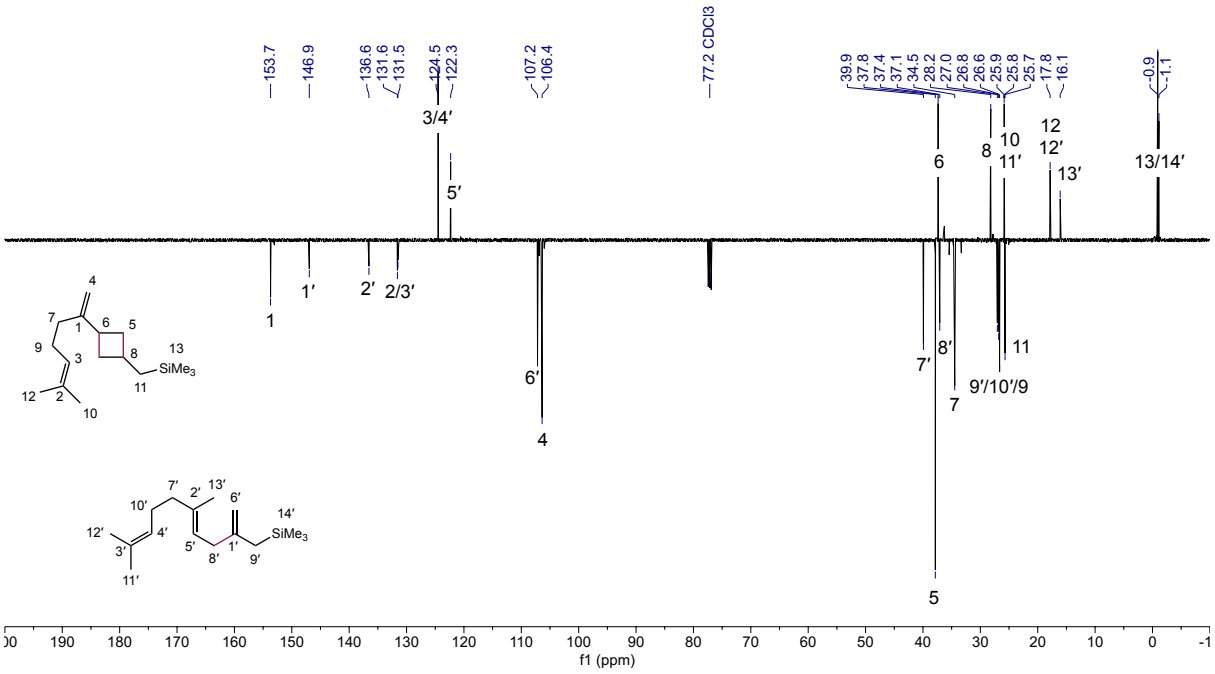

Figure S58. ^{13}C NMR (126 MHz, $CDCl_3$) spectrum of **14bj** and **16bj**.

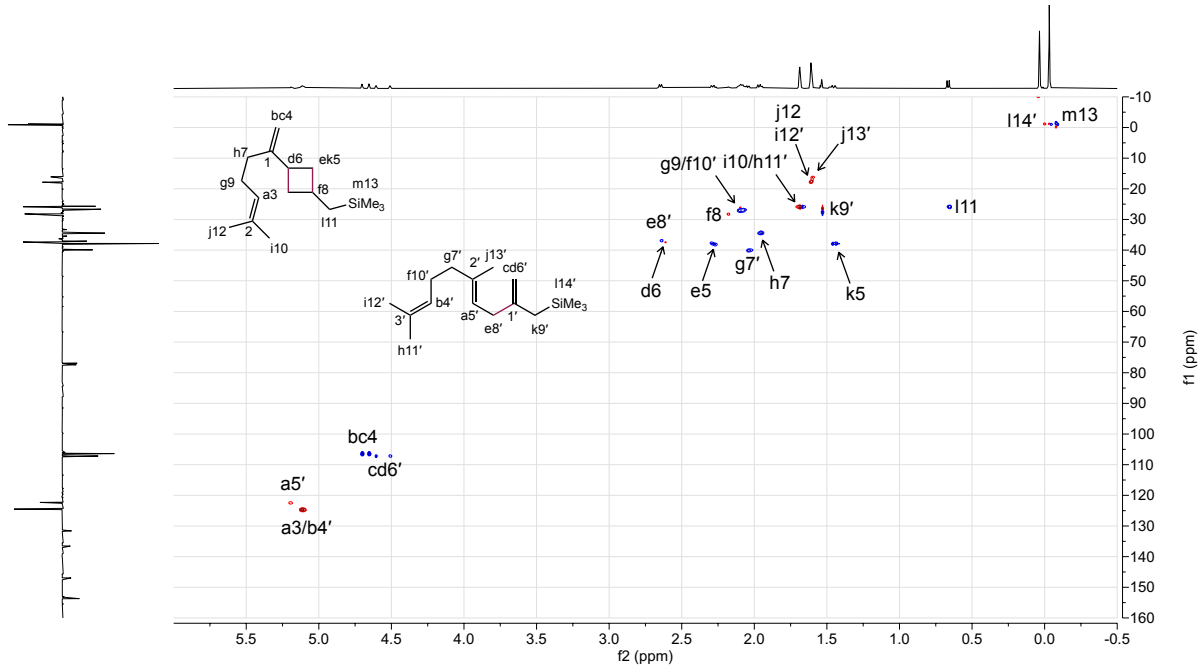

Figure S59. ^{1}H–^{13}C HSQC (500 MHz, $CDCl_3$) spectrum of **14bj** and **16bj**.

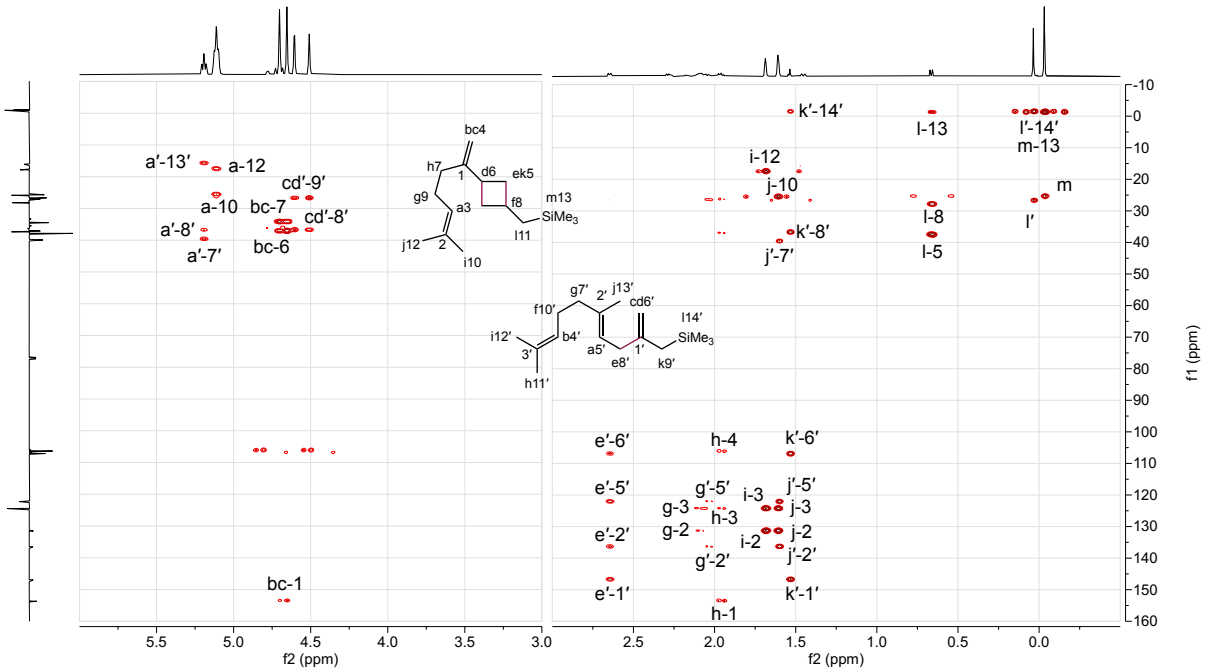

Figure S60. $^{1}H–^{13}C$ HMBC (500 MHz, $CDCl_3$) spectrum of **14bj** and **16bj**.

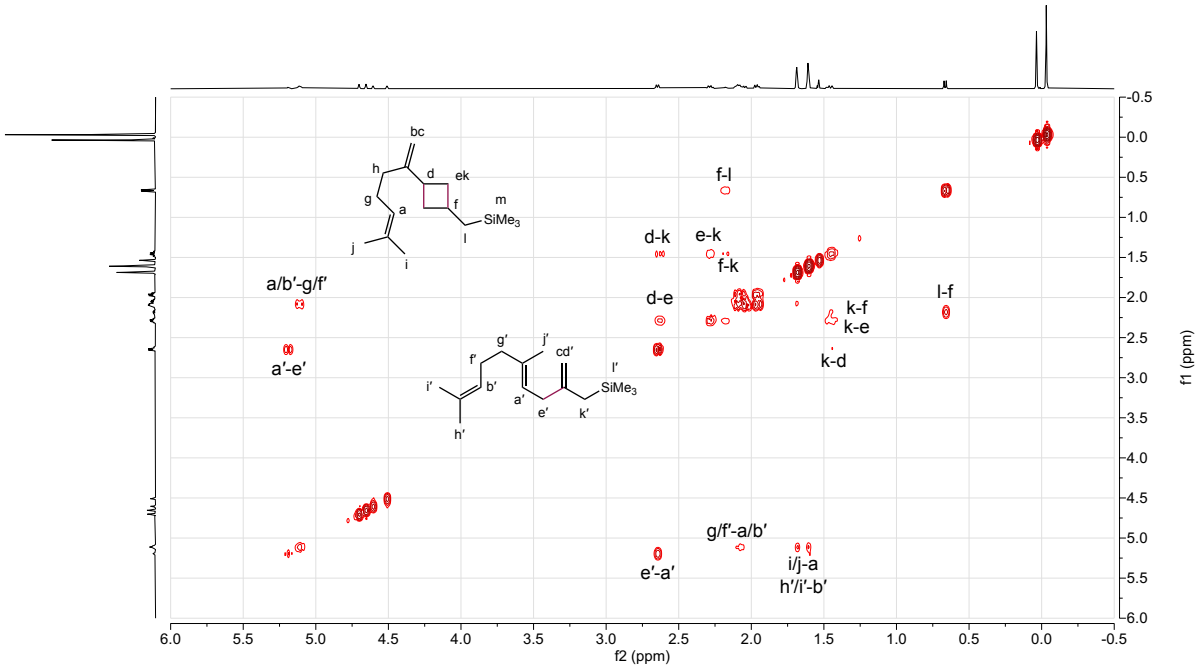

Figure S61. $^{1}H–^{1}H$ COSY (500 MHz, $CDCl_3$) spectrum of **14bj** and **16bj**.

(*E*)-trimethyl(3-(prop-1-en-1-yl)cyclobutyl)silane (17aa) was prepared in 87% isolated yield, 95% [2+2]-selectivity, 56:44 d.r. after 48 hours as described in 3.2.

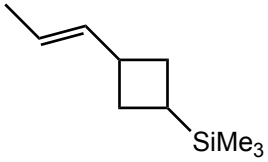

17aa

^{1}H NMR (500 MHz, $CDCl_3$) δ 5.60§ (ddd, *J* = 15.2, 7.1, 1.7 Hz, 1H), 5.47* (ddd, *J* = 15.1, 7.0, 1.6 Hz, 1H), 5.41 – 5.29 (m, 1H), 3.01* (dq, *J* = 16.8, 8.1 Hz, 1H), 2.81§ (h, *J* = 7.9 Hz, 1H), 2.12 – 2.03* (m, 1H), 2.01§ (t, *J* = 8.1 Hz, 2H), 1.72 – 1.66* (m, 1H), 1.65§ (d, *J* = 6.8 Hz, 3H), 1.63* (d, *J* = 6.3 Hz, 3H), 1.61 – 1.49* (m, 2H), 1.53 – 1.46§ (m, 1H), -0.01 (s, 9H), -0.07 (s, 9H) where resolved resonances arising from the *cis*(*) and *trans*(§) diastereomers are indicated.

^{13}C NMR (126 MHz, $CDCl_3$) δ 136.7*, 136.4§, 122.9§, 122.6*, 39.3§, 37.3*, 30.0§, 29.0*, 19.2*, 18.0* or §, 17.9* or §, 17.1§, -3.3* or §, -3.3* or § where resolved resonances arising from the *cis*(*) and *trans*(§) diastereomers are indicated.

GC-MS (EI): for $[M]^+$ = $C_{10}H_{20}Si$, calculated *m/z* = 168.13, found *m/z* = 168

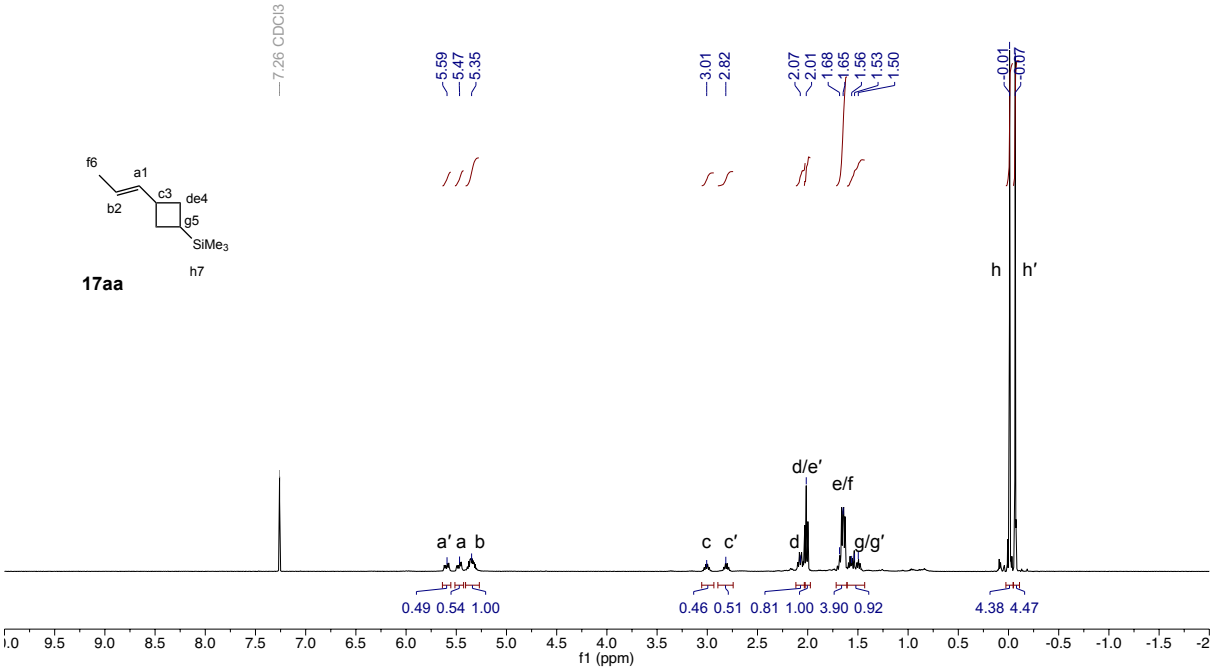

Figure S62. ^{1}H NMR (500 MHz, $CDCl_3$) spectrum of **17aa**.

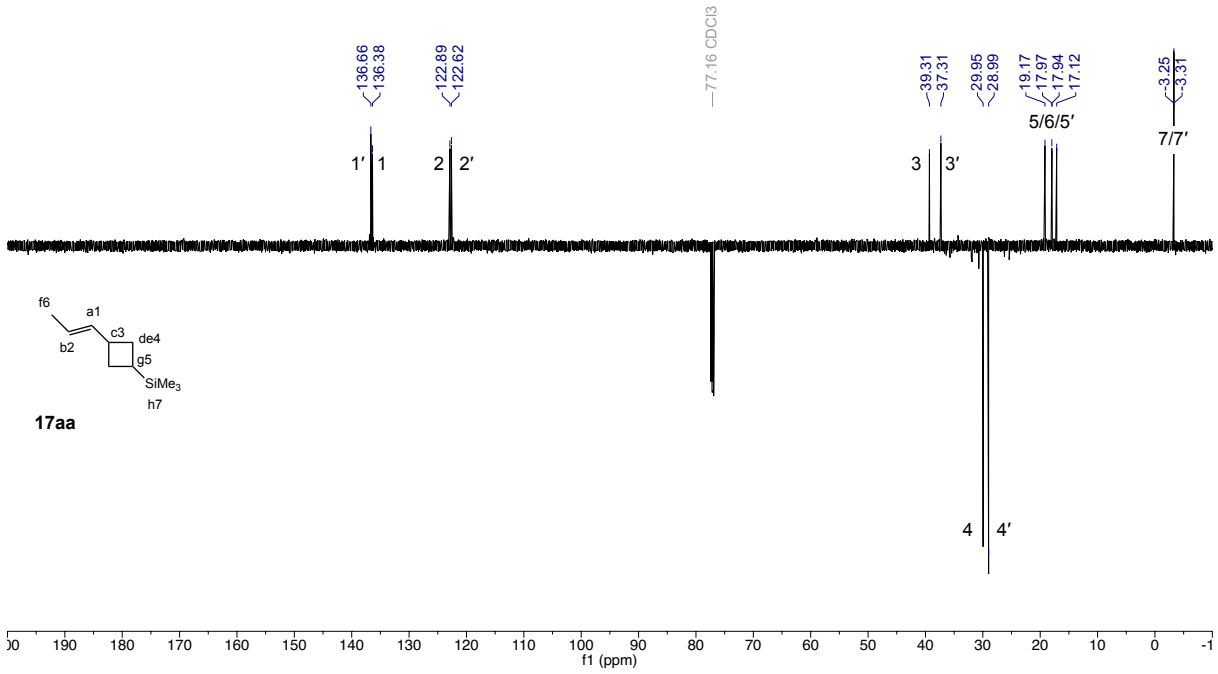

Figure S63. ^{13}C NMR (126 MHz, $CDCl_3$) spectrum of **17aa**.

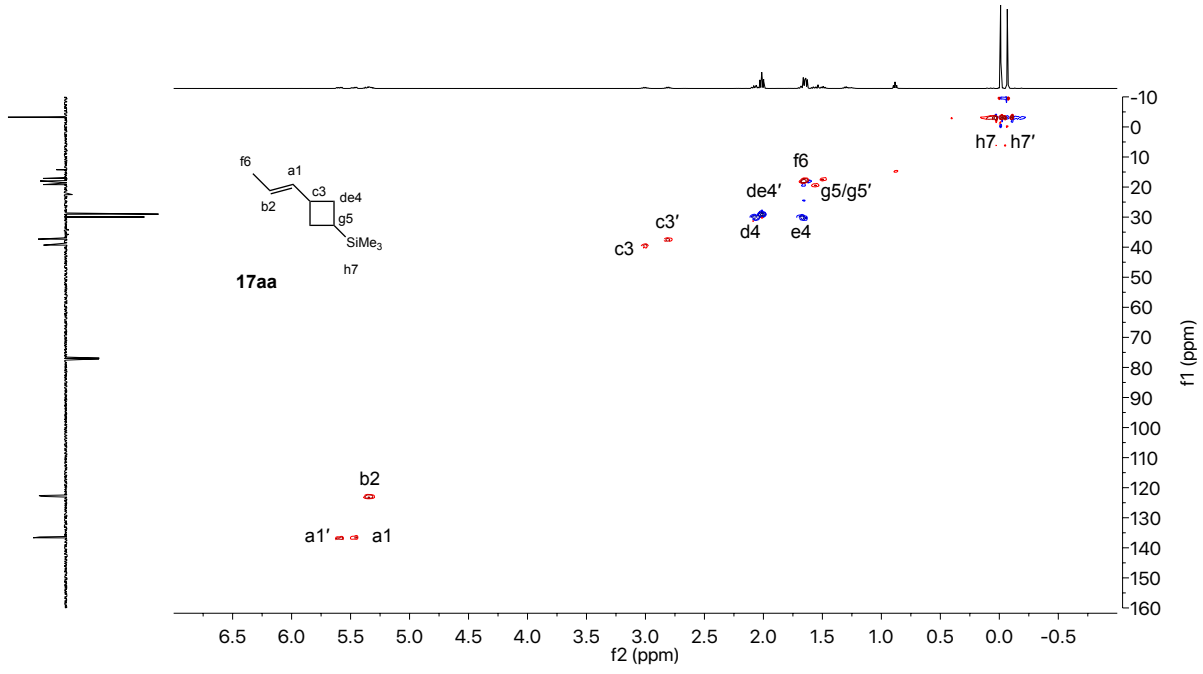

Figure S64. ^{1}H–^{13}C HSQC (500 MHz, $CDCl_3$) spectrum of **17aa**.

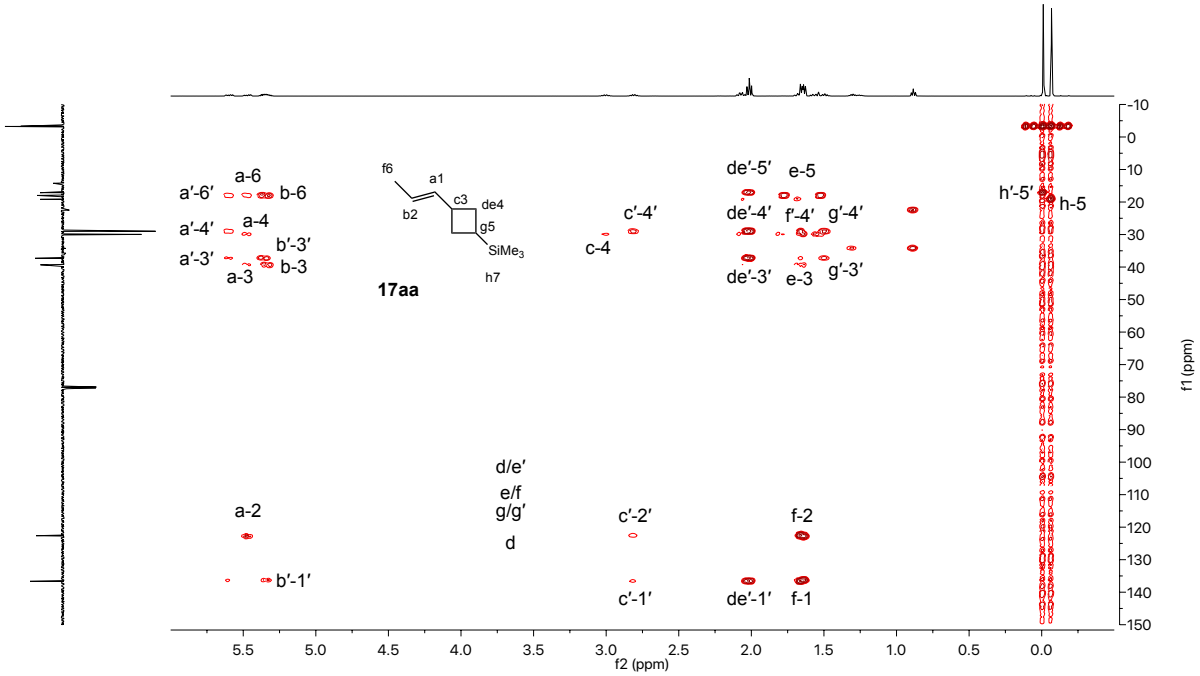

Figure S65. $^{1}H–^{13}C$ HMBC (500 MHz, $CDCl_3$) spectrum of **17aa**.

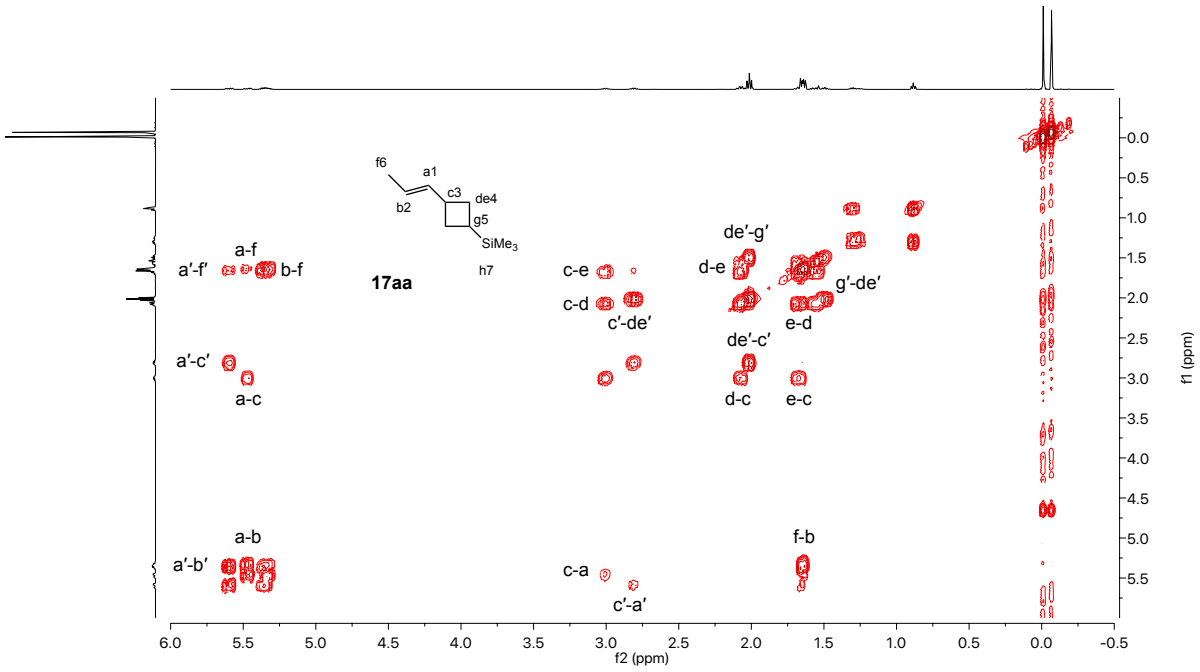

Figure S66. $^{1}H–^{1}H$ COSY (500 MHz, $CDCl_3$) spectrum of **17aa**.

(*E*)-dimethyl(phenyl)(3-(prop-1-en-1-yl)cyclobutyl)silane (17ba) was prepared in 87% isolated yield, 98% [2+2]-selectivity, 50:50 d.r. after 72 hours as described in 3.2.

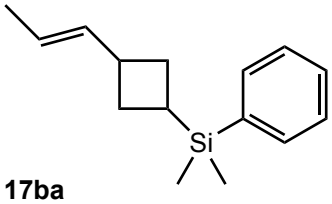

17ba

^{1}H NMR (500 MHz, $CDCl_3$) δ 7.50 (ddd, *J* = 16.1, 6.5, 2.9 Hz, 2H), 7.42 – 7.29 (m, 3H), 5.60[§] (dd, *J* = 15.1, 5.7 Hz, 1H), 5.45* (dd, *J* = 15.1, 5.3 Hz, 1H), 5.40 – 5.21 (m, 1H), 3.06* (h, *J* = 7.6 Hz, 1H), 2.75[§] (h, *J* = 7.1 Hz, 1H), 2.19 – 2.00 (m, 3H), 1.96 – 1.71 (m, 2H), 1.66[§] (d, *J* = 6.5 Hz, 3H), 1.63* (d, *J* = 6.2 Hz, 3H), 0.30 (s, 6H)[§], 0.24 (s, 6H)* where resolved resonances arising from the *cis*(*) and *trans*([§]) diastereomers are indicated.

^{13}C NMR (126 MHz, $CDCl_3$) δ 139.20*, 139.05[§], 136.36[§], 136.12*, 133.88, 133.84, 128.98, 128.91, 127.83, 127.80, 123.06*, 122.74[§], 39.61*, 37.18[§], 30.27*, 29.06[§], 18.39*, 17.96, 17.94, 16.51[§], -4.66[§], -4.75* where resolved resonances arising from the *cis*(*) and *trans*([§]) diastereomers are indicated.

GC-MS (EI): for $[M]^+$ = $C_{15}H_{22}Si$, calculated *m/z* = 230.14908, found *m/z* = 230.14889

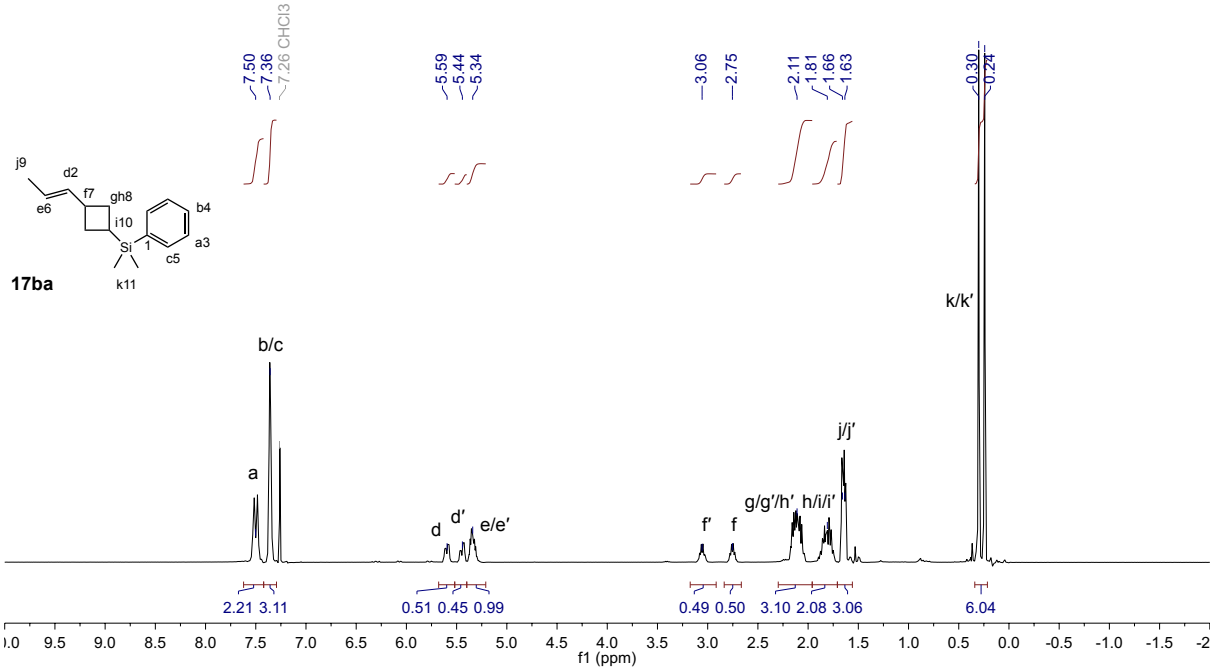

Figure S67. ^{1}H NMR (500 MHz, $CDCl_3$) spectrum of **17ba**.

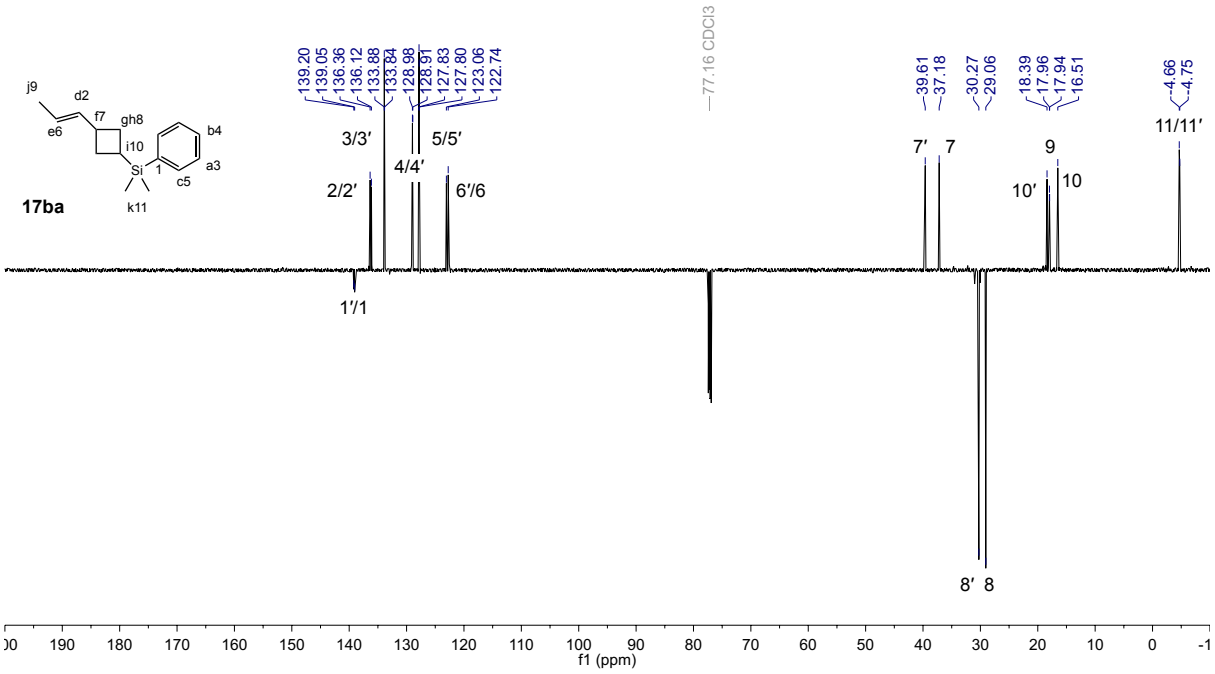

Figure S68. ^{13}C NMR (126 MHz, $CDCl_3$) spectrum of **17ba**.

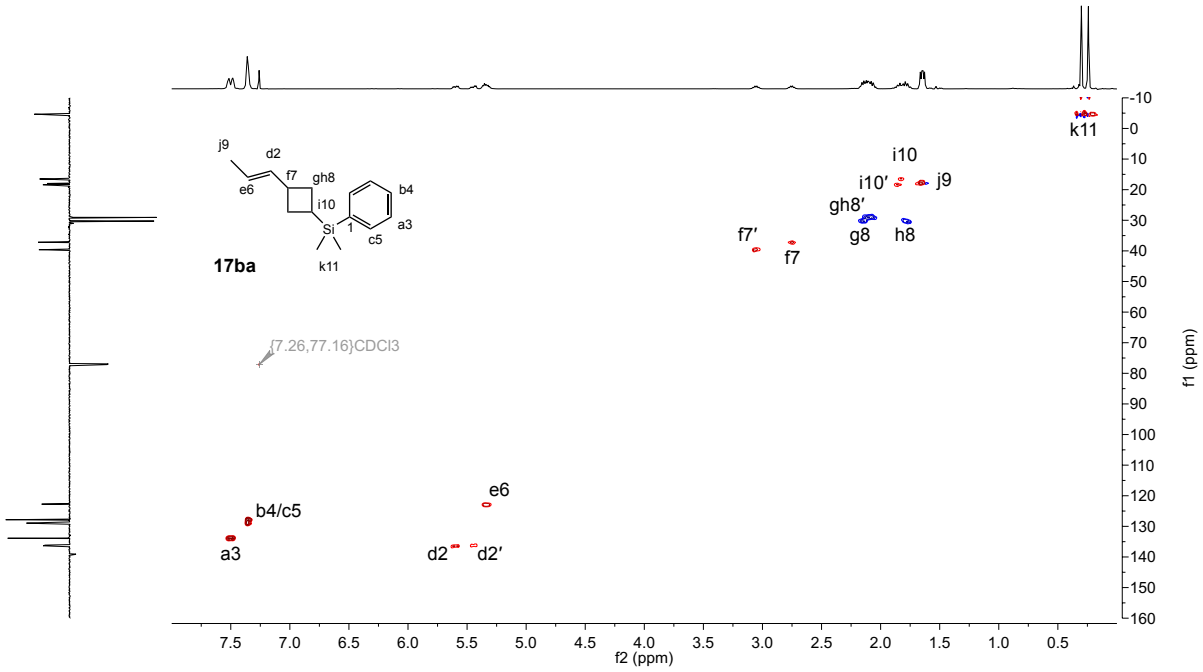

Figure S69. ^{1}H–^{13}C HSQC (500 MHz, $CDCl_3$) spectrum of **17ba**.

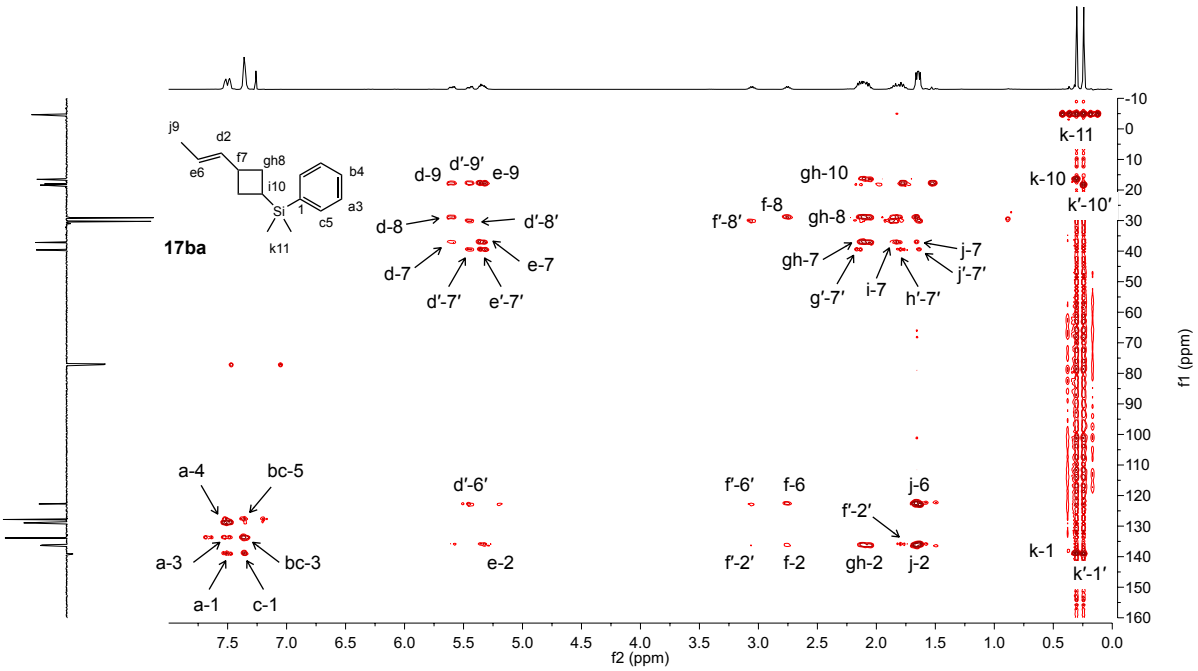

Figure S70. ^{1}H–^{13}C HMBC (500 MHz, $CDCl_3$) spectrum of **17ba**.

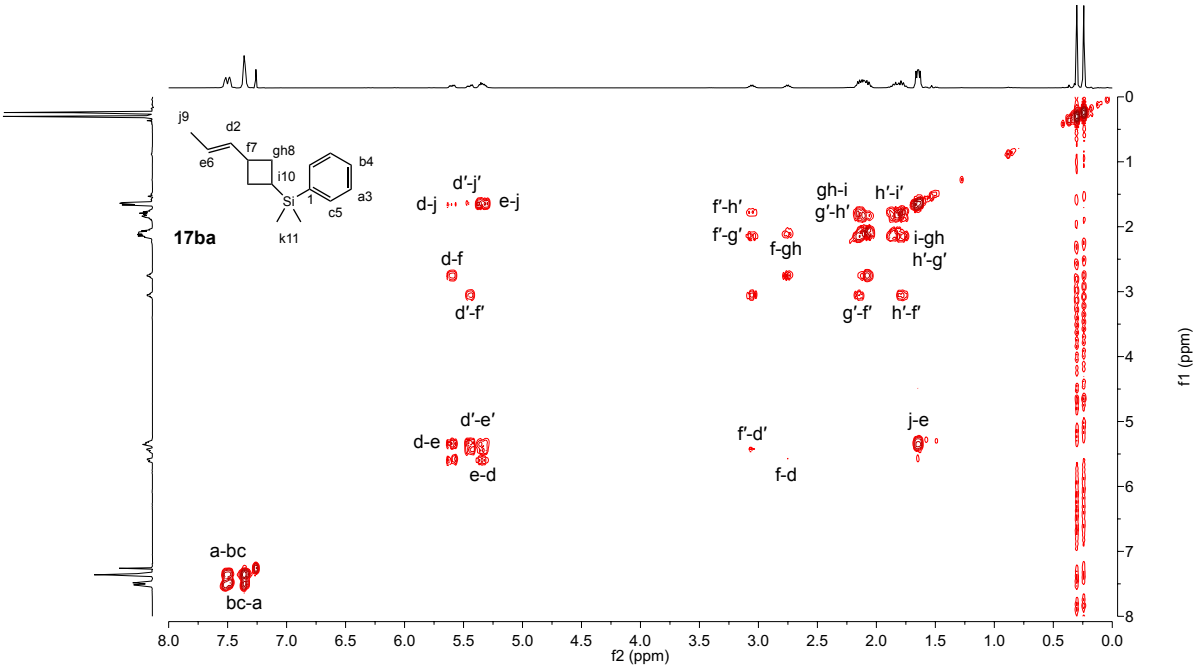

Figure S71. ^{1}H–^{1}H COSY (500 MHz, $CDCl_3$) spectrum of **17ba**.

(*E*)-triphenyl(3-(prop-1-en-1-yl)cyclobutyl)silane (17ca) was prepared in 87% isolated yield, 97% [2+2]-selectivity, 13:87 d.r. after 7 days as described in 3.2.

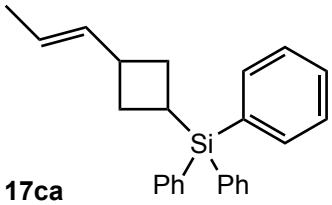

17ca

^{1}H NMR (500 MHz, $CDCl_3$) δ 7.59 – 7.52 (m, 6H), 7.47 – 7.39 (m, 3H), 7.39 – 7.32 (m, 6H), 5.60 (ddd, *J* = 15.1, 6.9, 1.7 Hz, 1H), 5.27 (dqd, *J* = 15.2, 6.3, 1.1 Hz, 1H), 2.67 (tt, *J* = 10.5, 6.2 Hz, 1H), 2.47 (h, *J* = 7.6 Hz, 1H), 2.40 – 2.20 (m, 2H), 1.64 (d, *J* = 6.5 Hz, 3H).

^{13}C NMR (126 MHz, $CDCl_3$) δ 137.0, 136.1, 136.0, 136.0, 135.1, 129.7, 128.0, 127.9, 122.8, 40.5, 36.7, 30.9, 29.2, 17.9, 16.4, 14.4.

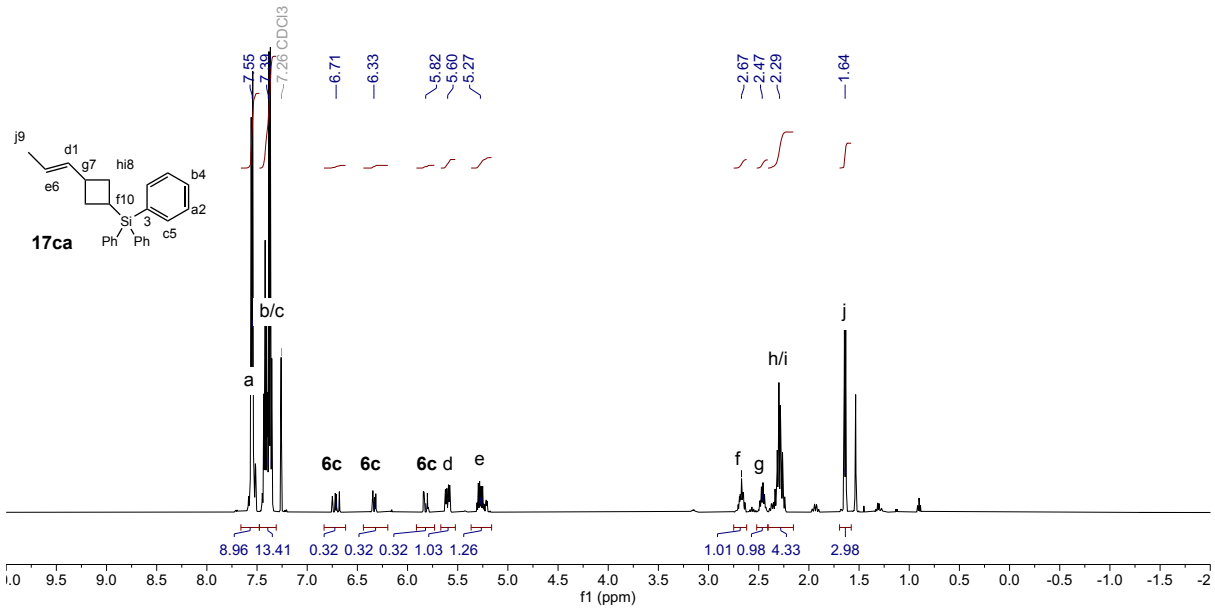

Figure S72. ^{1}H NMR (500 MHz, $CDCl_3$) spectrum of **17ca**.

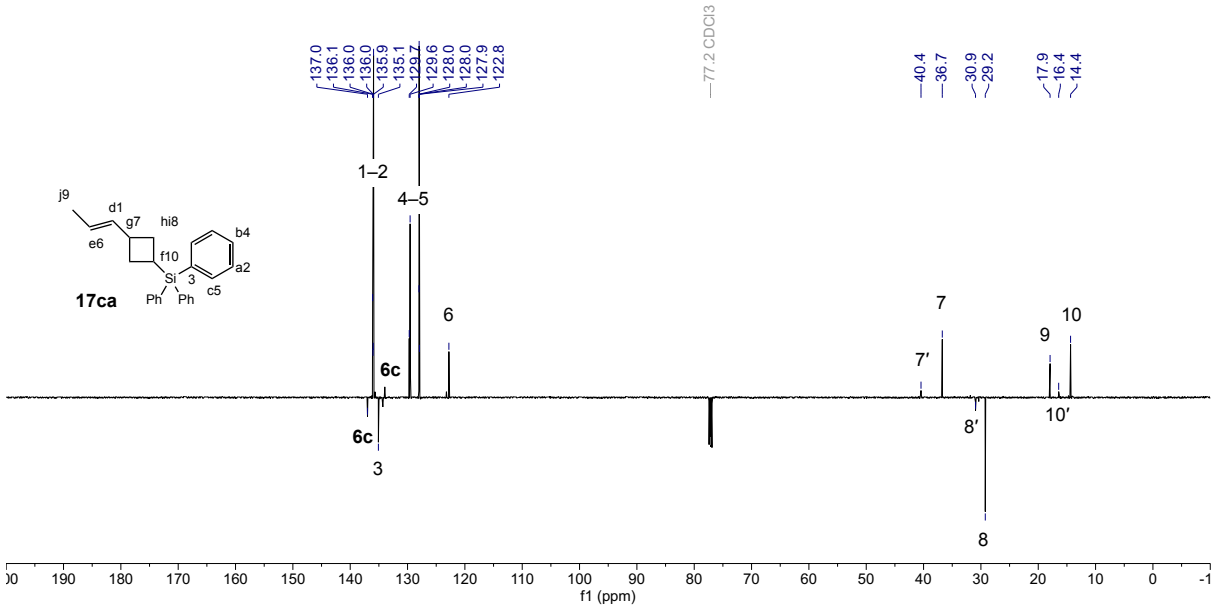

Figure S73. ^{13}C NMR (126 MHz, $CDCl_3$) spectrum of **17ca**

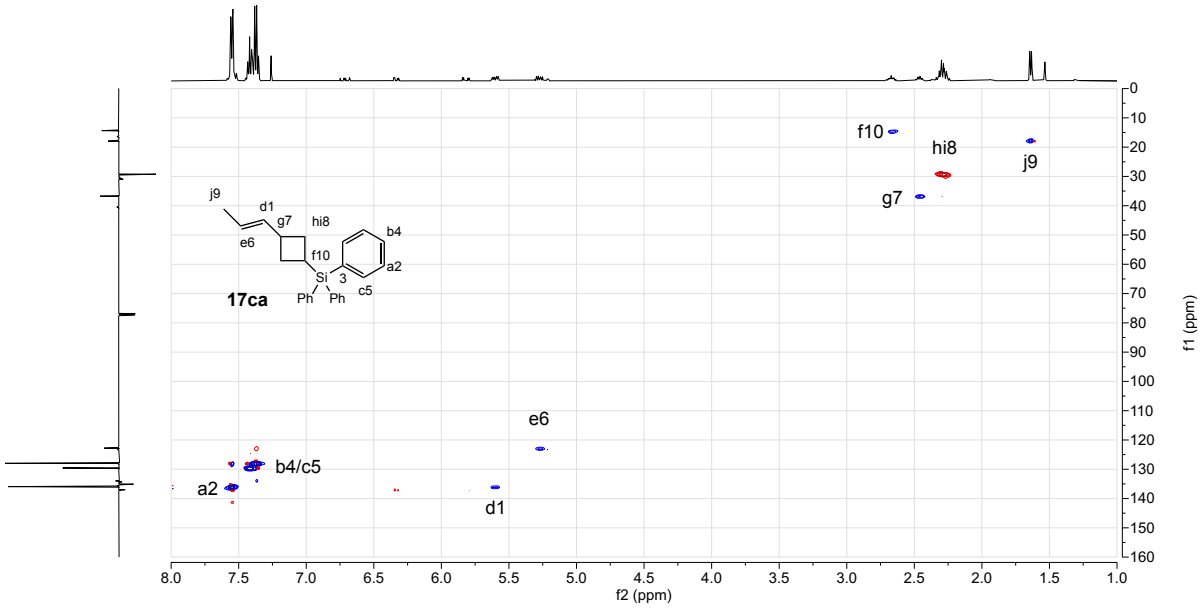

Figure S74. $^{1}H–^{13}C$ HSQC (500 MHz, $CDCl_3$) spectrum of **17ca**.

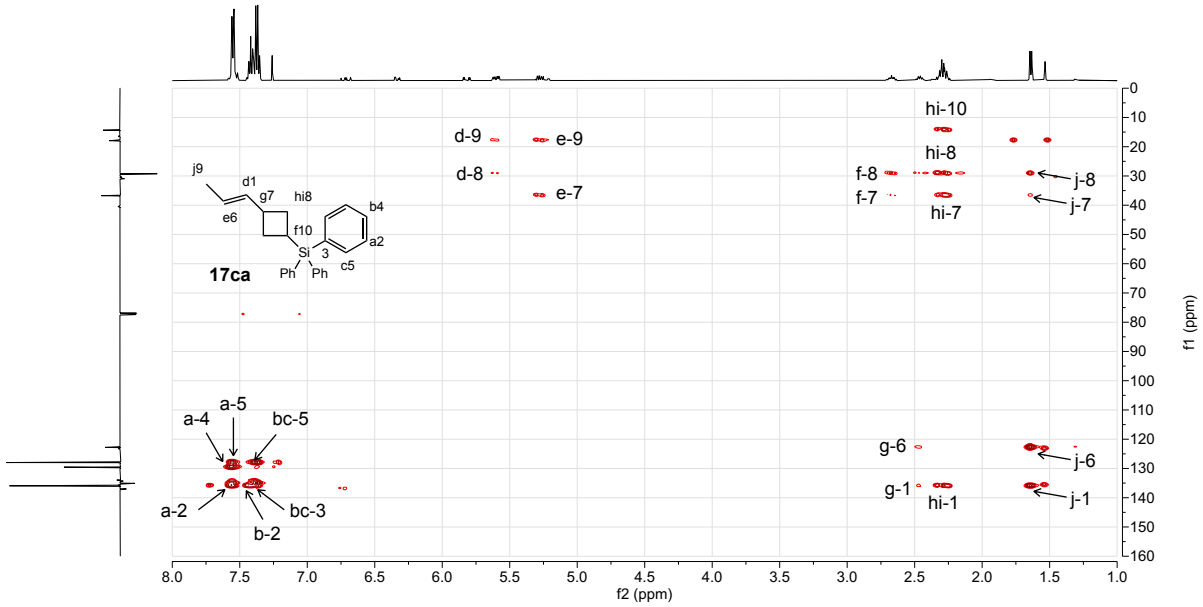

Figure S75. $^{1}H–^{13}C$ HMBC (500 MHz, $CDCl_3$) spectrum of **17ca**.

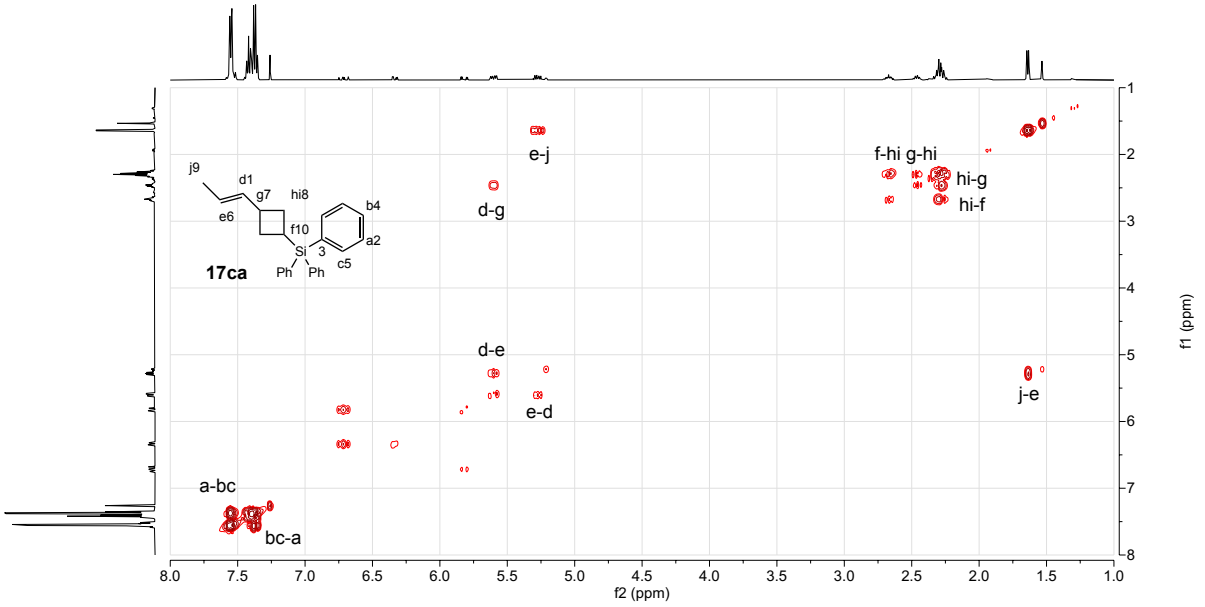

Figure S76. $^{1}H–^{1}H$ COSY (500 MHz, $CDCl_3$) spectrum of **17ca**.

(*E*)-diethoxy(methyl)(3-(prop-1-en-1-yl)cyclobutyl)silane (17da) was prepared in 91% isolated yield, 96% [2+2]-selectivity, 33:67 d.r. after 72 hours as described in 3.2.

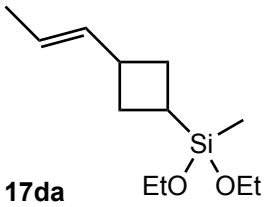

17da

^{1}H NMR (500 MHz, $CDCl_3$) δ 5.59§ (dd, *J* = 15.2, 6.1 Hz, 1H), 5.48* (dd, *J* = 14.9, 6.5 Hz, 1H), 5.41 – 5.28 (m, 1H), 3.76§ (q, *J* = 7.1 Hz, 4H), 3.74* (q, *J* = 7.1 Hz, 4H), 3.03* (h, *J* = 8.3 Hz, 1H), 2.93§ (h, *J* = 7.6 Hz, 1H), 2.23 – 2.15§ (m, 1H), 2.12* (qd, *J* = 10.9, 8.5, 2.8 Hz, 1H), 2.02§ (q, *J* = 10.6 Hz, 1H), 1.86* (qd, *J* = 11.8, 10.0, 9.8, 2.4 Hz, 1H), 1.76 – 1.65 (m, 1H), 1.65§ (d, *J* = 7.4 Hz, 3H), 1.63* (d, *J* = 6.3 Hz, 3H), 1.20 (t, *J* = 7.0 Hz, 6H), 0.16§ (s, 3H), 0.10* (s, 3H) where resolved resonances arising from the *cis* (*) and *trans* (§) diastereomers are indicated.

^{13}C NMR (126 MHz, $CDCl_3$) δ 136.23§, 136.11*, 123.19*, 122.86§, 58.39§, 58.34*, 39.94*, 37.52§, 29.78*, 28.52§, 18.60, 17.95§, 17.91*, 16.98*, 15.23§, -6.55§, -6.62* where resolved resonances arising from the major(*) and minor(§) diastereomers are indicated.

GC-MS (EI): for $[M + Na]^+$ = $C_{12}H_{24}O_2SiNa$, calculated *m/z* = 251.14434, found *m/z* = 250.9681; for $[M + H – OEt]^+$ = $C_{10}H_{20}OSi$, calculated *m/z* = 184.12835, found *m/z* = 184.12722

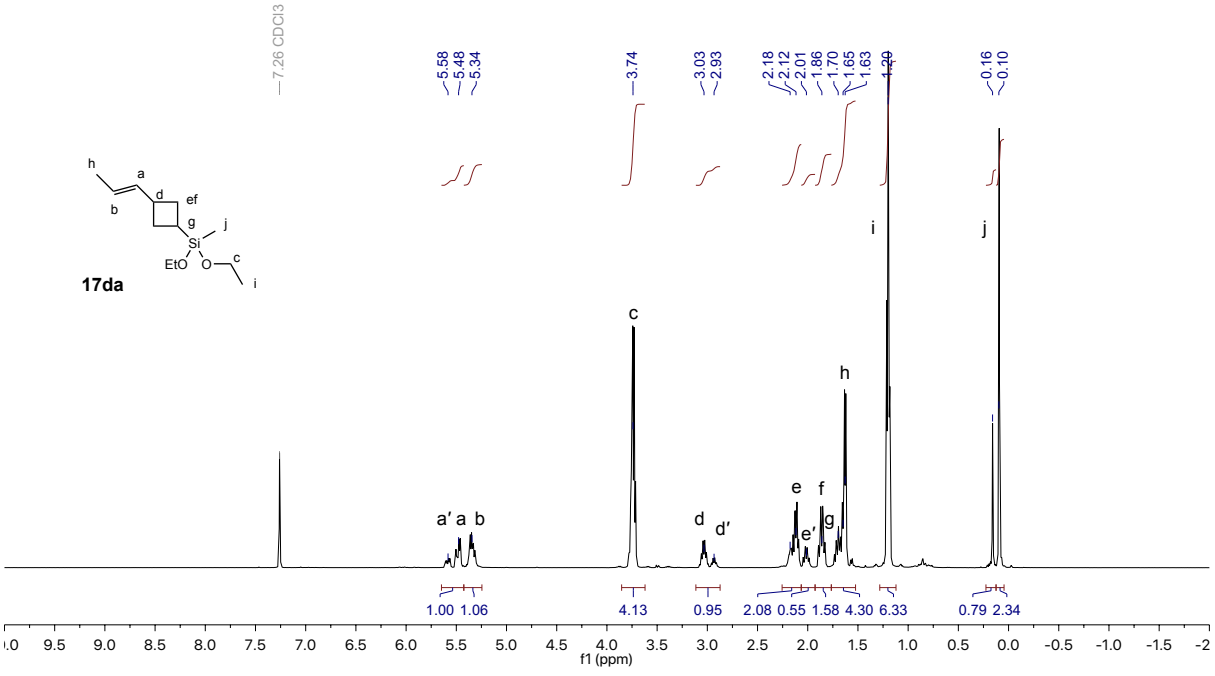

Figure S77. ^{1}H NMR (500 MHz, $CDCl_3$) spectrum of **17da**.

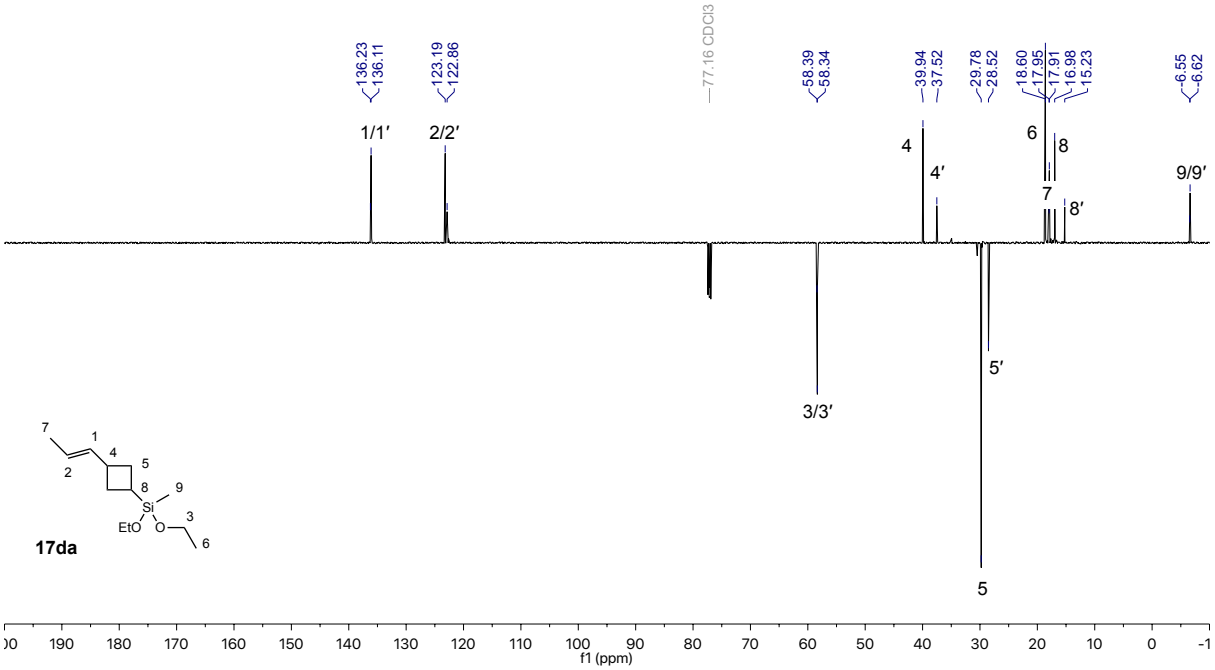

Figure S78. ^{13}C NMR (126 MHz, $CDCl_3$) spectrum of **17da**.

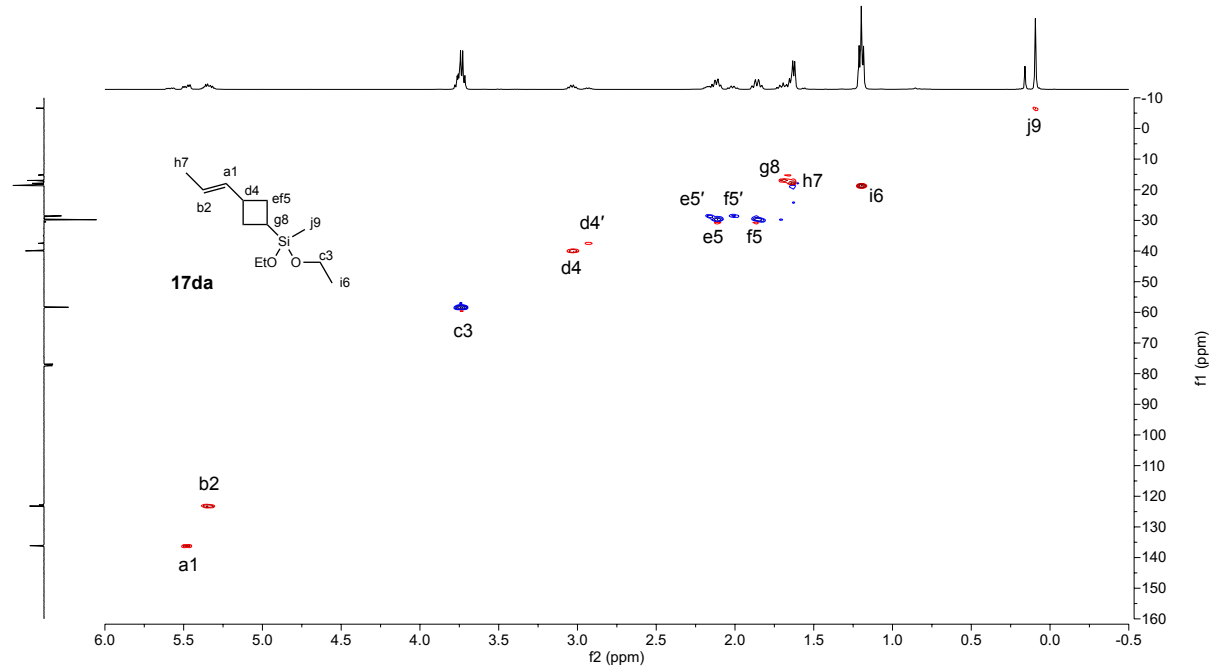

Figure S79. ^{1}H–^{13}C HSQC (500 MHz, $CDCl_3$) spectrum of **17da**.

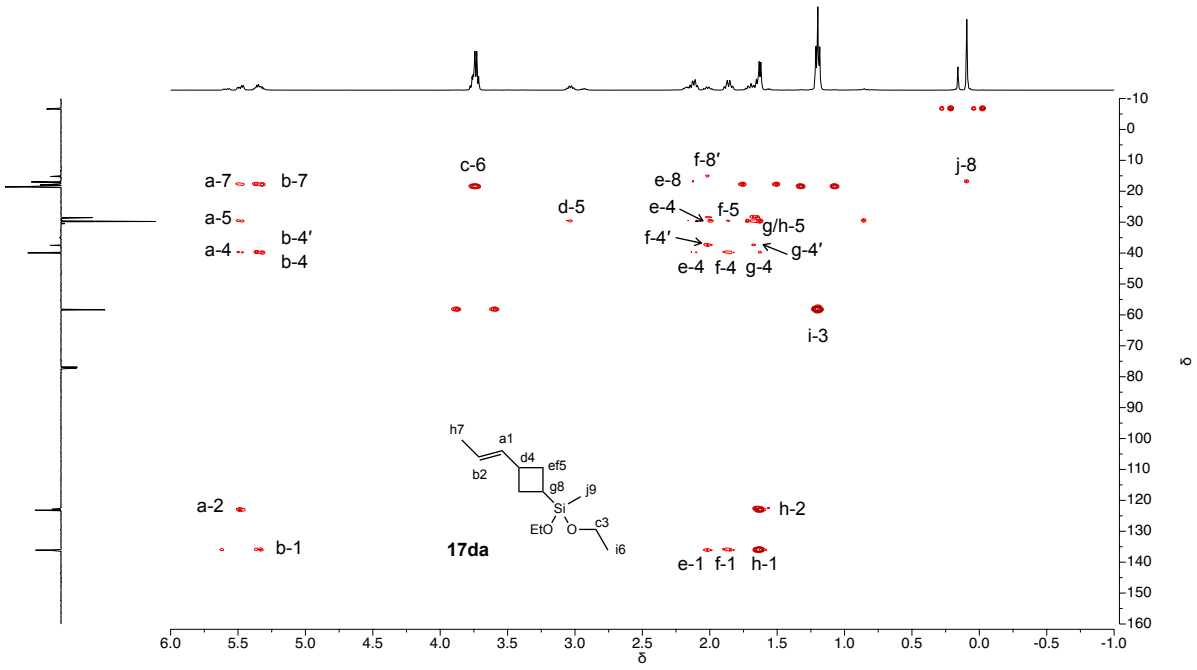

Figure S80. $^{1}H–^{13}C$ HMBC (500 MHz, $CDCl_3$) spectrum of **17da**.

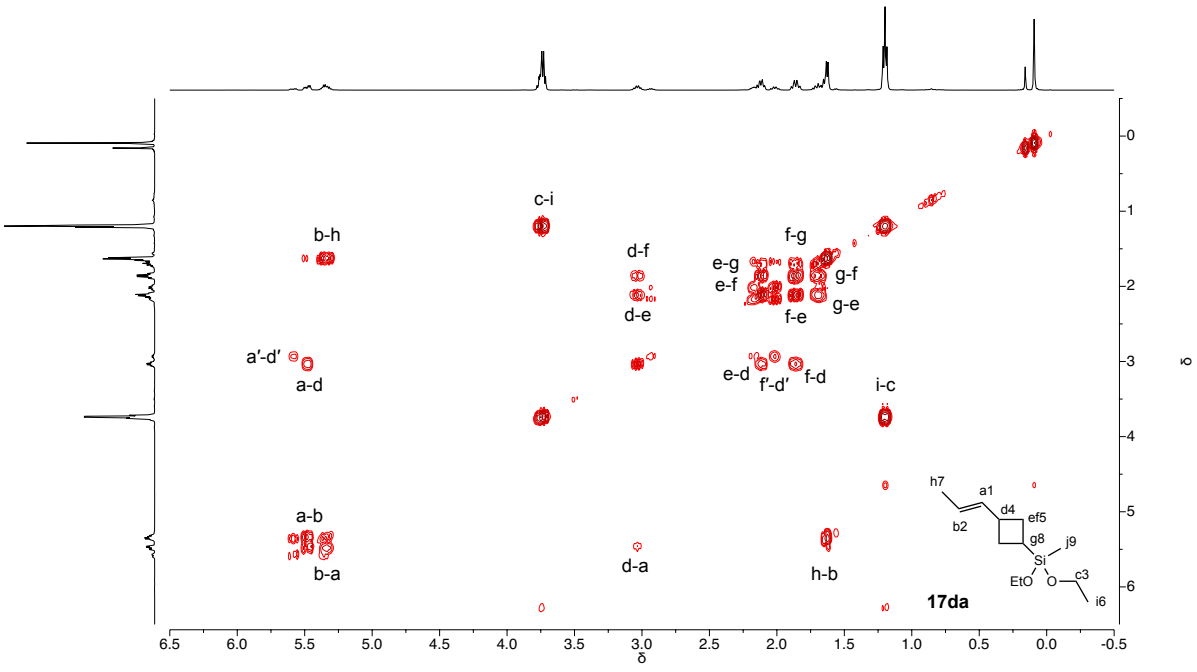

Figure S81. $^{1}H–^{1}H$ COSY (500 MHz, $CDCl_3$) spectrum of **17da**.

(*E*)-1,1,1,3,5,5,5-heptamethyl-3-(3-(prop-1-en-1-yl)cyclobutyl)trisiloxane (17ea) was prepared in 92% isolated yield, >98% [2+2]-selectivity, 33:67 d.r. after 72 hours as described in 3.2.

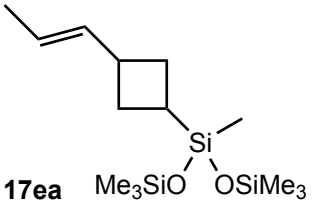

17ea

^{1}H NMR (500 MHz, $CDCl_3$) δ 5.59§ (ddd, *J* = 15.2, 7.1, 1.5 Hz, 1H), 5.48* (ddd, *J* = 15.2, 7.0, 1.3 Hz, 1H), 5.40 – 5.24 (m, 1H), 2.99* (h, *J* = 8.3, 7.5 Hz, 1H), 2.89§ (tq, *J* = 8.8, 7.5 Hz, 1H), 2.20 – 1.99 (m, 2H), 1.95§ (tdd, *J* = 10.4, 7.9, 1.5 Hz, 2H), 1.77* (qt, *J* = 11.3, 9.4, 2.4 Hz, 2H), 1.66§ (dq, *J* = 6.4, 1.5, 1.0 Hz, 3H), 1.63* (dq, *J* = 6.3, 1.0 Hz, 3H), 1.48* (tt, *J* = 10.9, 8.7 Hz, 1H), 1.41§ (tdd, *J* = 11.3, 5.5, 1.2 Hz, 0H), 0.09 (s, 18H), -0.03 (s, 3H) where resolved resonances arising from the *cis* (*) and *trans* (§) diastereomers are indicated.

^{13}C NMR (126 MHz, $CDCl_3$) δ 136.66§, 136.36*, 123.00*, 122.62§, 39.27*, 37.22§, 29.43*, 28.47§, 19.39, 17.94*, 17.60§, 2.04*, 1.99§, -2.12 where resolved resonances arising from the *cis* (*) and *trans* (§) diastereomers are indicated.

GC-MS (EI): for $[M - Me]^+$ = $C_{13}H_{29}O_2Si_3$, calculated *m/z* = 301.14756, found *m/z* = 301.14834

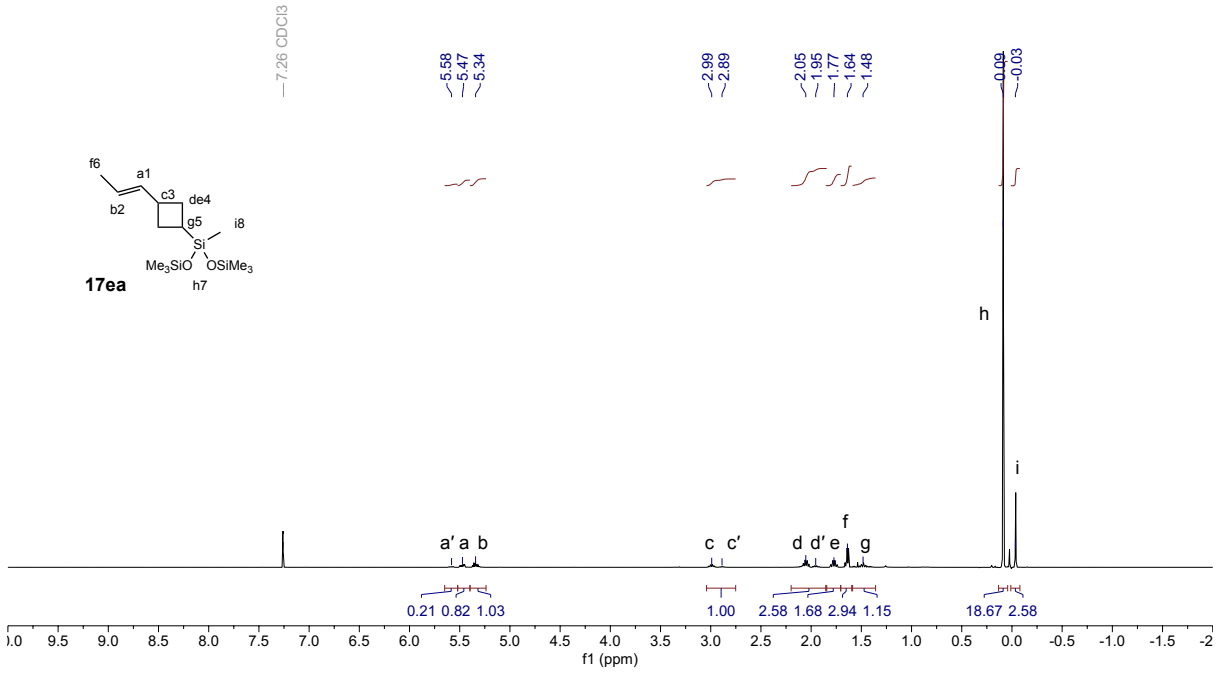

Figure S82. ^{1}H NMR (500 MHz, $CDCl_3$) spectrum of **17ea**.

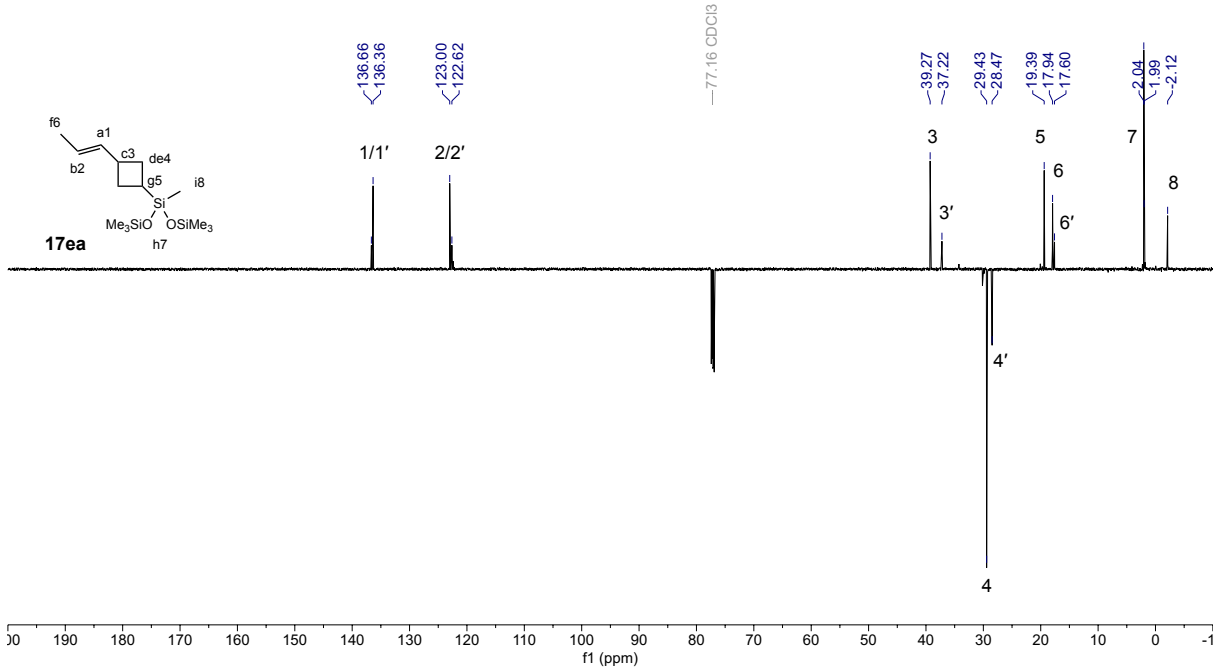

Figure S83. ^{13}C NMR (126 MHz, $CDCl_3$) spectrum of **17ea**.

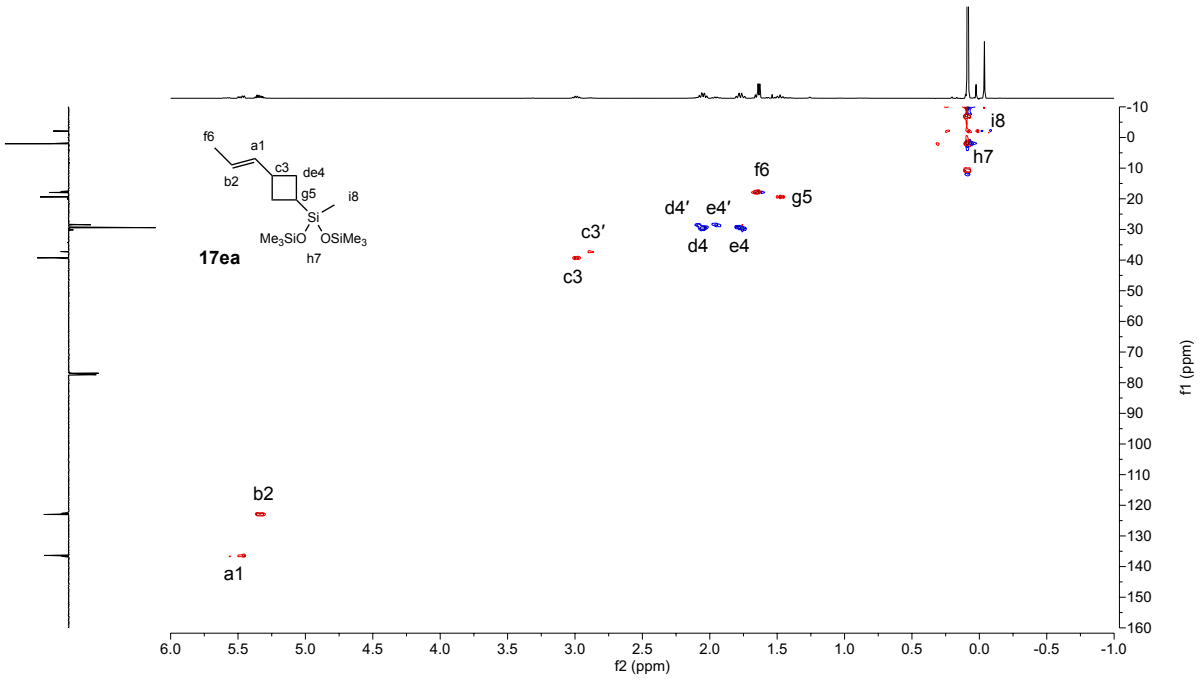

Figure S84. ^{1}H–^{13}C HSQC (500 MHz, $CDCl_3$) spectrum of **17ea**.

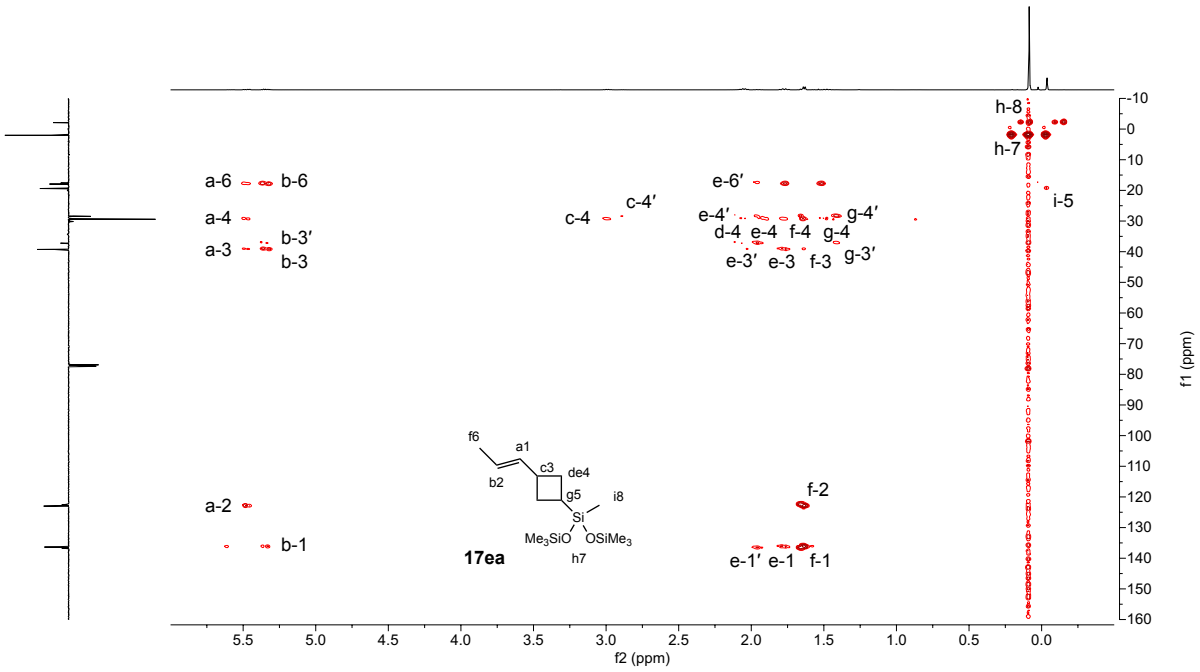

Figure S85. $^{1}H–^{13}C$ HMBC (500 MHz, $CDCl_3$) spectrum of **17ea**.

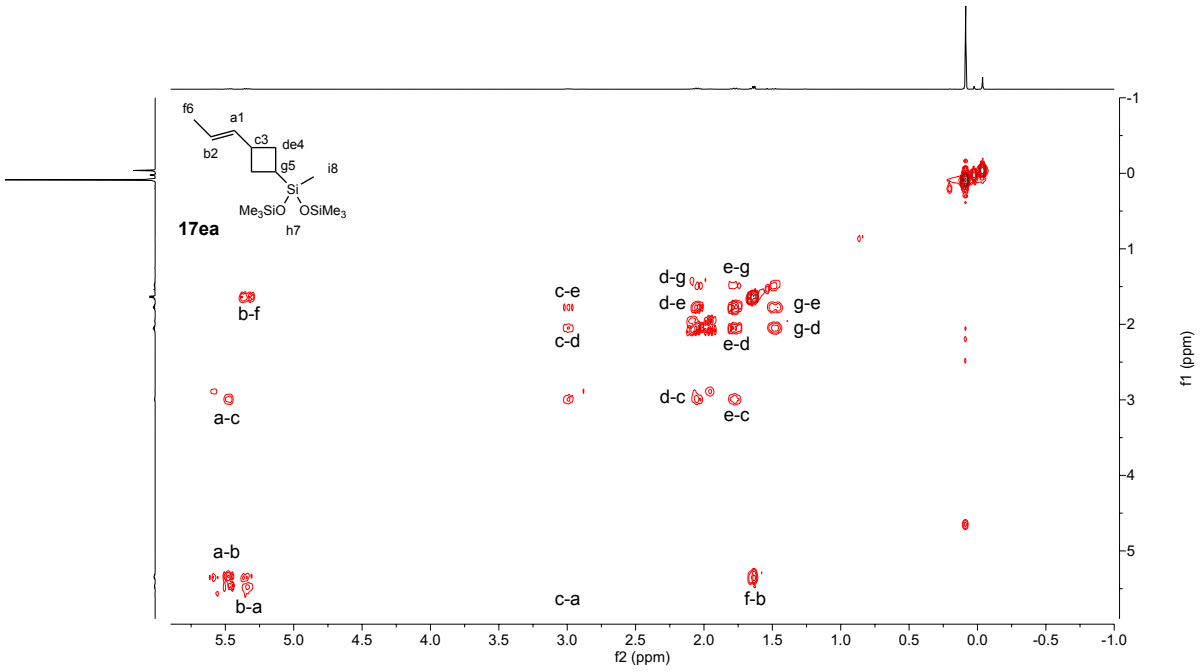

Figure S86. $^{1}H–^{1}H$ COSY (500 MHz, $CDCl_3$) spectrum of **17ea**.

(*E*)-triethoxy(3-(prop-1-en-1-yl)cyclobutyl)silane (17fa) was prepared in 89% isolated yield, 95% [2+2]-selectivity, 30:70 d.r. after 72 hours as described in 3.2.

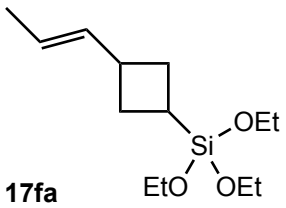

17fa

^{1}H NMR (500 MHz, $CDCl_3$) δ 5.59§ (ddd, *J* = 15.3, 7.1, 1.7 Hz, 1H), 5.50* (ddq, *J* = 15.3, 7.1, 1.6 Hz, 1H), 5.42 – 5.27 (m, 1H), 3.83§ (q, *J* = 6.9 Hz, 6H), 3.81* (q, *J* = 7.1 Hz, 6H), 3.10 – 2.95 (m, 1H), 2.24§ (dddd, *J* = 10.0, 8.2, 5.8, 1.8 Hz, 1H), 2.14* (qd, *J* = 8.5, 2.9 Hz, 1H), 2.09 – 1.91 (m, 2H), 1.73 – 1.54 (m, 1H), 1.65§ (ddd, *J* = 7.1, 1.6, 0.9 Hz, 3H), 1.63* (ddd, *J* = 6.4, 1.6, 0.9 Hz, 3H), 1.23§ (t, *J* = 6.9 Hz, 9H), 1.22* (t, *J* = 7.1 Hz, 6H) where resolved resonances arising from the *cis*(*) and *trans*(§) diastereomers are indicated.

^{13}C NMR (126 MHz, $CDCl_3$) δ 136.18§, 136.07*, 123.29*, 122.90§, 58.69§, 58.57*, 40.31*, 37.61§, 30.02*, 28.70§, 18.52, 17.96§, 17.91*, 14.37*, 14.37*, 12.69§ where resolved resonances arising from the *cis*(*) and *trans*(§) diastereomers are indicated.

GC-MS (EI): for $[M + H - OEt]^+$ = $C_{11}H_{22}O_2Si$, calculated *m/z* = 214.13892, found *m/z* = 214.13867

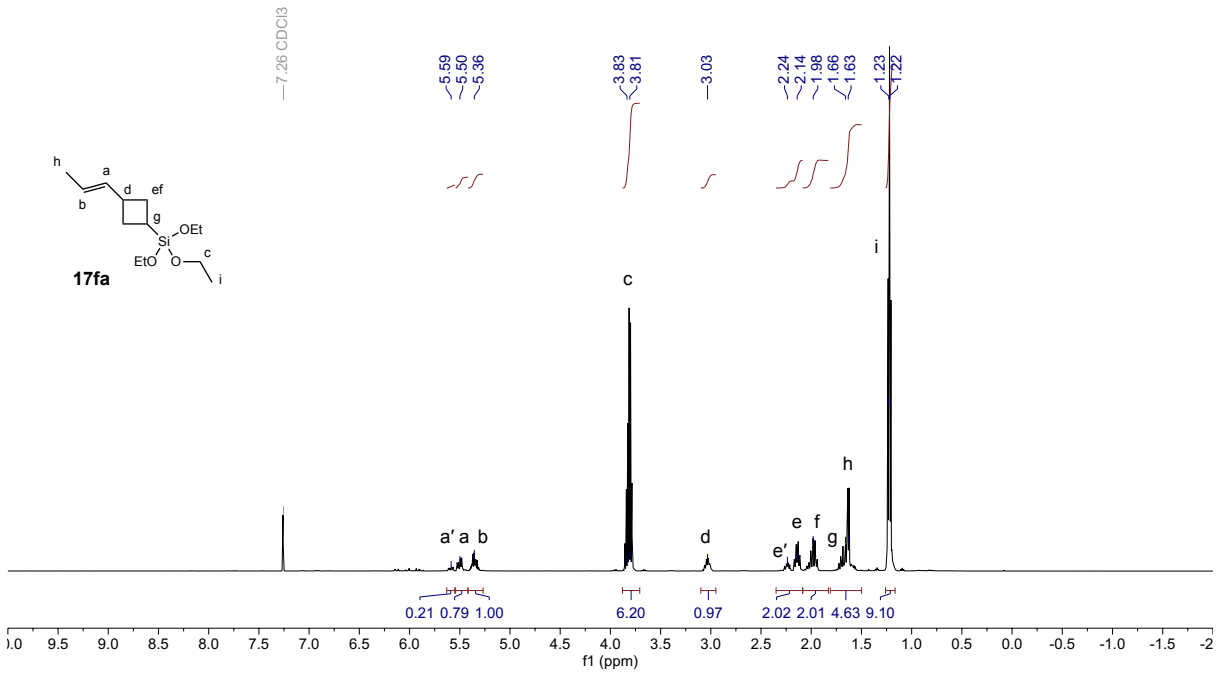

Figure S87. ^{1}H NMR (500 MHz, $CDCl_3$) spectrum of **17fa**.

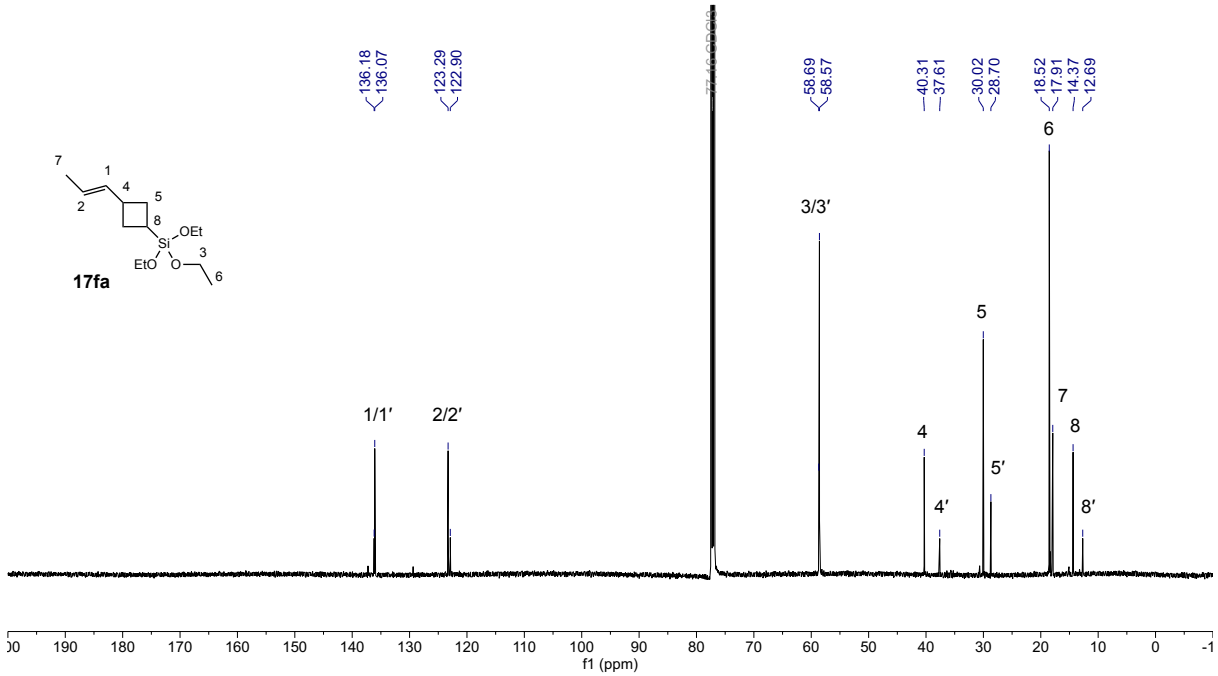

Figure S88. ^{13}C NMR (126 MHz, $CDCl_3$) spectrum of **17fa**.

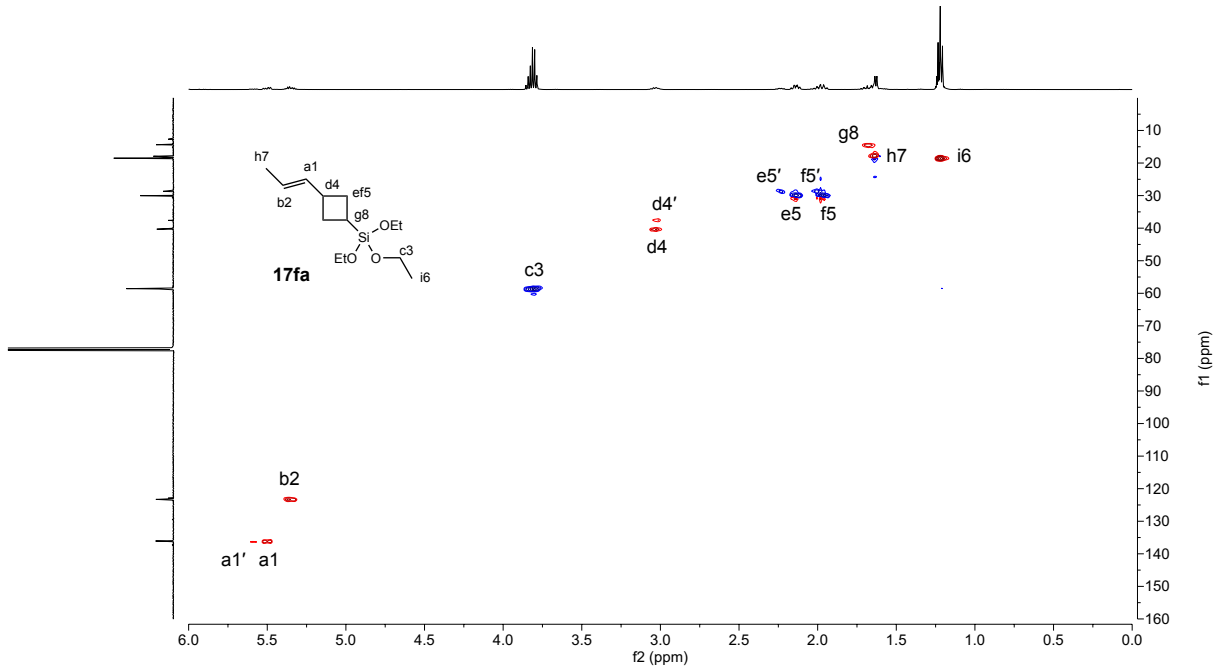

Figure S89. ^{1}H–^{13}C HSQC (500 MHz, $CDCl_3$) spectrum of **17fa**.

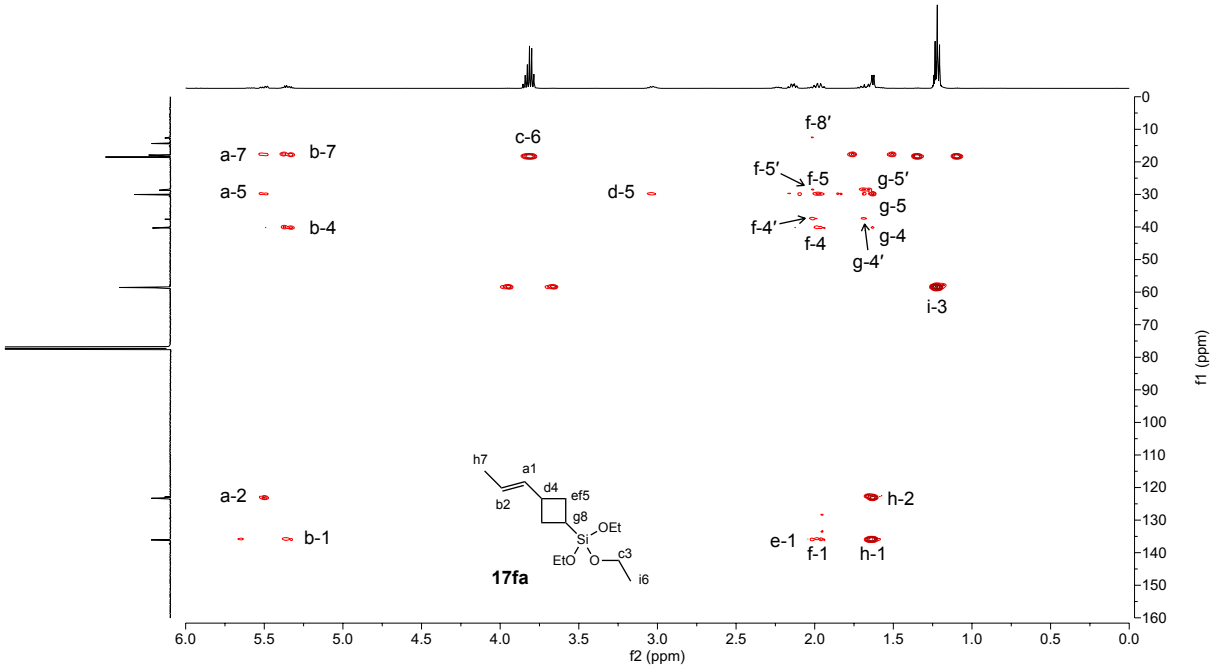

Figure S90. $^{1}H–^{13}C$ HMBC (500 MHz, $CDCl_3$) spectrum of **17fa**.

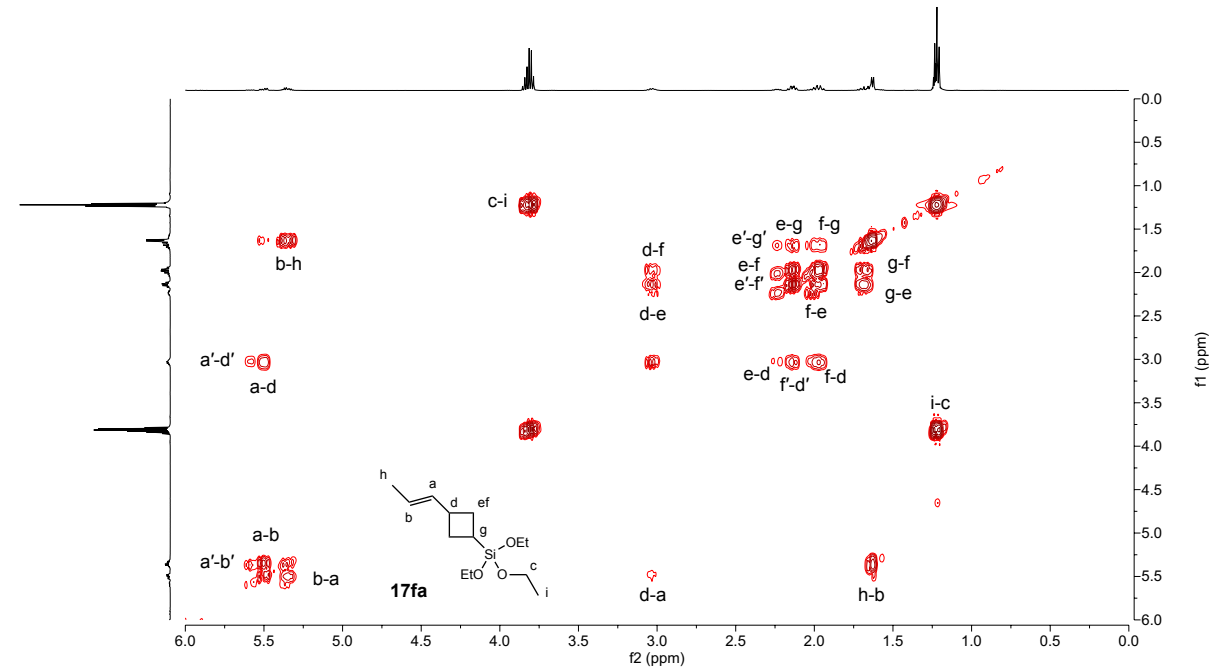

Figure S91. $^{1}H–^{1}H$ COSY (500 MHz, $CDCl_3$) spectrum of **17fa**.

1,1,3,3-tetramethyl-1,3-bis(3-((*E*)-prop-1-en-1-yl)cyclobutyl)disiloxane (17ga) was prepared in 90% isolated yield, 86% [2+2]-selectivity, 37:47:16 d.r. after 72 hours as described in 3.2. The mass balance of the material consists of the [2+2] cycloadduct where only one of the two vinyl groups of **6g** reacted (60:40 d.r.). The two products were not separated.

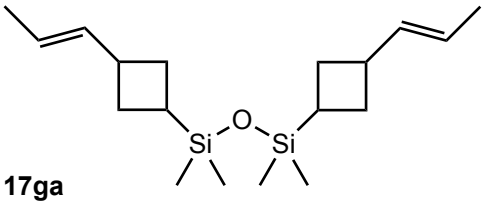

17ga

^{1}H NMR (500 MHz, $CDCl_3$) δ 5.59§ (ddt, *J* = 15.2, 7.1, 1.6 Hz, 1H), 5.48 (dddd, *J* = 15.2, 6.8, 3.0, 1.5 Hz, 1H), 5.41 – 5.23 (m, 1H), 3.01 (ttd, *J* = 9.9, 8.4, 7.2 Hz, 1H), 2.86§ (h, *J* = 7.8 Hz, 1H), 2.12 – 2.03 (m, 2H), 1.99*(ddd, *J* = 11.8, 10.2, 7.8 Hz, 2H), 1.75§(dtd, *J* = 11.5, 9.1, 2.4 Hz, 2H), 1.66§ (d, *J* = 6.4 Hz, 3H), 1.64 (dd, *J* = 6.4, 1.3 Hz, 3H), 1.61 – 1.50 (m, 1H), 1.51 – 1.42 (m, 1H), 0.06* (s, 3H), 0.06*(s, 3H), -0.00§ (s, 3H), -0.00§(s, 3H) where resolved resonances arising from the major(*) and minor(§) diastereomers are indicated.

^{13}C NMR (126 MHz, $CDCl_3$) δ 136.7, 136.4, 122.9, 122.6, 39.3, 39.2, 37.3, 37.3, 29.5, 28.6, 20.3, 18.4, 18.3, 18.0, 17.9, 0.60, -1.3, -1.3, -1.4, -1.4

GC-MS (EI): for $[M - C_9H_{11}]^+ = C_{11}H_{23}OSi_2$, calculated *m/z* = 227.12876, found *m/z* = 227.12729

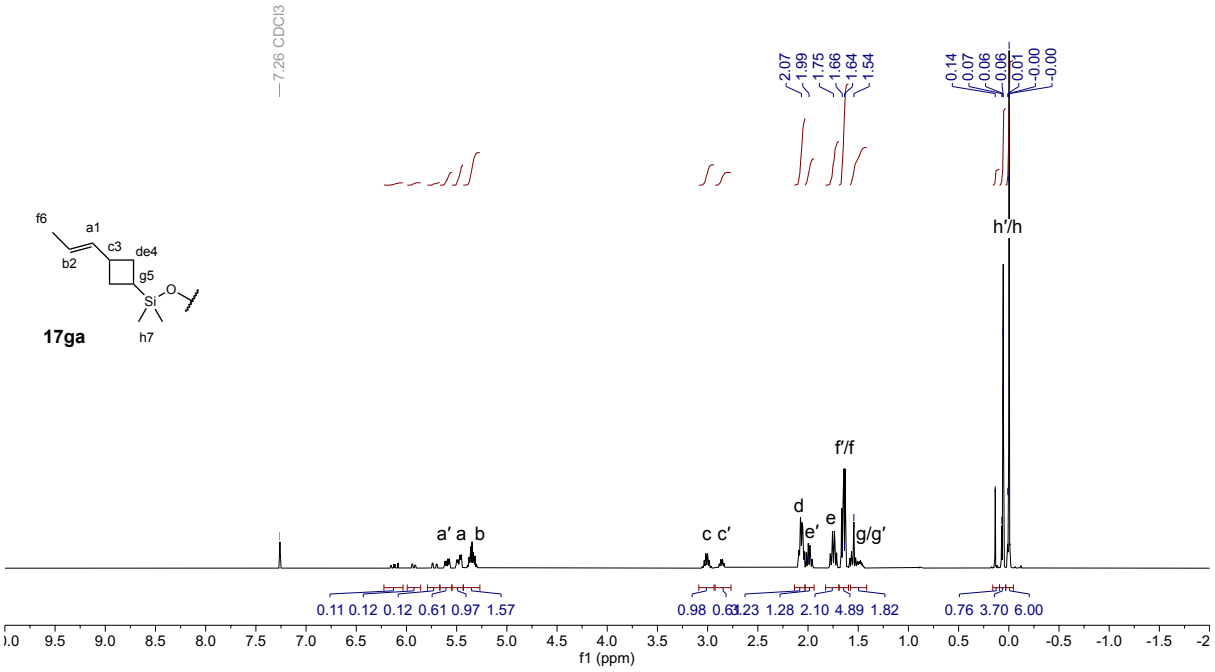

Figure S92. ^{1}H NMR (500 MHz, $CDCl_3$) spectrum of **17ga**.

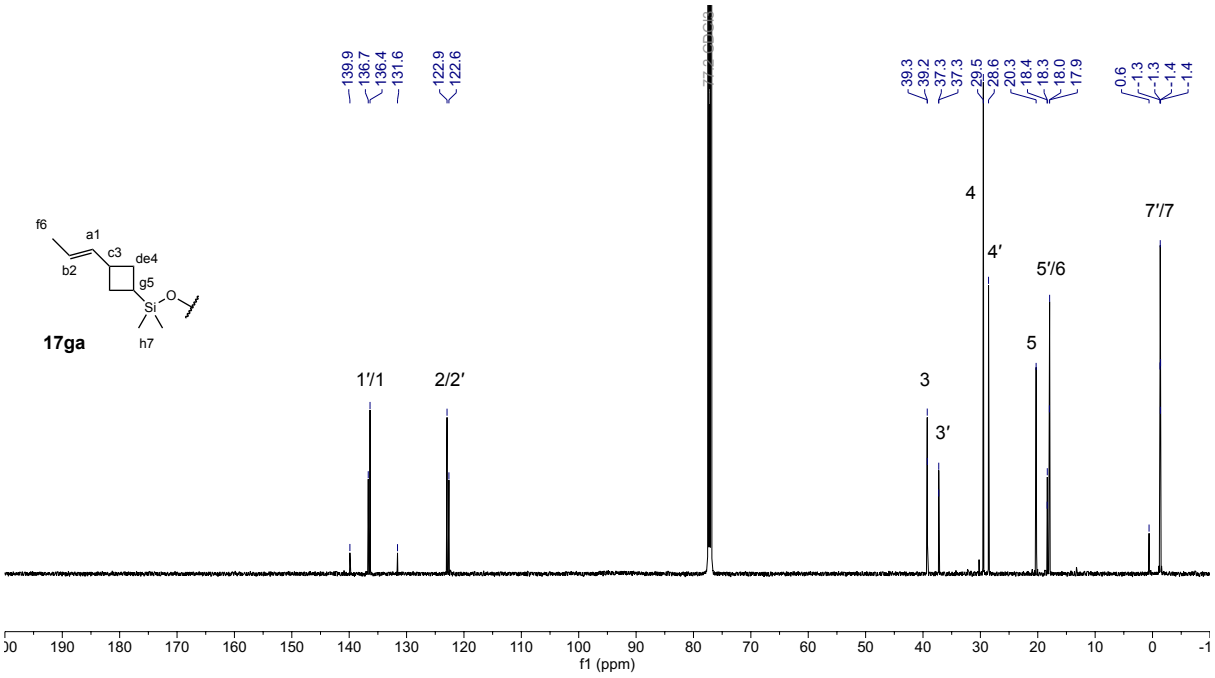

Figure S93. ^{13}C NMR (126 MHz, $CDCl_3$) spectrum of **17ga**.

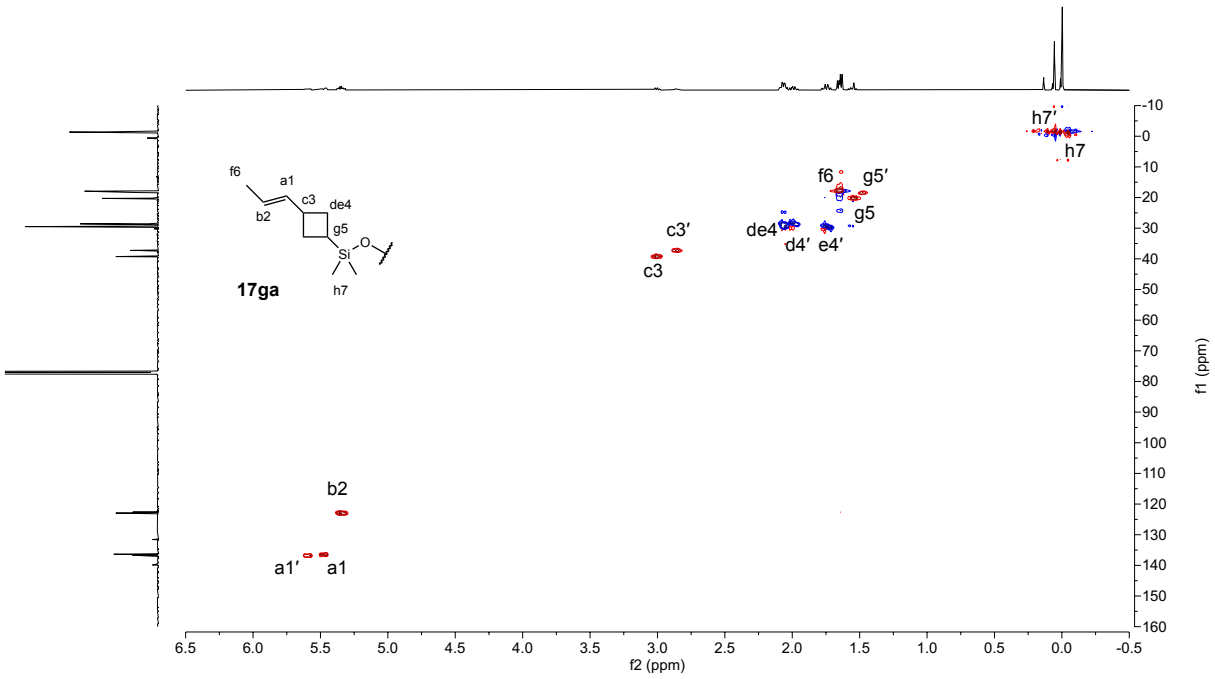

Figure S94. ^{1}H–^{13}C HSQC (500 MHz, $CDCl_3$) spectrum of **17ga**.

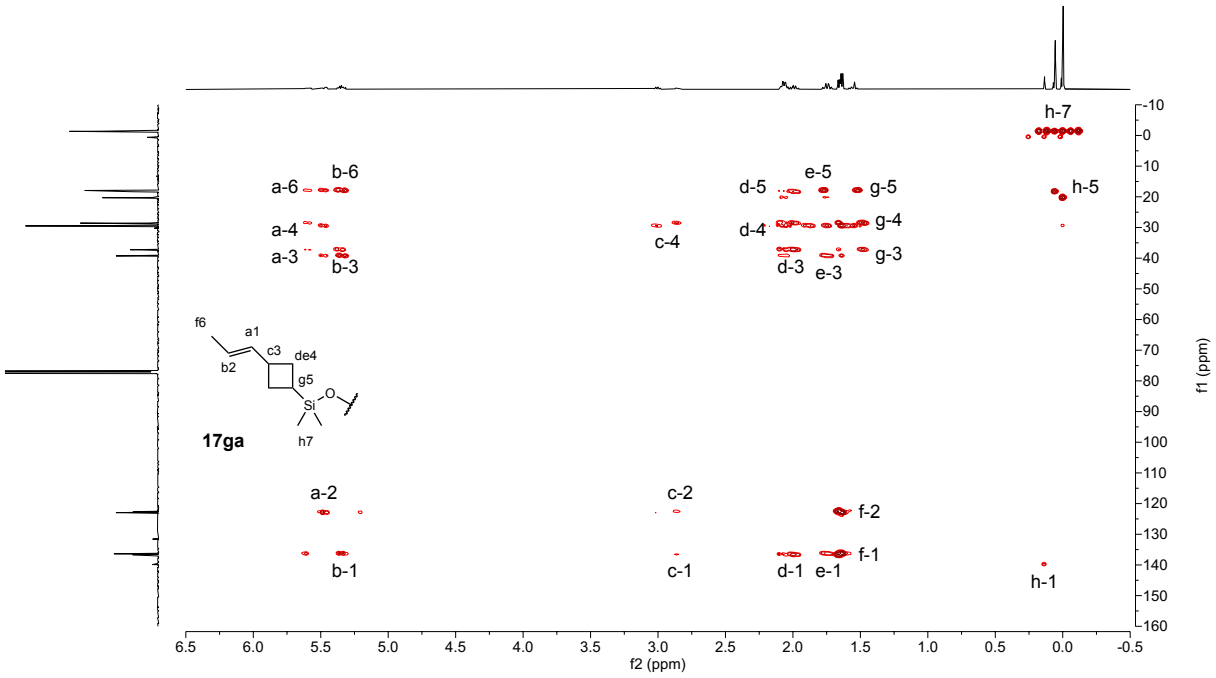

Figure S95. $^{1}H–^{13}C$ HMBC (500 MHz, $CDCl_3$) spectrum of **17ga**.

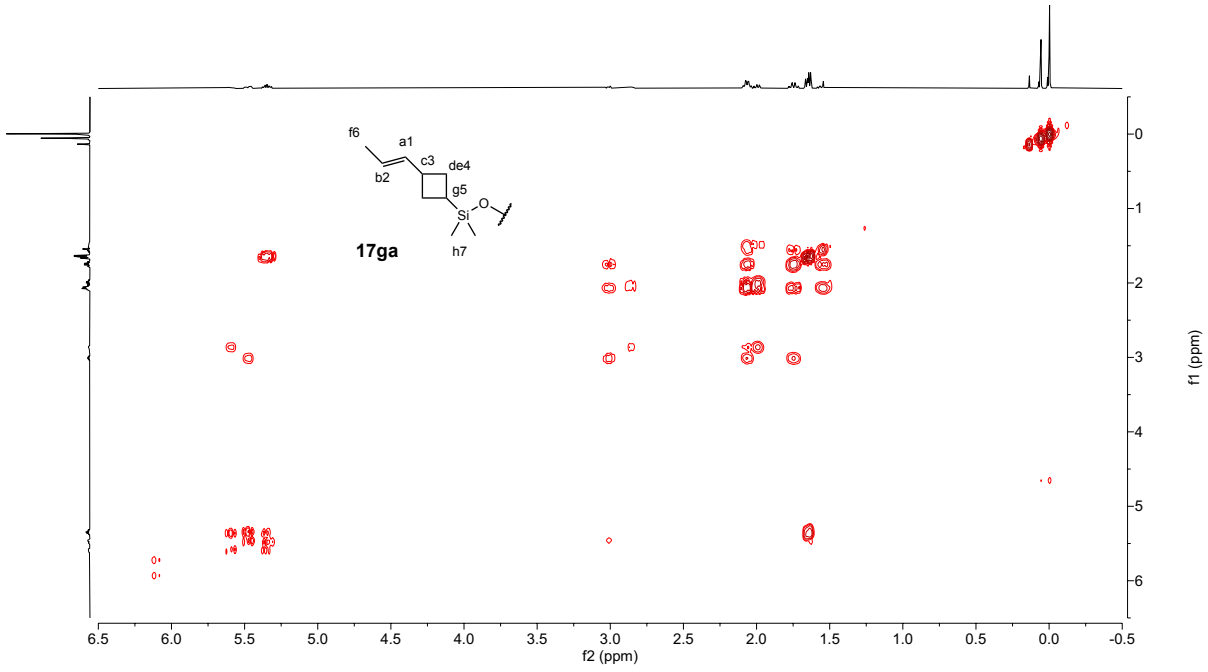

Figure S96. $^{1}H–^{1}H$ COSY (500 MHz, $CDCl_3$) spectrum of **17ga**.

(*E*)-trimethylsilyl-3-styrylcyclobutane (17ab) was prepared in a 26% isolated yeild, >98% [2+2]-selectivity, 51:49 d.r. after 48 hours as described in 3.2, with 1 mol% (^{Me}PDI)Fe(butadiene). The mass balance of the material consists of the [4+2] cycloaddition product from the dimerization of **13b**.

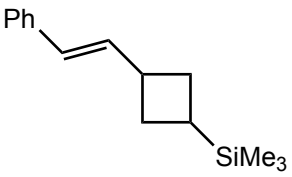

17ab

^{1}H NMR (500 MHz, $CDCl_3$) δ7.36 (dd, *J* =13.7, 6.8 Hz, 2H), 7.29(m, 2H), 7.20(m, 1H) 6.4 (m, 1H), 6.40-6.29 (m, 1H), 3.25* (m, 1H), 3.05§ (m, 1H), 2.16 (m, 3H), 1.82* (m, 1H), 1.75–1.55 (m, 1H), 0.03§ (s, 9H), -0.03* (s, 9H) where resolved resonances arising from the *cis*(*) and *trans*(§) diastereomers are indicated.

^{13}C NMR (126 MHz, $CDCl_3$) δ 137.94, 137.91, 135.7, 135.3, 128.62, 128.60, 127.7, 127.5, 126.95, 126.94, 126.1, 39.6, 37.7, 29.9, 28.9, 19.4, 17.3, -3.2, -3.3.

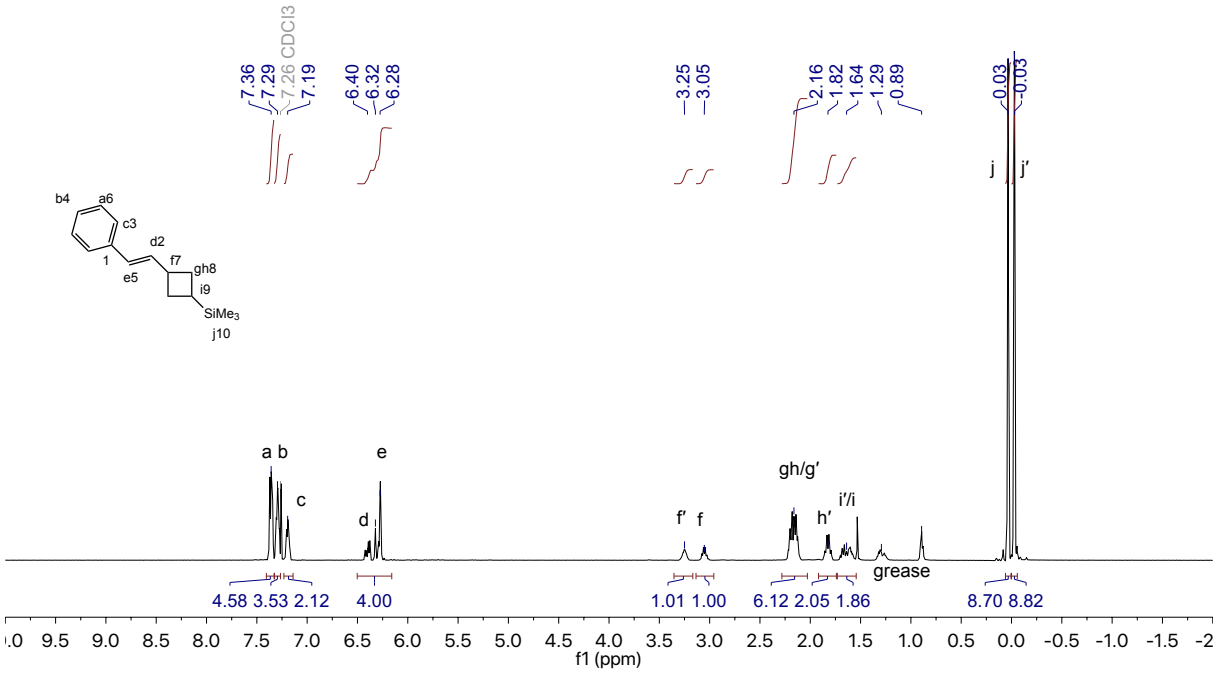

Figure S97. ^{1}H NMR (500 MHz, $CDCl_3$) spectrum of **17ab.**

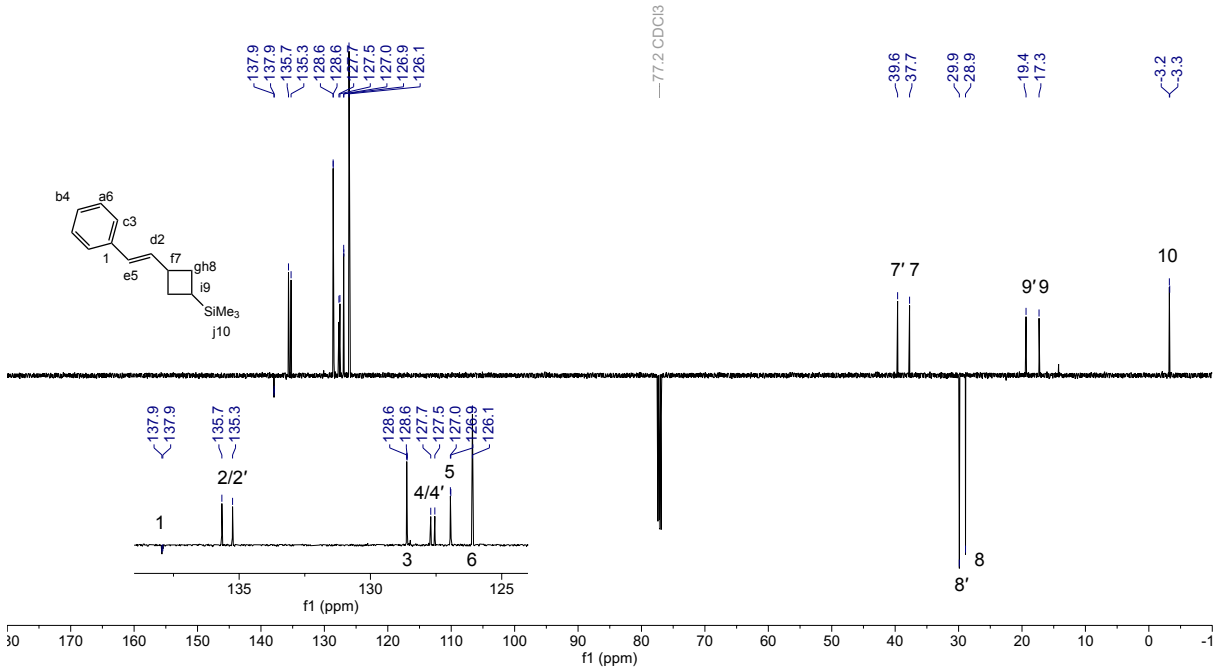

Figure S98. ^{13}C NMR (126 MHz, $CDCl_3$) spectrum of **17ab.**

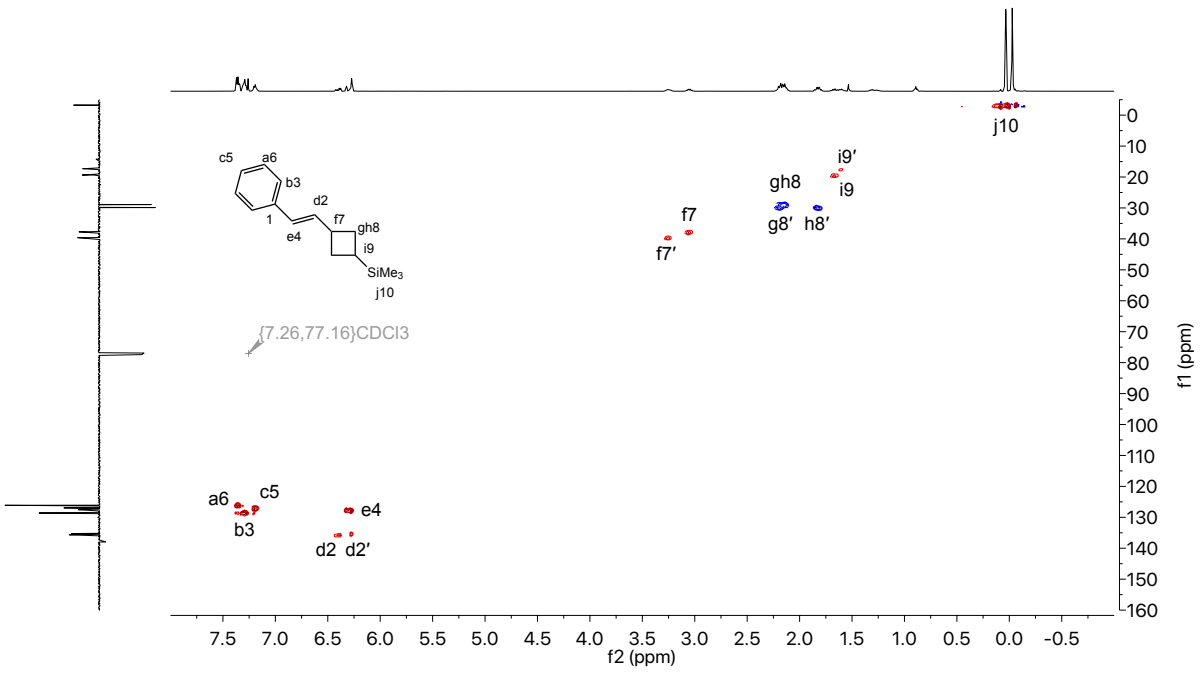

Figure S99. ^{1}H–^{13}C HSQC (500 MHz, $CDCl_3$) spectrum of **17ab.**

((*E*)-(3-(hept-1-en-1-yl)cyclobutyl)trimethylsilane (17ac) was prepared in an 85% isolated yeild, >98% [2+2]-selectivity, 48:55 d.r. after 70 hours as described in 3.2, with 1 mol% (^{Me}PDI)Fe(butadiene).

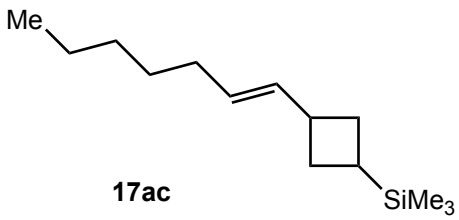

17ac

^{1}H NMR (500 MHz, $CDCl_3$) δ 5.57§ (ddt, *J* = 15.3, 7.1, 1.5 Hz, 1H), 5.44* (dd, *J* = 15.3, 6.9 Hz, 1H), 5.41 – 5.23 (m, 1H), 3.01* (h, *J* = 8.4 Hz, 1H), 2.81§ (h, *J* = 8.1 Hz, 1H), 2.13 – 1.87 (m, 6H), 1.67* (qd, *J* = 9.3, 8.9, 2.7 Hz, 1H), 1.62 – 1.46 (m, 2H), 1.46 – 1.11 (m, 6H), 0.88 (t, *J* = 7.0 Hz, 3H), -0.01§ (s, 9H), -0.07* (s, 9H) where resolved resonances arising from the *cis* (*) and *trans* (§) diastereomers are indicated.

^{13}C NMR (126 MHz, $CDCl_3$) δ 135.3, 135.0, 128.6, 128.3, 39.2, 37.3, 32.6, 31.6, 30.0, 29.5, 29.1, 22.7, 19.1, 17.1, 14.2, -3.2, -3.3.

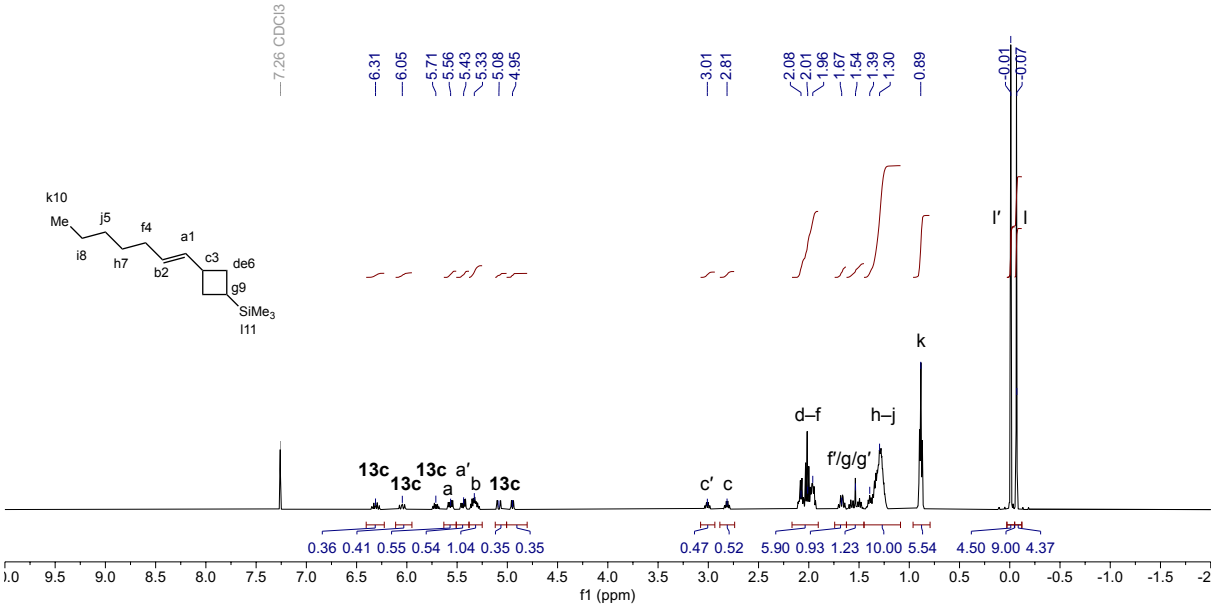

Figure S100. ^{1}H NMR (500 MHz, $CDCl_3$) spectrum of **17ac.**

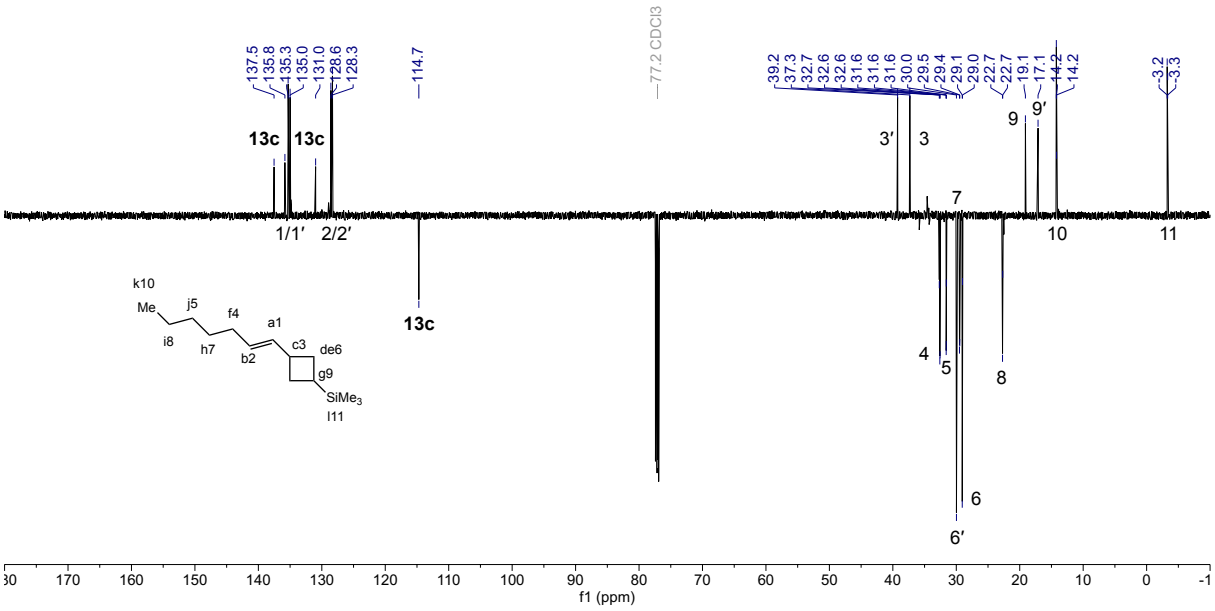

Figure S101. ^{13}C NMR (126 MHz, $CDCl_3$) spectrum of **17ac.**

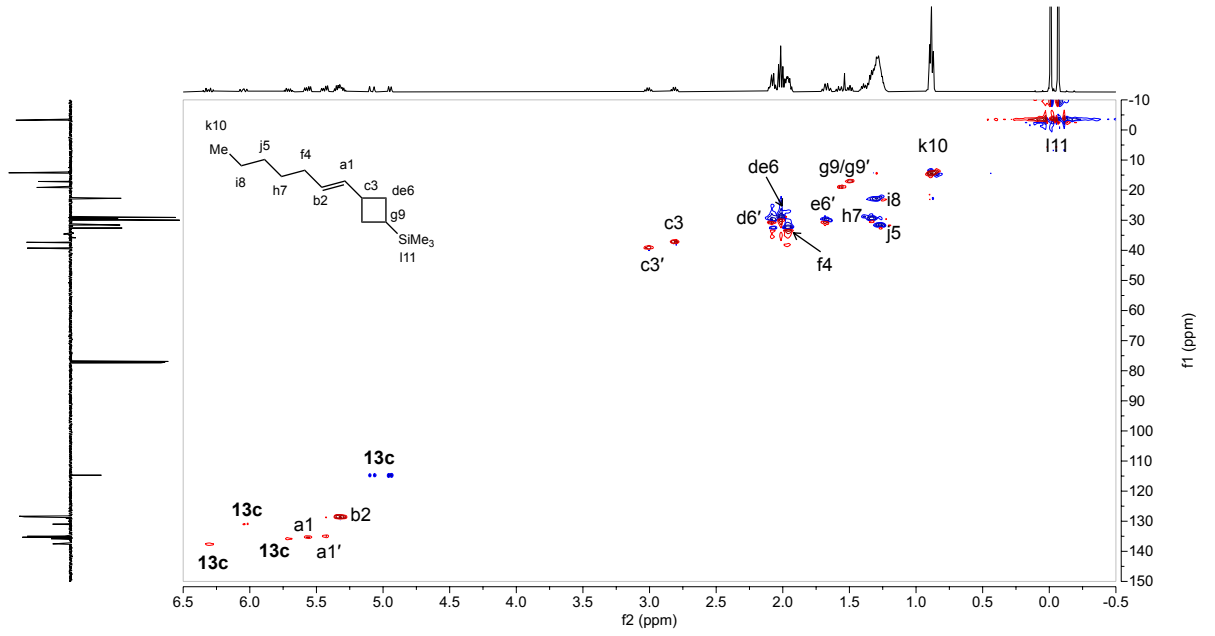

Figure S102. ^{1}H–^{13}C HSQC (500 MHz, $CDCl_3$) spectrum of **17ac.**

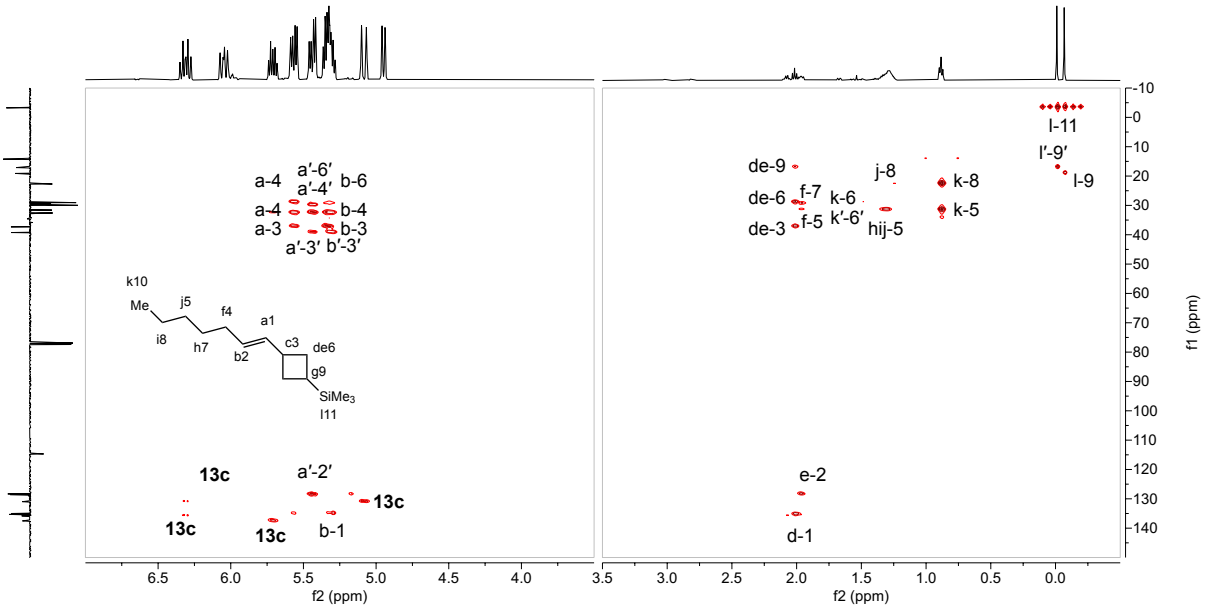

Figure S103. $^{1}H–^{13}C$ HMBC (500 MHz, $CDCl_3$) spectrum of **17ac.**

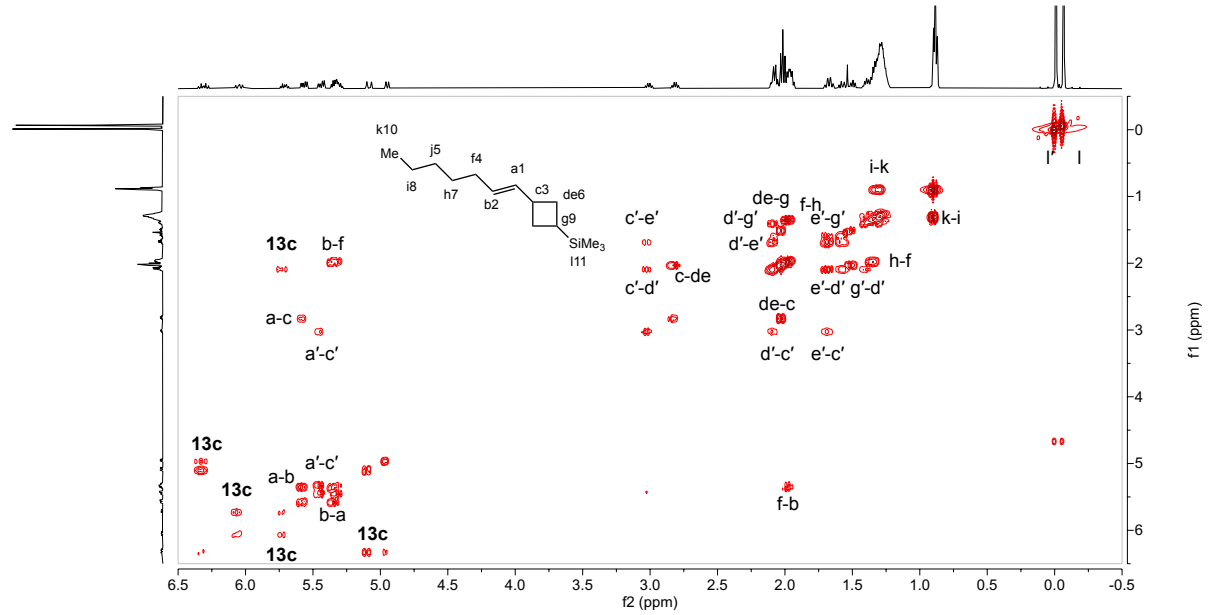

Figure S104. $^{1}H–^{1}H$ COSY (500 MHz, $CDCl_3$) spectrum of **17ac.**

(*E*)-trimethyl(3-(4-phenylbut-1-en-1-yl)cyclobutyl)silane (17ad) was obtained in an 83% yield >98% [2+2]-selectivity, 62:38 d.r.after 70 hours as described in 3.2, with 1 mol% (^{Me}PDI)Fe(butadiene).

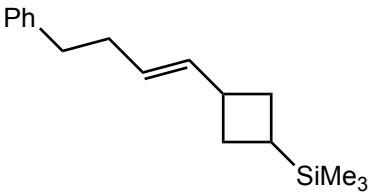

17ad

^{1}H NMR (500 MHz, $CDCl_3$) δ 7.31 (m, 1H), 7.22 (m, 4H), 5.64 (dd, *J* = 13.8, 7.7 Hz, 1H), 5.52 (dd, *J* = 15.3, 8.8 Hz, 1H), 5.42 (m, 1H), 3.06 (m, 1H), 2.84 (m, 1H), 2.69 (m, 1H), 2.34 (m, 1H), 2.15-1.91 (m, 8H), 1.74-1.49 (m, 3H), 0.03 (s, 9H) * or §, -0.03 (s, 9H) * or § where resolved resonances arising from the *cis* (*) and *trans* (§) diastereomers are indicated.

^{13}C NMR (126 MHz, $CDCl_3$) δ 142.33, 136.05, 135.72, 128.62, 128.36, 127.47, 127.21, 125.83, 39.16, 37.24, 36.28, 34.50, 29.88, 28.42, 19.14, 17.14, -3.25, -3.31 where resolved resonances arising from the *cis* (*) and *trans* (§) diastereomers are indicated.

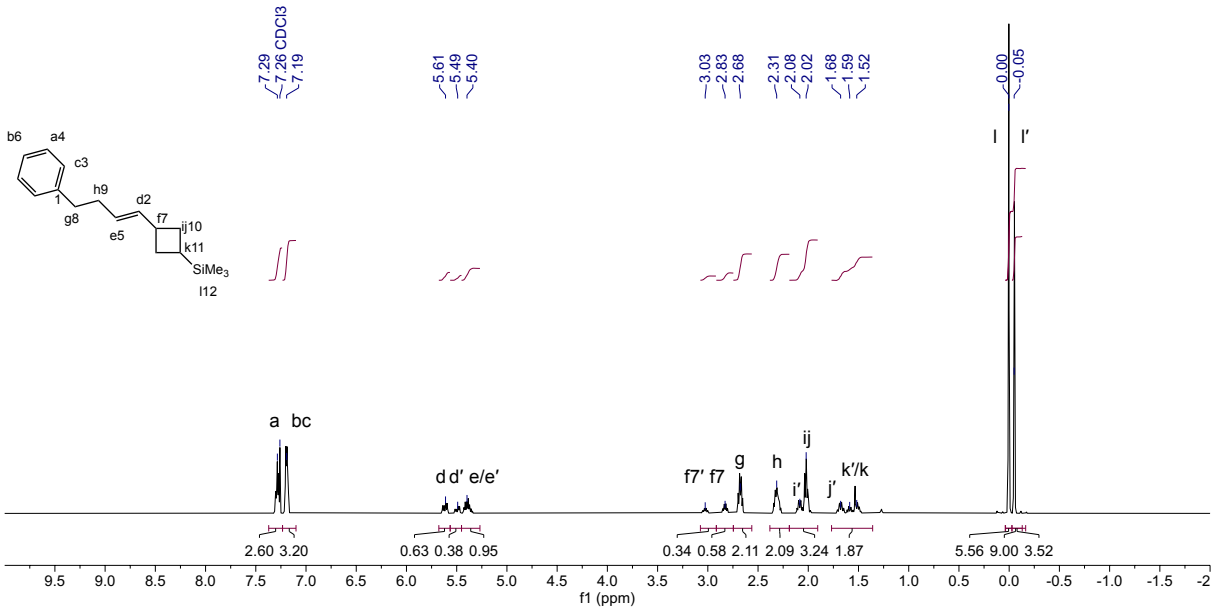

Figure S105. ^{1}H NMR (500 MHz, $CDCl_3$) spectrum of **17ad.**

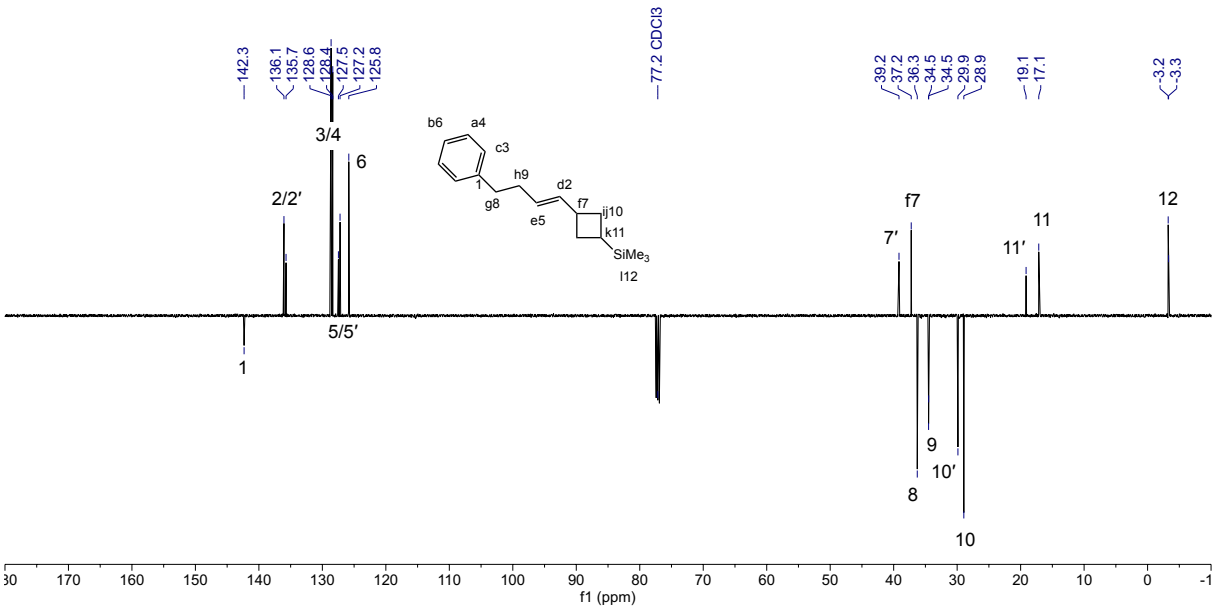

Figure S106. ^{13}C NMR (126 MHz, $CDCl_3$) spectrum of **17ad.**

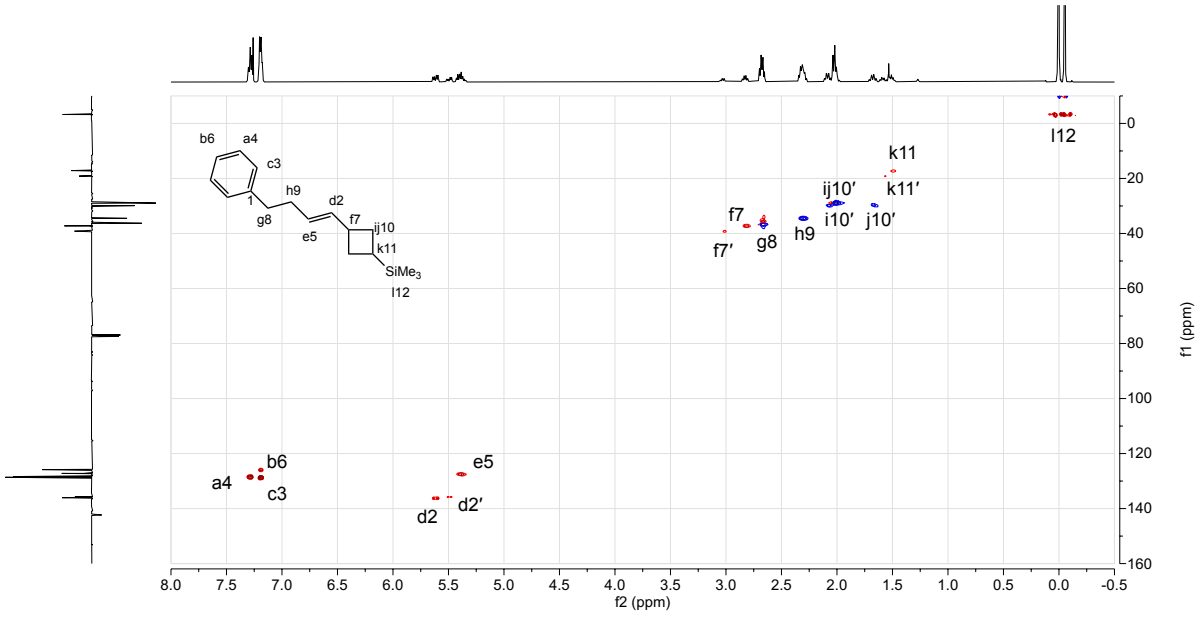

Figure S107. ^{1}H–^{13}C HSQC (500 MHz, $CDCl_3$) spectrum of **17ad.**

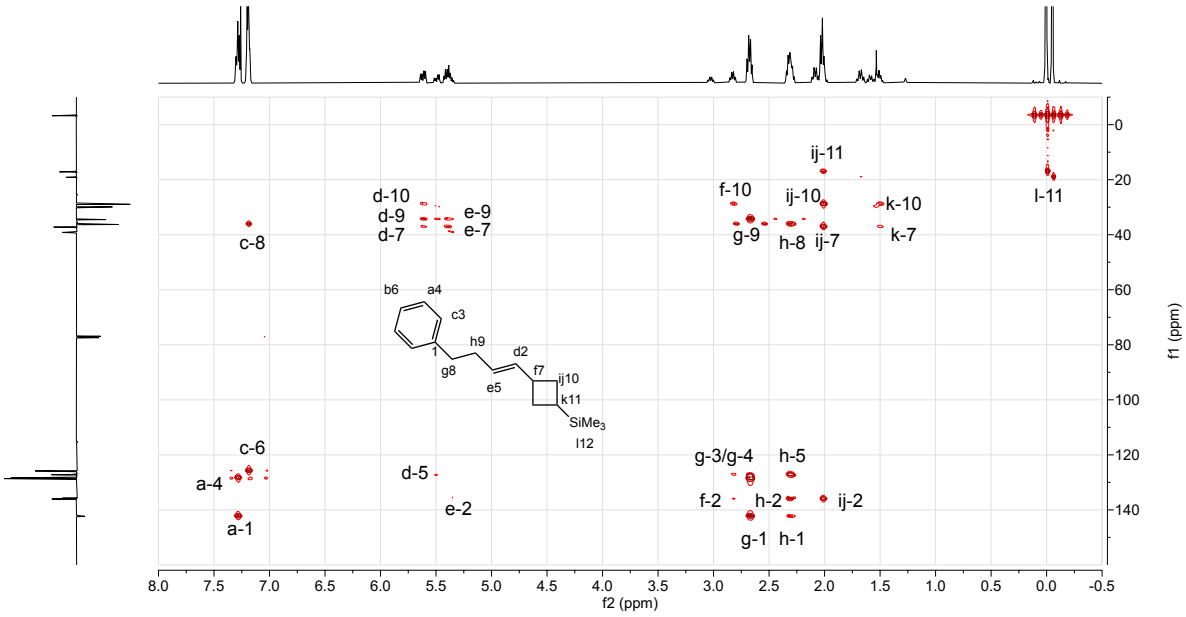

Figure S108. $^{1}H–^{13}C$ HMBC (500 MHz, $CDCl_3$) spectrum of **17ad.**

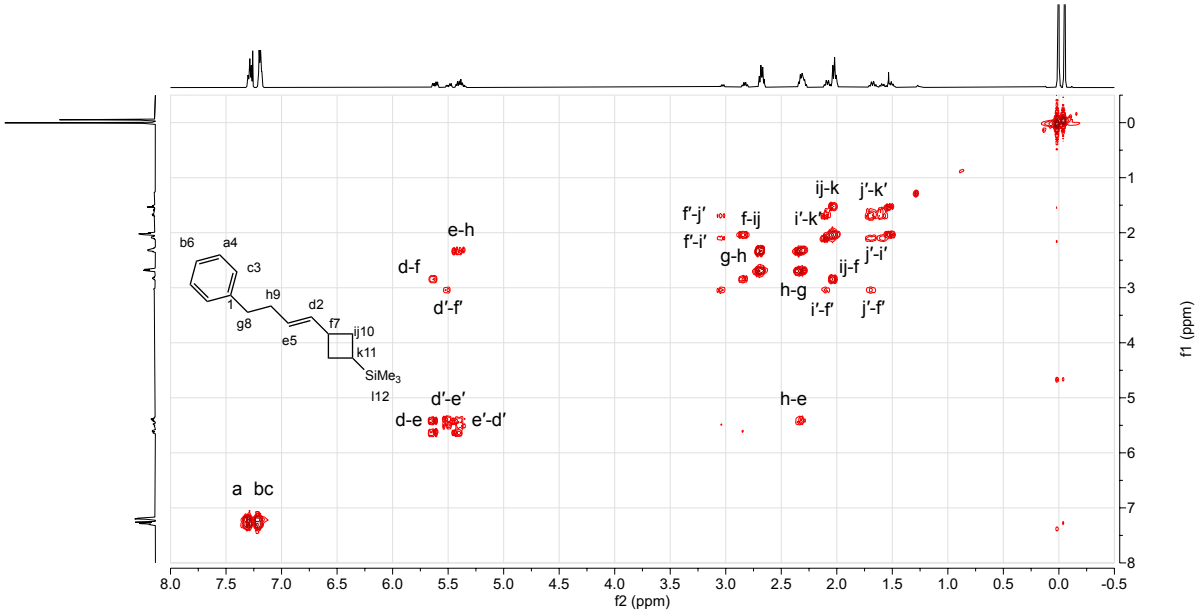

Figure S109. $^{1}H–^{1}H$ COSY (500 MHz, $CDCl_3$) spectrum of **17ad.**

(*E*)-*tert*-butyldiphenyl((3-(3-(trimethylsilyl)cyclobutyl)allyl)oxy)silane (17ae) was obtained in a 90% yield, 57:43 d.r. after 48 hours as described in 3.2.

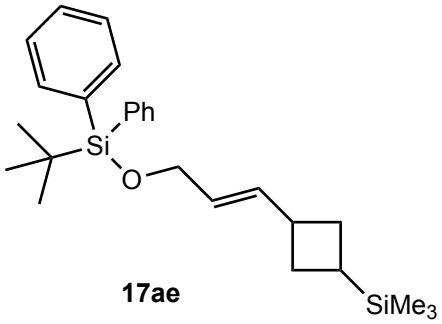

17ae

^{1}H NMR (500 MHz, $CDCl_3$) δ 7.76 – 7.66 (m, 4H), 7.49 – 7.32 (m, 6H), 5.81§ (ddt, *J* = 15.3, 6.9, 1.5 Hz, 1H), 5.70* (ddt, *J* = 15.4, 6.6, 1.5 Hz, 1H), 5.58 – 5.37 (m, 1H), 4.20§ (dt, *J* = 5.2, 1.4 Hz, 2H), 4.18* (dt, *J* = 5.3, 1.3 Hz, 2H), 3.08* (h, *J* = 8.9, 8.0 Hz, 1H), 2.88§ (h, *J* = 8.0 Hz, 1H), 2.12* (qd, *J* = 8.1, 2.1 Hz, 1H), 2.05§ (t, *J* = 8.2 Hz, 2H), 1.71* (qt, *J* = 10.6, 9.9, 2.6, 1.1 Hz, 1H), 1.66 – 1.58* (m, 1H), 1.58 – 1.48§ (m, 1H), 1.08 (s, 9H), 0.02§ (s, 9H), -0.04* (s, 9H) where resolved resonances arising from the *cis*(*) and *trans*(§) diastereomers are indicated.

^{13}C NMR (126 MHz, $CDCl_3$) δ 136.02§, 135.74, 135.72*, 134.07, 129.68, 127.72, 126.74*, 126.55§, 64.83§, 64.76*, 38.62*, 36.84§, 29.59*, 28.68§, 27.02, 19.38, 19.09*, 17.17§, -3.24§, -3.31* where resolved resonances arising from the *cis*(*) and *trans*(§) diastereomers are indicated.

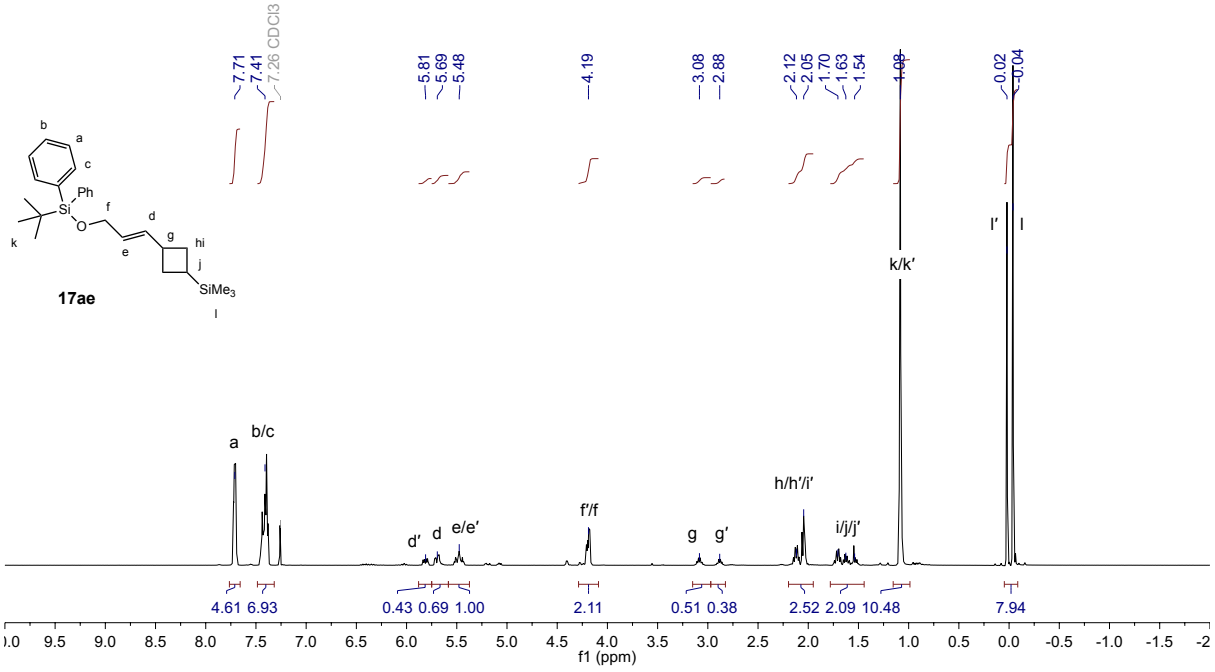

Figure S110. ^{1}H NMR (500 MHz, $CDCl_3$) spectrum of **17ae.**

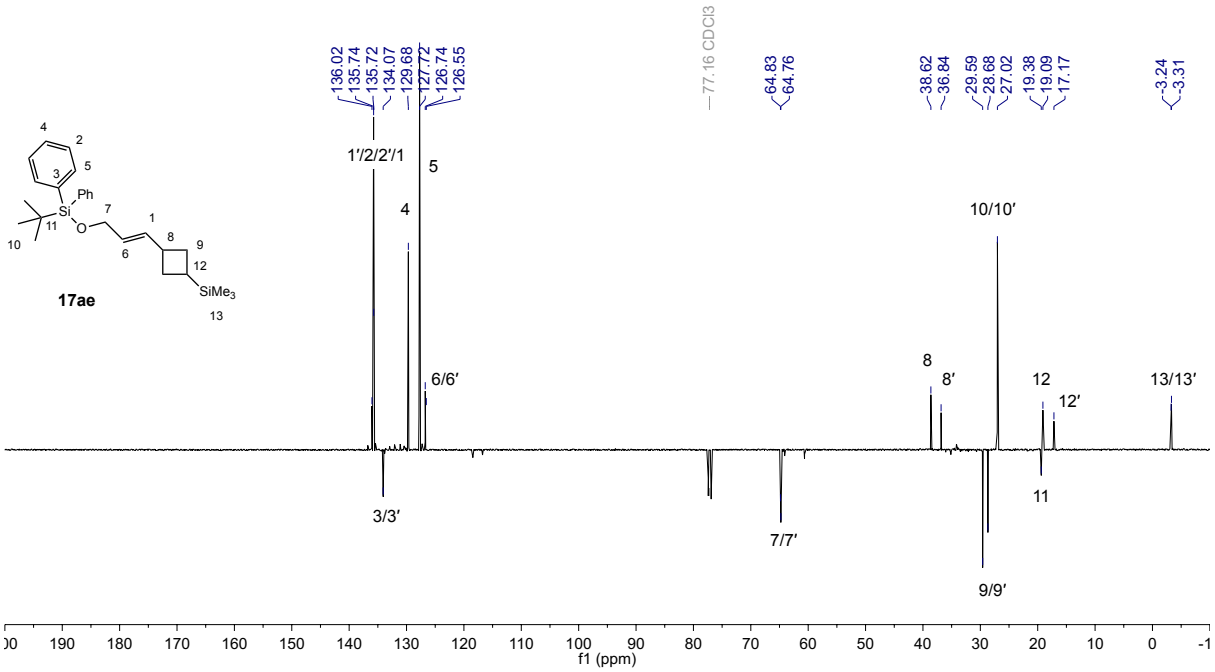

Figure S111. ^{13}C NMR (126 MHz, $CDCl_3$) spectrum of **17ae.**

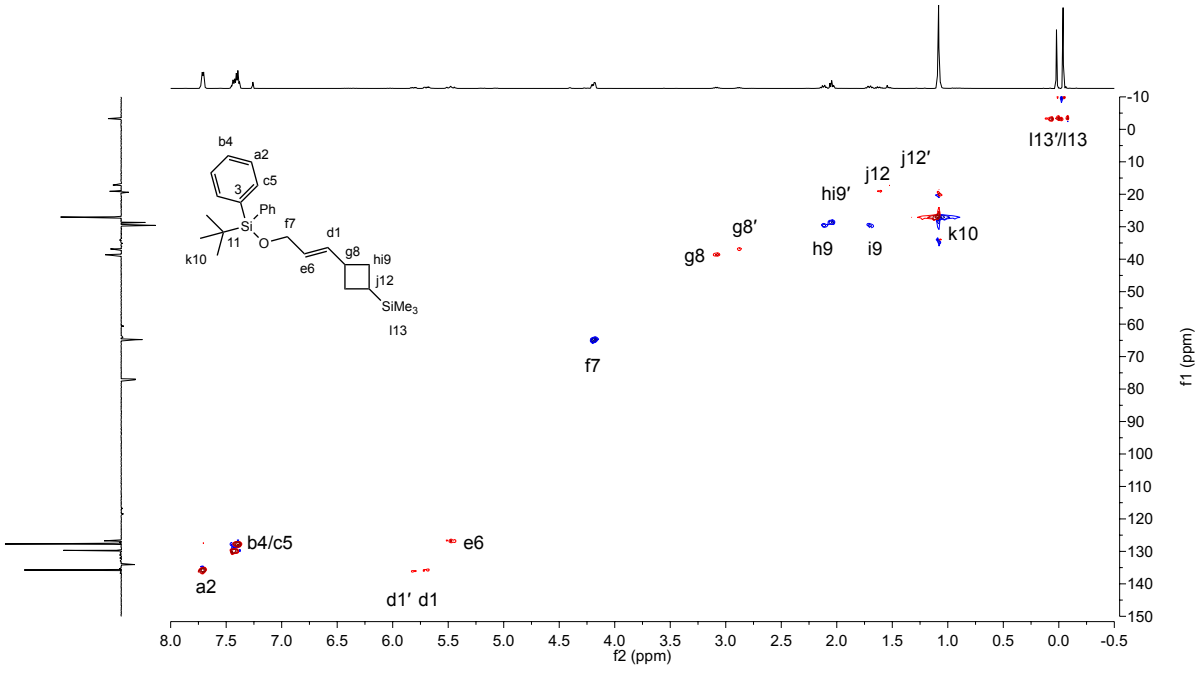

Figure S112. $^{1}H–^{13}C$ HSQC (500 MHz, $CDCl_3$) spectrum of **17ae.**

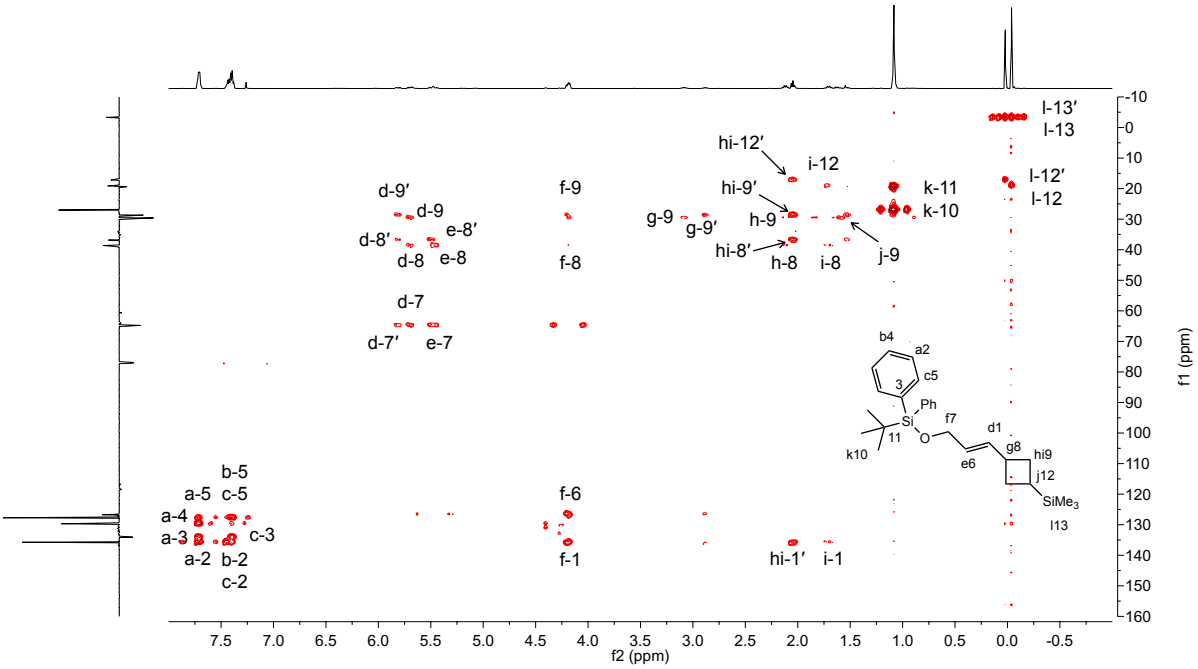

Figure S113. $^{1}H–^{13}C$ HMBC (500 MHz, $CDCl_3$) spectrum of **17ae.**

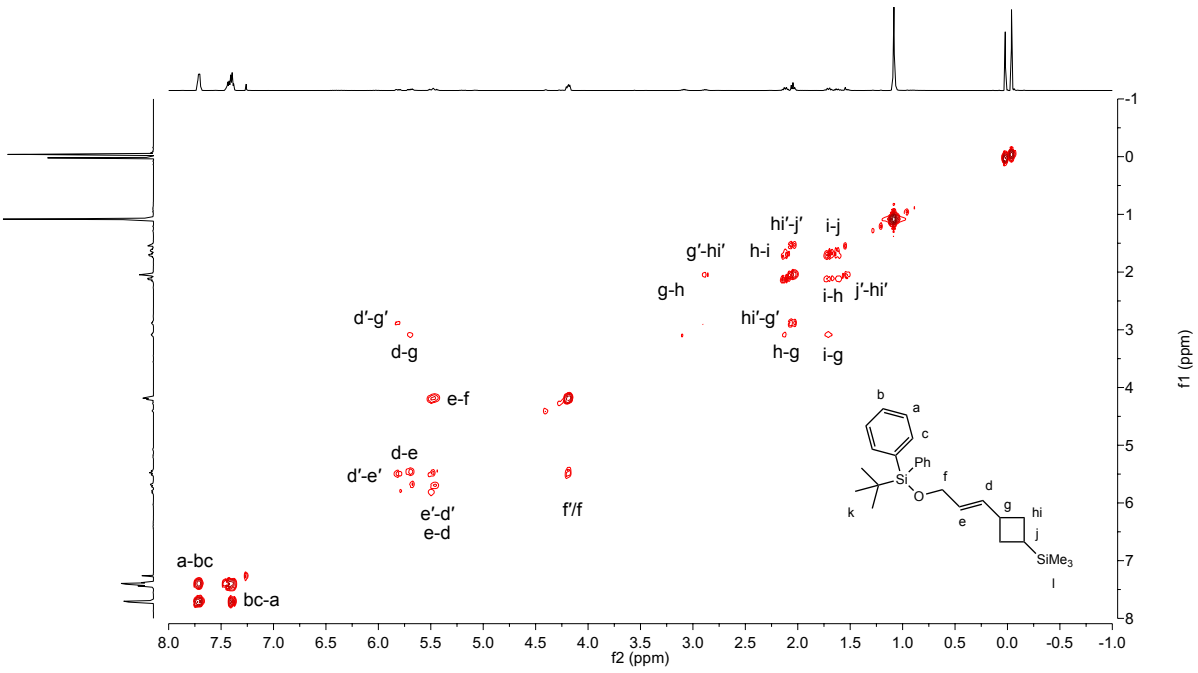

Figure S114. $^{1}H–^{1}H$ COSY (500 MHz, $CDCl_3$) spectrum of **17ae.**

((*E*)-(3-(4-(benzyloxy)but-1-en-1-yl)cyclobutyl)trimethylsilane **(17af)** was obtained in a 73% yield, >98% [2+2]-selectivity, 56:44 d.r.after 48 hours as described in 3.2, with 1 mol% (^{Me}PDI)Fe(butadiene).

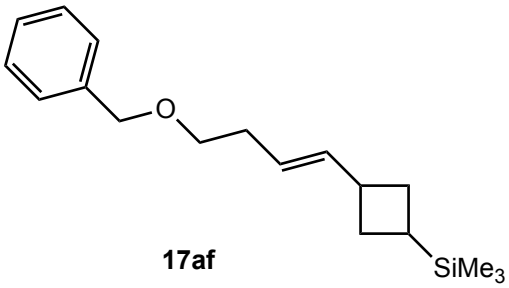

17af

^{1}H NMR (500 MHz, $CDCl_3$) δ 7.36 (dd, *J* = 4.5, 1.4 Hz, 4H), 7.30 (dt, *J* = 5.3, 3.9 Hz, 1H), 5.68§ (ddd, *J* = 15.1, 7.2, 1.7 Hz, 1H), 5.56* (ddd, *J* = 15.4, 6.9, 1.6 Hz, 1H), 5.46 – 5.28 (m, 1H), 4.53 (d, *J* = 2.8 Hz, 2H), 3.49 (q, *J* = 6.9 Hz, 2H), 3.04* (h, *J* = 8.3 Hz, 1H), 2.85§ (h, *J* = 7.9 Hz, 1H), 2.33 (h, *J* = 7.6, 7.0, 6.3, 5.4 Hz, 2H), 2.17 – 2.05* (m, 1H), 2.04§ (td, *J* = 8.0, 1.6 Hz, 2H), 1.75 – 1.65* (m, 1H), 1.65 – 1.54* (m, 1H), 1.56 – 1.46§ (m, 1H), 0.01§ (s, 9H), -0.05* (s, 9H) where resolved resonances arising from the *cis*(*) and *trans*(§) diastereomers are indicated.

^{13}C NMR (126 MHz, $CDCl_3$) δ 138.7, 137.5§, 137.2*, 128.5, 127.8, 127.6, 124.3*, 124.1§, 73.0, 70.4, 70.3, 39.2*, 37.3§, 33.1§, 33.0*, 29.8*, 28.9§, 19.1*, 17.1§, -3.3§, -3.3* where resolved resonances arising from the *cis*(*) and *trans*(§) diastereomers are indicated.

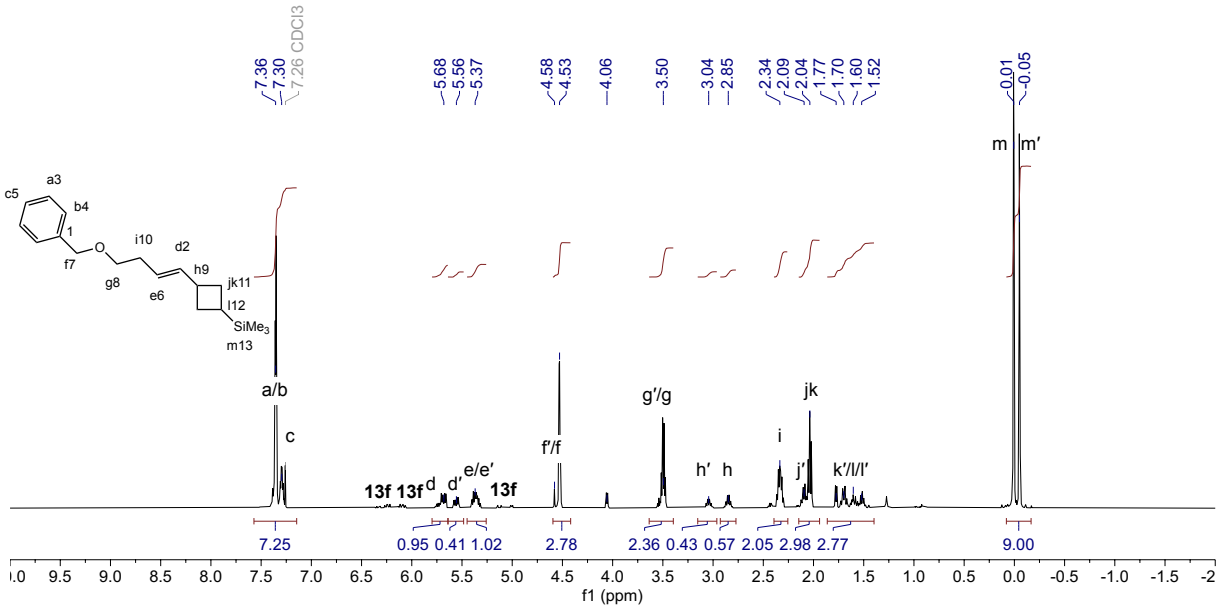

Figure S115. ^{1}H NMR (500 MHz, $CDCl_3$) spectrum of **17af.**

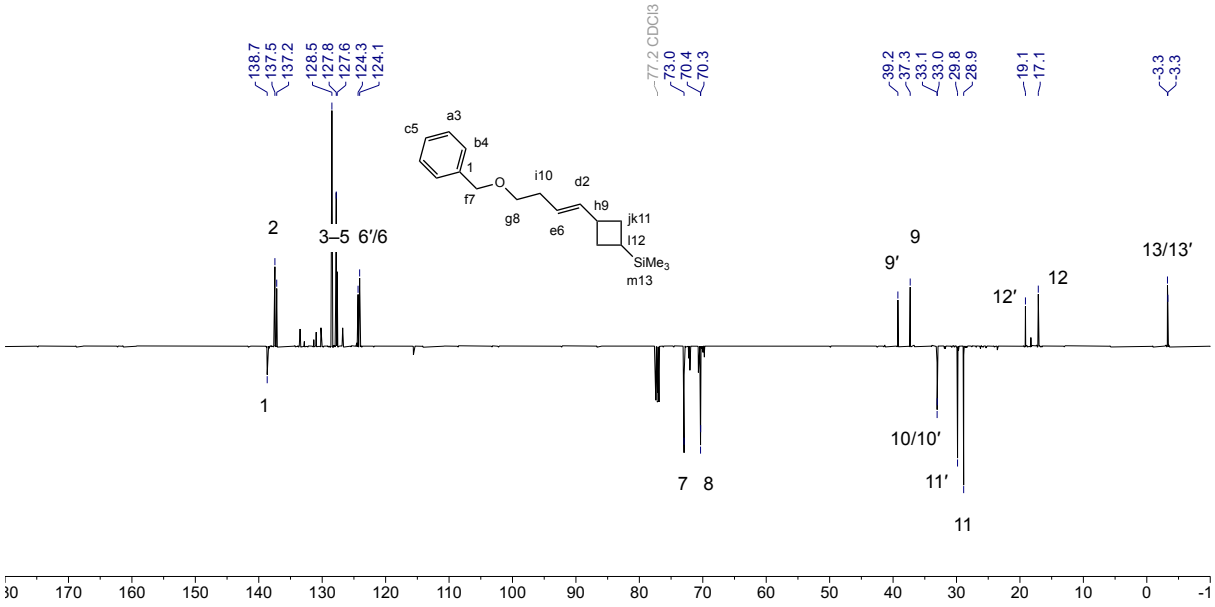

Figure S116. ^{13}C NMR (126 MHz, $CDCl_3$) spectrum of **17af**.

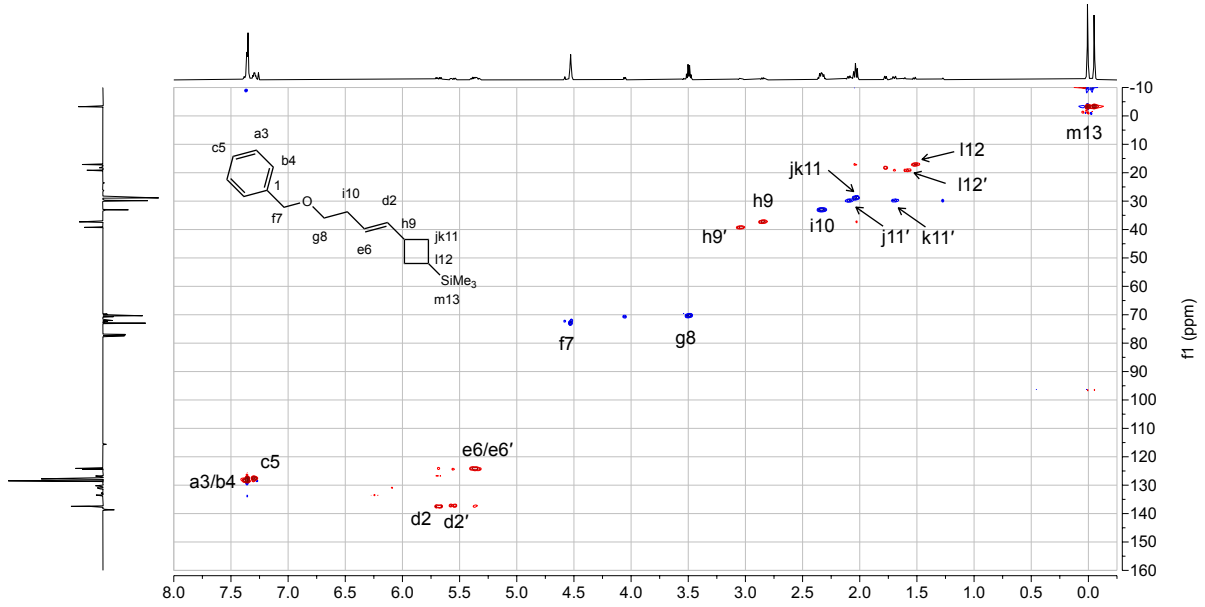

Figure S117. $^{1}H–^{13}C$ HSQC (500 MHz, $CDCl_3$) spectrum of **17af.**

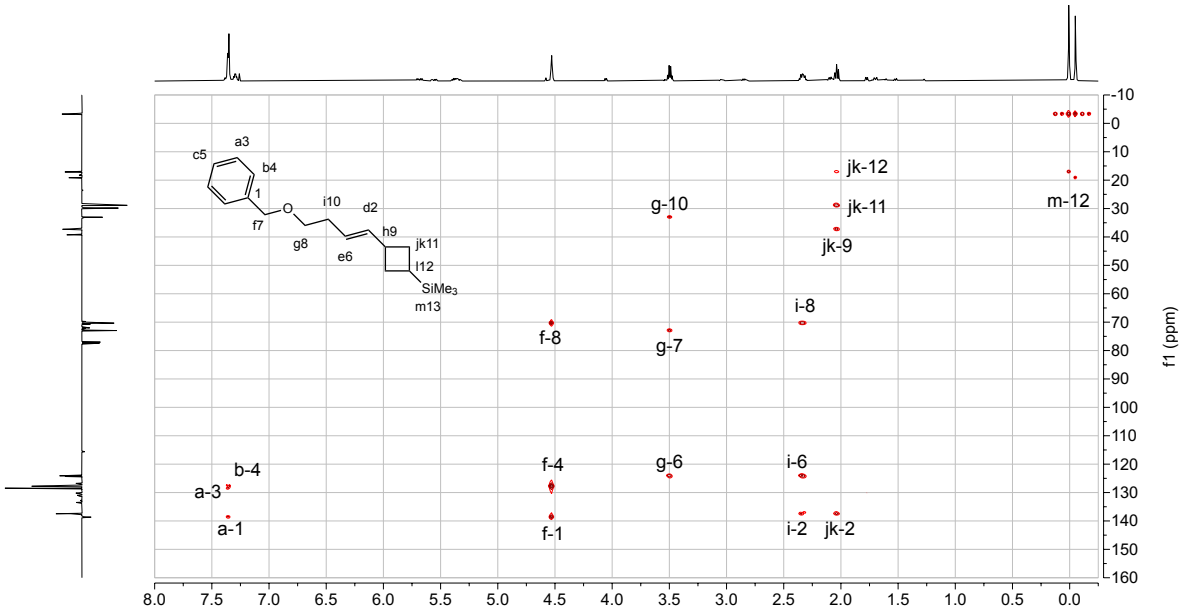

Figure S118. $^{1}H–^{13}C$ HMBC (500 MHz, $CDCl_3$) spectrum of **17af.**

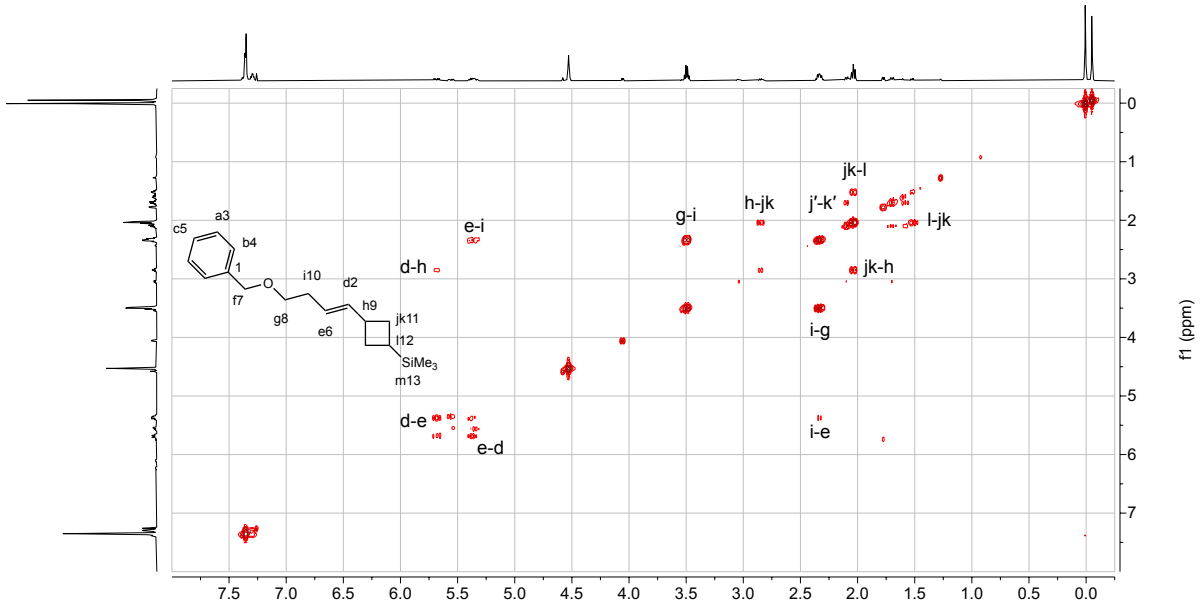

Figure S119. $^{1}H–^{1}H$ COSY (500 MHz, $CDCl_3$) spectrum of **17af.**

Trimethyl(4-(4-methylpent-3-en-1-yl)cyclohex-3-en-1-yl)silane (18aj) was prepared in an 88% isolated yield with 93% [4+2]-selectivity, 62:38 after 24 hours as described in 3.2, with 2.5 mol% (^{Me}PDI)Fe(butadiene).

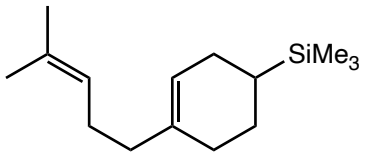

18aj

^{1}H NMR (500 MHz, $CDCl_3$) δ 5.46 (s, 1H), 5.11 (t, *J* = 7.8 Hz, 1H), 2.10-1.74 (m, 9 H) , 1.68 (s, 3H), 1.60 (s, 3H), 1.30 (m, 1H), 0.70 (m, 1H), -0.04 (s, 9H).

^{13}C NMR (126 MHz, $CDCl_3$) δ 138.0, 131.4, 124.7, 121.6, 38.3, 29.5, 26.7, 26.2, 25.9, 24.0, 21.3, 17.8, -3.4.

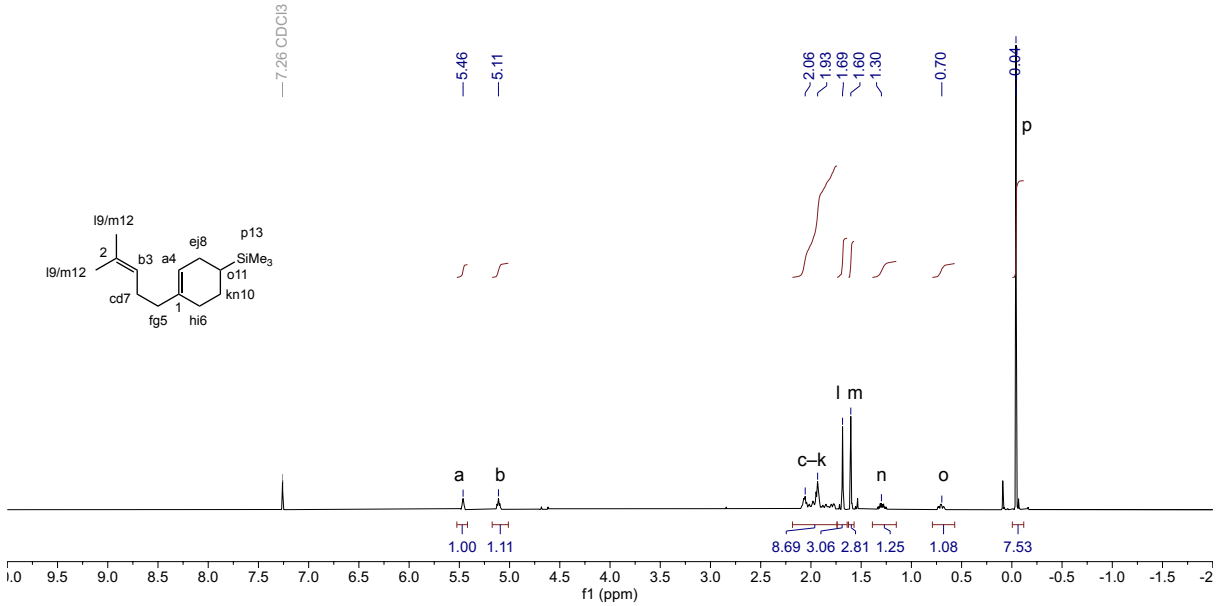

Figure S120. ^{1}H NMR (500 MHz, $CDCl_3$) spectrum of **18aj**.

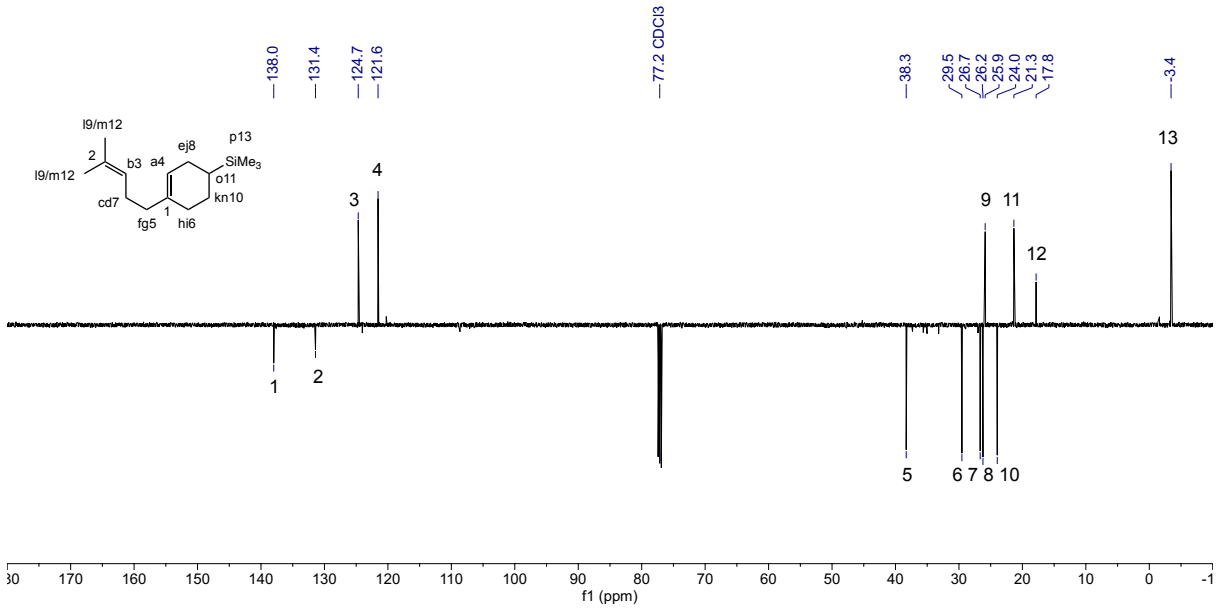

Figure S121. ^{13}C NMR (126 MHz, $CDCl_3$) spectrum of **18aj**.

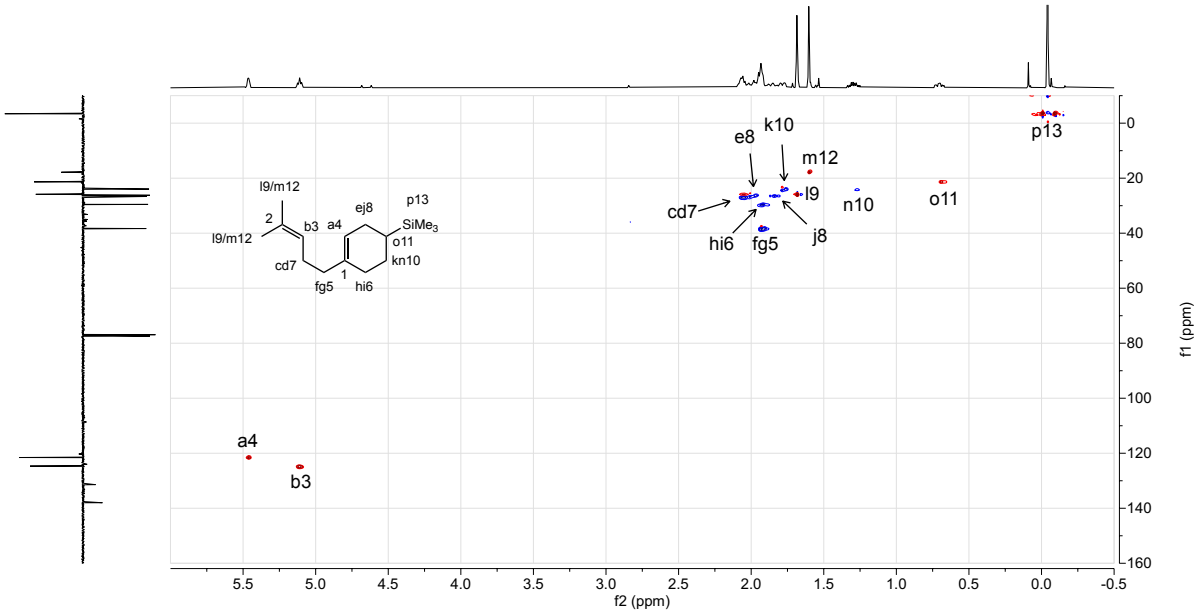

Figure S122. ^{1}H–^{13}C HSQC (500 MHz, $CDCl_3$) spectrum of **18aj**.

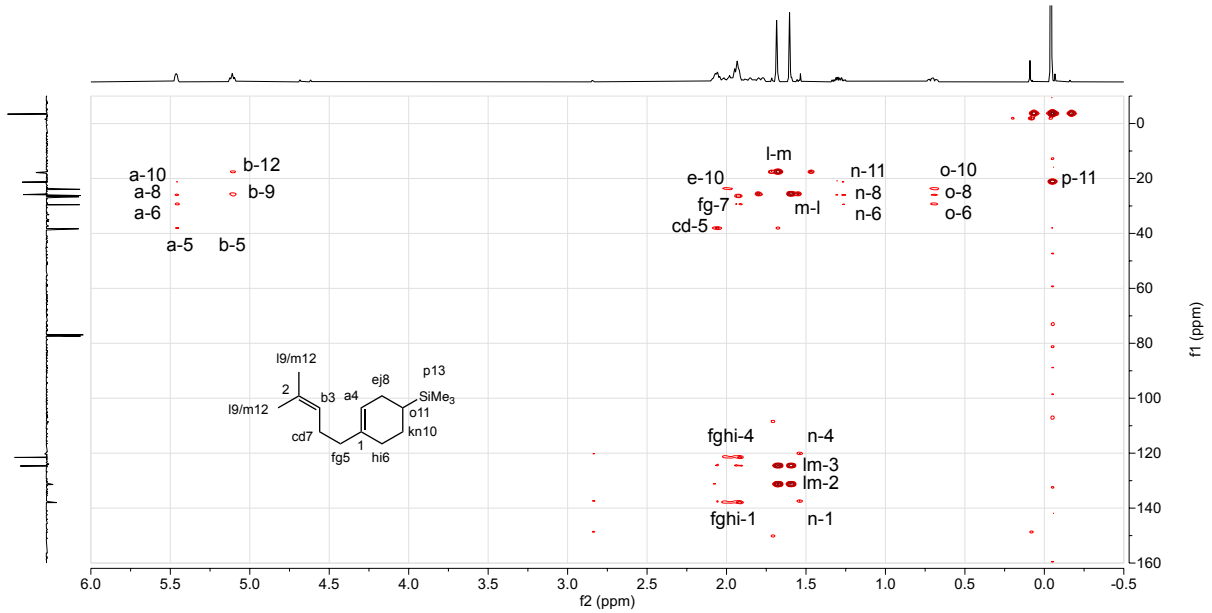

Figure S123. $^{1}H–^{13}C$ HMBC (500 MHz, $CDCl_3$) spectrum of **18aj**.

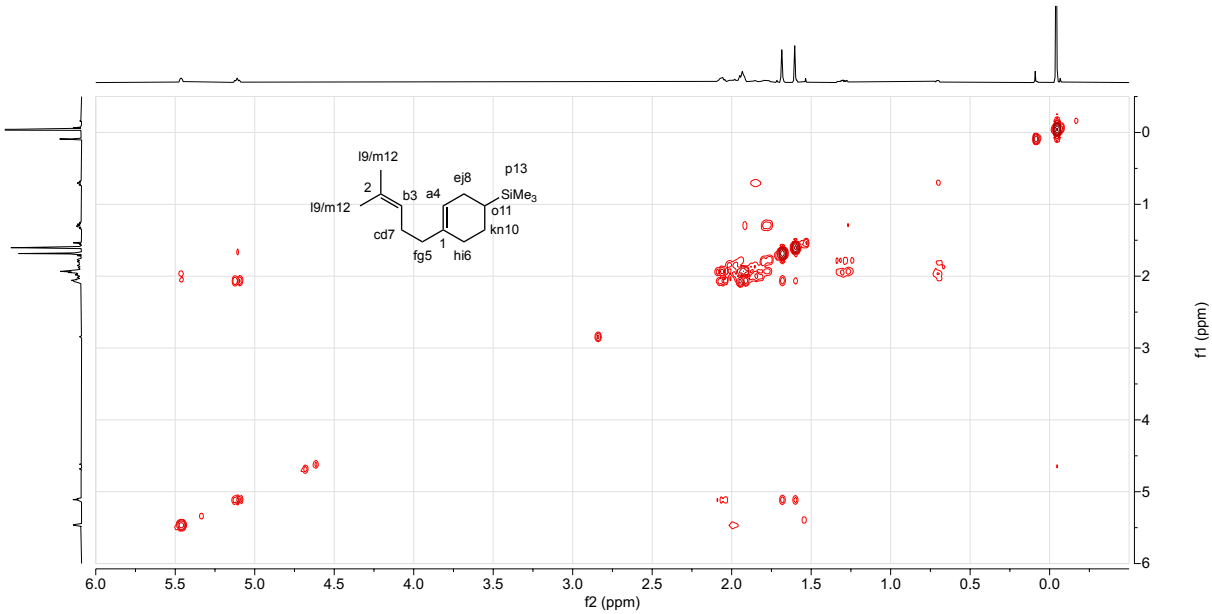

Figure S124. $^{1}H–^{1}H$ COSY (500 MHz, $CDCl_3$) spectrum of **18aj**.

Dimethyl(4-(4-methylpent-3-en-1-yl)cyclohex-3-en-1-yl)(phenyl)silane (18bj) was prepared in a 74% isolated yield with >98% [4+2]-selectivity, 62:38 after 70 hours as described in 3.2, with 2.5 mol% (^{Me}PDI)Fe(butadiene).

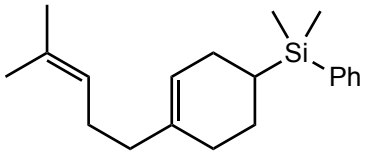

18bj

^{1}H NMR (500 MHz, $CDCl_3$) δ 7.60 – 7.43 (m, 2H), 7.43 – 7.31 (m, 3H), 5.43 (d, *J* = 3.5 Hz, 1H), 5.10 (tt, *J* = 7.1, 1.4 Hz, 1H), 2.18 – 1.75 (m, 9H), 1.68 (s, 3H), 1.59 (s, 3H), 1.32 (tdd, *J* = 13.0, 10.9, 5.5 Hz, 1H), 0.97 (dddd, *J* = 15.0, 12.9, 5.2, 2.4 Hz, 1H), 0.27 (s, 3H), 0.26 (s, 3H).

^{13}C NMR (126 MHz, $CDCl_3$) δ 138.54, 137.94, 134.09, 131.42, 128.94, 127.77, 124.63, 121.39, 38.25, 29.46, 26.61, 26.32, 25.85, 24.01, 20.99, 17.83, -4.95, -5.12.

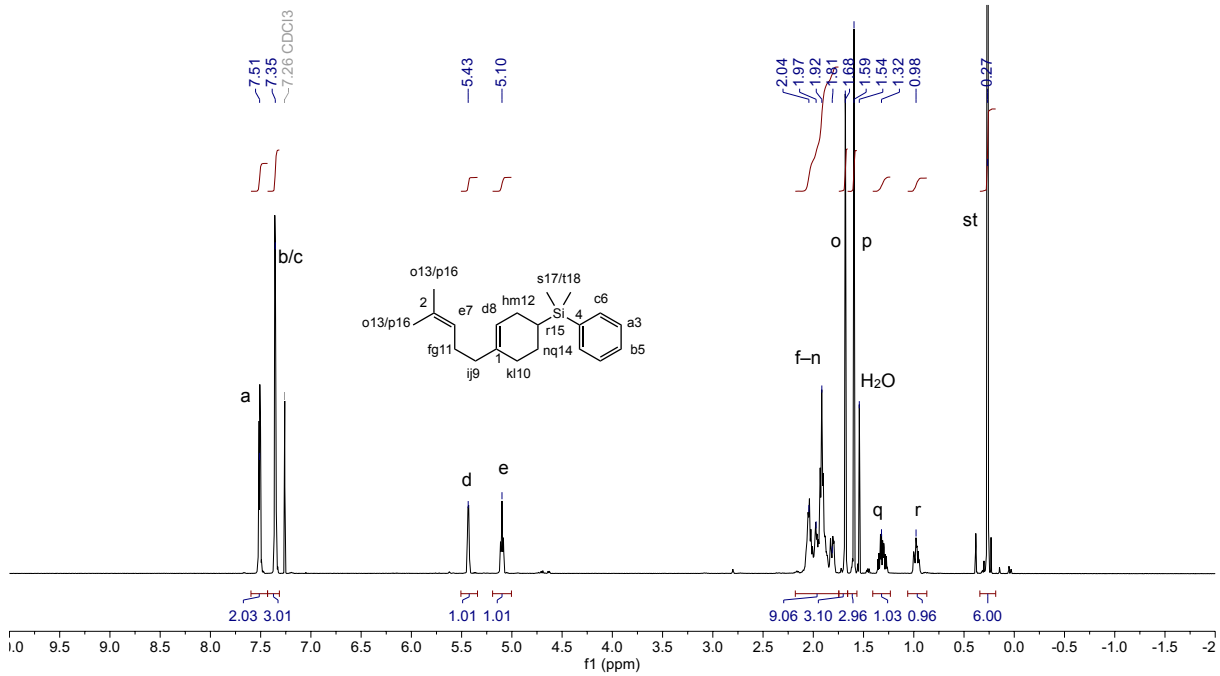

Figure S125. ^{1}H NMR (500 MHz, $CDCl_3$) spectrum of **18bj**.

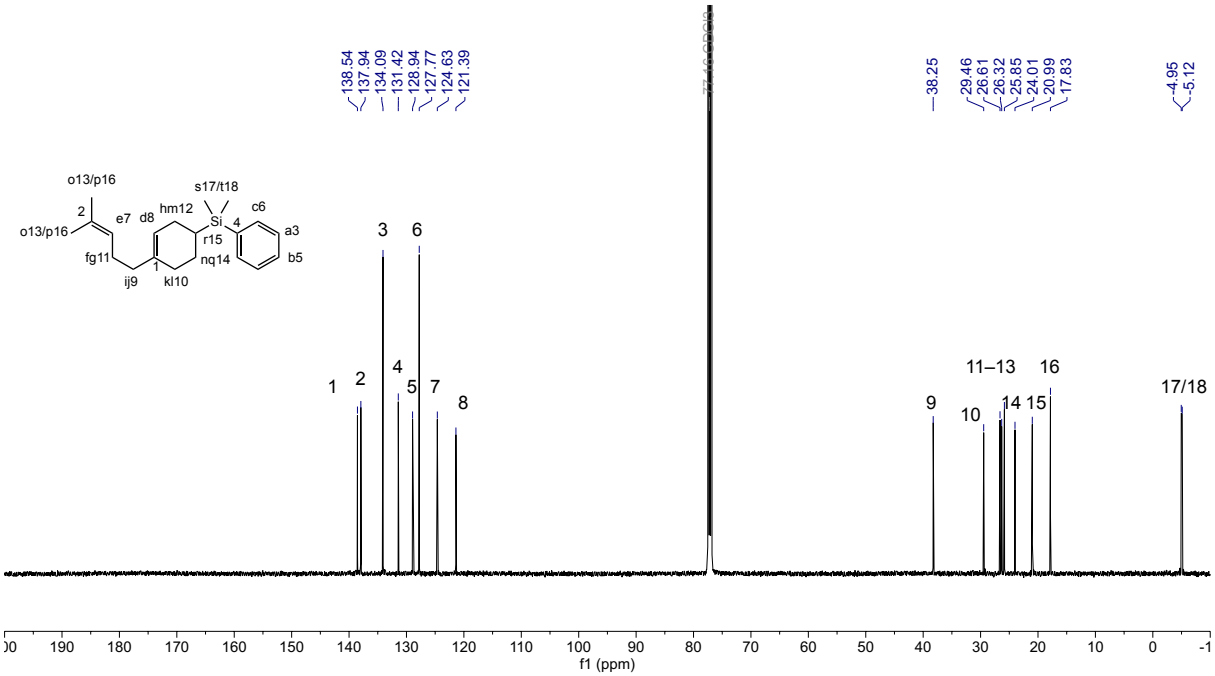

Figure S126. ^{13}C NMR (126 MHz, $CDCl_3$) spectrum of **18bj**.

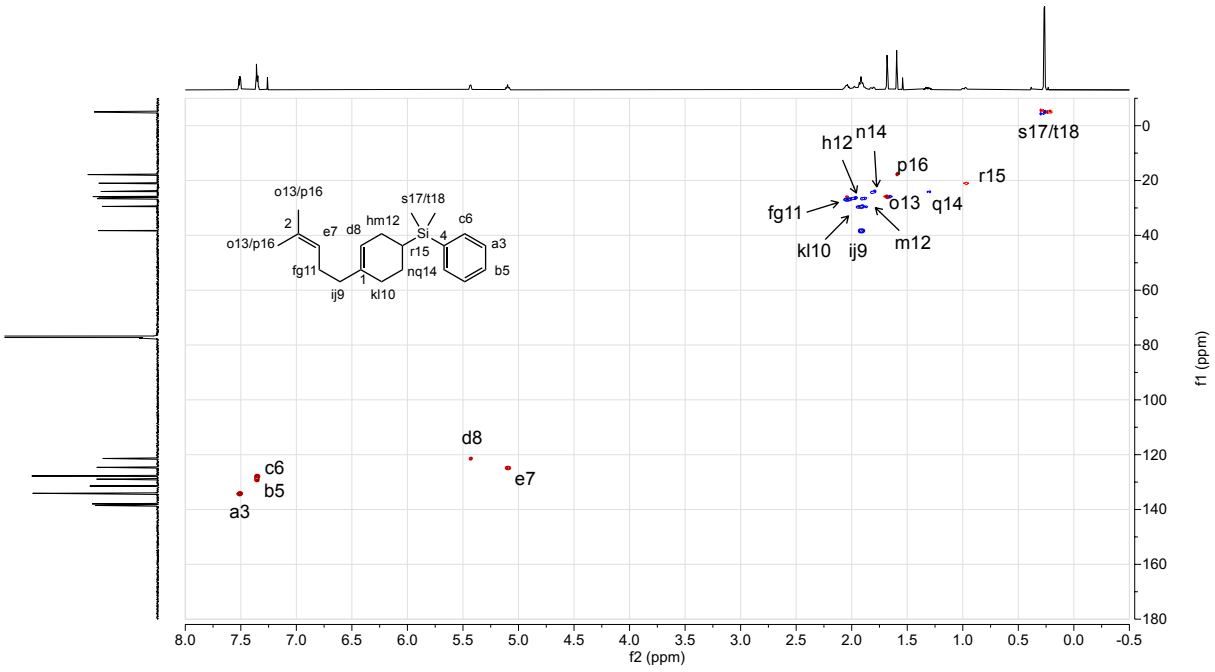

Figure S127. ^{1}H–^{13}C HSQC (500 MHz, $CDCl_3$) spectrum of **18bj**.

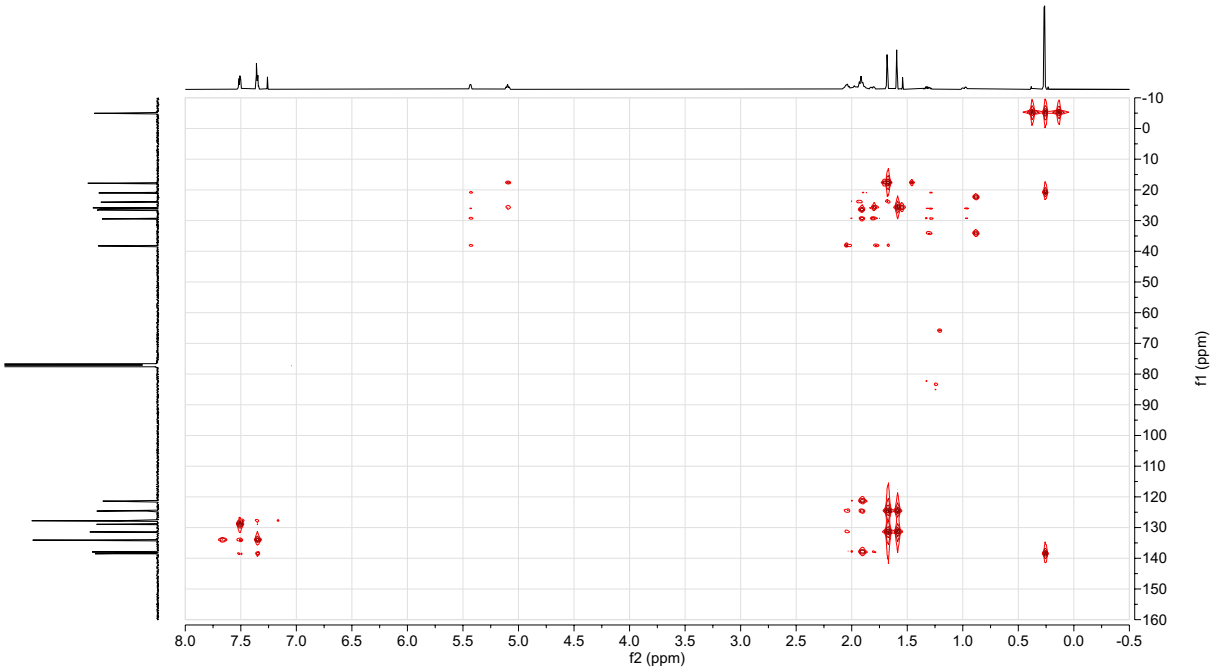

Figure S128. $^{1}H–^{13}C$ HMBC (500 MHz, $CDCl_3$) spectrum of **18bj**.

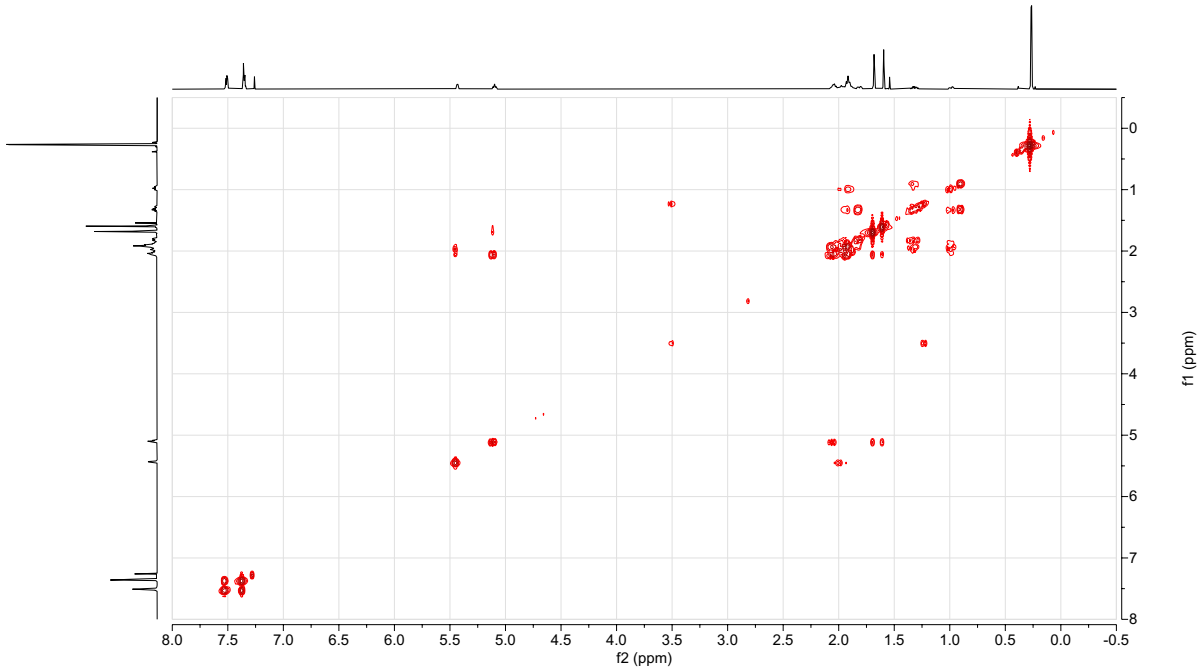

Figure S129. $^{1}H–^{1}H$ COSY (500 MHz, $CDCl_3$) spectrum of **18bj**.

(4-(4-methylpent-3-en-1-yl)cyclohex-3-en-1-yl)triphenylsilane (18cj) was prepared in a 56% isolated yield with 98% [4+2]-selectivity, after 70 hours as described in 3.2, with 2.5 mol% (^{Me}PDI)Fe(butadiene).

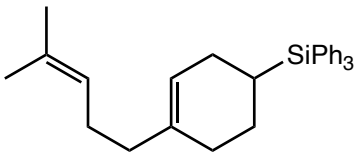

18cj

^{1}H NMR (500 MHz, $CDCl_3$) δ 7.57 (d, *J* = 6.4 Hz, 6H), 7.40 (t, *J* = 7.2 Hz, 3H), 7.39 – 7.32 (m, 6H), 5.44 (d, *J* = 5.0 Hz, 1H), 5.21 – 4.95 (m, 1H), 2.26 (d, *J* = 17.2 Hz, 1H), 2.17 – 1.97 (m, 5H), 1.98 – 1.85 (m, 3H), 1.77 (td, *J* = 11.5, 3.0 Hz, 1H), 1.68 (s, 3H), 1.59 (s, 3H), 1.53 – 1.35 (m, 1H).

^{13}C NMR (126 MHz, $CDCl_3$) δ 137.9, 136.2, 134.5, 131.5, 129.4, 127.9, 124.6, 121.4, 38.2, 29.7, 26.9, 26.6, 25.8, 24.8, 19.4, 17.8.

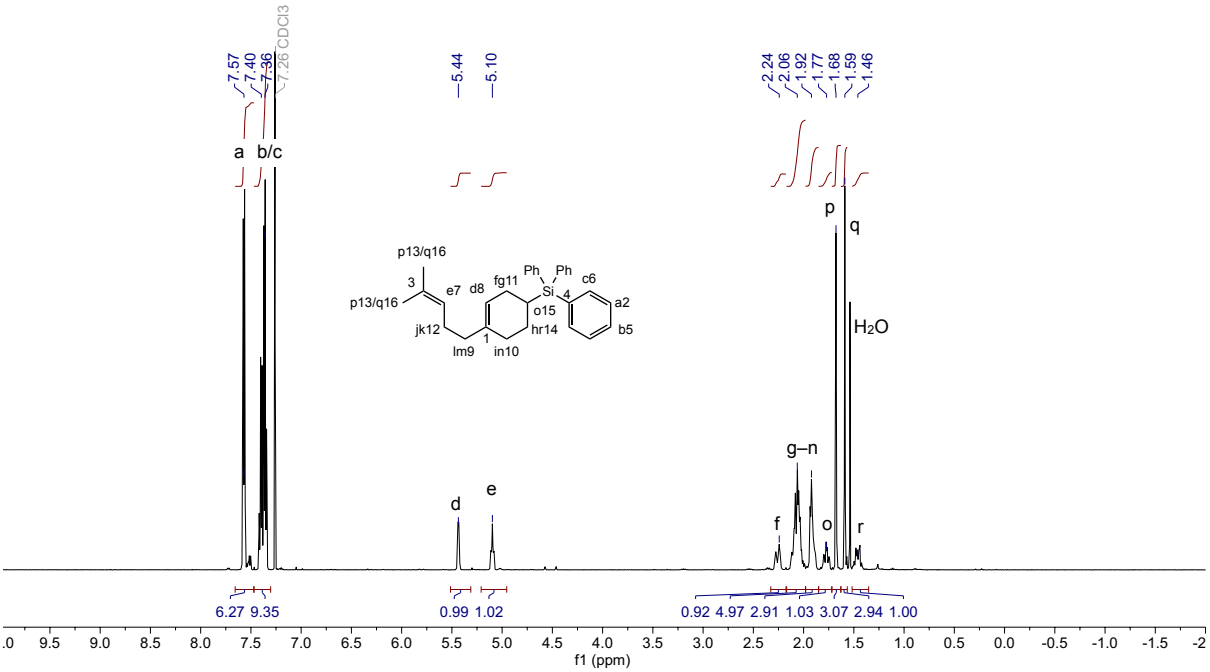

Figure S130. ^{1}H NMR (500 MHz, $CDCl_3$) spectrum of **18cj**.

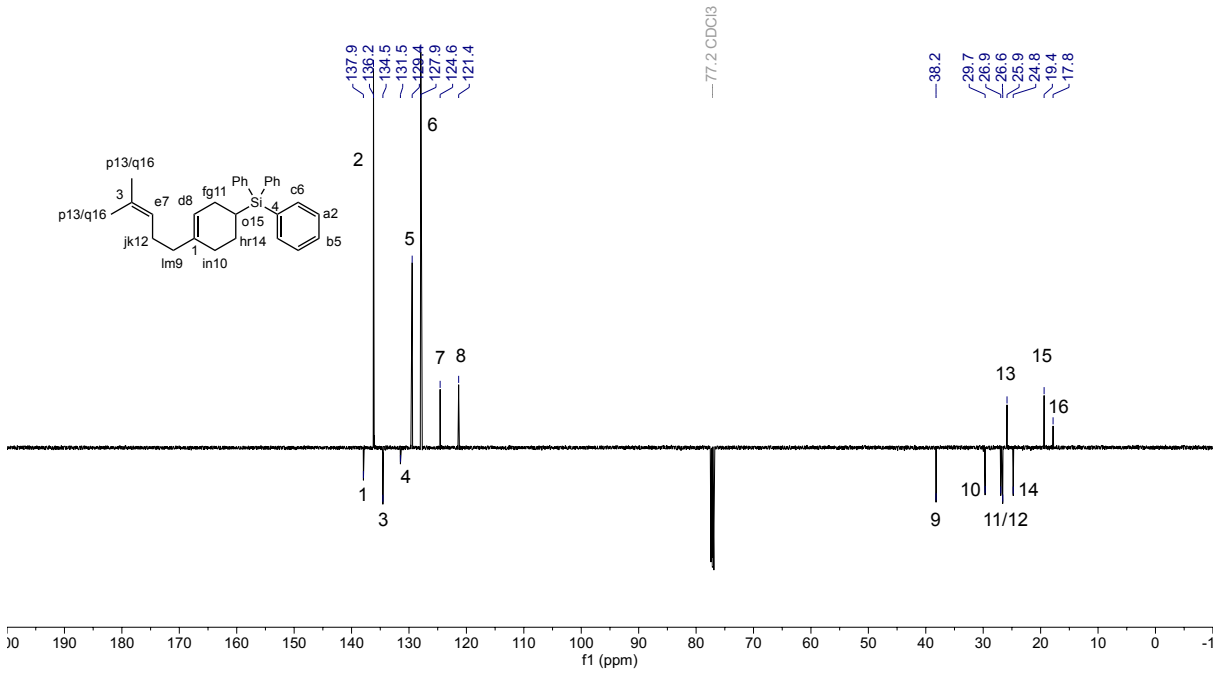

Figure S131. ^{13}C NMR (126 MHz, $CDCl_3$) spectrum of **18cj**.

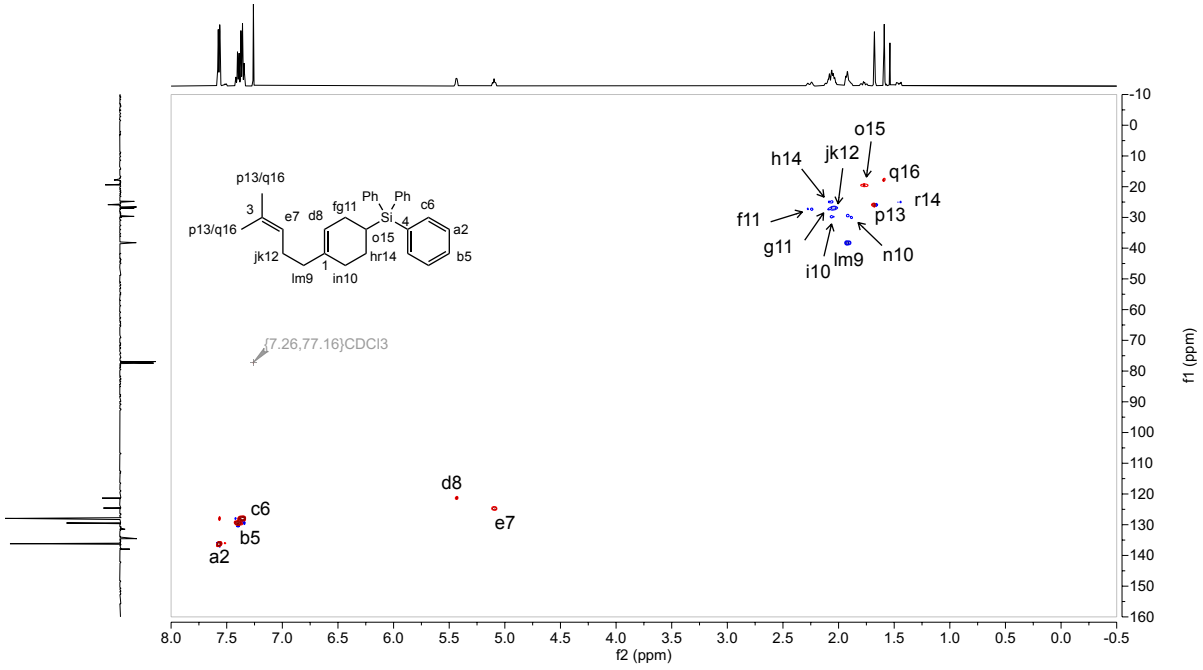

Figure S132. ^{1}H–^{13}C HSQC (500 MHz, $CDCl_3$) spectrum of **18cj**.

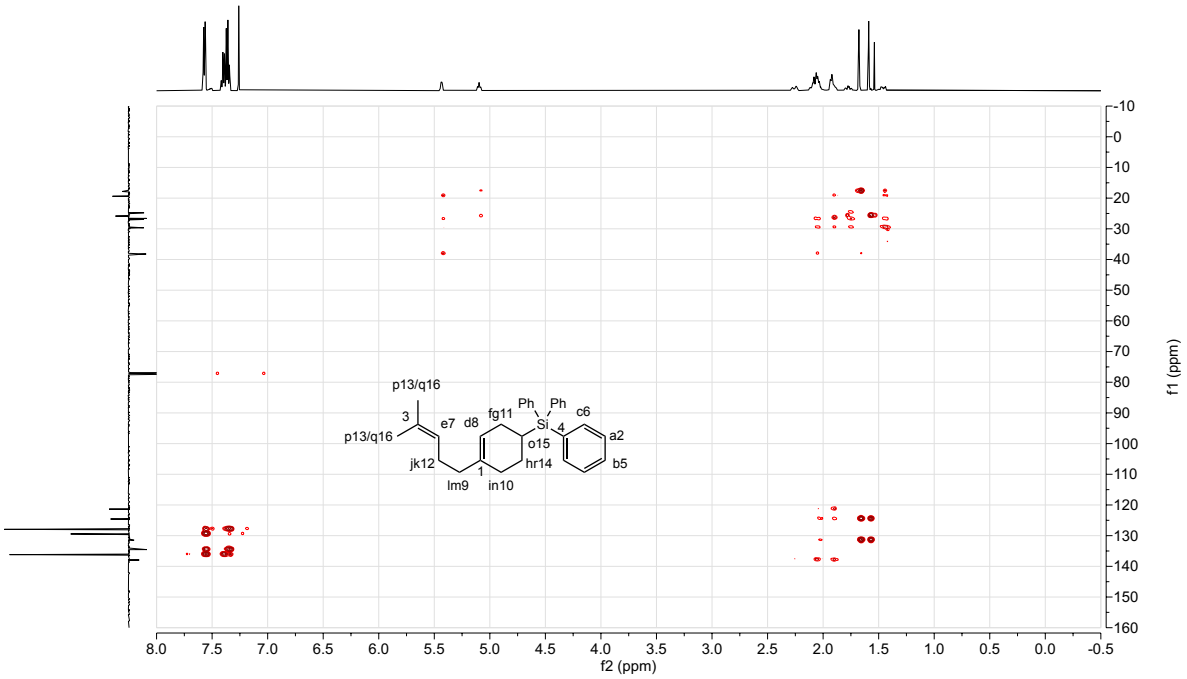

Figure S133. $^{1}H–^{13}C$ HMBC (500 MHz, $CDCl_3$) spectrum of **18cj**.

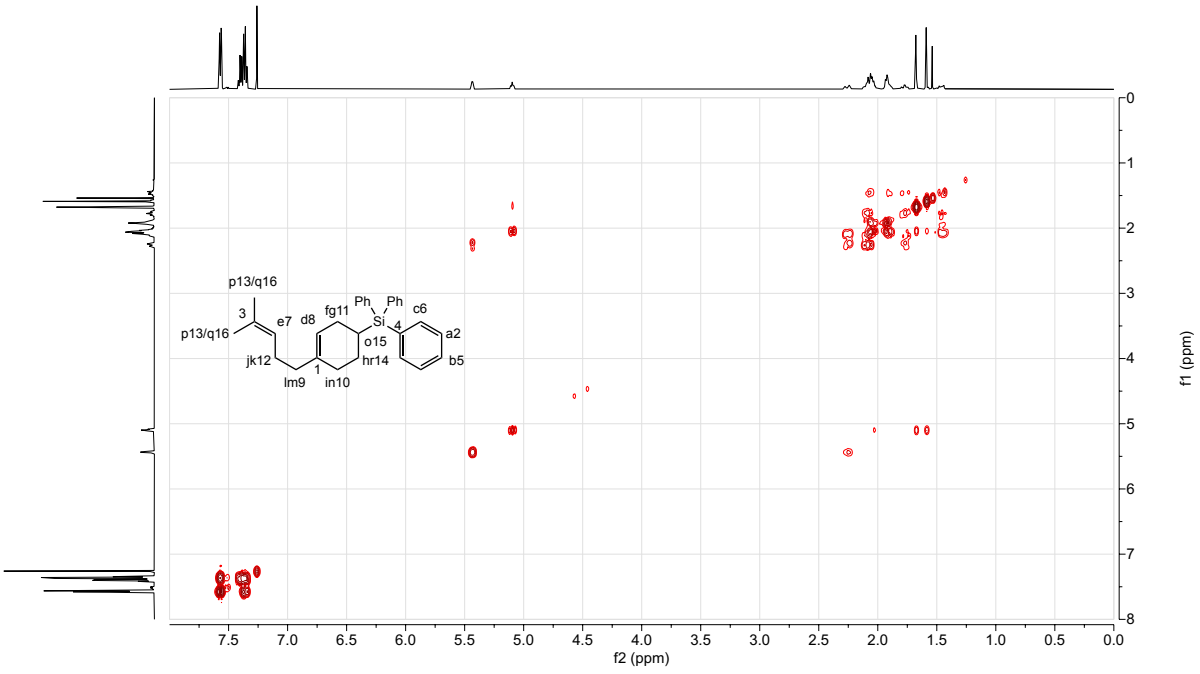

Figure S134. $^{1}H–^{1}H$ COSY (500 MHz, $CDCl_3$) spectrum of **18cj**.

Diethoxy(methyl)(4-(4-methylpent-3-en-1-yl)cyclohex-3-en-1-yl)silane (18dj) and **(*E*)-(5,9-dimethyldeca-1,4,8-trien-2-yl)diethoxy(methyl)silane** (**19dj**)

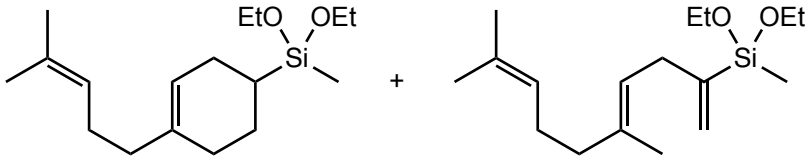

18dj **19dj**

were prepared as a mixture in a 74% combined isolated yield with 84% [4+2]-selectivity for **18dj** and 10% selectivity for hydroalkenylation product **19dj** after 72 hours as described in 3.2, with 1 mol% (^{Me}PDI)Fe(butadiene).

^{1}H NMR (500 MHz, $CDCl_3$) δ 5.44 (d, *J* = 3.6 Hz, 1H), 5.10 (tt, *J* = 7.0, 1.5 Hz, 1H), 3.78 (q, *J* = 7.0 Hz, 2H), 3.77 (q, *J* = 7.0 Hz, 2H), 2.18 – 1.77 (m, 9H), 1.67 (s, 3H), 1.59 (s, 3H), 1.39 (tdd, *J* = 12.9, 10.6, 5.7 Hz, 1H), 1.21 (t, *J* = 7.0 Hz, 3H), 1.21 (t, *J* = 7.0 Hz, 3H), 0.93 (tdd, *J* = 11.4, 5.6, 2.4 Hz, 1H), 0.07 (s, 3H).

^{13}C NMR (126 MHz, $CDCl_3$) δ 137.9, 131.4, 124.6, 121.1, 58.4, 58.3, 38.3, 29.1, 26.6, 25.8, 25.4, 23.3, 20.2, 18.6, 17.8, -6.9.

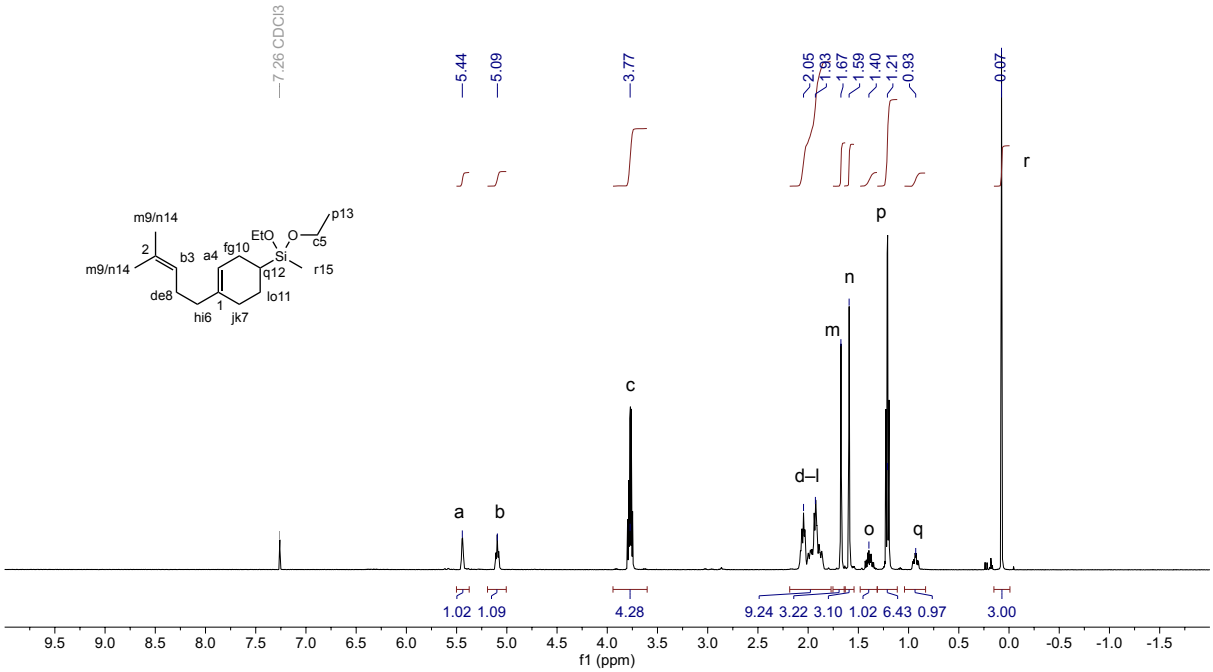

Figure S135. ^{1}H NMR (500 MHz, $CDCl_3$) spectrum of **18dj** and **19dj**.

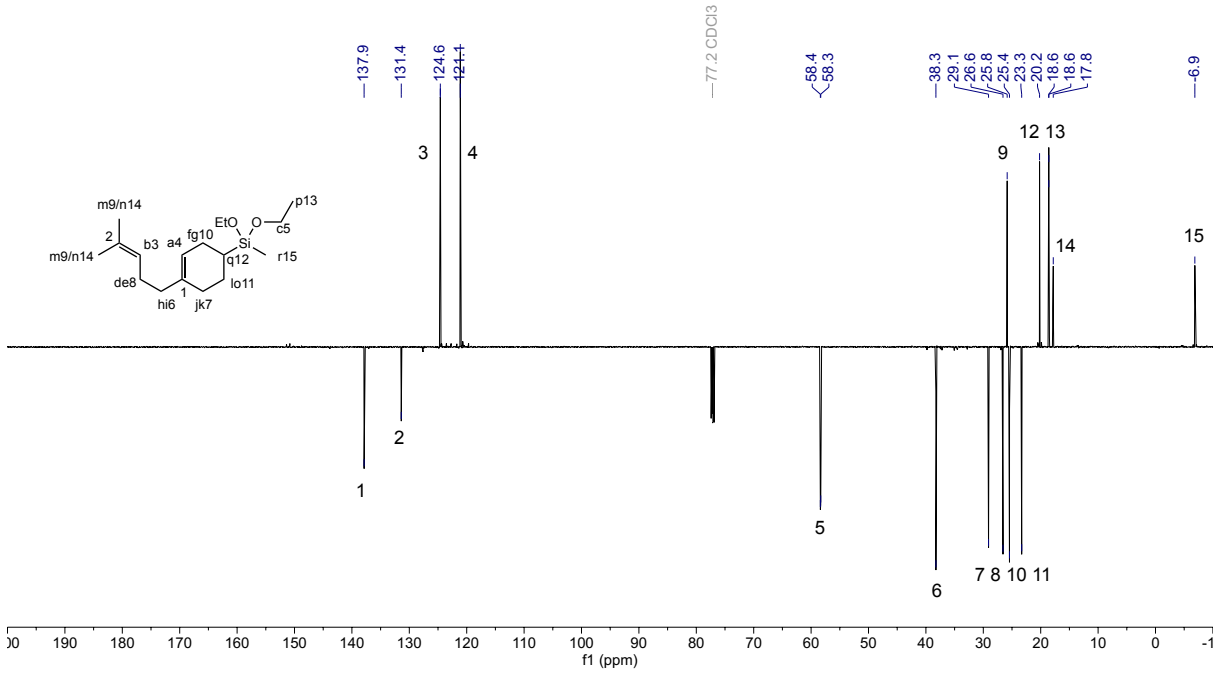

Figure S136. ^{13}C NMR (126 MHz, $CDCl_3$) spectrum of **18dj** and **19dj**.

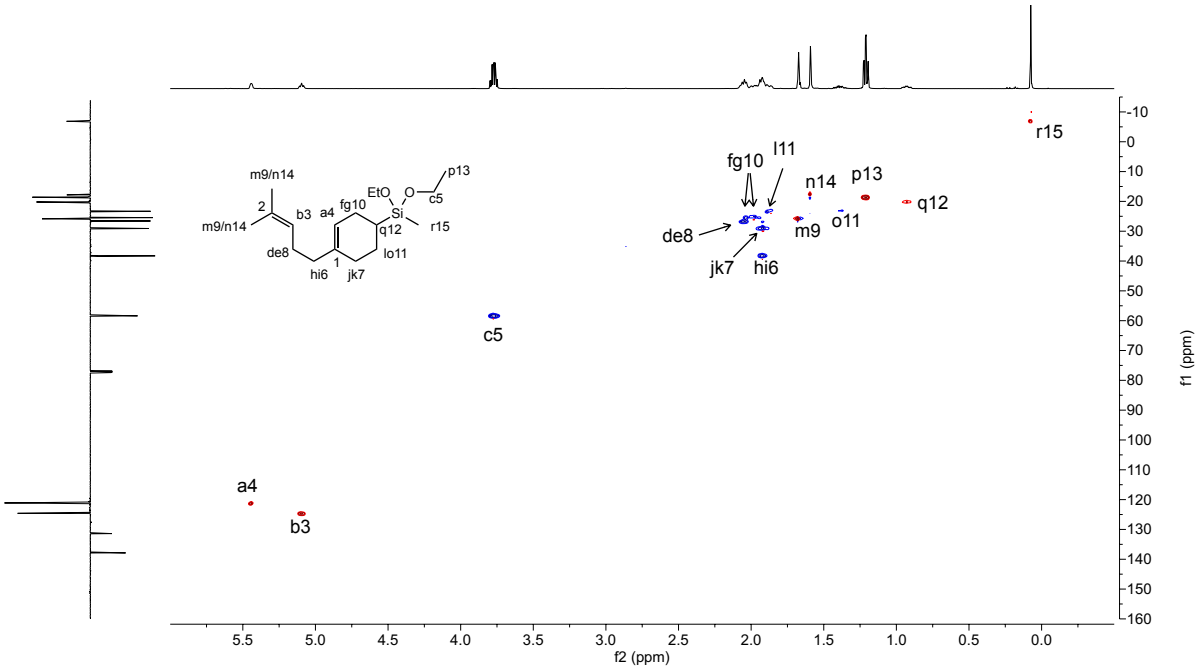

Figure S137. ^{1}H–^{13}C HSQC (500 MHz, $CDCl_3$) spectrum of **18dj** and **19dj**.

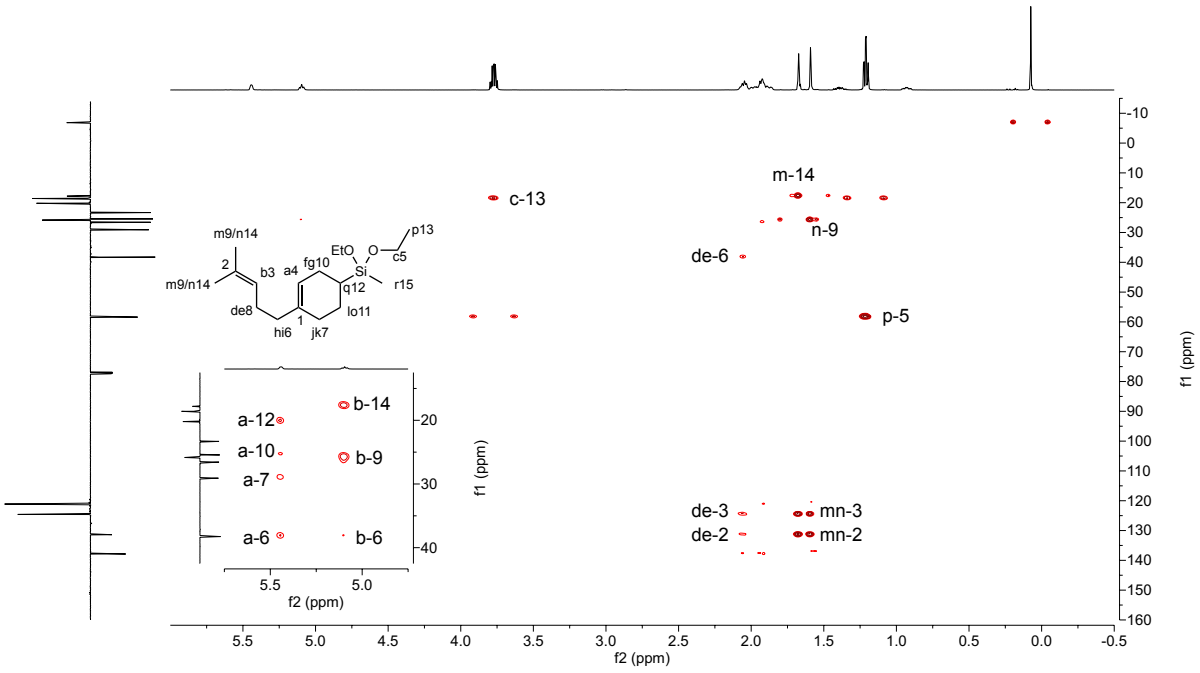

Figure S138. $^{1}H–^{13}C$ HMBC (500 MHz, $CDCl_3$) spectrum of **18dj** and **19dj**.

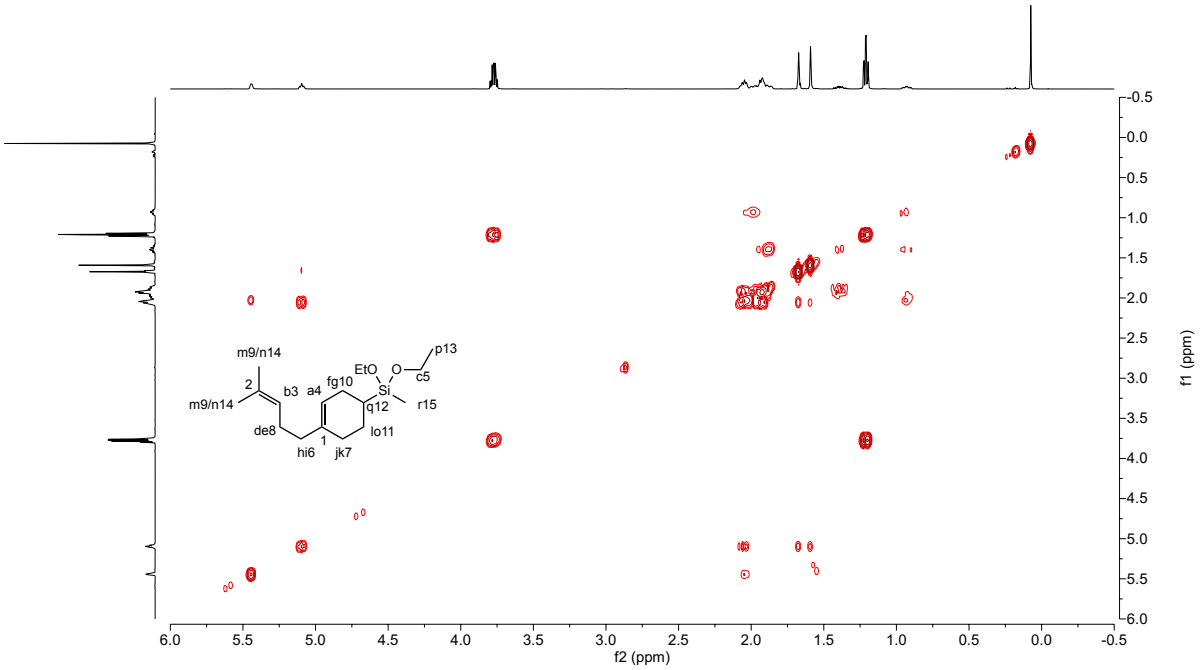

Figure S139. $^{1}H–^{1}H$ COSY (500 MHz, $CDCl_3$) spectrum of **18dj** and **19dj**.

1,1,1,3,5,5,5-heptamethyl-3-(4-(4-methylpent-3-en-1-yl)cyclohex-3-en-1-yl)trisiloxane (**18ej**) and **(*E*)-3-(5,9-dimethyldeca-1,4,8-trien-2-yl)-1,1,1,3,5,5,5-heptamethyltrisiloxane** (**19ej**) were prepared as a mixture in a 74% isolated yield with 77% [4+2]-selectivity for **18ej** and 12% selectivity for hydroalkenylation product **19ej** after 72 hours as described in 3.2, with 2 mol% (^{Me}PDI)Fe(butadiene).

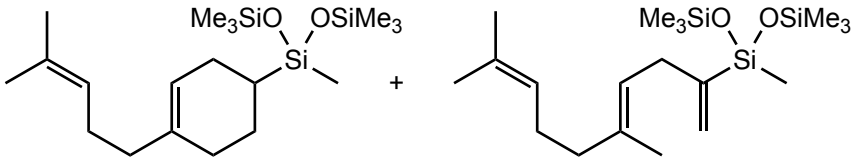

18ej **19ej**

Triethoxy(4-(4-methylpent-3-en-1-yl)cyclohex-3-en-1-yl)silane (18fj) was prepared in a 32% isolated yield with 81% [4+2]-selectivity for **18fj** after 72 hours as described in 3.2, with 5 mol% (^{Me}PDI)Fe(N_2)$_{1.5}$.

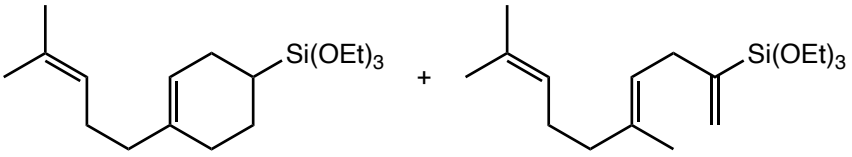

18fj **19fj**

^{1}H NMR (500 MHz, $CDCl_3$) δ 5.44 (s, 1H), 5.10 (t, *J* = 7.2 Hz, 1H), 3.83 (q, *J* = 7.0 Hz, 6H), 2.14 – 1.99 (m, 4H), 1.99 – 1.84 (m, 5H), 1.67 (s, 3H), 1.60 (s, 3H), 1.53 – 1.42 (m, 1H), 1.23 (t, *J* = 7.0 Hz, 9H), 0.96 (dtd, *J* = 12.5, 9.8, 7.8, 2.0 Hz, 1H)

^{13}C NMR (126 MHz, $CDCl_3$) δ 137.8, 131.4, 124.7, 121.1, 58.6, 38.3, 29.1, 26.6, 25.8, 25.6, 23.4, 18.5, 18.2, 17.8

((4*E*)-5,9-dimethyldeca-1,4,8-trien-1-yl)triethoxysilane (19fj) was prepared in a 27% isolated yield with 69% purity as in the procedure above.

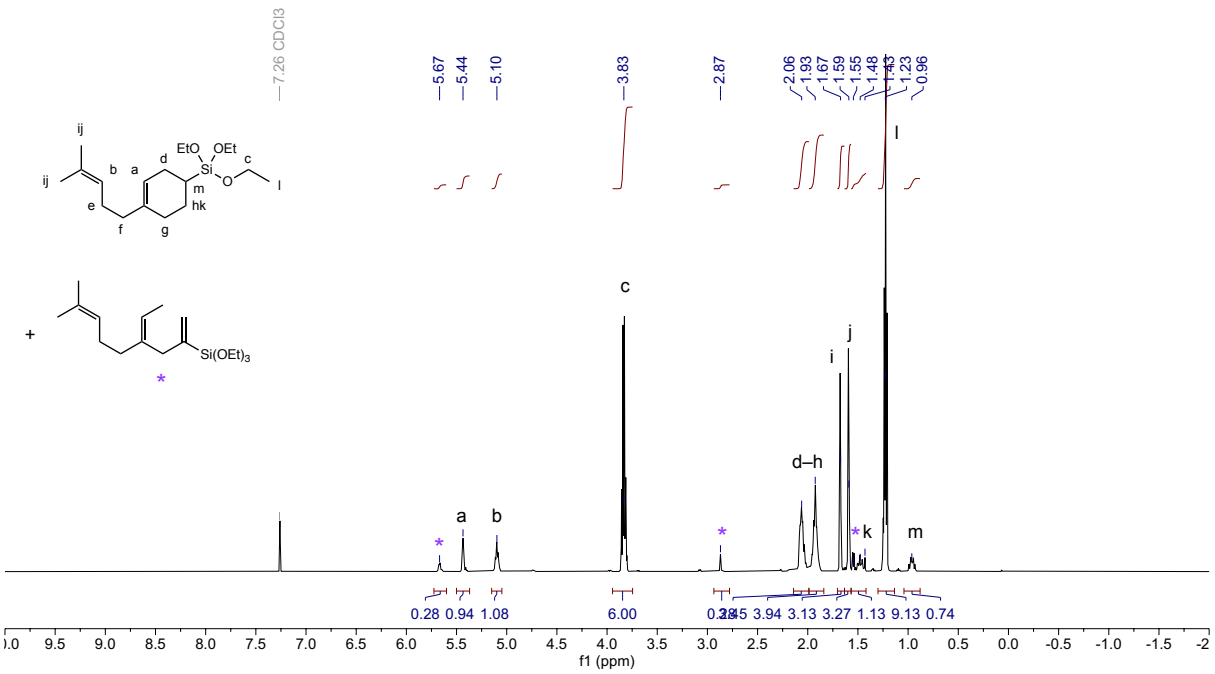

Figure S140. ^{1}H NMR (500 MHz, $CDCl_3$) spectrum of **18fj**.

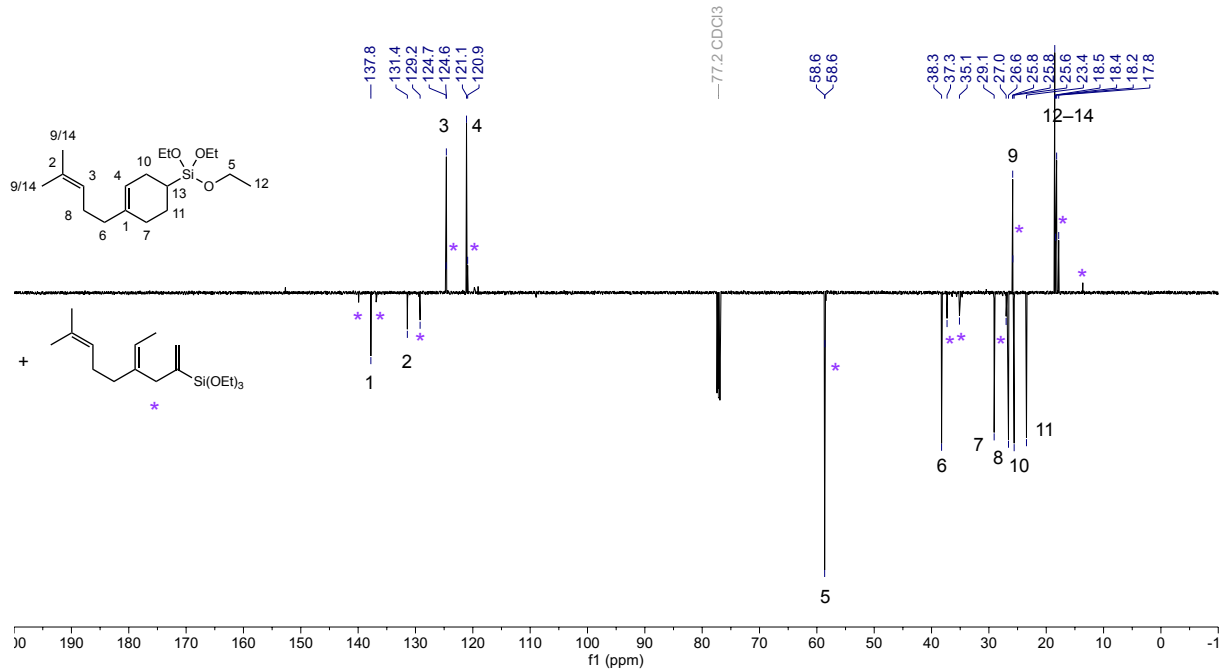

Figure S141. ^{13}C NMR (126 MHz, $CDCl_3$) spectrum of **18fj**.

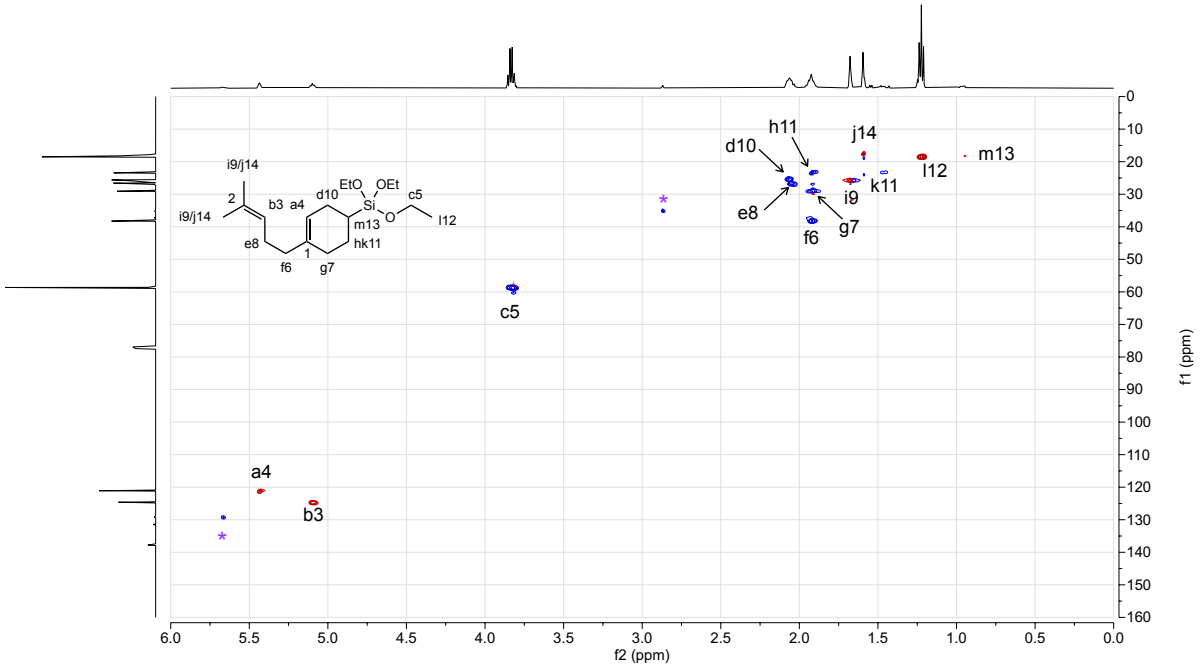

Figure S142. $^{1}H–^{13}C$ HSQC (500 MHz, $CDCl_3$) spectrum of **18fj**.

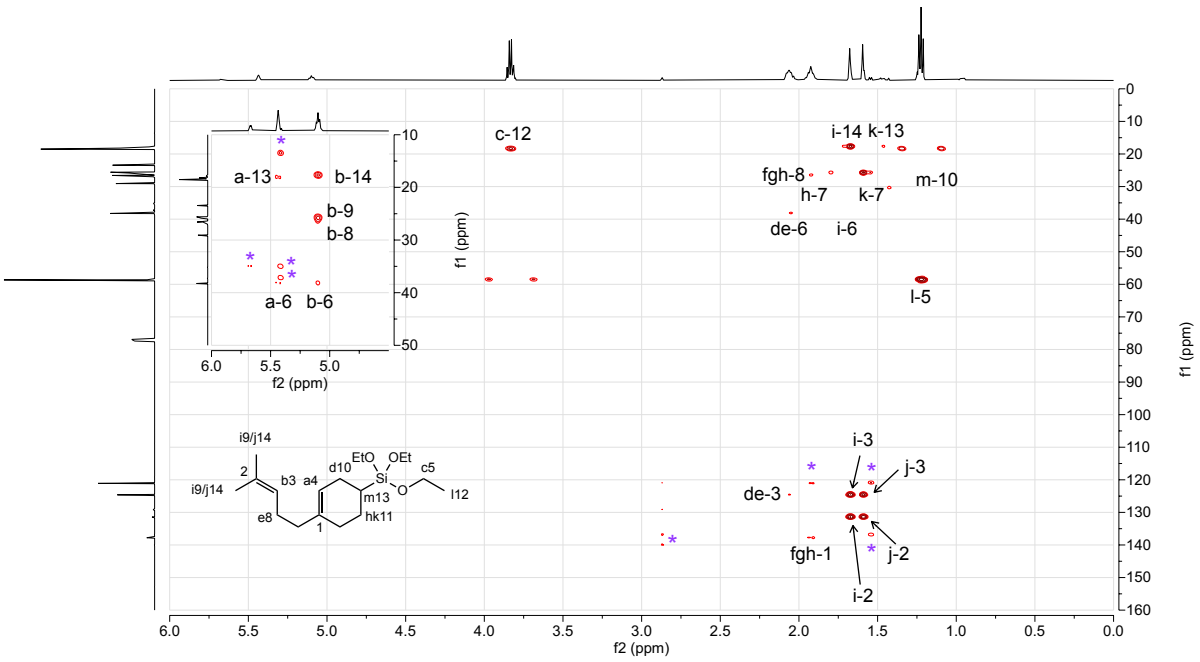

Figure S143. $^{1}H–^{13}C$ HMBC (500 MHz, $CDCl_3$) spectrum of **18fj**.

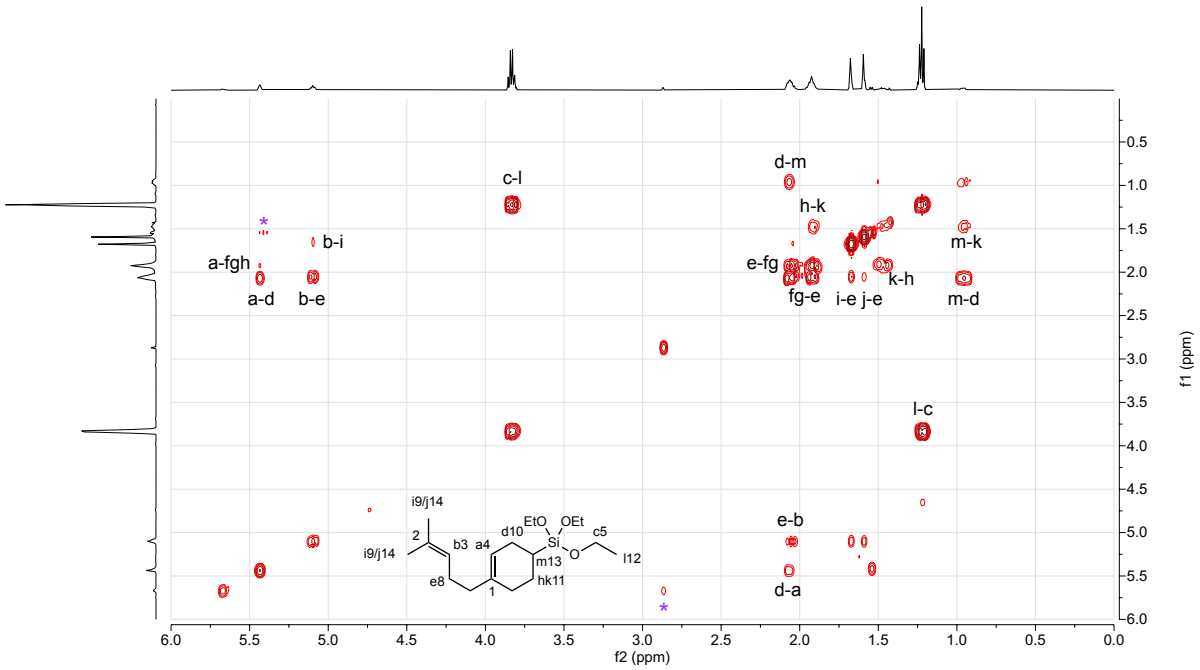

Figure S144. ^{1}H–^{1}H COSY (500 MHz, $CDCl_3$) spectrum of **18fj**.

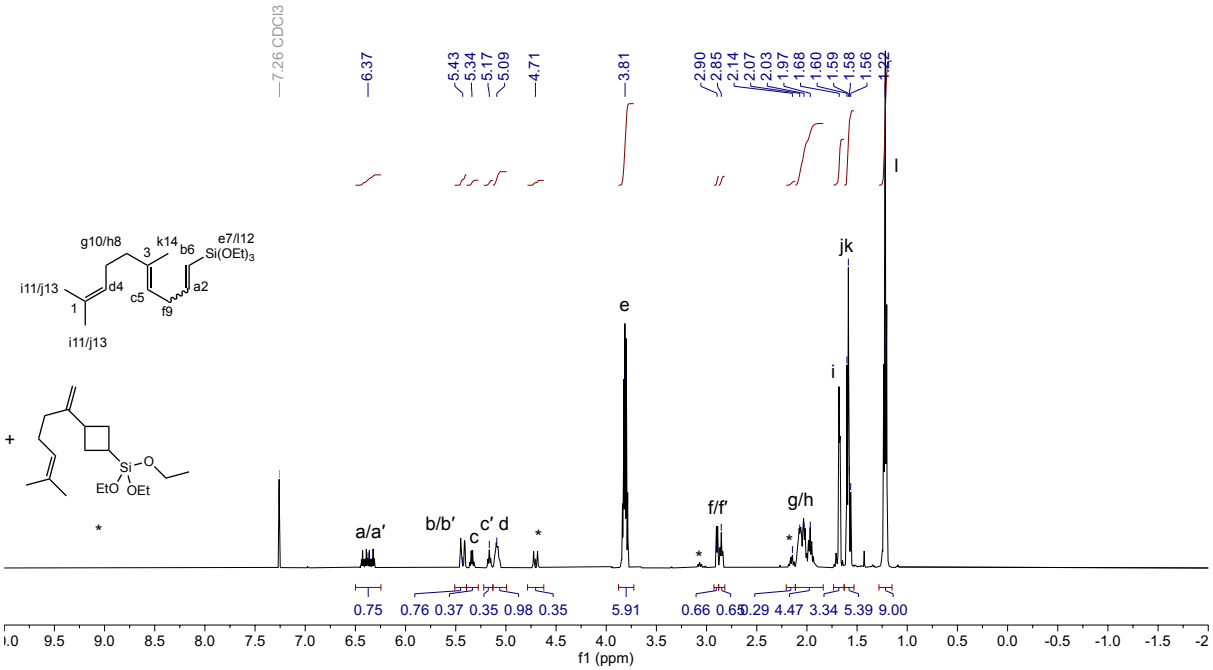

Figure S145. ^{1}H NMR (500 MHz, $CDCl_3$) spectrum of **19fj**.

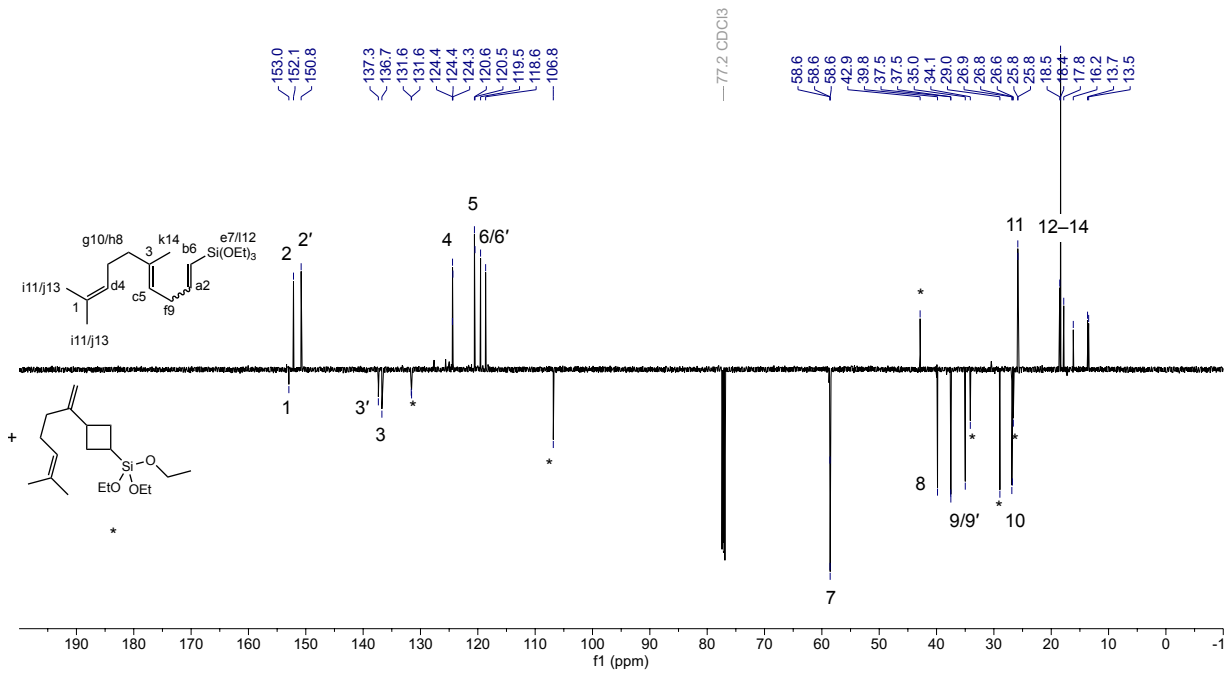

Figure S146. ^{13}C NMR (126 MHz, $CDCl_3$) spectrum of **19fj**.

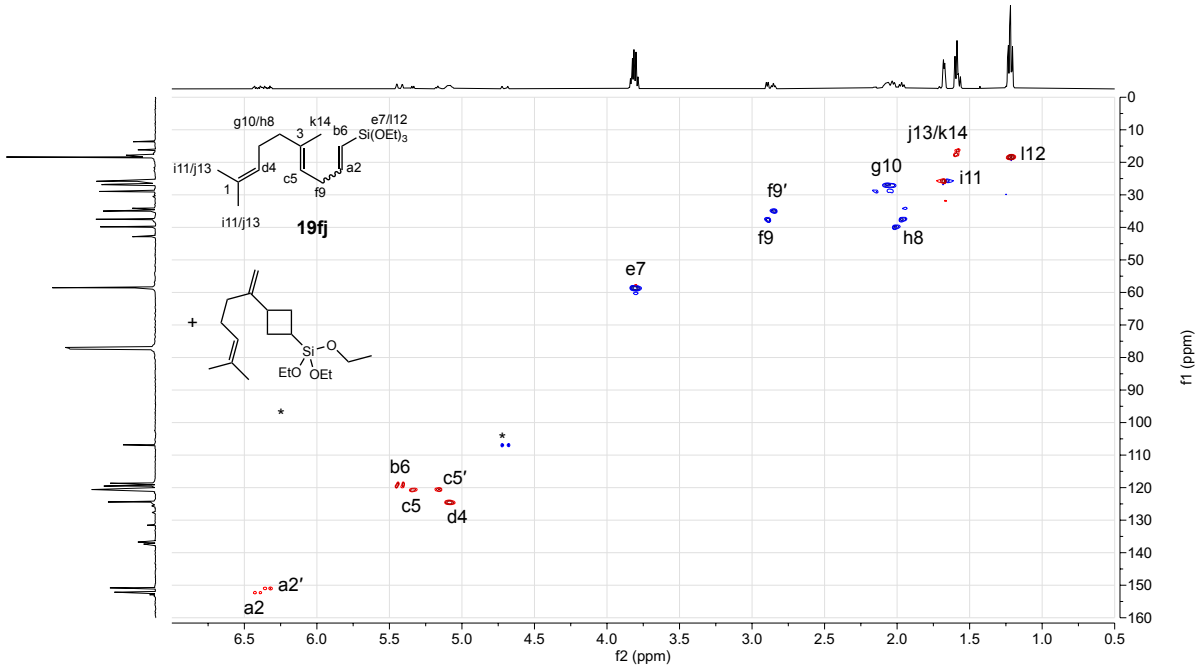

Figure S147. ^{1}H–^{13}C HSQC (500 MHz, $CDCl_3$) spectrum of **19fj**.

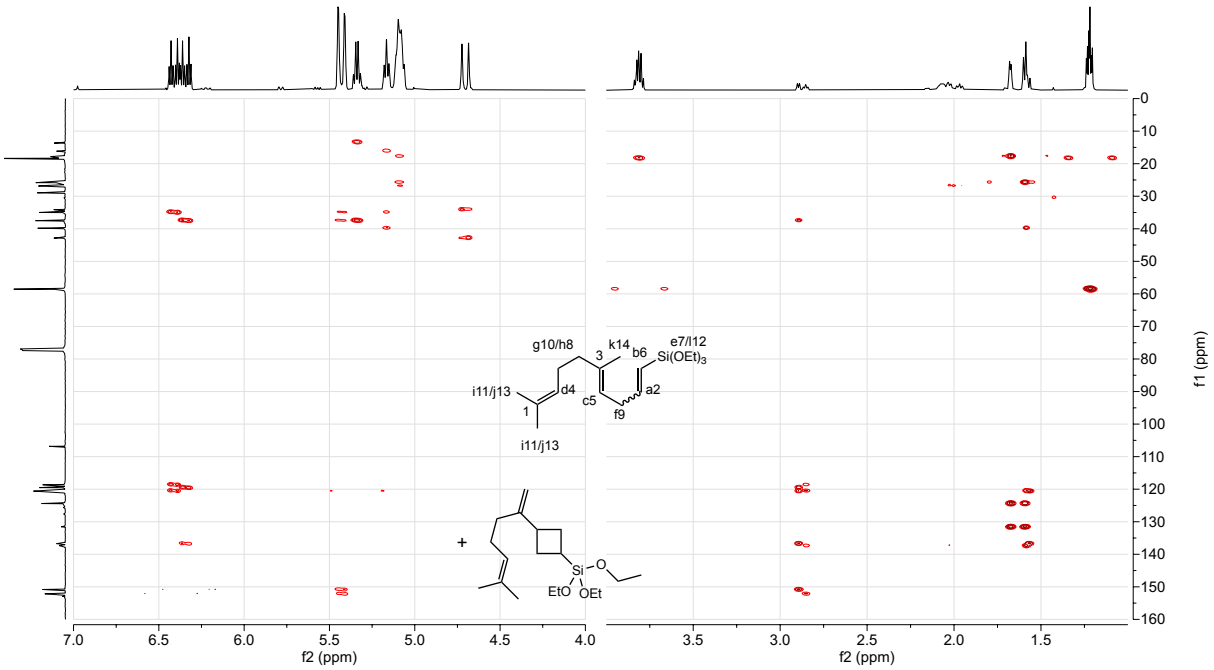

Figure S148. $^{1}H–^{13}C$ HMBC (500 MHz, $CDCl_3$) spectrum of **19fj**.

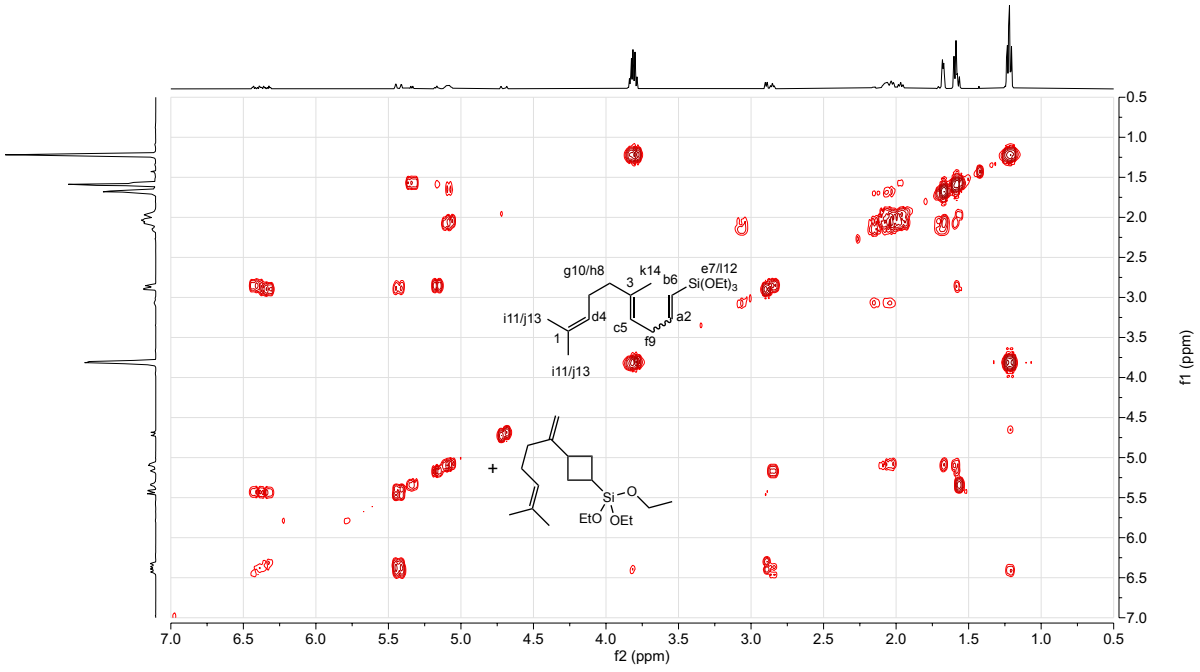

Figure S149. $^{1}H–^{1}H$ COSY (500 MHz, $CDCl_3$) spectrum of **19fj**.

1,1,3,3-tetramethyl-1,3-bis(4-(4-methylpent-3-en-1-yl)cyclohex-3-en-1-yl)disiloxane (18gj) was prepared as a mixture in 84% isolated yield with 74% [4+2]-selectivity for **18gj** after 24 hours as described in 3.2, with 2 mol% (^{Me}PDI)Fe(N_2)$_{1.5}$.

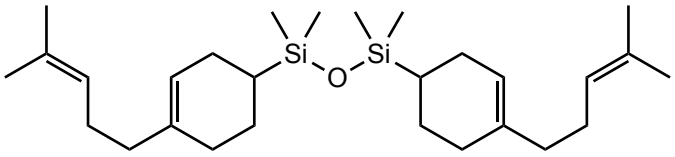

18gj

^{1}H NMR (500 MHz, $CDCl_3$) δ 5.46 (m, 1H), 5.11 (m, 1H), 2.10-1.73 (m, 9H), 1.61 (m, 3H), 1.53 (m, 3H), 1.30 (m, 1H), 0.72 (m, 1H), 0.05 (s, 6H) , -0.03 (s, 6H)

^{13}C NMR (126 MHz, $CDCl_3$) δ 148.39, 148.24, 137.94, 137.93, 137.41, 137.37, 131.42, 131.37, 124.70, 124.68, 124.67, 124.44, 124.25, 121.45, 121.39, 120.44, 120.40, 38.30, 37.39, 34.79, 29.42, 29.38, 27.01, 26.63, 25.87, 25.85, 25.61, 25.60, 23.41, 23.39, 23.10, 23.09, 17.84, 17.82, 13.67, 0.41, 0.35, -1.33, -1.38, -1.45, -1.53.

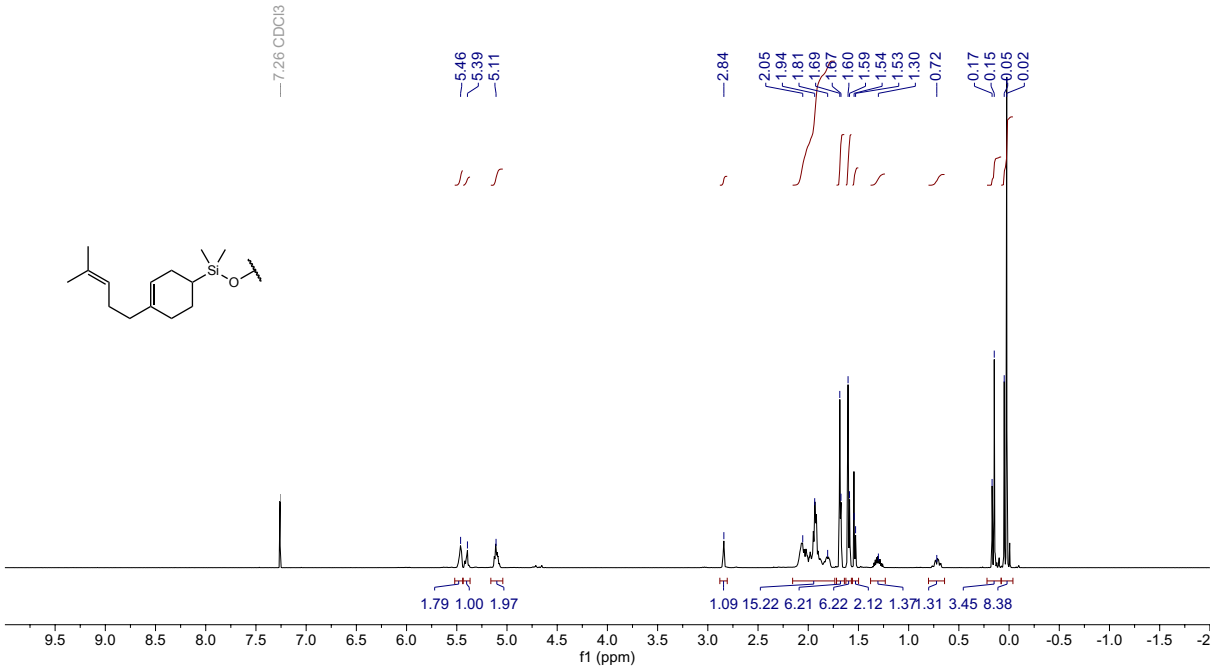

Figure S150. ^{1}H NMR (500 MHz, $CDCl_3$) spectrum of **18gj and 19gj**.

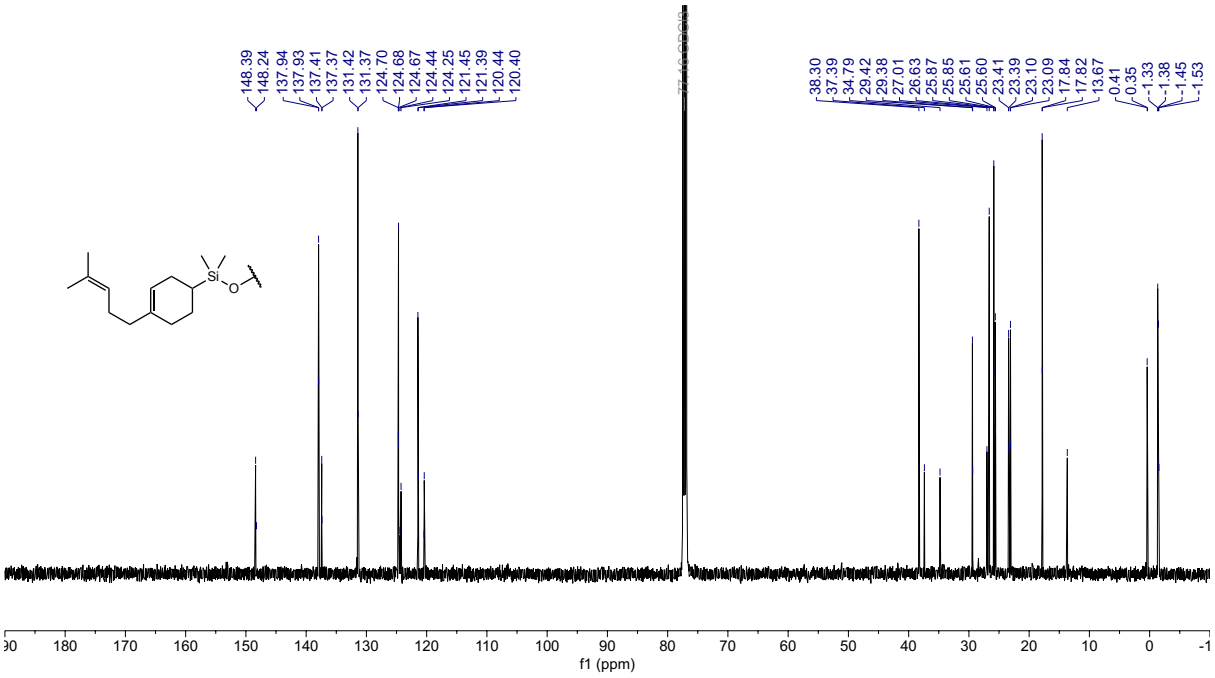

Figure S151. ^{13}C NMR (126 MHz, $CDCl_3$) spectrum of **18gj**.

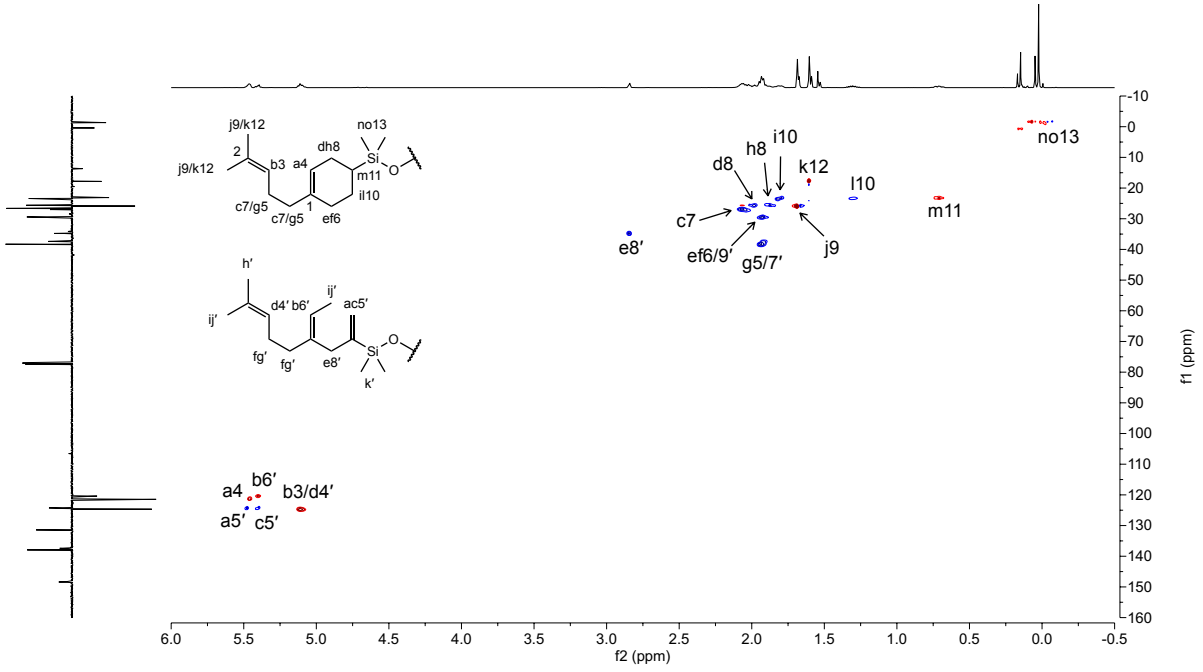

Figure S152. ^{1}H–^{13}C HSQC (500 MHz, $CDCl_3$) spectrum of **18gj**.

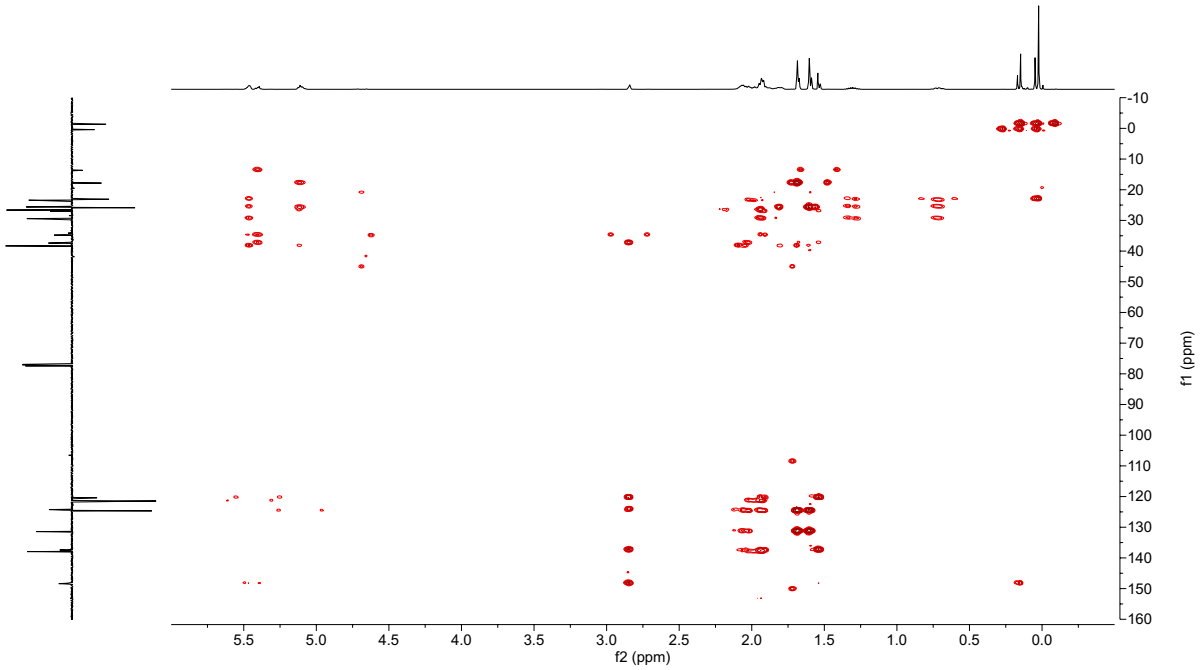

Figure S153. $^{1}H–^{13}C$ HMBC (500 MHz, $CDCl_3$) spectrum of **18gj**.

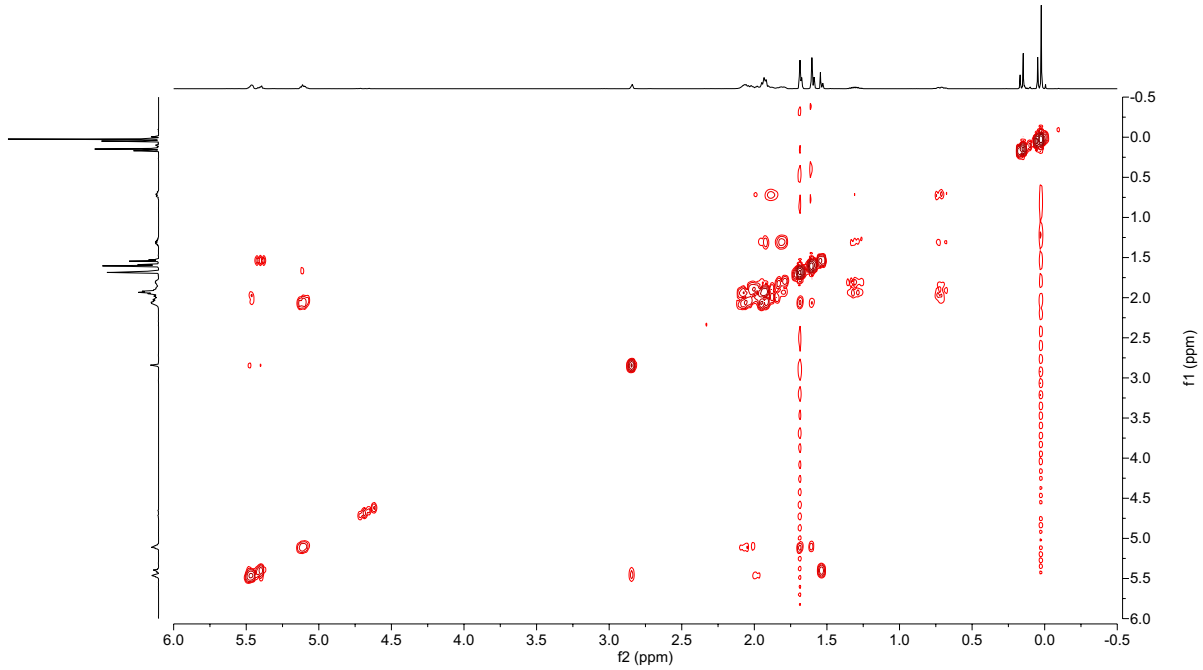

Figure S154. $^{1}H–^{1}H$ COSY (500 MHz, $CDCl_3$) spectrum of **18gj**.

trimethyl(4-methylcyclohex-3-en-1-yl)silane (18ai) was prepared in a 74% isolated yield with 90% [4+2]-selectivity, after 30 hours as described in 3.2, with 2.5 mol% (^{Me}PDI)Fe(butadiene).

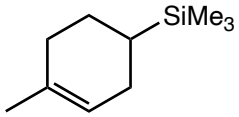

18ai

^{1}H NMR (500 MHz, $CDCl_3$) δ 5.43 (m, 1H), 2.01-1.70 (m, 5H), 1.64 (s, 3H), 1.31 (m, 1H), 0.69 (m, 1H), 0.09 (m, 1H), 0.04 (s, 9H).

^{13}C NMR (126 MHz, $CDCl_3$) δ 134.27, 121.90, 31.11, 26.24, 24.11, 23.92, 21.07, -3.44.

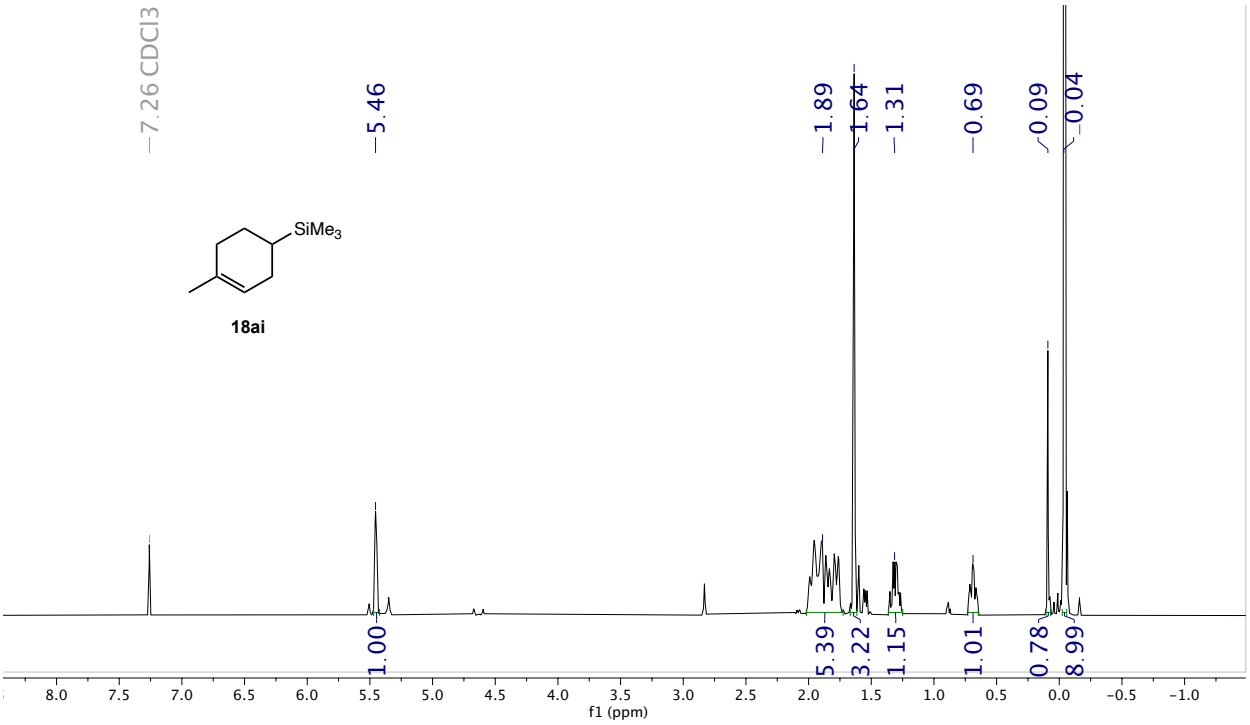

Figure S155. ^{1}H NMR (500 MHz, $CDCl_3$) spectrum of **18ai**.

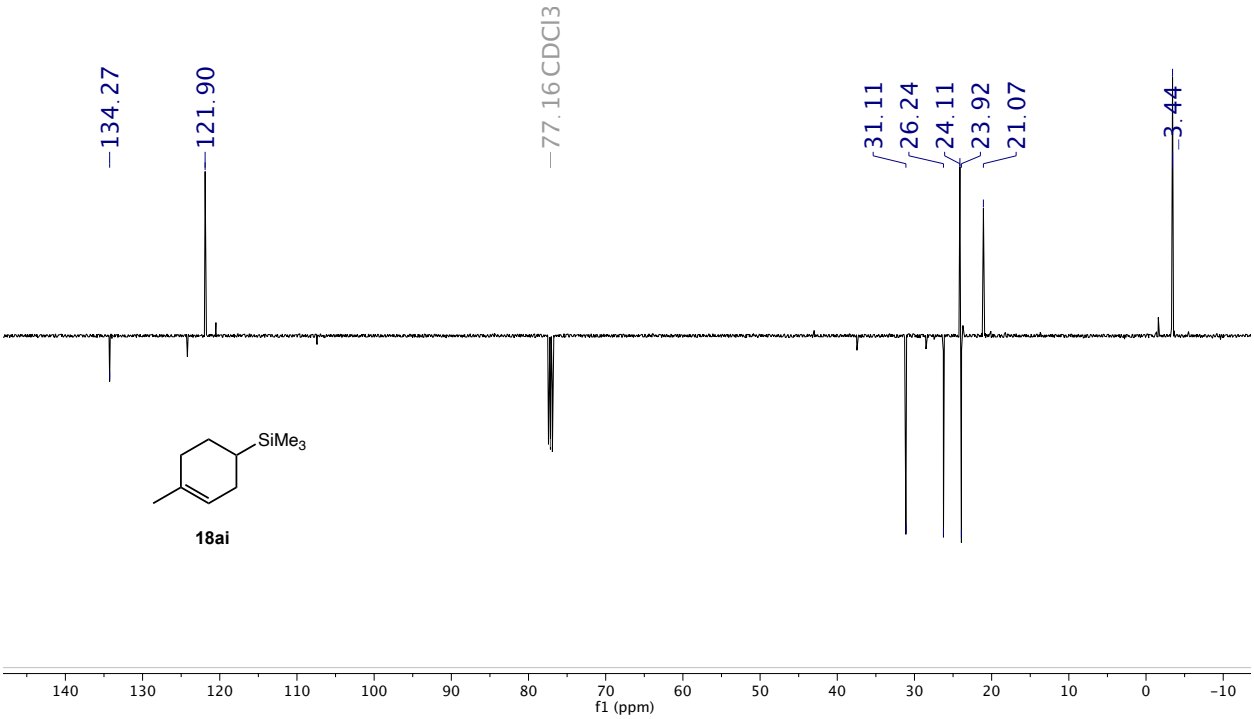

Figure S156. ^{13}C NMR (126 MHz, $CDCl_3$) spectrum of **18ai**.

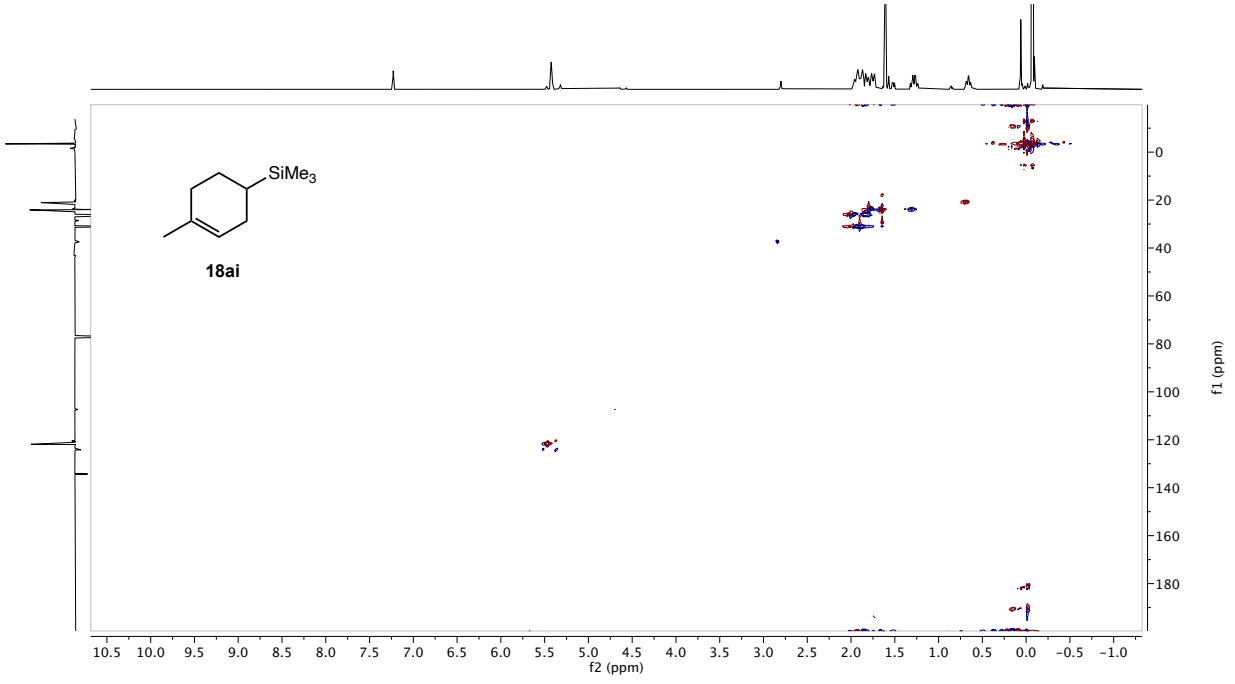

Figure S157. ^{1}H–^{13}C HSQC (500 MHz, $CDCl_3$) spectrum of **18ai**.

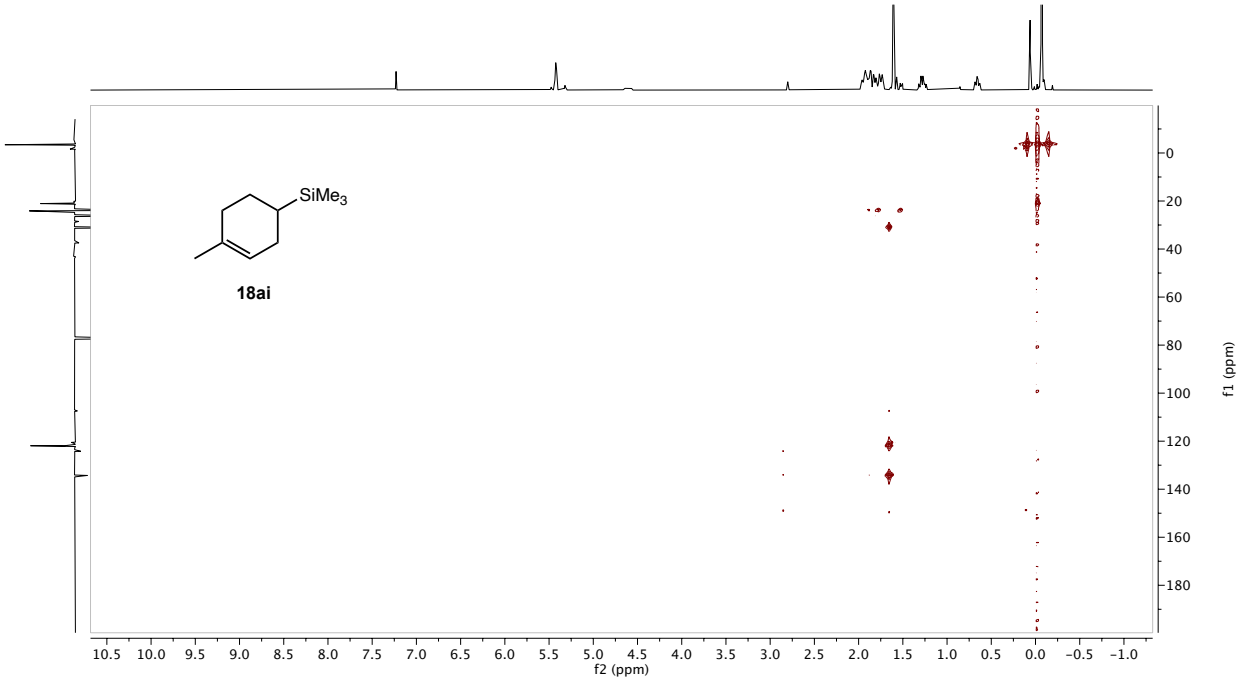

Figure S158. $^{1}H–^{13}C$ HMBC (500 MHz, $CDCl_3$) spectrum of **18ai**.

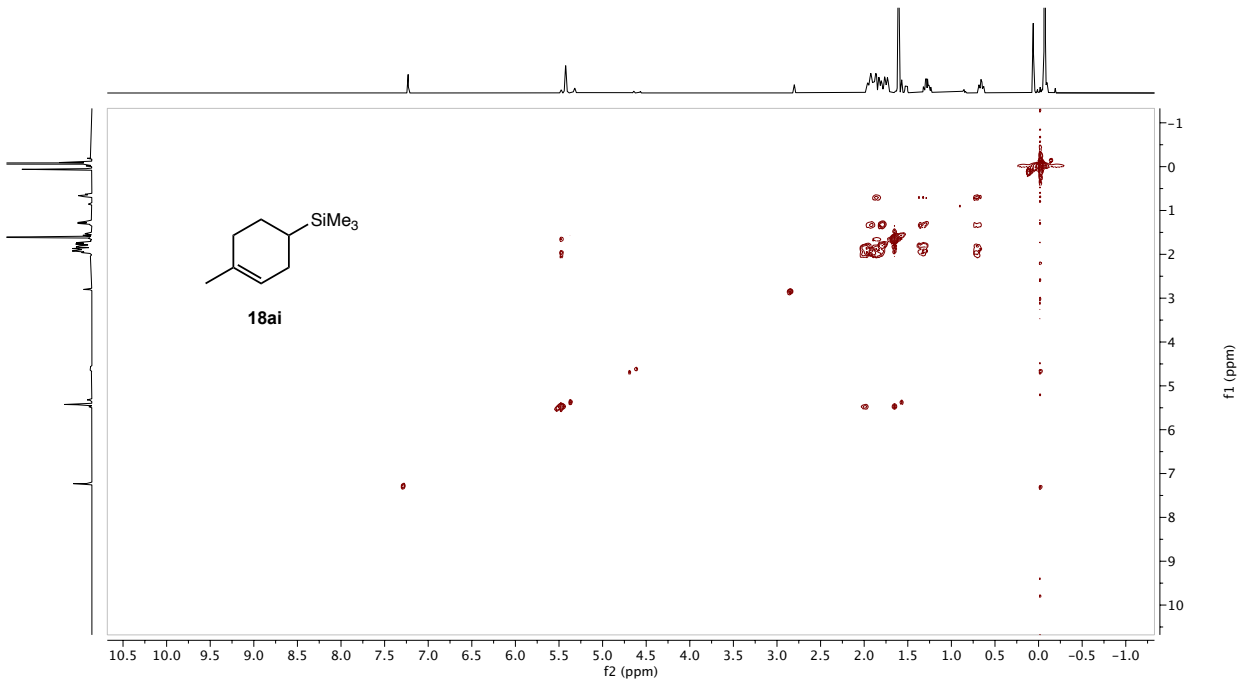

Figure S159. $^{1}H–^{1}H$ COSY (500 MHz, $CDCl_3$) spectrum of **18ai**.

trimethyl(2,3,4,5-tetrahydro-[1,1'-biphenyl]-4-yl)silane (18ak) was prepared in a 92% isolated yield with >99% [4+2]-selectivity, after 24 hours as described in 3.2, with 2.5 mol% (^{Me}PDI)Fe(butadiene).

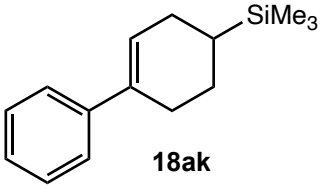

18ak

^{1}H NMR (500 MHz, $CDCl_3$) δ 7.38 (d, *J* = 8.6 Hz, 2H), 7.31 (t, *J* = 7.6 Hz, 2H), 7.21 (t, *J* = 7.2 Hz, 1H), 6.18 (s, 1H), 2.54 – 2.32 (m, 2H), 2.32 – 2.15 (m, 1H), 2.06 (td, *J* = 15.7, 4.1 Hz, 1H), 1.96 (dd, *J* = 13.0, 2.7 Hz, 1H), 1.53 – 1.38 (m, 1H), 0.91 – 0.75 (m, 1H), 0.01 (s, 9H).

^{13}C NMR (126 MHz, $CDCl_3$) δ 142.9, 136.8, 128.3, 126.6, 125.7, 125.1, 28.5, 26.9, 24.1, 20.9, -3.4.

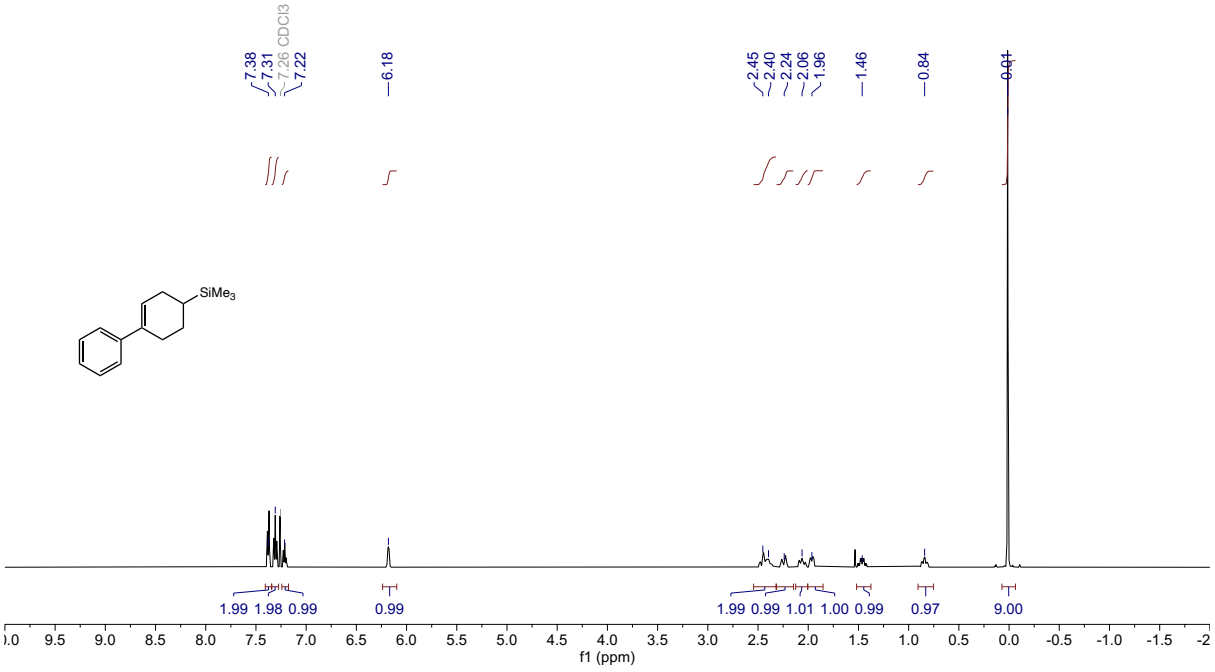

Figure S160. ^{1}H NMR (500 MHz, $CDCl_3$) spectrum of **18ak**.

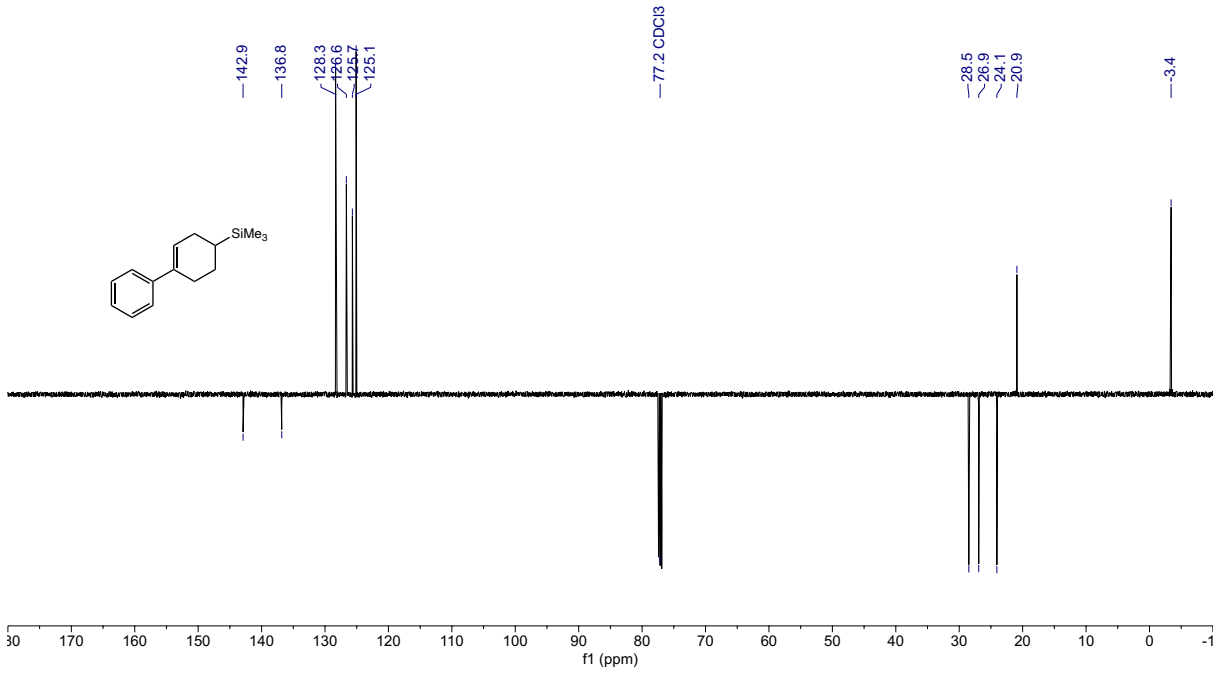

Figure S161. ^{13}C NMR (126 MHz, $CDCl_3$) spectrum of **18ak**.

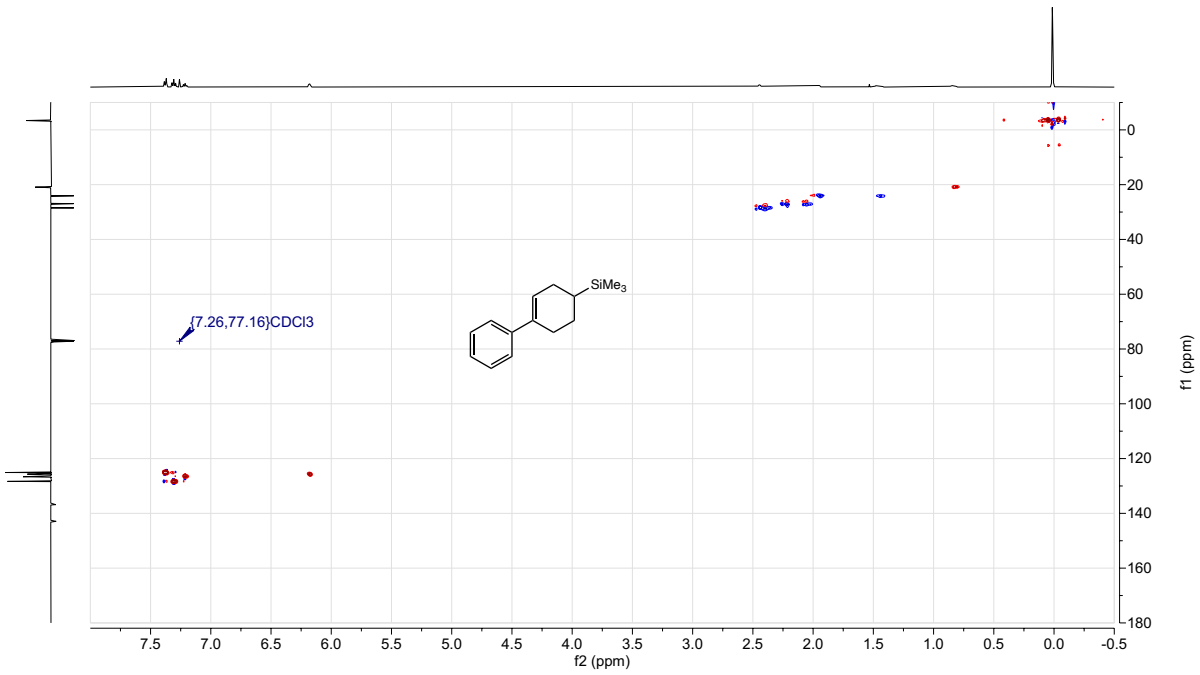

Figure S162. ^{1}H–^{13}C HSQC (500 MHz, $CDCl_3$) spectrum of **18ak**.

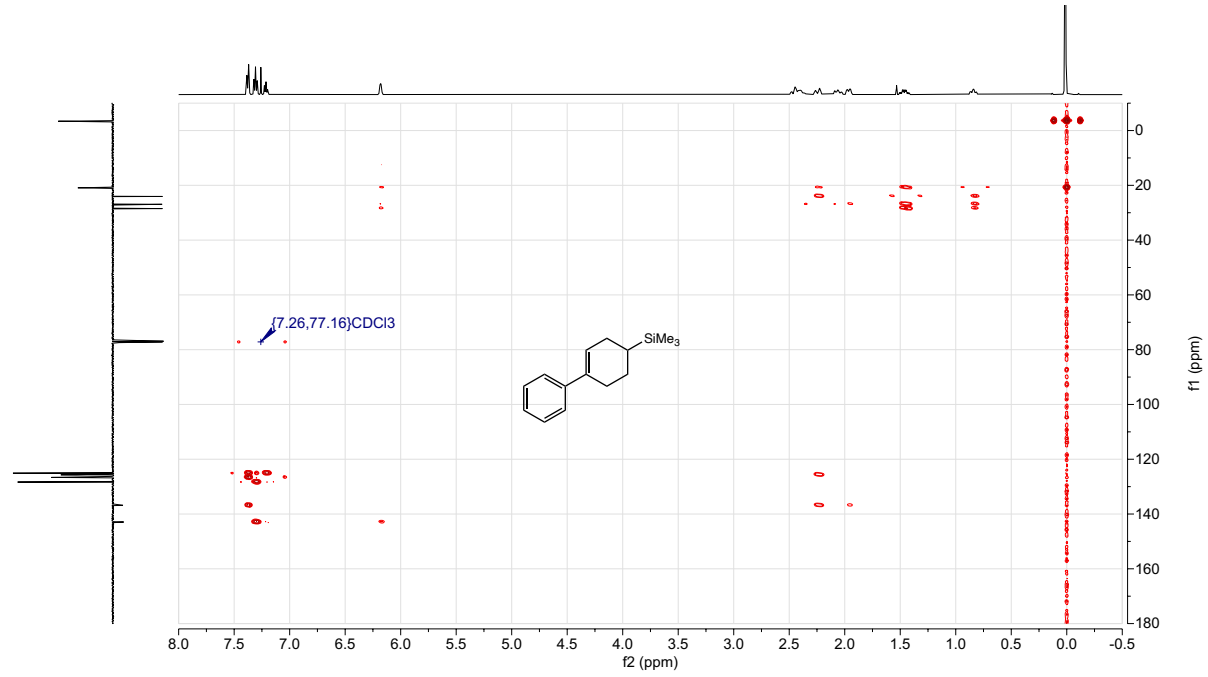

Figure S163. $^{1}H–^{13}C$ HMBC (500 MHz, $CDCl_3$) spectrum of **18ak**.

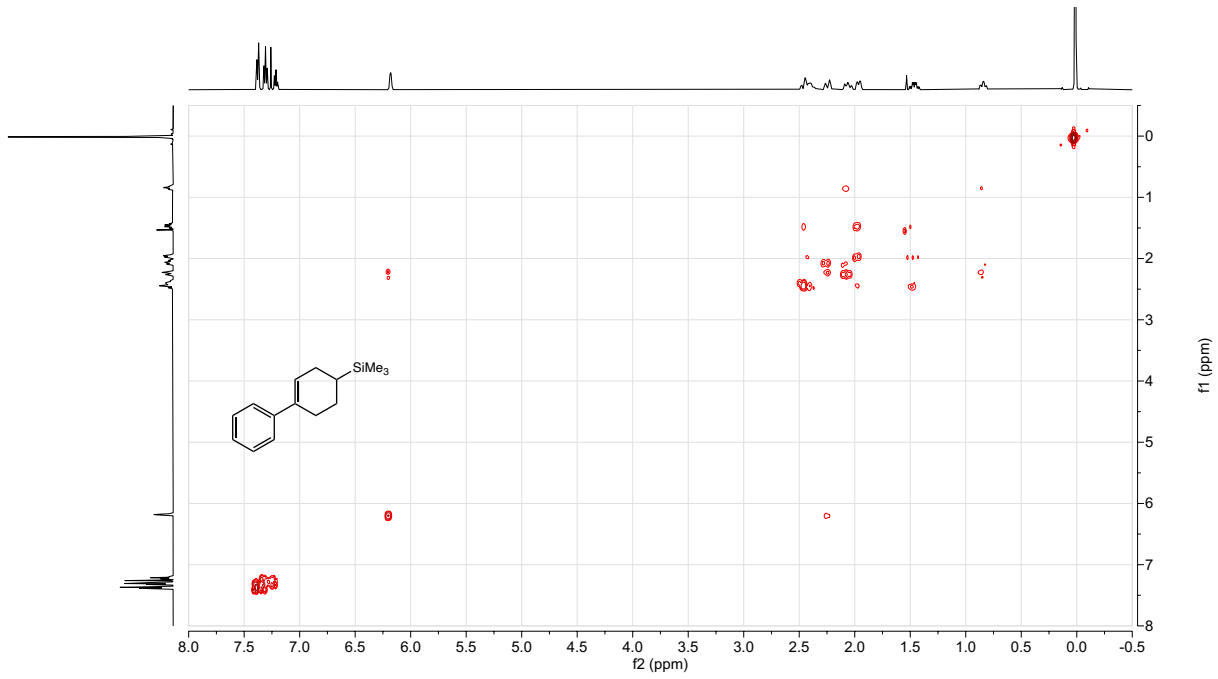

Figure S164. $^{1}H–^{1}H$ COSY (500 MHz, $CDCl_3$) spectrum of **18ak**.

[1,1'-bi(cyclohexan)]-1-en-4-yltrimethylsilane (**18al)** was prepared in an 85% isolated yield with 97% [4+2]-selectivity, after 27 hours as described in 3.2, with 2.5 mol% (^{Me}PDI)Fe(butadiene).

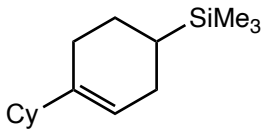

18al

^{1}H NMR (500 MHz, $CDCl_3$) δ 5.43 (s, 1H), 2.05-1.65 (m, 10H), 1.30-1.09 (m, 7H), 0.71 (1H), -0.05 (s, 9H).

^{13}C NMR (126 MHz, $CDCl_3$) δ 143.33, 119.56, 46.04, 32.27, 31.83, 27.91, 26.98, 26.65, 25.79, 24.13, 21.63, -3.42.

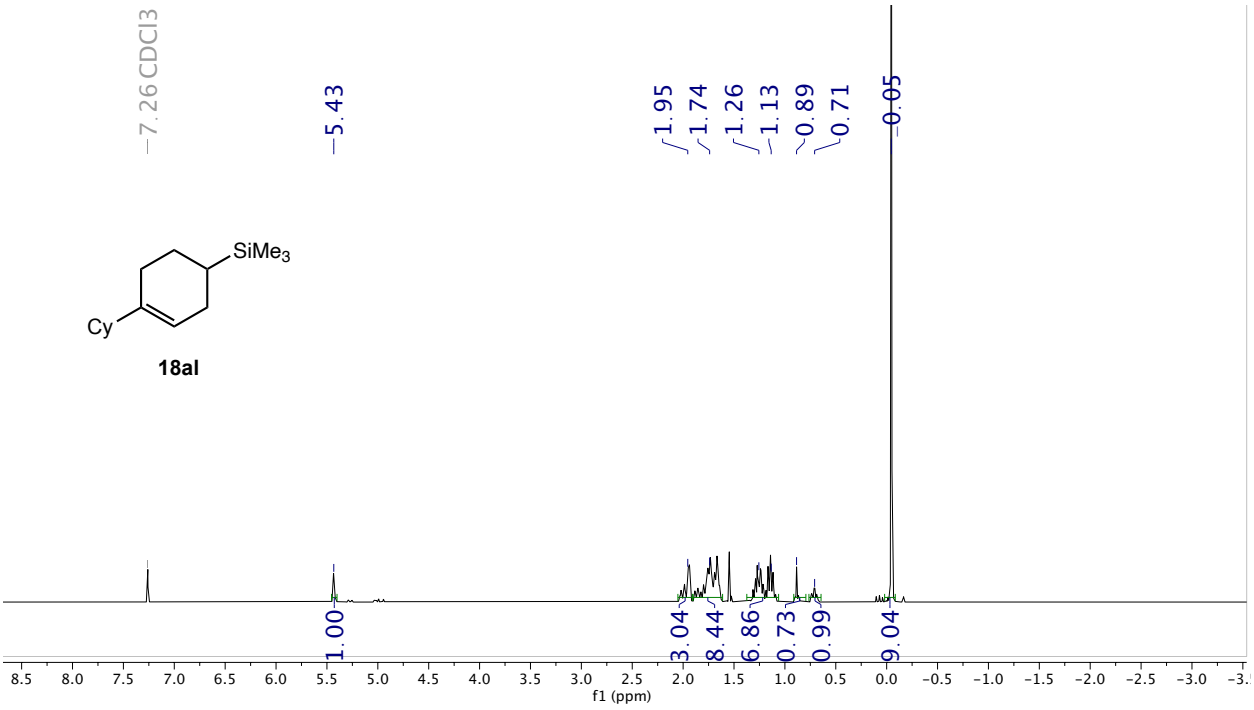

Figure S165. ^{1}H NMR (500 MHz, $CDCl_3$) spectrum of **18al**.

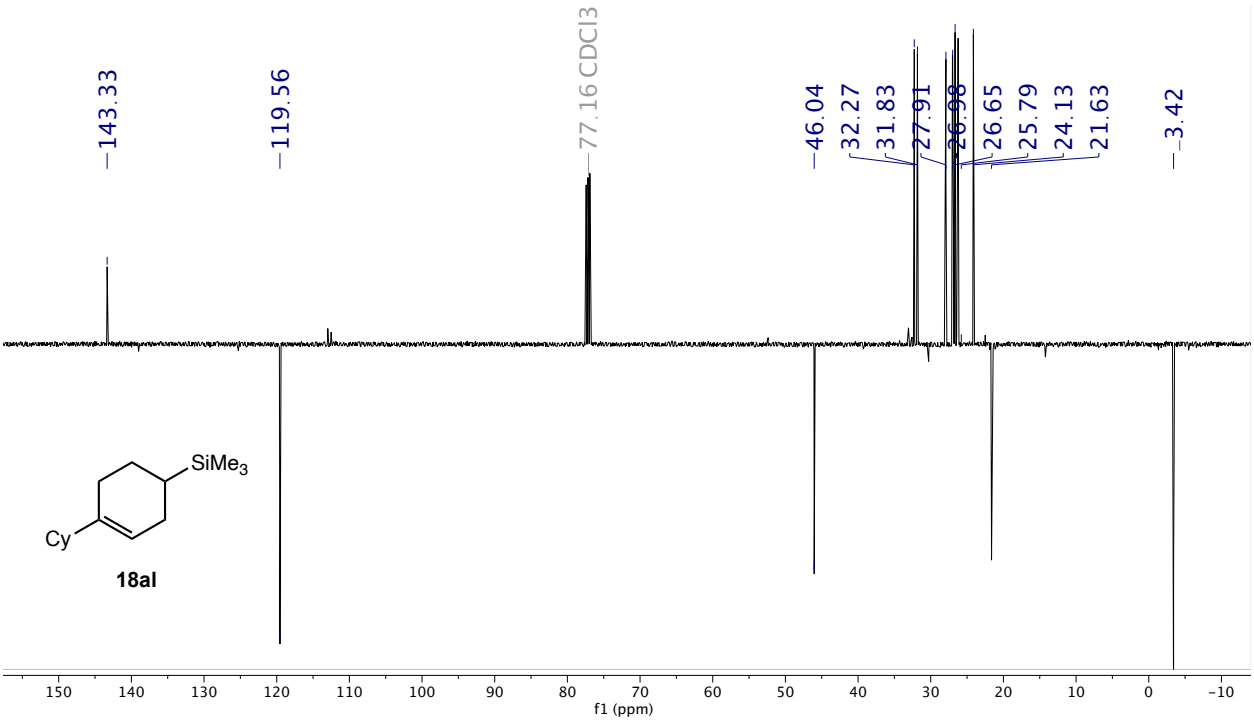

Figure S166. ^{13}C NMR (126 MHz, $CDCl_3$) spectrum of **18al**.

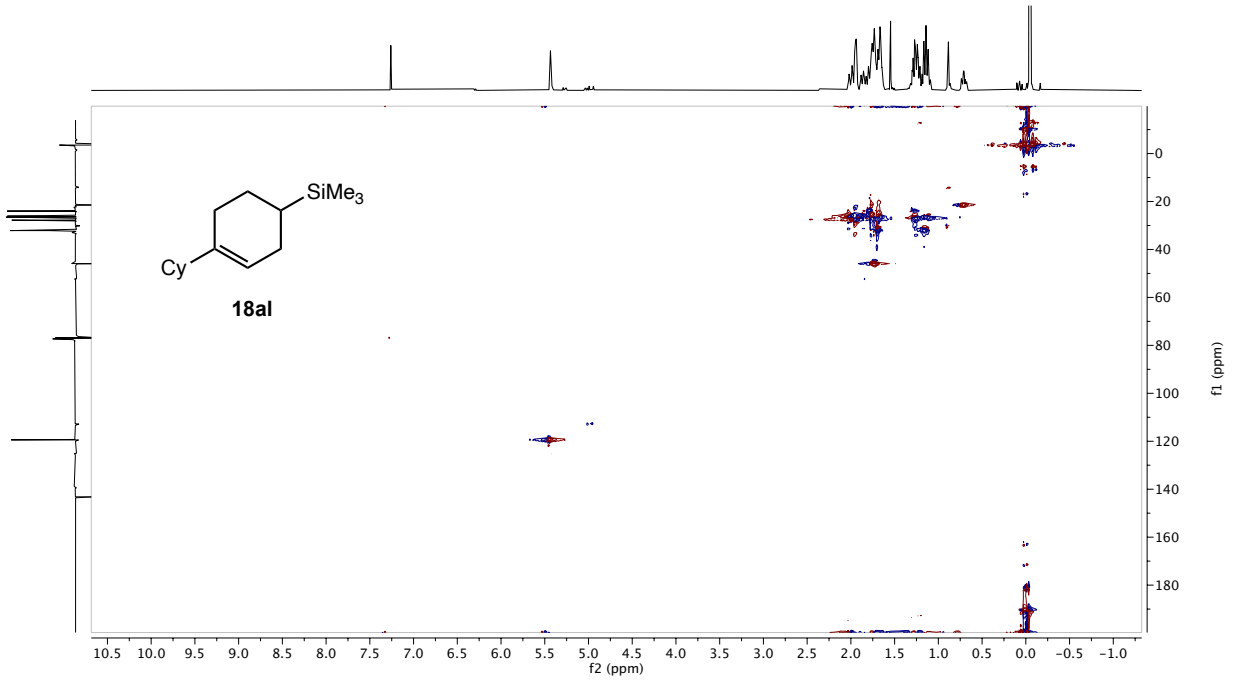

Figure S167. ^{1}H–^{13}C HSQC (500 MHz, $CDCl_3$) spectrum of **18al**.

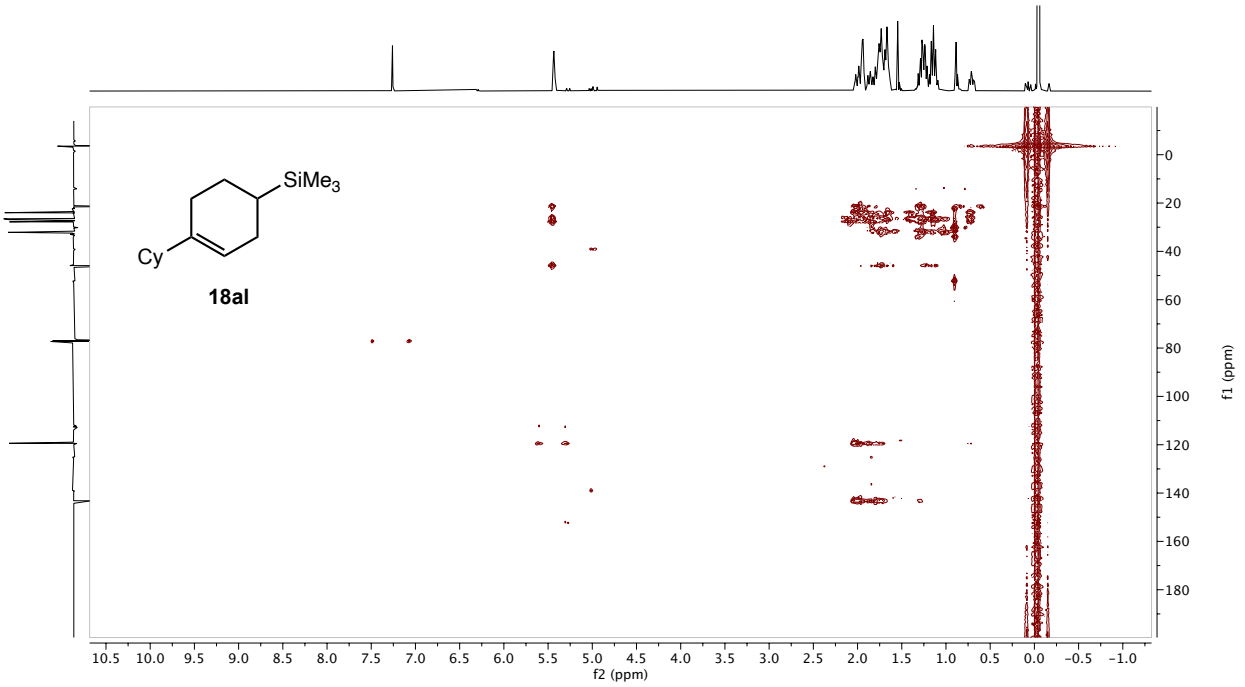

Figure S168. $^{1}H–^{13}C$ HMBC (500 MHz, $CDCl_3$) spectrum of **18al**.

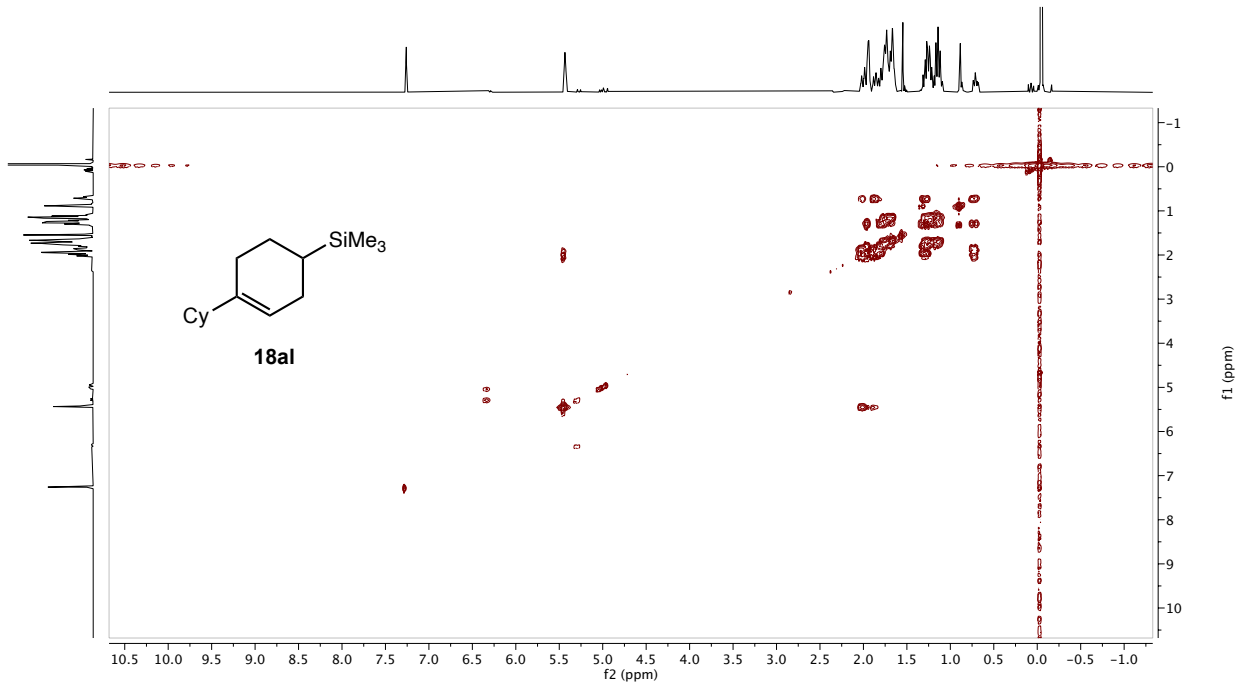

Figure S169. $^{1}H–^{1}H$ COSY (500 MHz, $CDCl_3$) spectrum of **18al**.

Trimethyl(4-phenethylcyclohex-3-en-1-yl)silane (18am) was prepared in an 88% isolated yield with 97% [4+2]-selectivity, after 48 hours as described in 3.2, with 2.5 mol% (^{Me}PDI)Fe(butadiene).

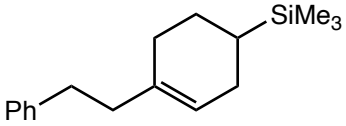

18am

^{1}H NMR (500 MHz, $CDCl_3$) δ 7.28 (t, *J* = 7.7, 7.2 Hz, 2H), 7.20 (d, *J* = 7.7 Hz, 2H), 7.18 (t, *J* = 7.2 Hz, 1H), 5.51 (s, 1H), 2.72 (td, *J* = 7.7, 4.4 Hz, 2H), 2.24 (t, *J* = 8.3 Hz, 2H), 2.10 – 1.92 (m, 3H), 1.91 – 1.85 (m, 1H), 1.85 – 1.78 (m, 1H), 1.40 – 1.20 (m, 1H), 0.73 (tt, *J* = 12.1, 4.9, 2.2 Hz, 1H), –0.02 (s, 9H).

^{13}C NMR (126 MHz, $CDCl_3$) δ 142.81, 137.56, 128.50, 128.37, 125.77, 122.06, 40.23, 34.64, 29.64, 26.21, 23.94, 21.31, -3.43.

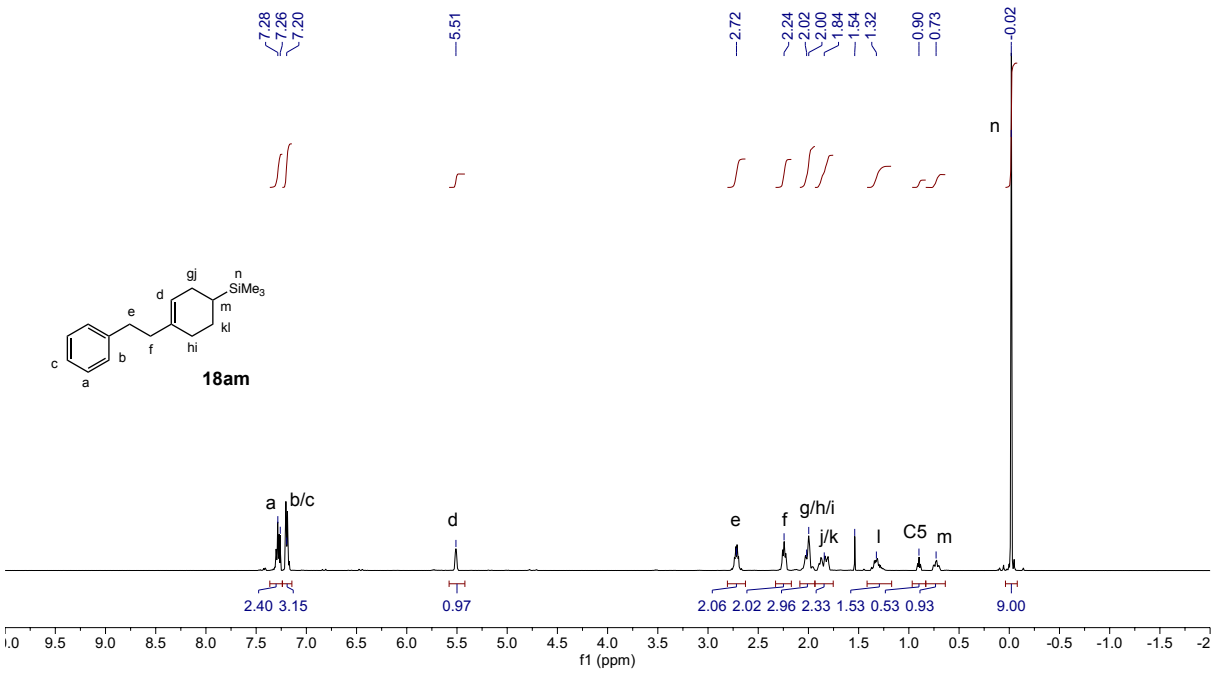

Figure S170. ^{1}H NMR (500 MHz, $CDCl_3$) spectrum of **18am**.

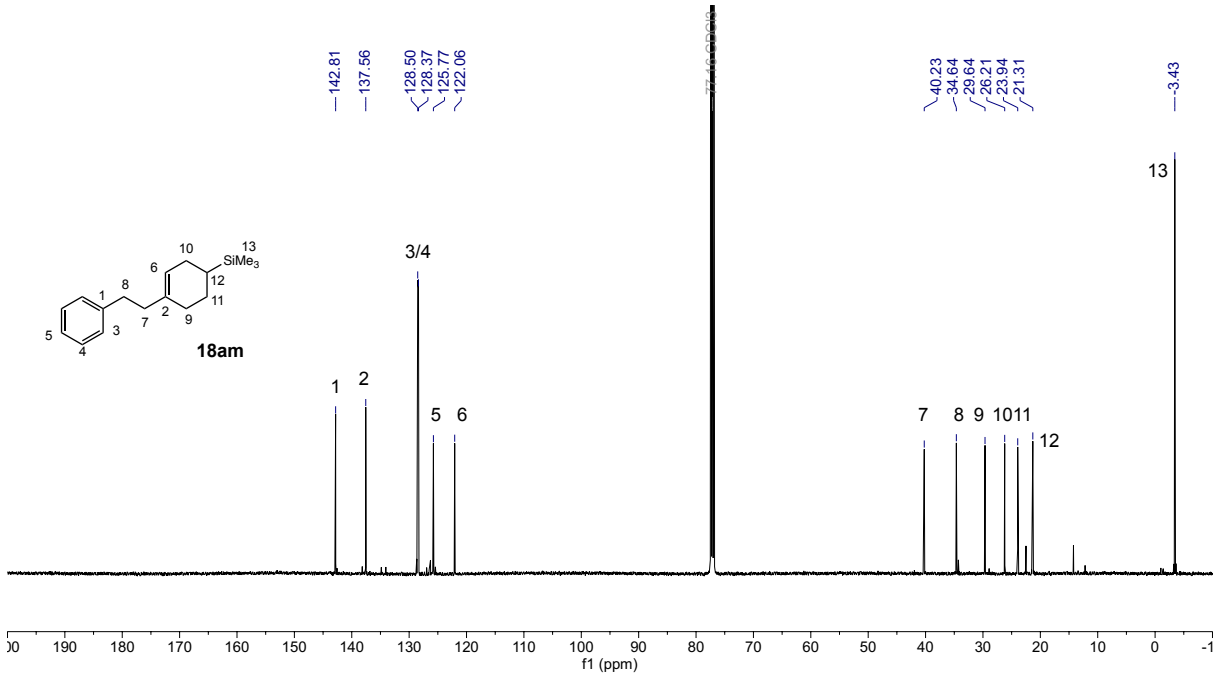

Figure S171. ^{13}C NMR (126 MHz, $CDCl_3$) spectrum of **18am**.

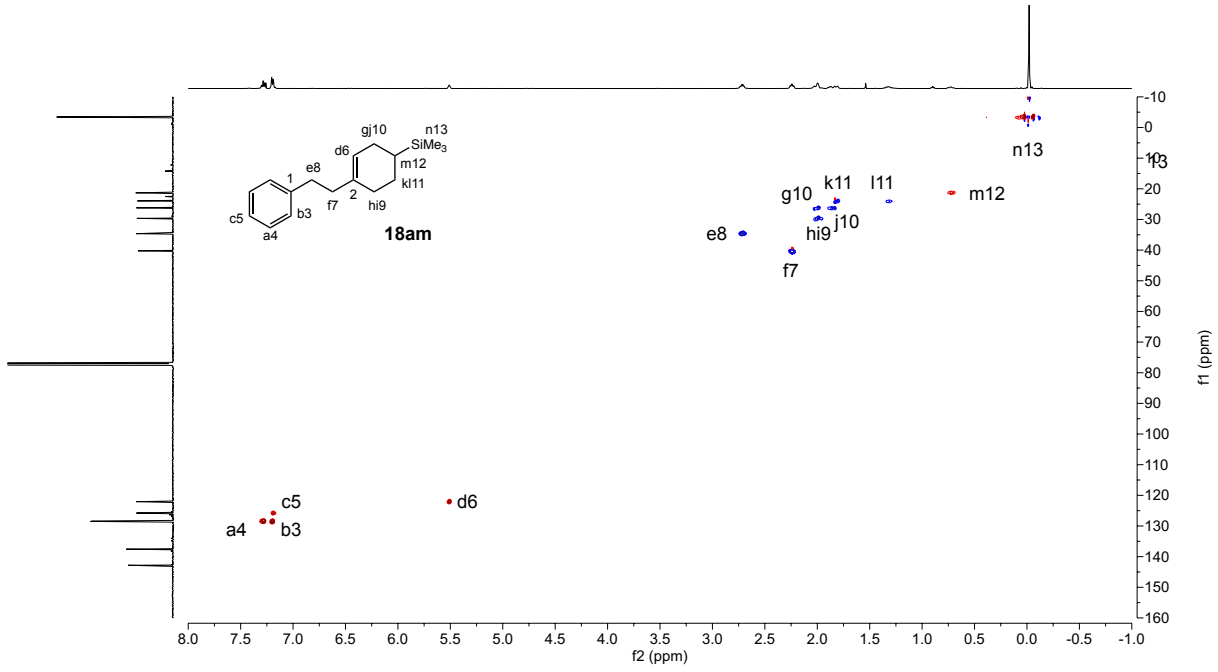

Figure S172. ^{1}H–^{13}C HSQC (500 MHz, $CDCl_3$) spectrum of **18am**.

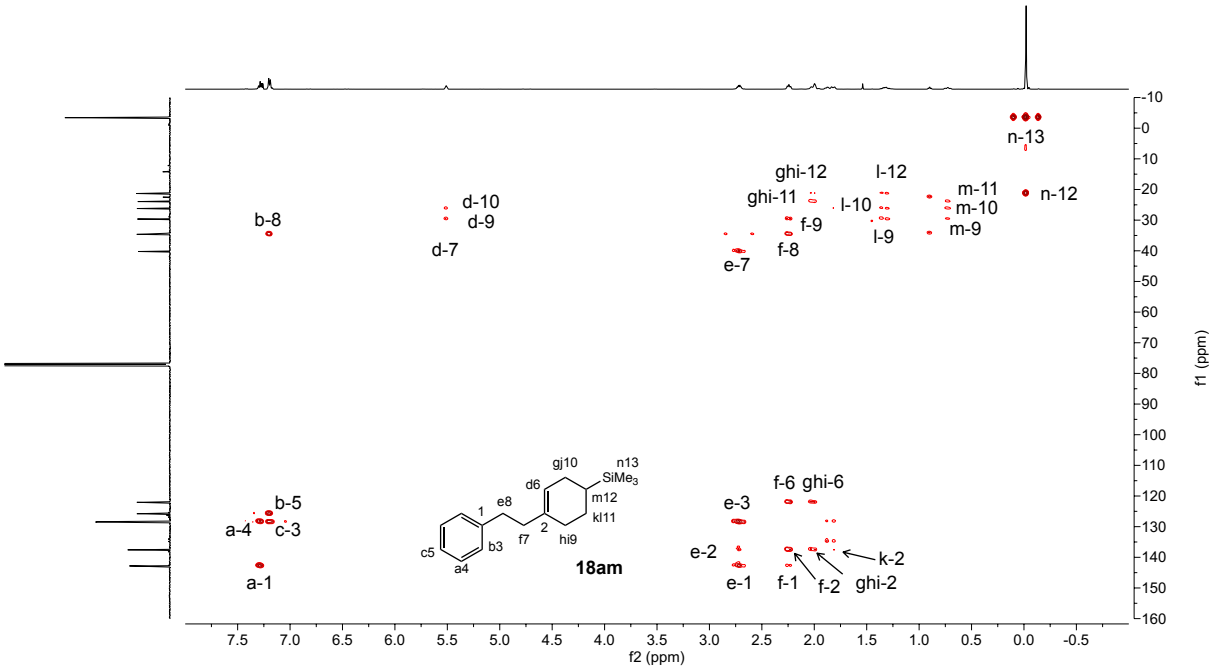

Figure S173. $^{1}H–^{13}C$ HMBC (500 MHz, $CDCl_3$) spectrum of **18am**.

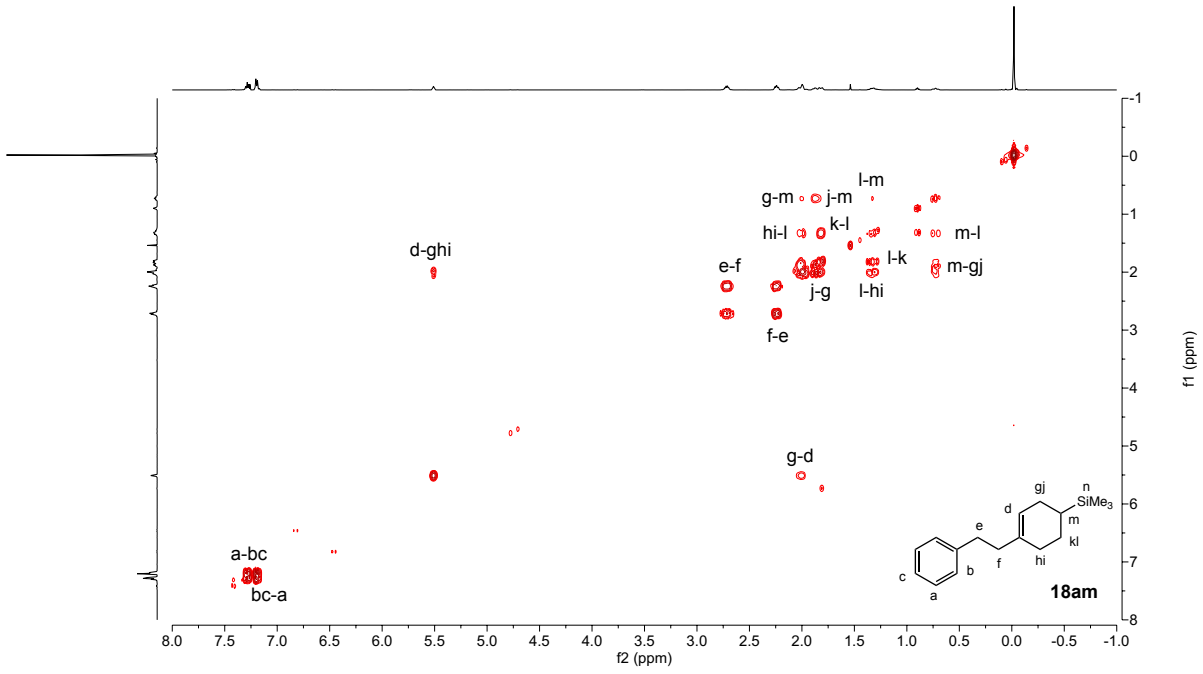

Figure S174. $^{1}H–^{1}H$ COSY (500 MHz, $CDCl_3$) spectrum of **18am**.

***tert*-butyldimethyl(3-(4-(trimethylsilyl)cyclohex-1-en-1-yl)propoxy)silane** (**18an)** was prepared in an 88% isolated yield with 95% [4+2]-selectivity, after 24 hours as described in 3.2, with 2.5 mol% (^{Me}PDI)Fe(butadiene).

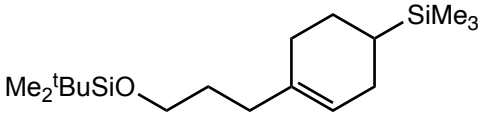

18an

^{1}H NMR (500 MHz, $CDCl_3$) δ 5.46 (s, 1H), 3.59 (t, *J* = 7.6 Hz, 2H) 2.04-1.76 (m, 2H), 1.60 (m, 3H), 1.30 (m, 3H), 0.89 (s, 13H), 0.69 (m, 1H), 0.05 (s, 7H), -0.04 (s, 9H).

^{13}C NMR (126 MHz, $CDCl_3$) δ 137.64, 121.67, 63.21, 34.35, 31.07, 29.49, 26.20, 26.13, 23.95, 21.35, 13.67, -3.44, -5.09.

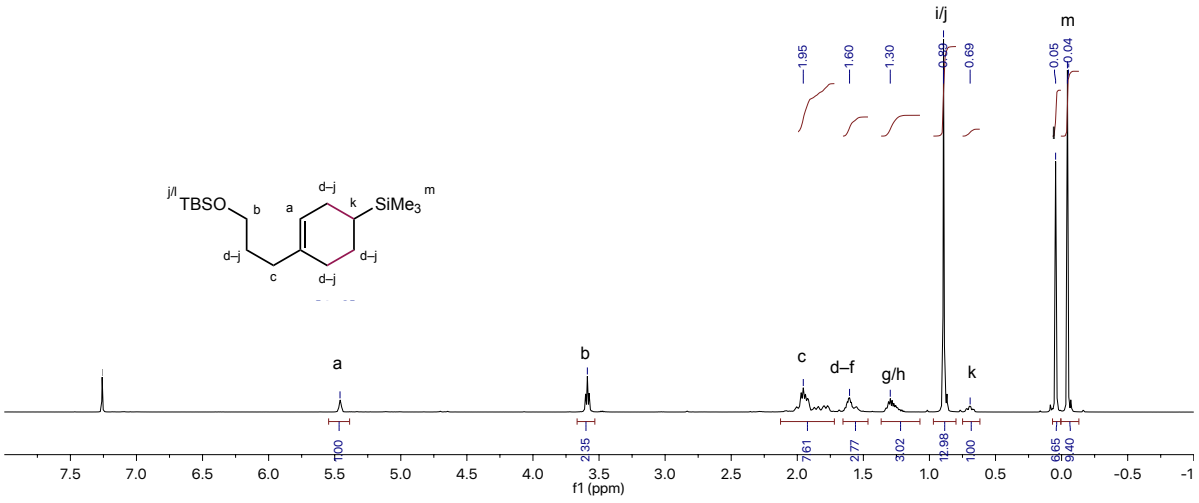

Figure S175. ^{1}H NMR (500 MHz, $CDCl_3$) spectrum of **18an**.

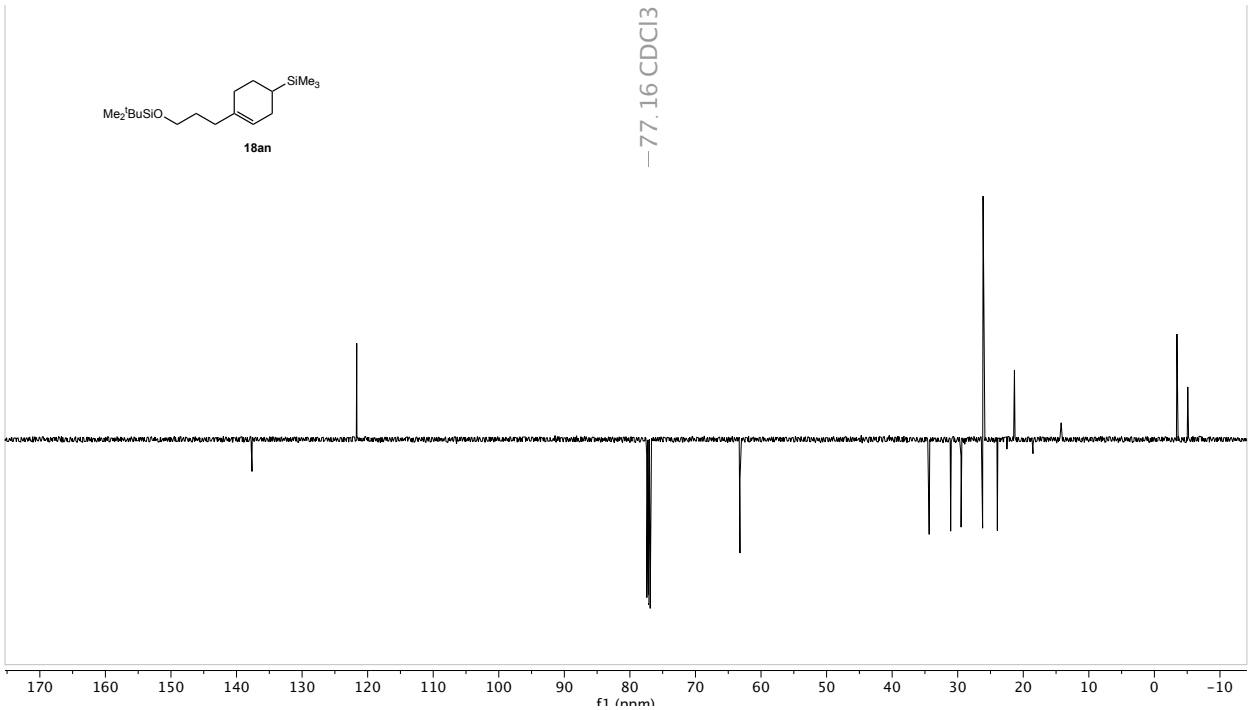

Figure S176. ^{13}C NMR (126 MHz, $CDCl_3$) spectrum of **18an**.

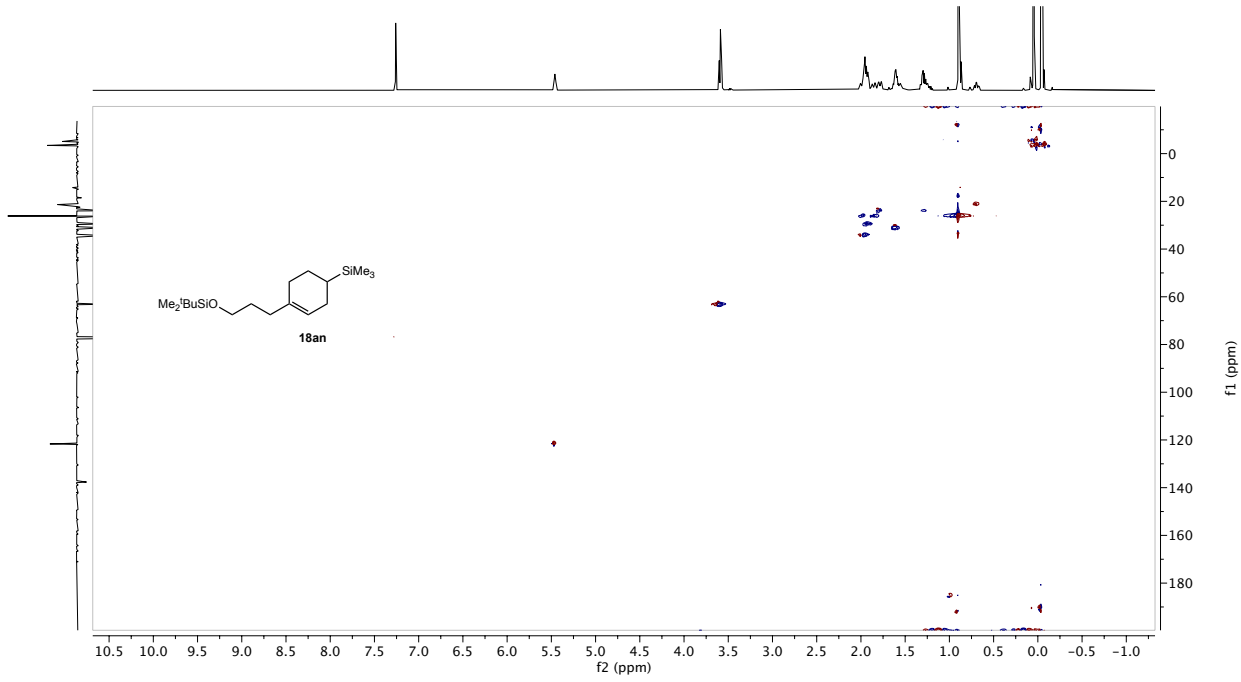

Figure S177. ^{1}H–^{13}C HSQC (500 MHz, $CDCl_3$) spectrum of **18an**.

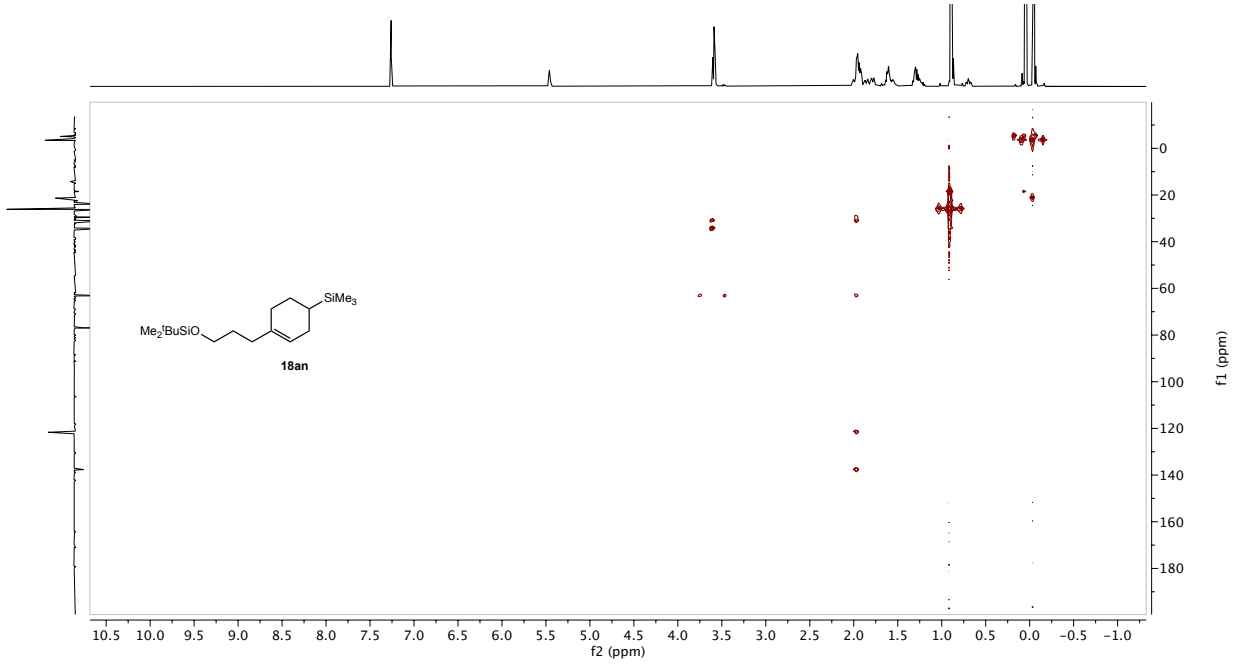

Figure S178. $^{1}H–^{13}C$ HMBC (500 MHz, $CDCl_3$) spectrum of **18an**.

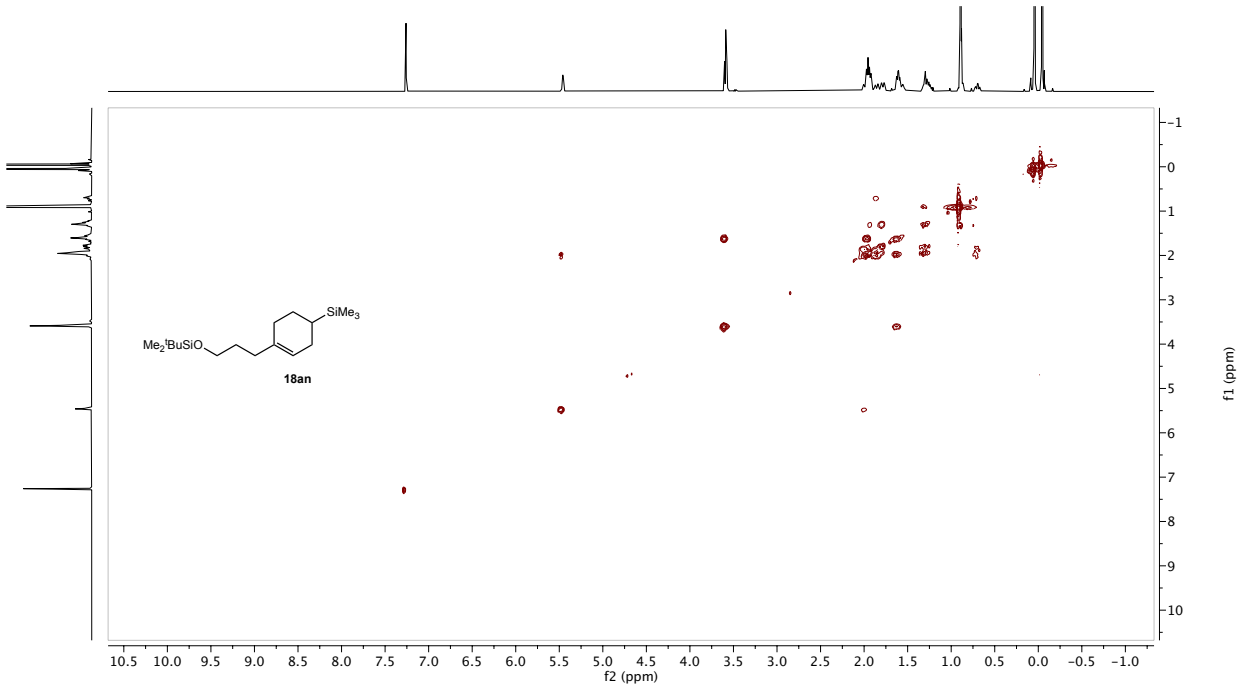

Figure S179. $^{1}H–^{1}H$ COSY (500 MHz, $CDCl_3$) spectrum of **18an**.

(4-(3,3-dimethoxypropyl)cyclohex-3-en-1-yl)trimethylsilane (**18ao)** was prepared in an 88% isolated yield with 95% [4+2]-selectivity, after 24 hours as described in 3.2, with 2.5 mol% (^{Me}PDI)Fe(butadiene).

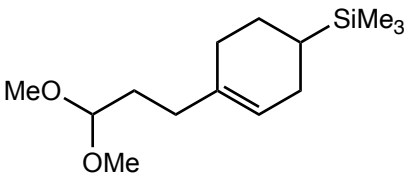

18ao

^{1}H NMR (500 MHz, $CDCl_3$) δ 5.50 (s, 1H), 4.37 (t, *J* = 5.7 Hz, 1H), 3.34 (s, 6H), 2.06-1.67 (m, 6H), 1.35 (m, 2H), 0.88 (m, 1H), 0.70 (m, 1H) -0.05 (s, 9H).

^{13}C NMR (126 MHz, $CDCl_3$) δ 138.83, 137.14, 121.92, 116.01, 113.59, 104.43, 52.91, 52.83, 33.05, 31.11, 30.79, 29.48, 27.11, 23.91, 21.29, -3.44.

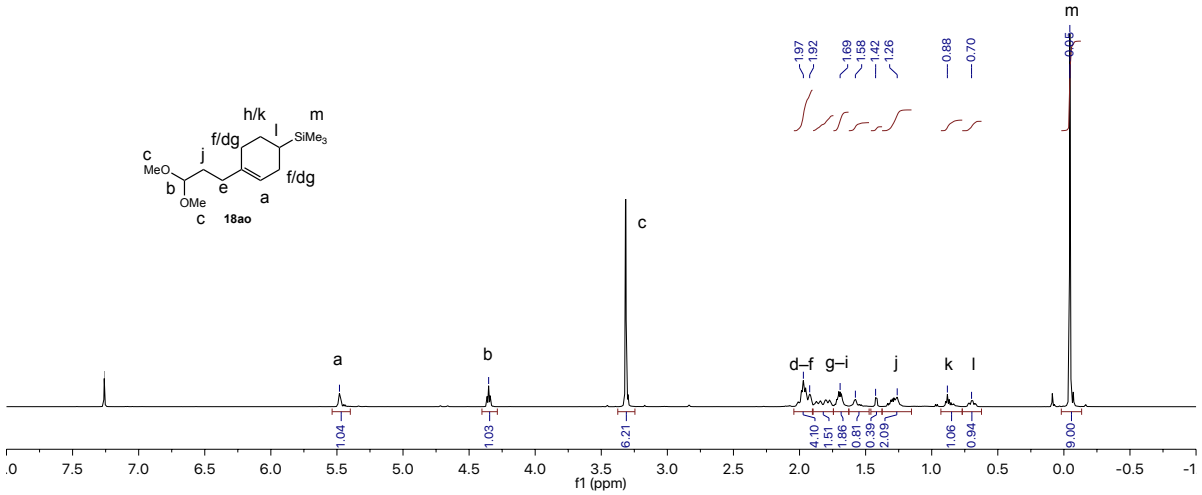

Figure S180. ^{1}H NMR (500 MHz, $CDCl_3$) spectrum of **18ao**.

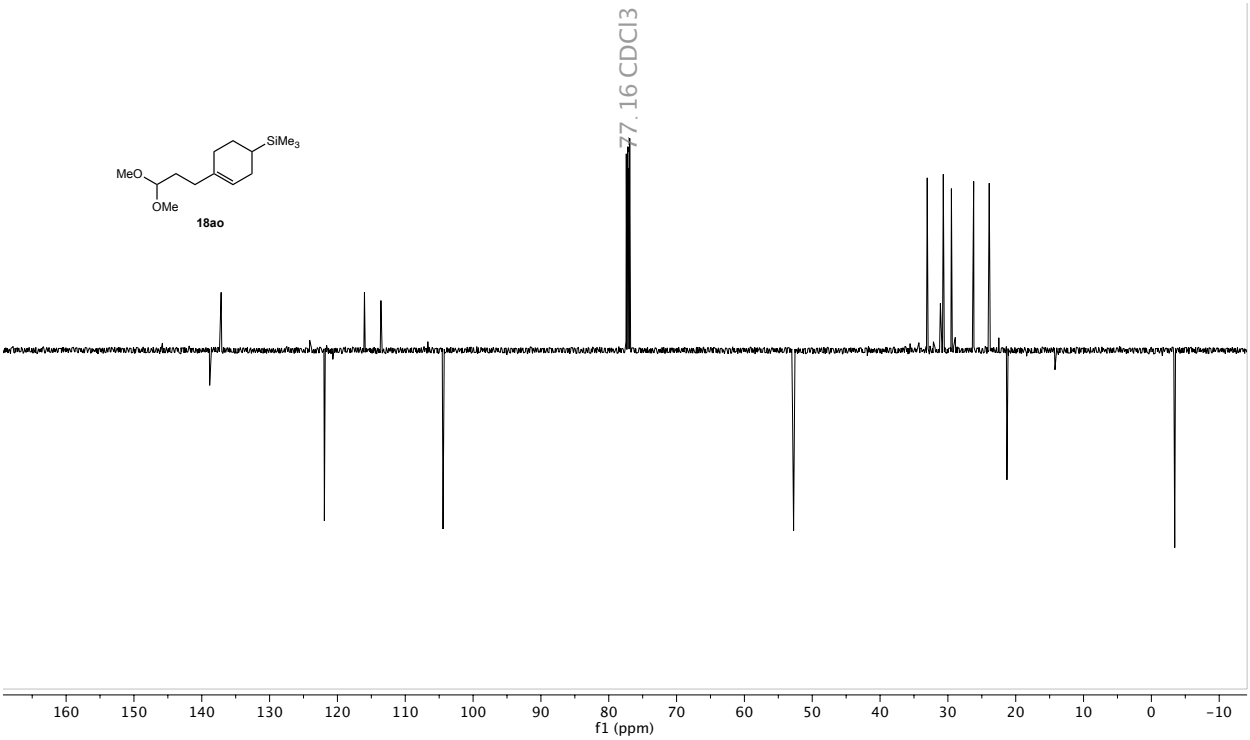

Figure S181. ^{13}C NMR (126 MHz, $CDCl_3$) spectrum of **18ao**.

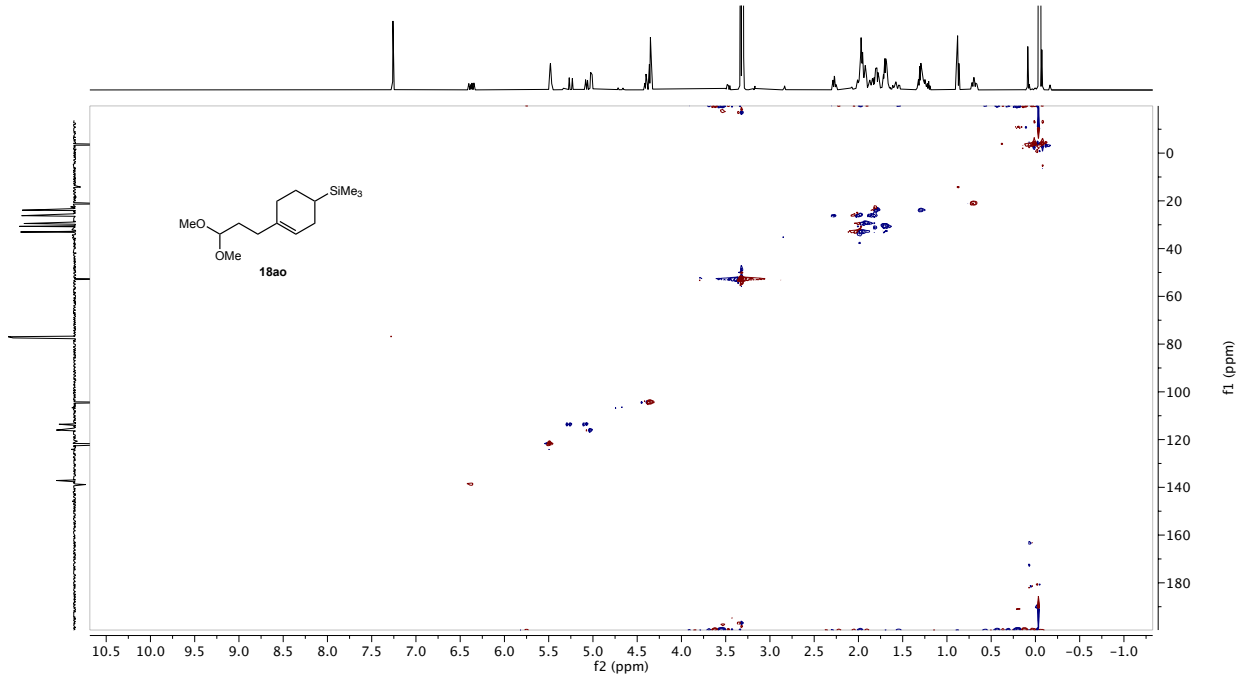

Figure S182. ^{1}H–^{13}C HSQC (500 MHz, $CDCl_3$) spectrum of **18ao**.

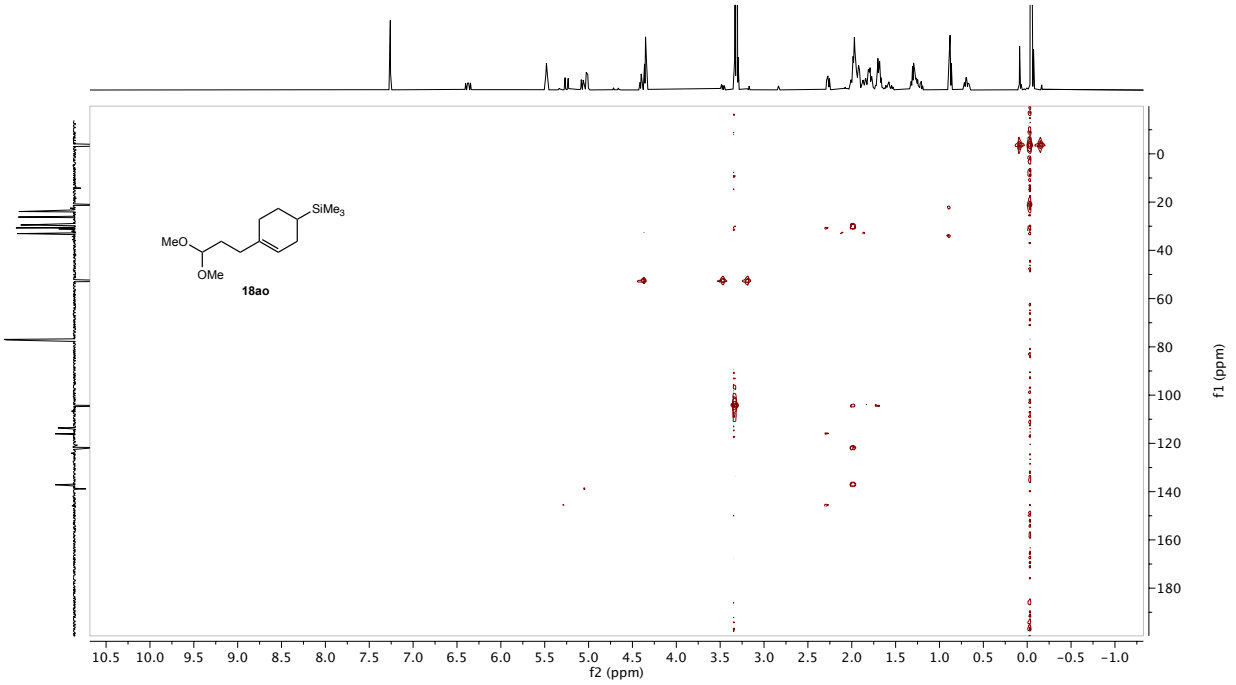

Figure S183. $^{1}H–^{13}C$ HMBC (500 MHz, $CDCl_3$) spectrum of **18ao**.

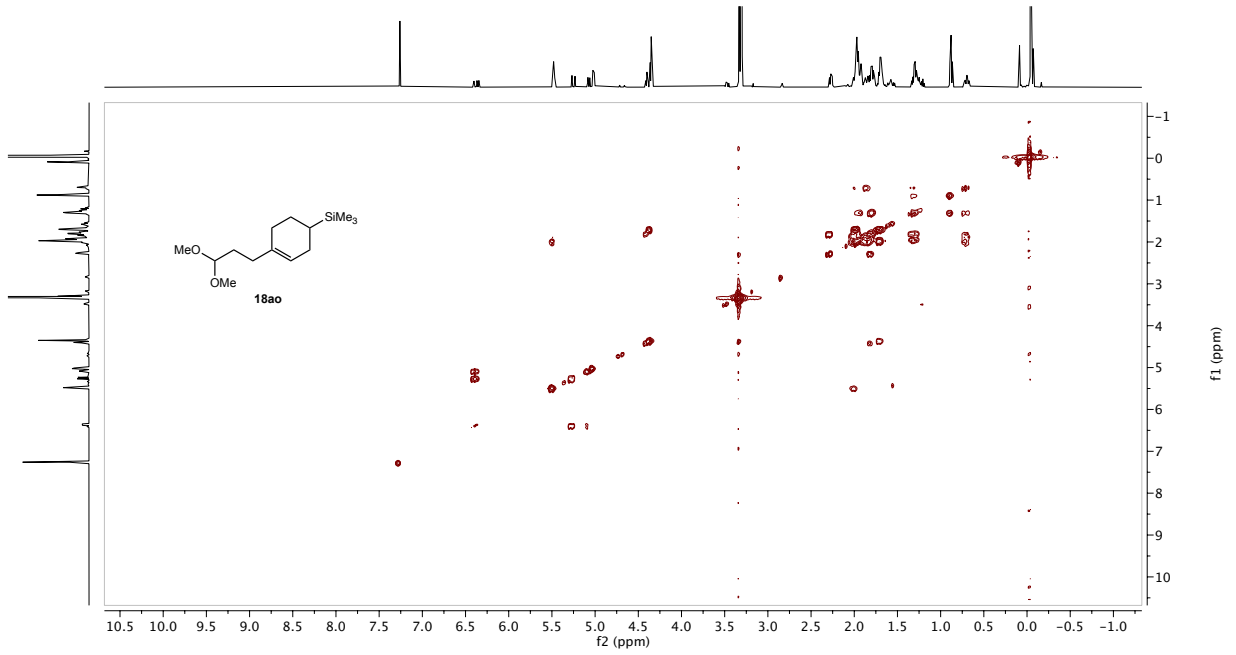

Figure S184. $^{1}H–^{1}H$ COSY (500 MHz, $CDCl_3$) spectrum of **18ao**.

1-(2-(4-(trimethylsilyl)cyclohex-1-en-1-yl)ethyl)pyrrolidine (18ap) was prepared in a 74% isolated yield with 93% [4+2]-selectivity, after 24 hours as described in 3.2, with 2.5 mol% (^{Me}PDI)Fe(butadiene).

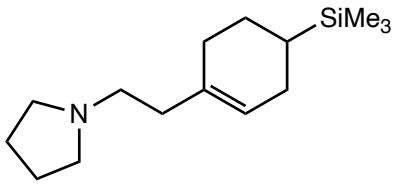

18ap

^{1}H NMR (500 MHz, $CDCl_3$) δ 5.46 (s, 1H), 2.48 (s, 4H), 2.39 (t, *J* = 8.1 Hz, 2H), 1.98-1.89 (m, 4H), 1.8-1.73 (m, 4H), 1.65-1.56 (m, 2H), 1.27(m, 1H), -0.05 (s, 9H).

^{13}C NMR (126 MHz, $CDCl_3$) δ 137.73, 121.63, 56.65, 54.40, 36.27, 29.39, 26.81, 26.19, 23.93, 23.54, 21.33, -3.64.

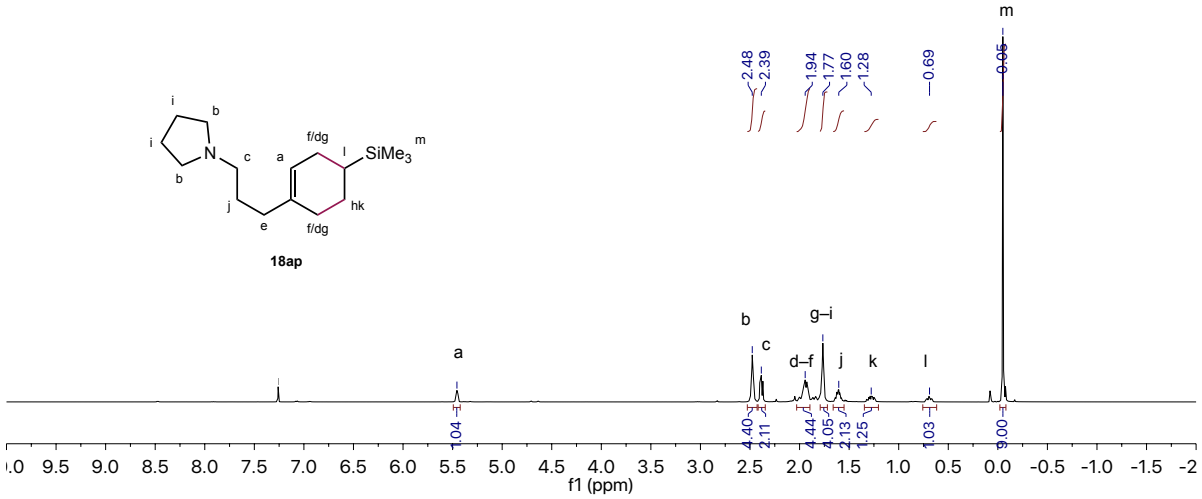

Figure S185. ^{1}H NMR (500 MHz, $CDCl_3$) spectrum of **18ap**.

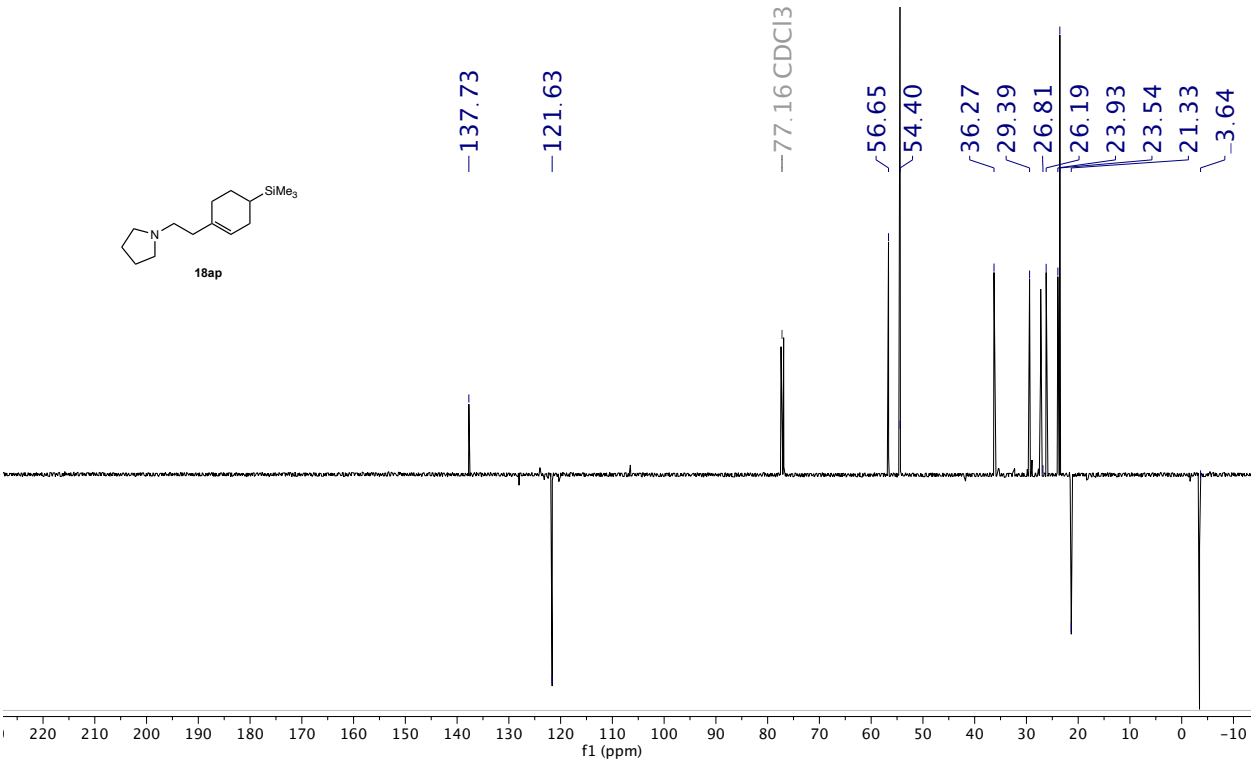

Figure S186. ^{13}C NMR (126 MHz, $CDCl_3$) spectrum of **18ap**.

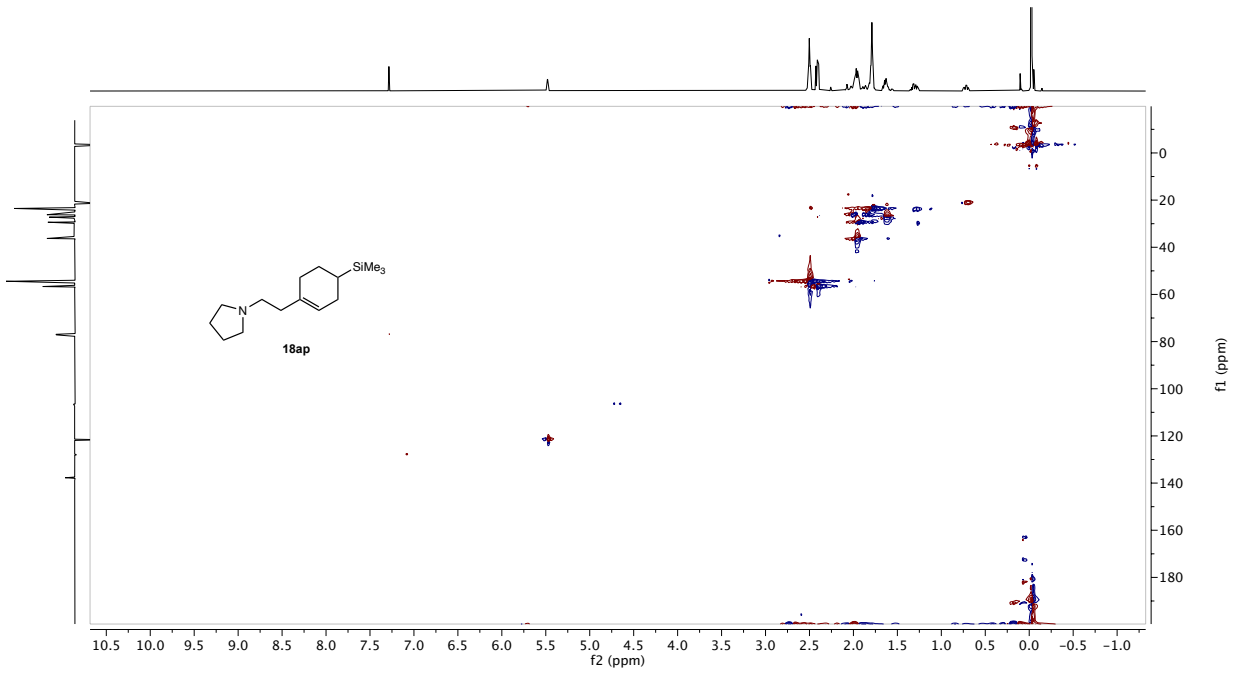

Figure S187. ^{1}H–^{13}C HSQC (500 MHz, $CDCl_3$) spectrum of **18ap**.

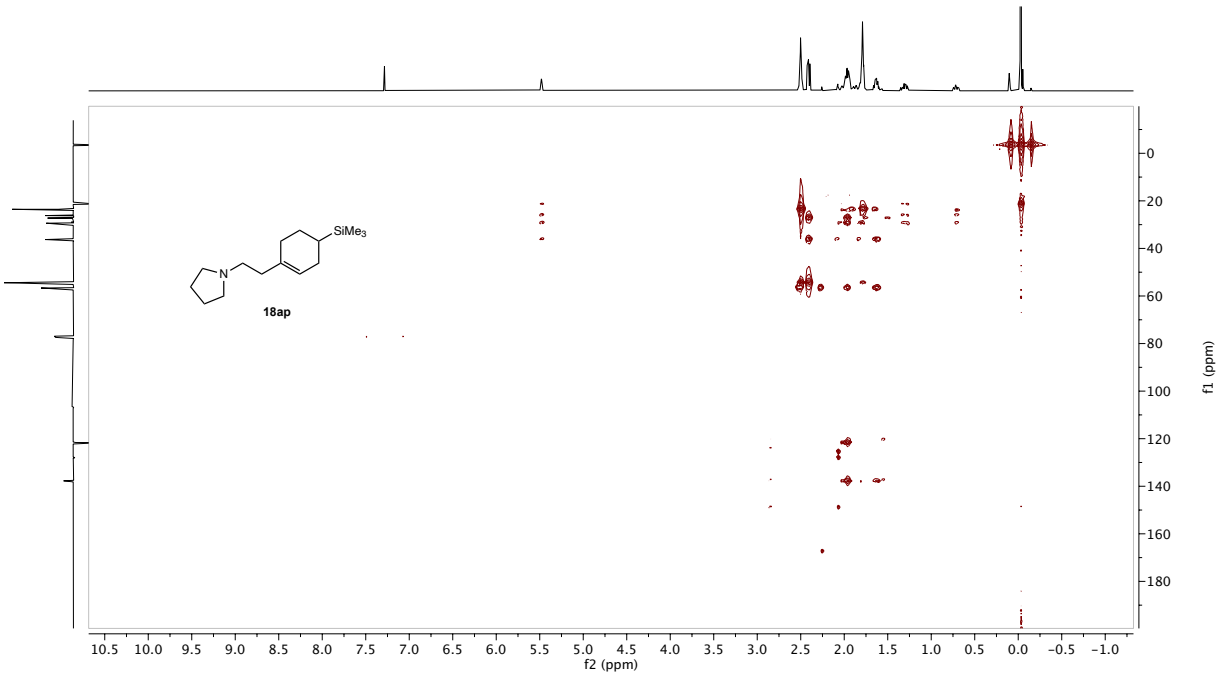

Figure S188. $^{1}H–^{13}C$ HMBC (500 MHz, $CDCl_3$) spectrum of **18ap**.

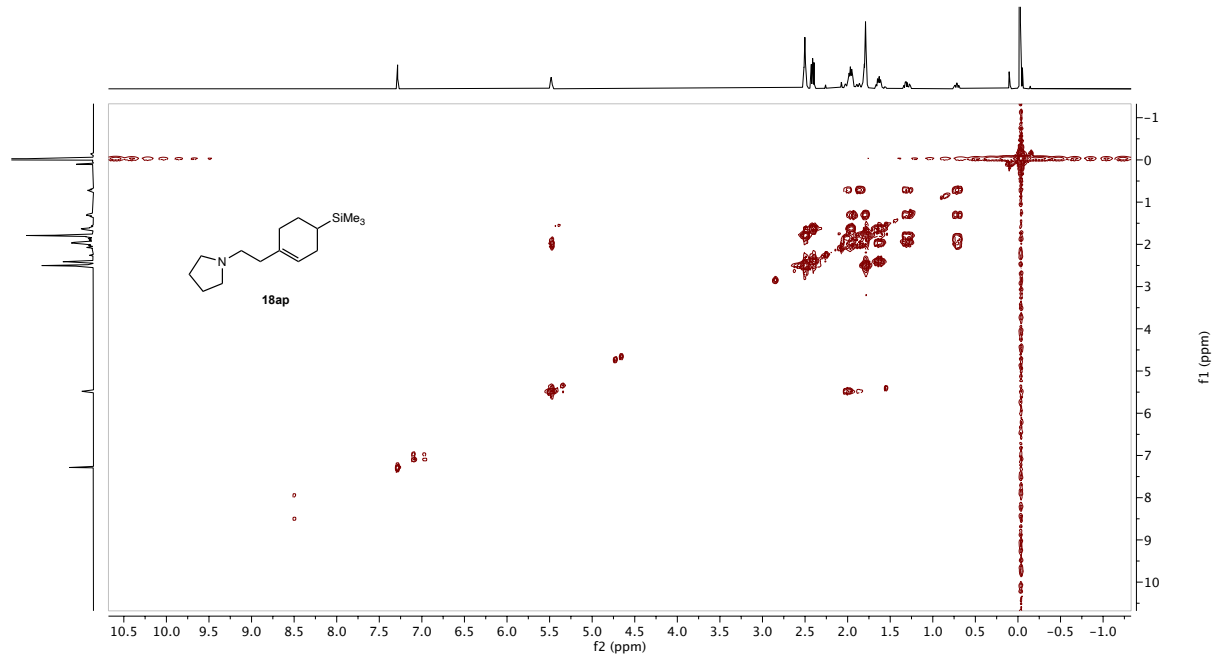

Figure S189. $^{1}H–^{1}H$ COSY (500 MHz, $CDCl_3$) spectrum of **18ap**.

4. Independent Synthesis of 17bi

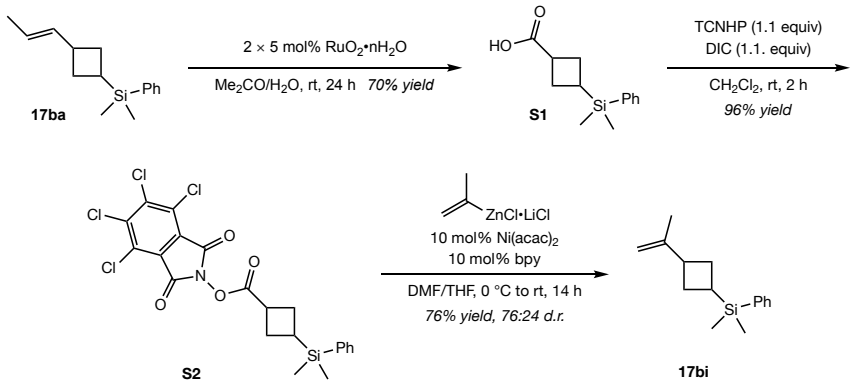

Figure S190. Independent synthesis of **17bi**

An authentic sample of **dimethyl(phenyl)(3-(prop-1-en-2-yl)cyclobutyl)silane (17bi)** was prepared through independent synthesis using procedures adapted from those reported previously for related molecules.[60,61]

^{1}H NMR (500 MHz, $CDCl_3$) δ 7.57 – 7.49§ (m, 2H), 7.51 – 7.45* (m, 2H), 7.40 – 7.29 (m, 3H), 4.70§ (s, 1H), 4.66* (s, 1H), 4.65§ (s, 1H), 4.58* (s, 1H), 3.04* (p, *J* = 9.0, 8.4 Hz, 1H), 2.74§ (p, *J* = 8.5 Hz, 1H), 2.27 – 2.03 (m, 2H), 1.92 – 1.81 (m, 1H), 1.74 (tt, *J* = 11.0, 4.6 Hz, 1H), 1.64§ (s, 3H), 1.61* (s, 3H), 0.31§ (s, 6H), 0.23* (s, 6H) where resolved resonances arising from the *cis*(*) and *trans*(§) diastereomers are indicated.

^{13}C NMR (126 MHz, $CDCl_3$) δ 149.3§, 149.2*, 139.0, 133.9§, 133.8*, 129.0§, 128.9*, 127.9§, 127.8*, 107.6*, 107.3§, 43.3*, 40.6§, 28.8*, 26.1§, 20.2§, 20.0*, 17.5*, 15.5§, -4.6§, -4.8* where resolved resonances arising from the *cis*(*) and *trans*(§) diastereomers are indicated.

GC-MS (EI): for $[M]^+ = C_{15}H_{22}Si$, calculated *m/z* = 230.14908, found *m/z* = 232.95.

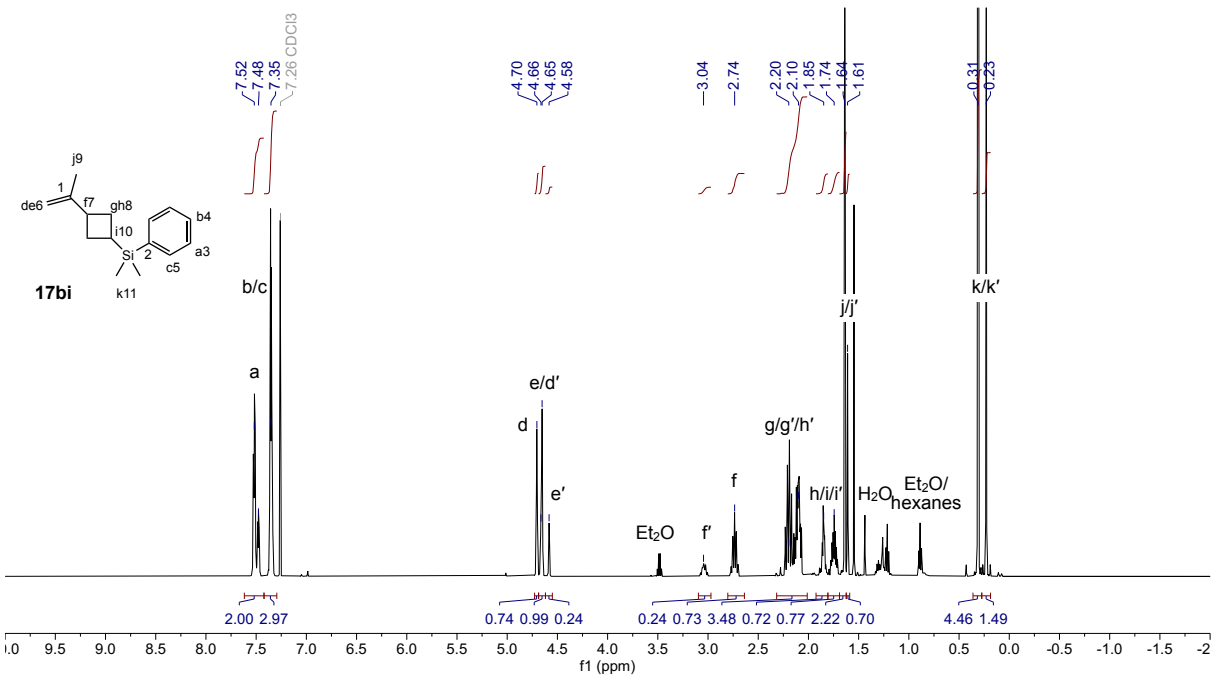

Figure S191. ^{1}H NMR (500 MHz, $CDCl_3$) spectrum of **17bi**.

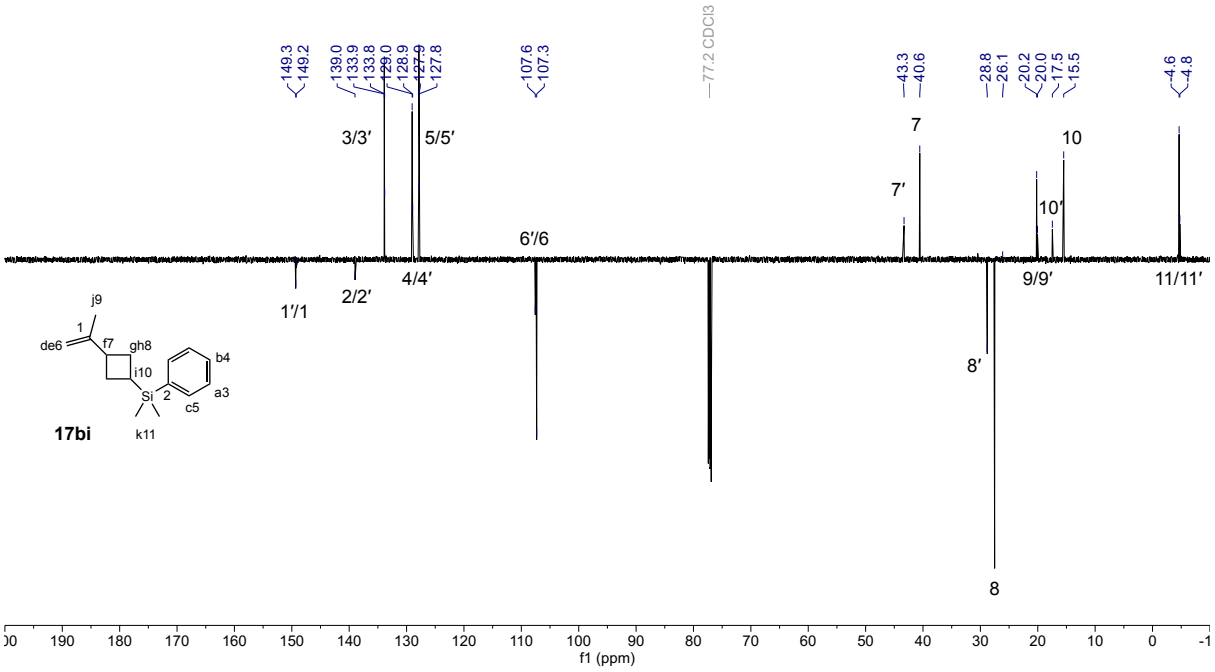

Figure S192. ^{13}C NMR (126 MHz, $CDCl_3$) spectrum of **17bi**.

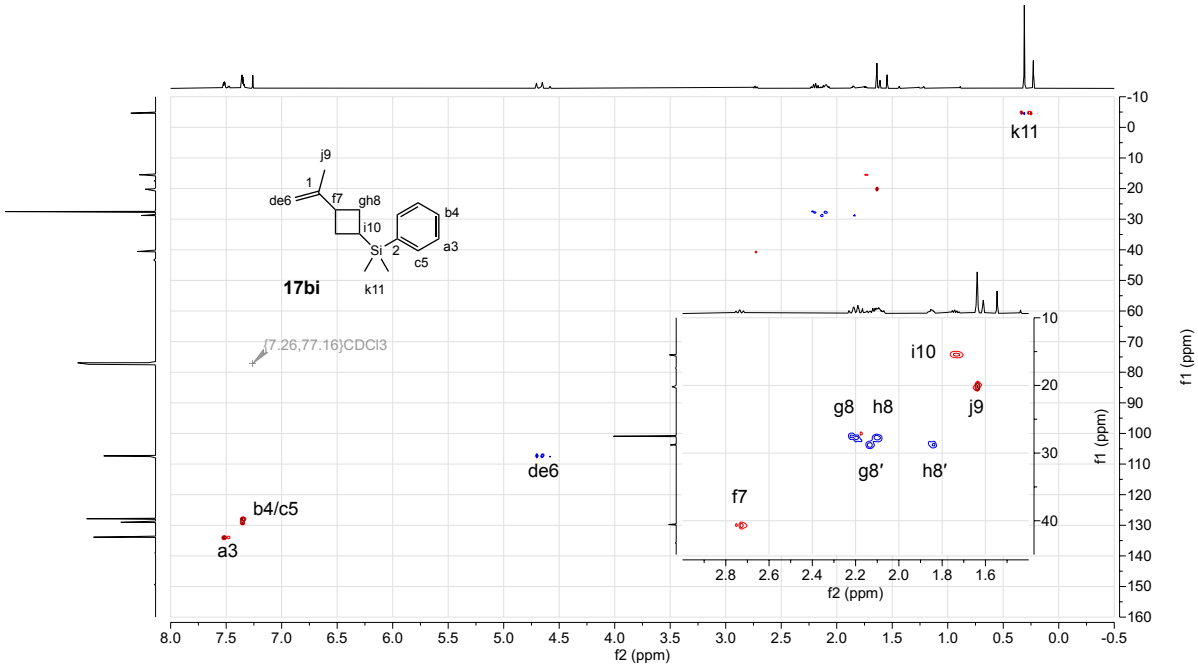

Figure S193. $^{1}H–^{13}C$ HSQC (500 MHz, $CDCl_3$) spectrum of **17bi**.

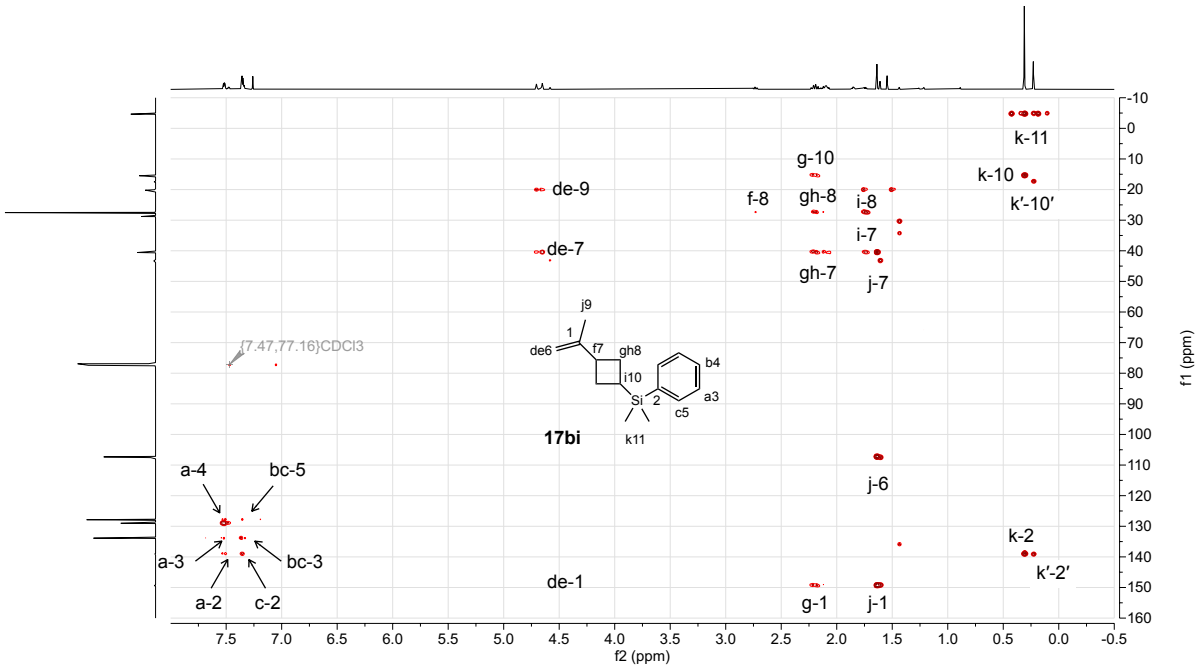

Figure S194. $^{1}H–^{13}C$ HMBC (500 MHz, $CDCl_3$) spectrum of **17bi**.

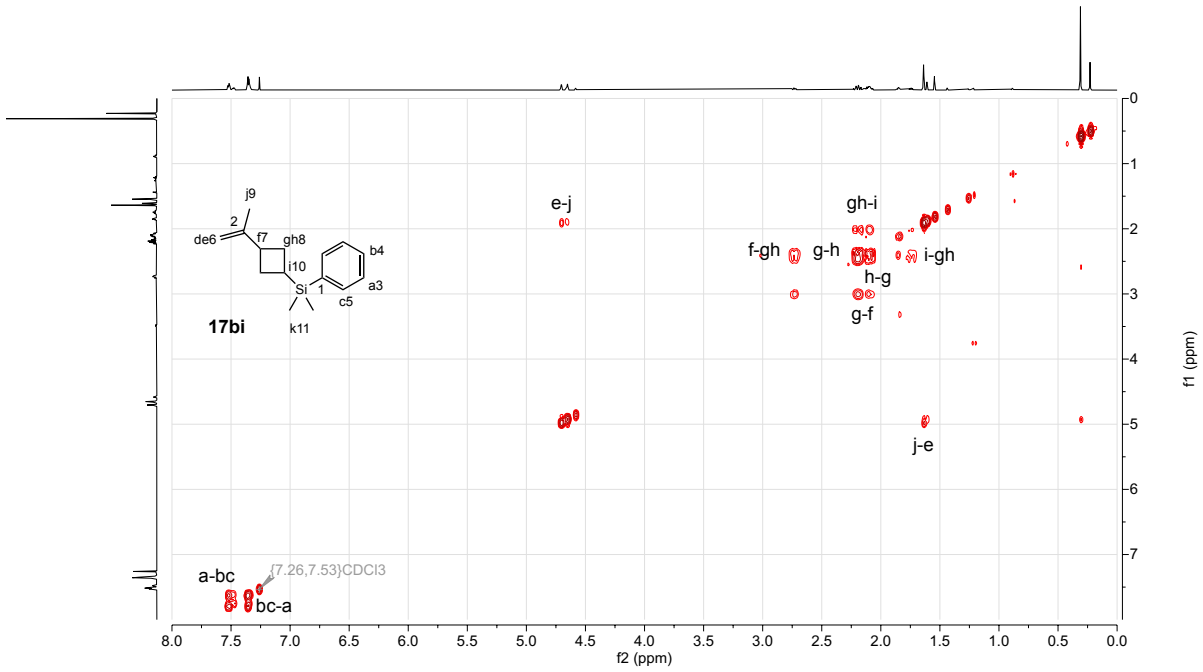

Figure S195. ^{1}H–^{1}H COSY (500 MHz, $CDCl_3$) spectrum of **17bi**.

5. Kinetic Analysis

5.1 General Kinetic Procedure

Kinetic experiments were performed in an N_2 atmosphere glovebox, using dimethylphenyl vinylsilane (**5b**) and myrcene (**9b**) as model substrates and cyclooctane as an internal standard. Stock mixtures of **5b**, **9b**, and [4+2]-cycloadduct **14bb** were prepared separately for to determine the GC response factors for each component relative to cyclooctane. The molar ratio vs. GC integrated area were fit with a linear regression to a function of the form:

$$\left({}^{n}/_{n_{\mathbf{ST}}}\right) = \alpha_{\mathbf{5b}}\left({}^{A}/_{A_{\mathbf{ST}}}\right) + b \tag{S1}$$

where α is the response factor relative to cyclooctane. The raw data and fit parameters are listed in Table S1 and depicted in Figures S194-S196.

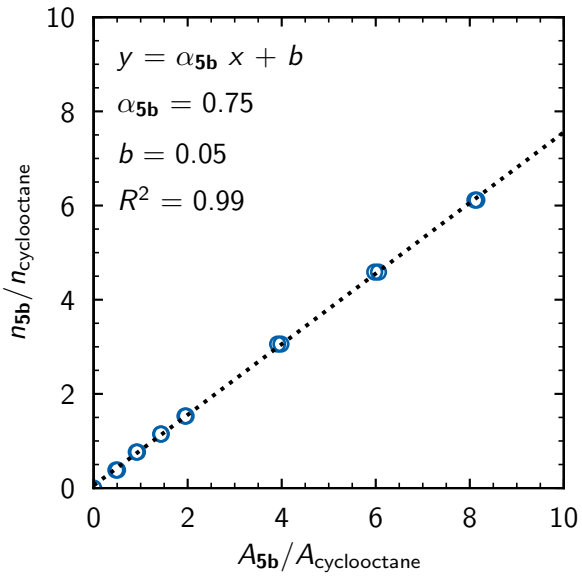

Figure S196. Calibration curve to determine the GC response factor ($\alpha_{\mathbf{5b}}$) of **5b** relative to cyclooctane. See Table S1 for tabulated values.

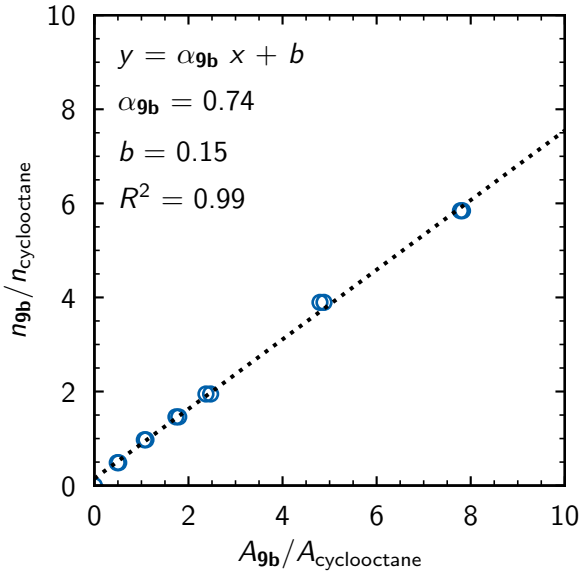

Figure S197. Calibration curve to determine the GC response factor ($\alpha_{\mathbf{9b}}$) of **9b** relative to cyclooctane. See Table S1 for tabulated values.

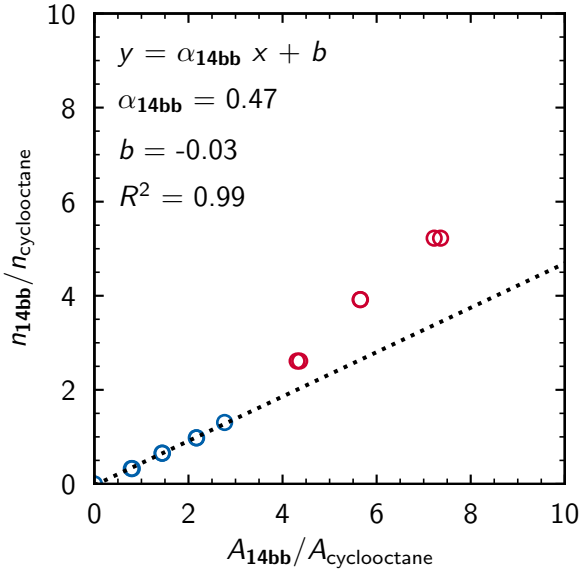

Figure S198. Calibration curve to determine the GC response factor ($\alpha_{\mathbf{14b}}$) of **14bb** relative to cyclooctane. Regression limited to the linear range shown in blue. See Table S1 for tabulated values.

Table S1. Calibration curves to determine the GC response factors relative to cyclooctane.[a]

Raw Data: [a]						
Entry	**5b**		**9b**		**14bb**	
	A_{5b}/A_{ST}	n_{5b}/n_{ST}	A_{9b}/A_{ST}	n_{9b}/n_{ST}	A_{14bb}/A_{ST}	n_{14bb}/n_{ST}
1	0.473	0.382	0.517	0.487	0.786	0.327
2	0.508	0.382	0.486	0.487	0.805	0.327
3	0.906	0.765	1.096	0.974	1.437	0.653
4	0.932	0.765	1.062	0.974	1.446	0.653
5	1.438	1.147	1.793	1.461	2.172	0.980
6	1.425	1.147	1.734	1.461	2.167	0.980
7	1.966	1.529	2.471	1.948	2.768	1.306
8	1.943	1.529	2.372	1.948	2.765	1.306
9	3.984	3.058	4.881	3.895	4.310	2.612
10	3.913	3.058	4.795	3.895	4.364	2.612
11	6.059	4.587	7.825	5.843	5.656	3.918
12	5.977	4.587	7.782	5.843	5.649	3.918
13	8.109	6.116	10.349	7.791	7.223	5.225
14	8.150	6.116	10.361	7.791	7.359	5.225
Fit Parameters: [b]						
α [b]	0.75		0.74		0.47 [c]	
b [b]	0.05		0.15		–0.03 [c]	
R^2 [b]	0.99		0.99		0.99 [c]	

[a] See Figures S194–S196. [b] Determined from the linear regression of the data to Equation S1. [c] Determined for the linear regime only where $A_{14bb}/A_{ST} \leq 2.768$.

To minimize any confounding effects arising, all trials necessary for comparison within a single experiment were performed side-by-side using the same batches of starting materials and precatalyst where possible. All kinetic experiments were conducted in a glovebox. While standard preparative conditions were conducted in neat substrate, kinetic experiments were performed in benzene solution to ensure uniform mixing and ease of analysis. The chemoselectivity for formation of [4+2]-cycloadduct **14bb** (XX% [4+2]) was the same under neat conditions as in benzene solution. For each trial, substrate **9b** was filtered through a monster pipette (9.75 mm OD, 14.6 cm body, 4.5 mL capacity) filled with activated Al_2O_3 immediately prior to use. Substrates **5b** and **9b** were dispensed by mass into a 1.5 mL oven-dried glass vial. Cyclooctane and benzene were added using microliter glass syringes, and the vial was charged with a PTFE-coated flea magnetic stir bar. Separately, a 5.00 mL volumetric flask was charged with $[(^{Me}PDI)Fe(N_2)]_2(\mu_2\text{-}N_2)$ (0.044 g, 0.106 mmol), and benzene was added to volume. The [Fe] precatalyst solution was mixed to homogeneity, filtered through a plug of glass wool, and dispensed using a microliter glass syringe to initiate reaction. The precatalyst solution was frozen and stored at –35 °C. The reaction vial was sealed with a PTFE-lined screw cap, and the reaction was maintained with stirring at ambient temperature (25 °C) in the glovebox.

Aliquots (~2 μL) were removed from the reaction mixture with the tip of a glass Pasteur pipette at regular intervals. Each aliquot was immediately diluted ~500-fold in Et_2O (1 mL). The samples were removed from

the glovebox, exposed to air, and analyzed by gas chromatography. The conversion of substrates **5b** and **9b** to product **14bb** was monitored over the full course of the reaction relative to the cyclooctane internal standard. Using the calibrated response factors, an empirically determined constant infinity point, and the known initial concentrations of cyclooctane and substrates **5b** and **9b**, the concentration of each reaction component was calculated from the raw GC integration data as a function of time. The total volume (V_{tot}) was assumed constant over the course of the reaction.

In general, the reaction time-courses demonstrated clean exponential substrate consumption and product formation. As such, the concentration vs. time data were fit to a net first-order rate law as shown in Equations S2–S4 for the limiting substrate ($[SM]_{limiting}$ = [**5b**] or [**9b**]), the substrate used in excess ($[SM]_{excess}$ = $[SM]_{limiting}$ + *excess* = [**5b**] or [**9b**]), and the product, respectively. Fit values for variable parameters describing the initial (or final) concentrations and the first-order rate constant, k_{obs}, were extracted.

$$[\mathrm{SM}]_{t,\mathrm{limiting}} = [\mathrm{SM}]_{0,\mathrm{limiting}} e^{-k_{\mathrm{obs}} t} \tag{S2}$$

$$[\mathrm{SM}]_{t,\mathrm{excess}} = [\mathrm{SM}]_{0,\mathrm{limiting}} e^{-k_{\mathrm{obs}} t} + excess \tag{S3}$$

$$[\mathbf{14bb}]_t = [\mathbf{14bb}]_{\infty}(1 - e^{-k_{\mathrm{obs}} t}) \tag{S4}$$

Alternatively, the initial rates (v_0) were determined from linear regression to concentration vs. time data obtained at time points where conversion of the limiting substrate ≤10%.

$$[\mathrm{SM}]_t = -v_0 t + [\mathrm{SM}]_0 \tag{S5}$$

$$[\mathbf{14bb}]_t = v_0 t + [\mathbf{14bb}]_0 \tag{S6}$$

5.2 Test for Catalyst Death and/or Product Inhibition

To evaluate whether the total concentration of active iron catalyst remained constant over the course of the reaction, a “same excess” experiment was performed as described by Blackmond.[62] Full reaction time courses were monitored for trials conducted with the same $[Fe]_{tot}$ and the same excess of one substrate (*excess* = $[\mathbf{9b}]_0 - [\mathbf{5b}]_0$) but with different absolute substrate concentrations. These variations mimic initiating the reaction at an intermediate substrate conversion. The overlay of time-shifted concentration vs. time plots from these experiments indicates that catalyst deactivation and product inhibition are negligible under the reaction conditions examined. The concentration and rate data are presented in Tables S2–4 and plotted in Figure S198.

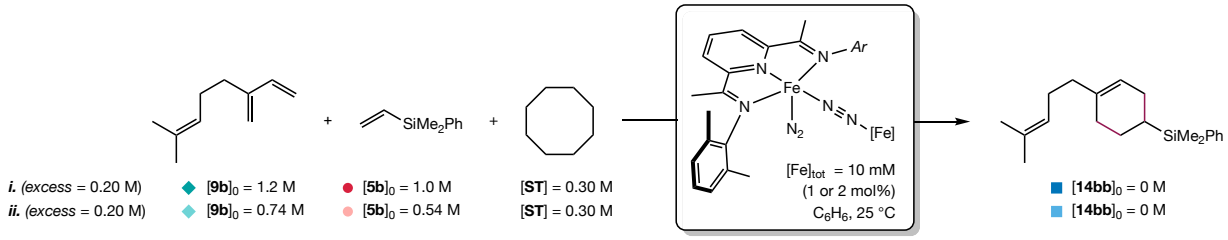

Figure S199. "Same-Excess" experiment to test for catalyst death and/or product inhibition.

Table S2. Concentration [**5b**] vs. time data from the "same-excess" experiment. [a]

time (min)	[**5b**]$_t$ (M), where:									
	where [**5b**]$_0$ = 1.0 M, [**9b**]$_0$ = 1.2 M					[**5b**]$_0$ = 0.54 M, [**9b**]$_0$ = 0.74 M				
	trial i	*trial ii*	*trial iii*	*trial iv*	*avg*	*trial i*	*trial ii*	*trial iii*	*trial iv*	*avg.*
10	0.901	0.944	0.917	0.928	0.922	0.494	0.498	0.500	0.503	0.499
20	0.896	0.931	0.905	0.910	0.910	0.489	0.498	0.488	0.492	0.492
30	0.899	0.910	0.879	0.934	0.905	0.480	0.490	0.477	0.476	0.481
45	0.886	0.888	0.858	0.871	0.876	0.463	0.487	0.466	0.467	0.471
60	0.863	0.849	0.852	0.860	0.856	0.453	0.465	0.451	0.457	0.456
80	0.852	0.846	0.829	0.831	0.839	0.439	0.442	0.448	0.441	0.443
100	0.828	0.826	0.815	0.814	0.821	0.425	0.450	0.429	0.447	0.438
120	0.799	0.812	0.783	0.777	0.793	0.421	0.428	0.414	0.447	0.428
150	0.785	0.795	0.759	0.762	0.775	0.406	0.417	0.399	0.430	0.413
180	0.757	0.753	0.721	0.728	0.740	0.392	0.403	0.384	0.389	0.392
210	0.733	0.740			0.736	0.376	0.383			0.379
240	0.700	0.704	0.669	0.675	0.687	0.363	0.366	0.349	0.391	0.367
270	0.676	0.697			0.687	0.346	0.366			0.356
300	0.678	0.685	0.628	0.642	0.658	0.349	0.367	0.328	0.330	0.344
330	0.661	0.674			0.667	0.335	0.342			0.339
360	0.633	0.641	0.584	0.576	0.609	0.319	0.332	0.300	0.309	0.315
420	0.582	0.585	0.539	0.535	0.560	0.285	0.290	0.275	0.280	0.283
480			0.495	0.495	0.495			0.257	0.286	0.271
540			0.459	0.475	0.467			0.232	0.241	0.237
600			0.420	0.417	0.418			0.188	0.222	0.205
720			0.358	0.354	0.356			0.187	0.189	0.188
1040	0.300	0.256			0.278	0.134	0.141			0.138
1255			0.166	0.179	0.172			0.095	0.103	0.099
1440			0.137	0.147	0.142			0.085	0.089	0.087
1620			0.114	0.119	0.117	0.080	0.057			0.069
1800			0.103	0.106	0.105	0.494	0.498	0.500	0.503	0.499
2880	0.137	0.084			0.110	0.489	0.498	0.488	0.492	0.492

[a] For all experiments, *excess* = 0.2 M, [Fe]$_{tot}$ = 0.010 M. Reactions conducted in benzene at 25 °C. See Figure **S197**.

Table S3. Concentration [**9b**] vs. time data from the "same-excess" experiment. [a]

time (min)	[**9b**]$_t$ (M), where:									
	where [**5b**]$_0$ = 1.0 M, [**9b**]$_0$ = 1.2 M					[**5b**]$_0$ = 0.54 M, [**9b**]$_0$ = 0.74 M				
	trial i	*trial ii*	*trial iii*	*trial iv*	*avg*	*trial i*	*trial ii*	*trial iii*	*trial iv*	*avg.*
10	1.041	1.128	1.112	1.137	1.105	0.674	0.652	0.721	0.653	0.675
20	1.027	1.110	1.103	1.121	1.090	0.671	0.664	0.713	0.638	0.672
30	1.034	1.091	1.067	1.098	1.072	0.657	0.651	0.695	0.625	0.657
45	1.008	1.061	1.051	1.076	1.049	0.644	0.638	0.685	0.619	0.646
60	0.997	1.036	1.044	1.067	1.036	0.635	0.625	0.671	0.604	0.634
80	0.972	1.026	1.019	1.032	1.012	0.620	0.604	0.659	0.589	0.618
100	0.963	0.994	0.999	1.005	0.990	0.609	0.606	0.636	0.586	0.609
120	0.931	0.972	0.970	0.980	0.963	0.587	0.578	0.624	0.596	0.596
150	0.914	0.970	0.933	0.949	0.942	0.575	0.572	0.605	0.559	0.578
180	0.883	0.929	0.898	0.920	0.908	0.563	0.560	0.590	0.535	0.562
210	0.861	0.902	--	--	0.882	0.552	0.541	--	--	0.547
240	0.828	0.865	0.841	0.859	0.848	0.541	0.521	0.555	0.547	0.541
270	0.799	0.866	--	--	0.832	0.514	0.520	--	--	0.517
300	0.795	0.848	0.791	0.813	0.812	0.516	0.518	0.523	0.470	0.507
330	0.783	0.842	--	--	0.812	0.505	0.486	--	--	0.495
360	0.750	0.815	0.755	0.757	0.769	0.483	0.481	0.501	0.444	0.477
420	0.707	0.749	0.709	0.712	0.719	0.457	0.436	0.473	0.414	0.445
480	--	--	0.660	0.669	0.665	--	--	0.451	0.414	0.432
540	--	--	0.610	0.605	0.607	--	--	0.423	0.367	0.395
600	--	--	0.564	0.571	0.568	--	--	0.368	0.344	0.356
720	--	--	0.496	0.499	0.498	--	--	0.364	0.311	0.338
1040	0.393	0.406	--	--	0.400	0.286	0.289	--	--	0.287
1255	--	--	0.298	0.305	0.301	--	--	0.269	0.220	0.245
1440	--	--	0.277	0.281	0.279	--	--	0.248	0.206	0.227
1620	--	--	0.254	0.262	0.258	--	--	--	--	--
1800	--	--	0.237	0.249	0.243	--	--	--	--	--
2880	0.231	0.213	--	--	0.222	0.223	0.186	--	--	0.204

[a] For all experiments, *excess* = 0.2 M, $[Fe]_{tot}$ = 0.010 M. Reactions conducted in benzene at 25 °C. See Figure **S197**.

Table S4. Concentration [**14bb**] vs. time data from the "same-excess" experiment. [a]

time (min)	[**14bb**]$_t$ (M), where:									
	where [**5b**]$_0$ = 1.0 M, [**9b**]$_0$ = 1.2 M					[**5b**]$_0$ = 0.54 M, [**9b**]$_0$ = 0.74 M				
	trial i	*trial ii*	*trial iii*	*trial iv*	*avg*	*trial i*	*trial ii*	*trial iii*	*trial iv*	*avg.*
10	0.002	0.003	0.006	0.009	0.005	0.000	0.000	0.006	0.005	0.003
20	0.015	0.018	0.023	0.025	0.020	0.011	0.010	0.016	0.017	0.013
30	0.028	0.029	0.039	0.045	0.035	0.019	0.020	0.029	0.028	0.024
45	0.045	0.047	0.061	0.062	0.054	0.030	0.034	0.048	0.041	0.038
60	0.065	0.065	0.078	0.080	0.072	0.045	0.047	0.054	0.053	0.050
80	0.085	0.086	0.100	0.104	0.094	0.058	0.057	0.070	0.068	0.063
100	0.104	0.105	0.124	0.130	0.116	0.069	0.072	0.083	0.085	0.077
120	0.119	0.123	0.144	0.143	0.132	0.080	0.079	0.092	0.098	0.087
150	0.148	0.153	0.174	0.178	0.163	0.098	0.099	0.113	0.119	0.107
180	0.169	0.172	0.203	0.207	0.188	0.113	0.118	0.129	0.133	0.123
210	0.197	0.207			0.202	0.131	0.130			0.130
240	0.226	0.234	0.256	0.268	0.246	0.151	0.145	0.164	0.173	0.158
270	0.254	0.259			0.256	0.157	0.167			0.162
300	0.284	0.296	0.322	0.333	0.309	0.177	0.191	0.208	0.198	0.193
330	0.306	0.325			0.316	0.192	0.194			0.193
360	0.330	0.338	0.377	0.391	0.359	0.210	0.214	0.230	0.231	0.221
420	0.370	0.375	0.429	0.435	0.402	0.227	0.235	0.257	0.255	0.243
480			0.476	0.491	0.483			0.294	0.321	0.308
540			0.537	0.537	0.537			0.315	0.306	0.311
600			0.575	0.608	0.592			0.340	0.339	0.339
720			0.662	0.667	0.664			0.388	0.378	0.383
1040	0.894	0.764			0.829	0.421	0.406			0.413
1255			0.861	0.928	0.895			0.496	0.483	0.490
1440			0.931	0.950	0.941			0.534	0.508	0.521
1620			0.938	0.965	0.952	0.500	0.551			0.526
1800			0.965	0.948	0.956	0.000	0.000	0.006	0.005	0.003
2880	0.974	1.014			0.994	0.011	0.010	0.016	0.017	0.013

[a] For all experiments, *excess* = 0.2 M, $[Fe]_{tot}$ = 0.010 M. Reactions conducted in benzene at 25 °C. See Figure **S197**.

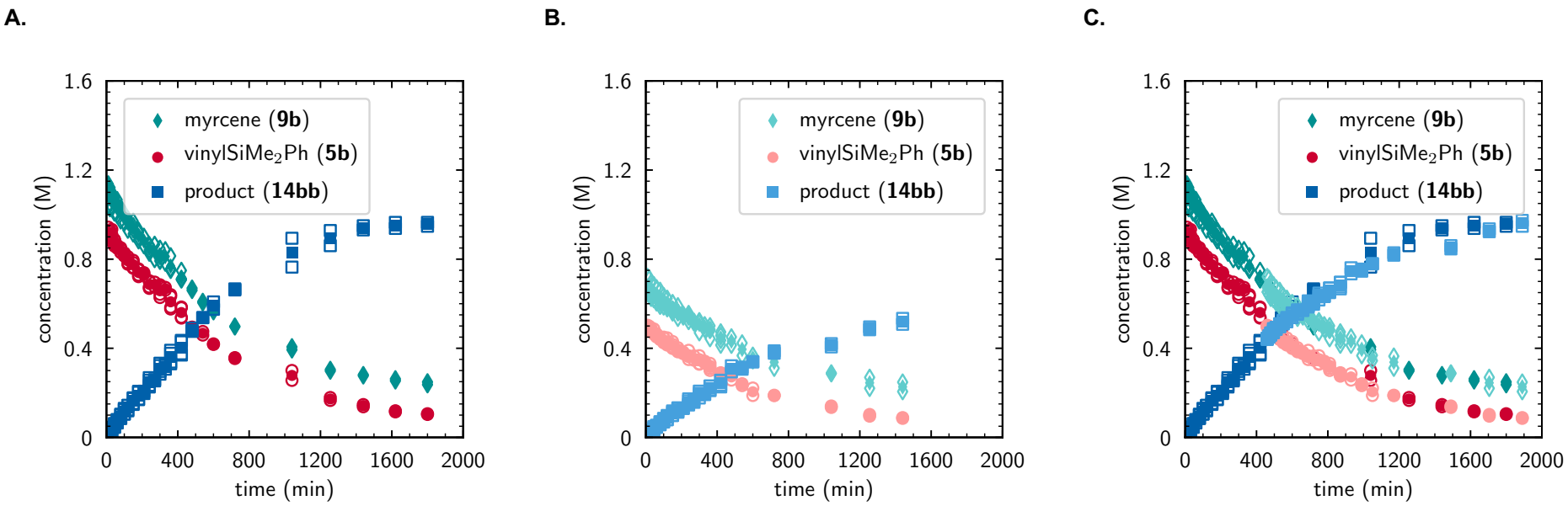

Figure S200. Concentration vs. time data for trials initiated with the "same excess" substrate concentrations. (**A.**) [**5b**]$_0$ = 1.0 M, [**9b**]$_0$ = 1.2 M, excess = 0.2 M, [Fe]$_{tot}$ = 0.010 M. (**B.**) [**5b**]$_0$ = 0.54 M, [**9b**]$_0$ = 0.74 M, excess = 0.20 M, [Fe]$_{tot}$ = 0.010 M. (**C.**) Overlay of plots A and B where the time-axis is shifted +450 minutes and [**14bb**] is shifted +0.44 M. Open markers represent data points obtained from individual trials; closed markers represent average values obtained from duplicate trials. See Table S2 for tabulated data.

5.3 Determination of Kinetic Order in Diene 9b

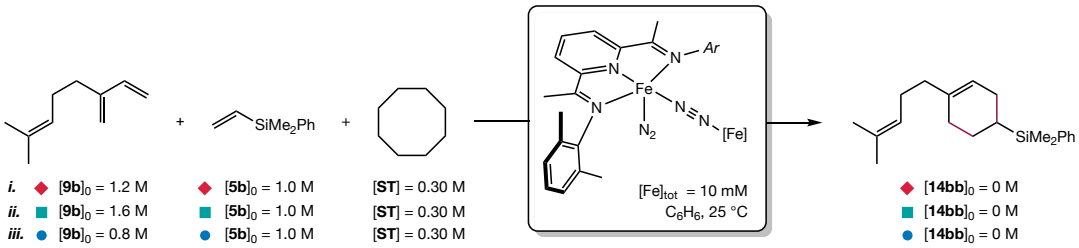

Figure S201. Determination of order in diene **9b**.

To determine the order in myrcene, initial rate measurements and full reaction time courses were monitored for trials conducted with the same $[Fe]_{tot}$ and $[\mathbf{5b}]_0$ but differing $[\mathbf{9b}]_0$. The overlay of concentration vs. time plots from these experiments indicates that the reaction exhibits a zero-order dependence on diene **9b** (i.e. no rate dependence) under the conditions examined. This is consistent with saturation of the iron catalyst with diene in the resting state (see Section 5.2). The concentration and rate data are presented in Tables S5–7 and plotted in Figure **S200**.

Table S5. Concentration [**5b**] vs. time data with varied [**9b**]$_0$. [a]

time (min)	[**5b**]$_t$ (M), where:								
	where [**9b**]$_0$ = 1.2 M			where [**9b**]$_0$ = 1.6 M			where [**9b**]$_0$ = 0.8 M		
	trial i	*trial ii*	*avg*	*trial i*	*trial ii*	*avg.*	*trial i*	*trial ii*	*avg.*
10	0.901	0.944	0.922	0.884	0.933	0.908	0.901	0.969	0.935
20	0.896	0.931	0.913	0.880	0.920	0.900	0.899	0.940	0.919
30	0.899	0.910	0.905	0.870	0.900	0.885	0.882	0.905	0.893
45	0.886	0.888	0.887	0.842	0.900	0.871	0.873	0.913	0.893
60	0.863	0.849	0.856	0.833	0.853	0.843	0.838	0.924	0.881
80	0.852	0.846	0.849	0.810	0.850	0.830	0.825	0.845	0.835
100	0.828	0.826	0.827	0.801	0.823	0.812	0.811	0.858	0.834
120	0.799	0.812	0.805	0.761	0.806	0.784	0.793	0.819	0.806
150	0.785	0.795	0.790	0.734	0.787	0.761	0.766	0.810	0.788
180	0.757	0.753	0.755	0.713	0.748	0.731	0.748	0.780	0.764
210	0.733	0.740	0.736	0.695	0.718	0.706	0.727	0.740	0.733
240	0.700	0.704	0.702	0.704	0.697	0.701	0.704	0.752	0.728
270	0.676	0.697	0.687	0.629	0.681	0.655	0.682	0.698	0.690
300	0.678	0.685	0.682	0.642	0.666	0.654	0.678	0.707	0.693
330	0.661	0.674	0.667	0.630	0.640	0.635	0.668	0.686	0.677
360	0.633	0.641	0.637	0.597	0.620	0.608	0.660	0.680	0.670
420	0.582	0.585	0.583	0.549	0.561	0.555	0.608	0.614	0.611
1040	0.300	0.256	0.278	0.197	0.212	0.204	0.344	0.356	0.350
2880	0.137	0.084	0.110	0.071	0.036	0.053	0.264	0.248	0.256
Initial Rate									
v_0 (10^{-3} M min^{-1})	0.84	1.36	1.10	1.01	1.22	1.11	1.18	1.36	1.27
[**5b**]$_0$ (M)	0.92	0.95	0.93	0.89	0.94	0.92	0.92	0.97	0.94
R^2	0.95	0.95	0.98	0.97	0.95	0.98	0.96	0.73	0.93
First-Order Fit									
k_{obs} (10^{-3} min^{-1})	1.01(5)	1.12(4)	1.07(4)	1.22(5)	1.26(3)	1.24(4)	1.49(8)	1.5(1)	1.51(8)
[**5b**]$_0$ (M)	0.91(1)	0.94(1)	0.92(1)	0.89(1)	0.95(1)	0.92(1)	0.91(2)	0.96(2)	0.94(2)
excess (M)	--	--	--	--	--	--	0.24(2)	0.23(2)	0.24(2)

[a] For all experiments, [**5b**]$_0$ = 1.0 M, [Fe]$_{tot}$ = 0.010 M. Reactions conducted in benzene at 25 °C. See Figures **S200**.

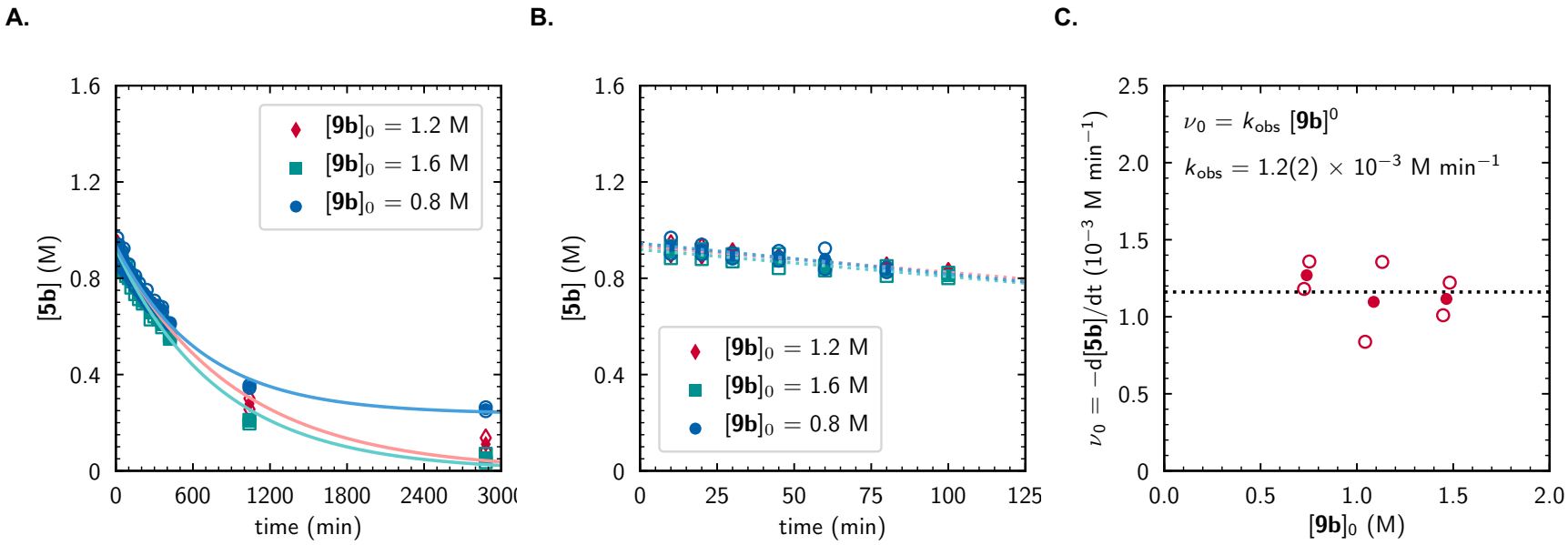

Figure S202. Concentration vs. time data, monitoring [**5b**]$_t$, for trials initiated with varied [**9b**]$_0$ where [**5b**]$_0$ = 1.0 M and [Fe]$_{tot}$ = 0.010 M. Open markers represent data points obtained from individual trials; closed markers represent average values obtained from duplicate trials. (**A.**) Full reaction time course fit to a first-order rate law (solid lines). (**B.**) Initial rate profiles obtained from linear regression (dotted lines) to data obtained where conversion ≤10%. (**C.**). Initial rate vs. initial concentration [**9b**]$_0$ with the average effective rate constant (k_{obs}, dotted line). See Table S5 for tabulated data and fit parameters.

Table S6. Concentration [**9b**] vs. time data with varied [**9b**]$_0$. [a]

time (min)	[9**b**]$_t$ (M), where:								
	where [**9b**]$_0$ = 1.2 M			where [**9b**]$_0$ = 1.6 M			where [**9b**]$_0$ = 0.8 M		
	trial i	*trial ii*	*avg*	*trial i*	*trial ii*	*avg.*	*trial i*	*trial ii*	*avg.*
10	1.041	1.128	1.084	1.445	1.478	1.461	0.724	0.752	0.738
20	1.027	1.110	1.069	1.425	1.461	1.443	0.715	0.738	0.726
30	1.034	1.091	1.062	1.414	1.451	1.433	0.703	0.719	0.711
45	1.008	1.061	1.034	1.396	1.446	1.421	0.702	0.717	0.710
60	0.997	1.036	1.017	1.386	1.374	1.380	0.671	0.718	0.694
80	0.972	1.026	0.999	1.371	1.382	1.377	0.655	0.655	0.655
100	0.963	0.994	0.979	1.361	1.363	1.362	0.654	0.660	0.657
120	0.931	0.972	0.951	1.312	1.327	1.319	0.618	0.621	0.619
150	0.914	0.970	0.942	1.285	1.308	1.297	0.592	0.615	0.603
180	0.883	0.929	0.906	1.264	1.254	1.259	0.576	0.590	0.583
210	0.861	0.902	0.882	1.247	1.250	1.248	0.546	0.559	0.552
240	0.828	0.865	0.846	1.236	1.206	1.221	0.528	0.588	0.558
270	0.799	0.866	0.832	1.179	1.208	1.194	0.506	0.518	0.512
300	0.795	0.848	0.821	1.185	1.191	1.188	0.495	0.504	0.500
330	0.783	0.842	0.812	1.176	1.165	1.170	0.484	0.488	0.486
360	0.750	0.815	0.782	1.149	1.136	1.142	0.465	0.478	0.472
420	0.707	0.749	0.728	1.066	1.079	1.073	0.425	0.422	0.424
1040	0.393	0.406	0.400	0.691	0.686	0.689	0.170	0.173	0.171
2880	0.231	0.213	0.222	0.540	0.483	0.511	0.094	0.075	0.085
Initial Rate									
v_0 (10^{-3} M min^{-1})	0.91	1.46	1.19	0.90	1.34	1.13	1.00	1.16	1.08
[**9b**]$_0$ (M)	1.05	1.14	1.09	1.44	1.49	1.47	0.74	0.76	0.75
R^2	0.97	0.97	0.99	0.96	0.88	0.94	0.96	0.83	0.94
First-Order Fit									
k_{obs} (10^{-3} min^{-1})	1.28(5)	1.20(7)	1.24(5)	1.22(8)	1.21(9)	1.21(7)	1.30(6)	1.33(6)	1.32(6)
[**9b**]$_0$ (M)	1.06(1)	1.12(2)	1.19(2)	1.46(3)	1.49(3)	1.47(3)	0.73(1)	0.75(1)	0.74(1)
excess (M)	0.20(1)	0.17(2)	0.19(2)	0.49(3)	0.44(3)	0.46(3)	--	--	--

[a] For all experiments, [**5b**]$_0$ = 1.0 M, [Fe]$_{tot}$ = 0.010 M. Reactions conducted in benzene at 25 °C. See Figures **S201**.

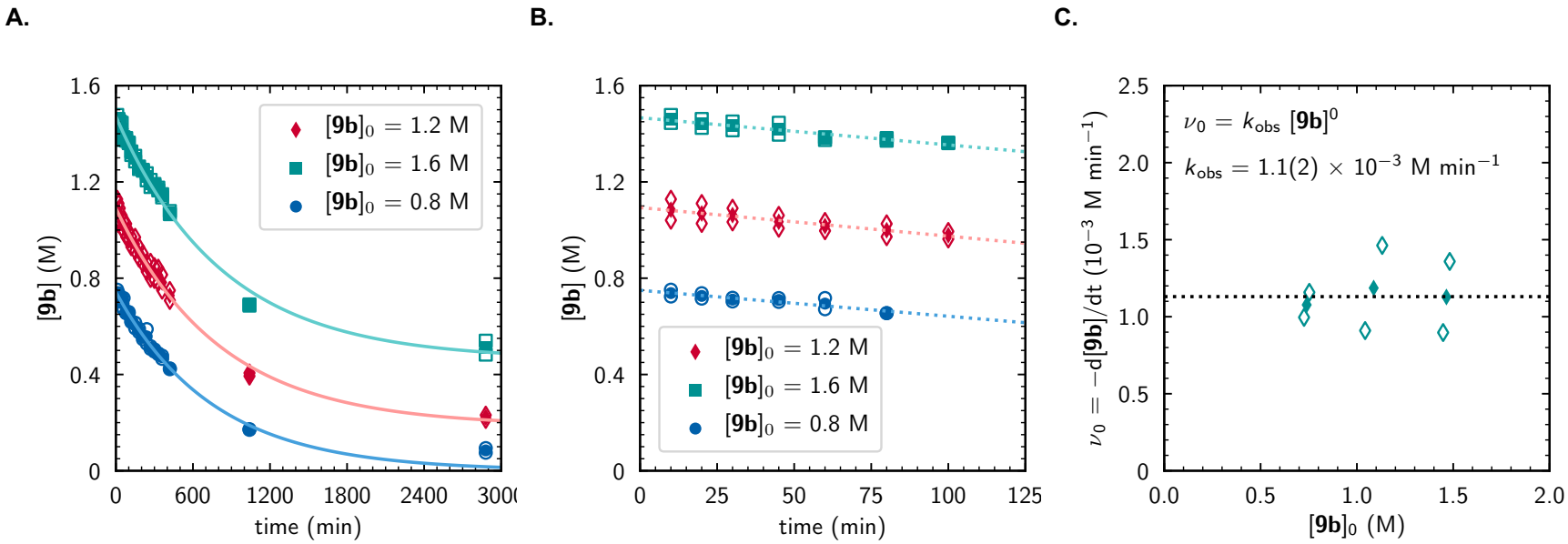

Figure S203. Concentration vs. time data, monitoring $[\mathbf{9b}]_t$, for trials initiated with varied $[\mathbf{9b}]_0$ where $[\mathbf{5b}]_0$ = 1.0 M and $[Fe]_{tot}$ = 0.010 M. Open markers represent data points obtained from individual trials; closed markers represent average values obtained from duplicate trials. (**A.**) Full reaction time course fit to a first-order rate law (solid lines). (**B.**) Initial rate profiles obtained from linear regression (dotted lines) to data obtained where conversion ≤10%. (**C.**). Initial rate vs. initial concentration $[\mathbf{9b}]_0$ with the average effective rate constant (k_{obs}, dotted line). See Table S6 for tabulated data and fit parameters.

Table S7. Concentration [**14bb**] vs. time data with varied [**9b**]$_0$. [a]

time (min)	[**14bb**]$_t$ (M), where:								
	where [**9b**]$_0$ = 1.2 M			where [**9b**]$_0$ = 1.6 M			where [**9b**]$_0$ = 0.8 M		
	trial i	*trial ii*	*avg*	*trial i*	*trial ii*	*avg.*	*trial i*	*trial ii*	*avg.*
10	0.002	0.003	0.003	0.003	0.004	0.003	0.002	0.001	0.001
20	0.015	0.018	0.016	0.017	0.018	0.017	0.013	0.016	0.015
30	0.028	0.029	0.029	0.030	0.029	0.030	0.026	0.027	0.026
45	0.045	0.047	0.046	0.047	0.047	0.047	0.041	0.045	0.043
60	0.065	0.065	0.065	0.067	0.071	0.069	0.059	0.068	0.063
80	0.085	0.086	0.085	0.086	0.088	0.087	0.075	0.079	0.077
100	0.104	0.105	0.105	0.106	0.110	0.108	0.094	0.099	0.096
120	0.119	0.123	0.121	0.126	0.128	0.127	0.113	0.114	0.113
150	0.148	0.153	0.150	0.155	0.160	0.157	0.138	0.140	0.139
180	0.169	0.172	0.171	0.177	0.183	0.180	0.163	0.161	0.162
210	0.197	0.207	0.202	0.209	0.212	0.211	0.192	0.186	0.189
240	0.226	0.234	0.230	0.215	0.247	0.231	0.215	0.226	0.221
270	0.254	0.259	0.256	0.270	0.274	0.272	0.234	0.230	0.232
300	0.284	0.296	0.290	0.305	0.306	0.306	0.259	0.265	0.262
330	0.306	0.325	0.316	0.330	0.327	0.328	0.281	0.289	0.285
360	0.330	0.338	0.334	0.363	0.362	0.363	0.316	0.316	0.316
420	0.370	0.375	0.373	0.396	0.390	0.393	0.334	0.337	0.336
1040	0.894	0.764	0.829	0.813	0.818	0.815	0.635	0.629	0.632
2880	0.974	1.014	0.994	0.979	1.056	1.017	0.732	0.806	0.769
Initial Rate									
v_0 (10^{-3} M min^{-1})	1.15	1.13	1.14	1.15	1.19	1.17	1.06	1.15	1.11
[**14bb**]$_0$ (M)	–0.007	–0.005	–0.006	–0.006	–0.006	–0.006	–0.007	–0.007	–0.008
R^2	0.99	0.99	0.99	0.99	0.99	0.99	0.99	0.98	0.99
First-Order Fit									
k_{obs} (10^{-3} min^{-1})	1.2(1)	1.06(3)	1.09(7)	1.17(6)	1.07(4)	1.08(3)	1.42(5)	1.27(3)	1.34(3)
[**14bb**]$_\infty$ (M)	1.06(6)	1.08(2)	1.07(4)	1.04(3)	1.13(2)	1.12(5)	0.76(1)	0.83(1)	0.80(1)

[a] For all experiments, [**5b**]$_0$ = 1.0 M, [Fe]$_{tot}$ = 0.010 M. Reactions conducted in benzene at 25 °C. See Figures **S202**.

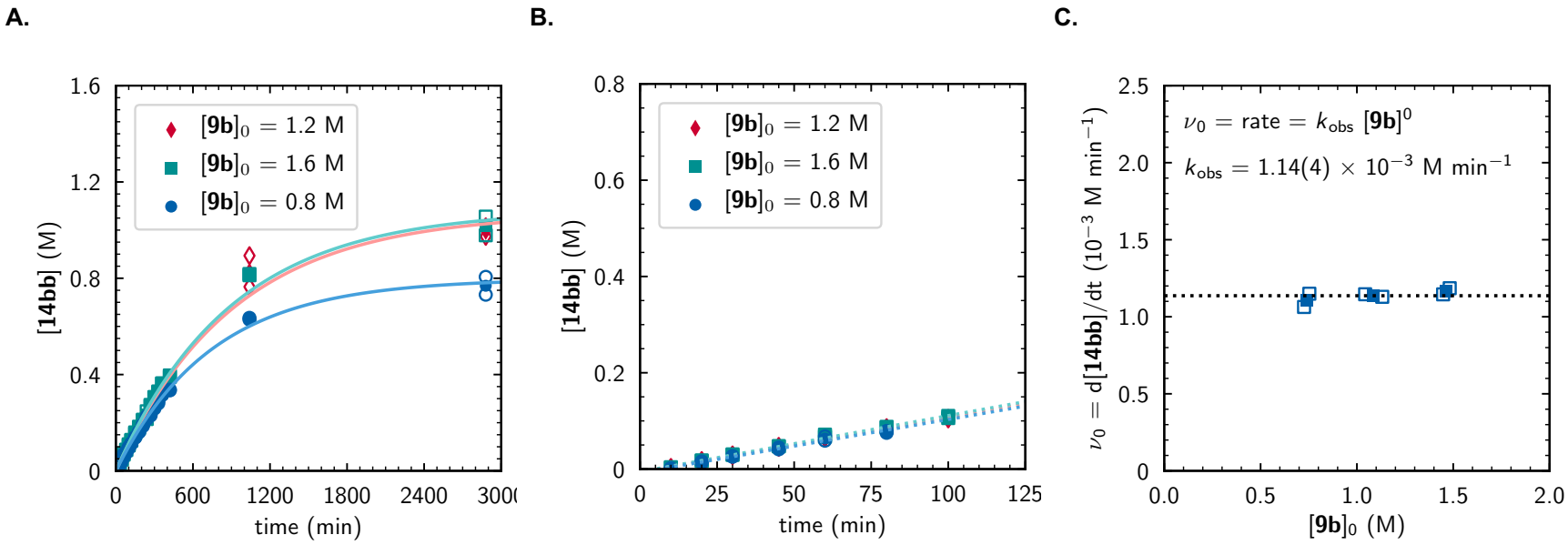

Figure S204. Concentration vs. time data, monitoring [**15bb**]$_t$, for trials initiated with varied [**9b**]$_0$ where [**5b**]$_0$ = 1.0 M and [Fe]$_{tot}$ = 0.010 M. Open markers represent data points obtained from individual trials; closed markers represent average values obtained from duplicate trials. (**A.**) Full reaction time course fit to a first-order rate law (solid lines). (**B.**) Initial rate profiles obtained from linear regression (dotted lines) to data obtained where conversion ≤10%. (**C.**). Initial rate vs. initial concentration [**9b**]$_0$ with the average effective rate constant (k_{obs}, dotted line). See Table S7 for tabulated data and fit parameters.

5.4 Determination of Kinetic Order in Vinyl Silane 5b

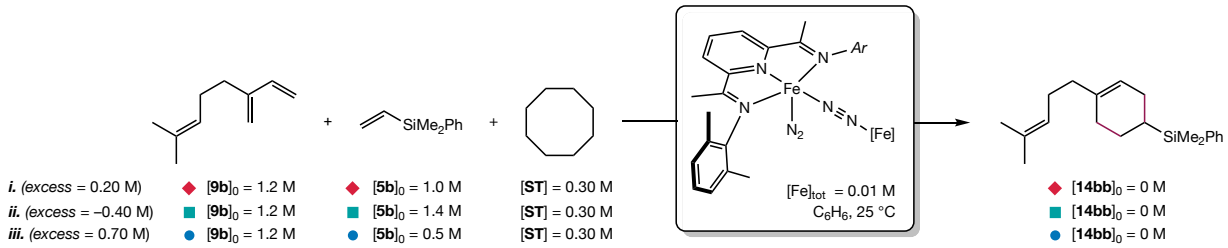

Figure S205. Determination of order in vinyl silane **5b**.

To determine the order in myrcene, initial rate measurements and full reaction time courses were monitored for trials conducted with the same $[Fe]_{tot}$ and $[\mathbf{9b}]_0$ but differing $[\mathbf{5b}]_0$. Under all of the conditions examined, the reaction exhibited clean exponential decay of substrate concentration and exponential growth of product concentration, indicative of a net first-order rate law (at constant $[Fe]_{tot}$). Given the zero-order dependence on diene [**9b**], this observation was most consistent with the first-order dependence arising from the changing vinyl silane [**5b**]. This conclusion was corroborated by the observation of a linear relationship between $[\mathbf{5b}]_0$ and the initial rate, v_0. at low $[\mathbf{5b}]_0$ and saturation at high $[\mathbf{5b}]_0$. The concentration and rate data are presented in Tables S8–10 and plotted in **Figures S204–206**.

Table S8. Concentration [**5b**] vs. time data with varied [**5b**]$_0$. [a]

time (min)	[**5b**]$_t$ (M), where:							
	where [**5b**]$_0$ = 1.4 M			where [**5b**]$_0$ = 1.0 M			where [**5b**]$_0$ = 0.54 M	
	trial i	*trial ii*	*avg.*	*trial i*	*trial ii*	*avg*	*trial i*	*trial ii*
10	1.324	1.341	1.333	0.917	0.928	0.922	0.487	0.492
20	1.314	1.301	1.308	0.905	0.910	0.908	0.489	0.482
30	1.297	1.295	1.296	0.879	0.934	0.906	0.463	0.467
45	1.284	1.273	1.279	0.858	0.871	0.865	0.453	0.453
60	1.266	1.253	1.260	0.852	0.860	0.856	0.438	0.444
80	1.227	1.255	1.241	0.829	0.831	0.830	0.447	0.427
100	1.189	1.199	1.194	0.815	0.814	0.815	0.418	0.415
120	1.166	1.175	1.170	0.783	0.777	0.780	0.407	0.410
150	1.135	1.143	1.139	0.759	0.762	0.761	0.392	0.391
180	1.112	1.100	1.106	0.721	0.728	0.725	0.377	0.367
240	1.022	1.054	1.038	0.669	0.675	0.672	0.346	0.341
300	0.976	0.981	0.978	0.628	0.642	0.635	0.314	0.310
360	0.911	0.918	0.914	0.584	0.576	0.580	0.287	0.286
420	0.859	0.872	0.866	0.539	0.535	0.537	0.261	0.254
480	0.808	0.808	0.808	0.495	0.495	0.495	0.243	0.229
540	0.750	0.749	0.750	0.459	0.475	0.467	0.208	0.212
600	0.709	0.710	0.710	0.420	0.417	0.418	0.189	0.189
720	0.613	0.618	0.616	0.358	0.354	0.356	0.155	0.156
1255	0.373	0.367	0.370	0.166	0.179	0.172	0.078	0.067
1440	0.330	0.340	0.335	0.137	0.147	0.142	0.057	0.052
1620	0.322	0.321	0.321	0.114	0.119	0.117	0.056	0.056
1800	0.300	0.301	0.301	0.103	0.106	0.105	0.053	0.000
1980	0.294	0.293	0.294	0.093	0.096	0.094	0.000	0.000
Initial Rate								
v_0 (10^{-3} M min^{-1})	1.34	1.17	1.13	1.25	1.47	1.36	1.07	1.00
[**5b**]$_0$ (M)	1.34	1.33	1.34	0.92	0.95	0.94	0.50	0.50
R^2	0.98	0.85	0.98	0.96	0.87	0.97	0.93	0.98
First-Order Fit								
k_{obs} (10^{-3} min^{-1})	1.34(4)	1.31(5)	1.34(4)	1.29(1)	1.30(2)	1.30(1)	1.52(4)	1.59(4)
[**5b**]$_0$ (M)	1.35(1)	1.35(2)	1.35(1)	0.92(1)	0.93(1)	0.93(1)	0.49(1)	0.49(1)
excess (M)	0.19(1)	0.18(2)	0.18(1)	--	--	--	--	--

[a] For all experiments, [**9b**]$_0$ = 1.2 M, [Fe]$_{tot}$ = 0.010 M. Reactions conducted in benzene at 25 °C. See Figure **S204**. Continued in Table S9.

Table S9. Concentration [**5b**] vs. time data with varied [**5b**]$_0$, continued. [a]

time (min)	[**5b**]$_t$ (M), where:								
	where [**5b**]$_0$ = 0.54 M, continued			where [**5b**]$_0$ = 0.39 M			where [**5b**]$_0$ = 0.22 M		
	trial iii	*trial iv*	*avg*				*trial i*	*trial ii*	*avg.*
10	0.471	0.495	0.486	0.362	0.415	0.389	0.221	0.208	0.215
20	0.460	0.485	0.479	0.349	0.407	0.378	0.214	0.202	0.208
30	0.452	0.475	0.464	0.341	0.394	0.367	0.212	0.193	0.203
45	0.443	0.462	0.453	0.330	0.384	0.357	0.200	0.187	0.194
60	0.427	0.444	0.438	0.324	0.376	0.350	0.194	0.182	0.188
80	0.417	0.427	0.430	0.315	0.353	0.334	0.196	0.182	0.189
100	0.397	0.417	0.412	0.299	0.348	0.323	0.179	0.168	0.173
120	0.383	0.397	0.399	0.289	0.327	0.308	0.172	0.159	0.166
150	0.366	0.392	0.385	0.272	0.318	0.295	0.169	0.156	0.163
180	0.350	0.365	0.365	0.261	0.305	0.283	0.161	0.157	0.159
240	0.321	0.338	0.337	0.236	0.275	0.255	0.135	0.146	0.140
300	0.294	0.308	0.307	0.219	0.250	0.234	0.128	0.121	0.125
360	0.265	0.279	0.279	0.194	0.220	0.207	0.112	0.106	0.109
420	--	--	0.258	--	--	--	--	--	--
480	--	--	0.236	--	--	--	--	--	--
540	0.195	0.206	0.205	0.143	0.163	0.153	0.088	0.081	0.085
600	--	--	0.189	--	--	--	--	--	--
720	0.143	0.146	0.150	0.103	0.115	0.109	0.060	0.063	0.062
1255	0.061	0.067	0.068	0.048	0.055	0.052	0.036	0.036	0.036
1440	0.054	0.054	0.054	0.045	0.046	0.045	0.033	0.031	0.032
1620	--	--	0.056	--	--	--	--	--	--
1800	--	--	0.026	--	--	--	--	--	--
1980	--	--	0.000	--	--	--	--	--	--
Initial Rate									
v_0 (10^{-3} M min^{-1})	0.84	1.00	0.98	0.76	0.80	0.78	0.47	0.76	0.62
[**5b**]$_0$ (M)	0.48	0.51	0.50	0.37	0.42	0.39	0.23	0.22	0.22
R^2	0.99	0.99	0.99	0.96	0.97	0.97	0.89	0.99	0.99
First-Order Fit									
k_{obs} (10^{-3} min^{-1})	1.63(2)	1.63(2)	1.57(3)	1.69(4)	1.72(3)	1.71(3)	1.72(8)	1.60(7)	1.66(7)
[**5b**]$_0$ (M)	0.47(1)	0.50(1)	0.49(1)	0.36(2)	0.41(1)	0.39(1)	0.22(1)	0.20(1)	0.21(1)

[a] For all experiments, [**9b**]$_0$ = 1.2 M, [Fe]$_{tot}$ = 0.010 M. Reactions conducted in benzene at 25 °C. See Figures **S204**. Continued from Table S8.

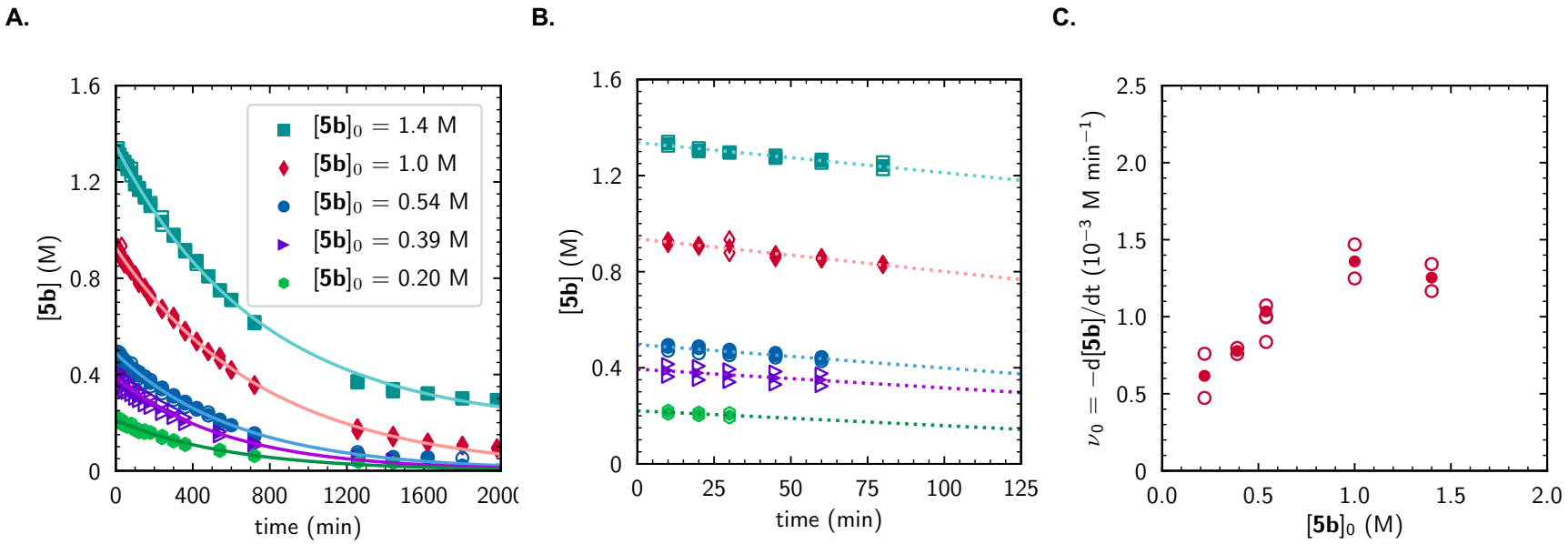

Figure S206. Concentration vs. time data, monitoring [**5b**]$_t$, for trials initiated with varied [**5b**]$_0$ where [**9b**]$_0$ = 1.2 M and [Fe]$_{tot}$ = 0.010 M. Open markers represent data points obtained from individual trials; closed markers represent average values obtained from duplicate trials. (**A.**) Full reaction time course fit to a first-order rate law (solid lines). (**B.**) Initial rate profiles obtained from linear regression (dotted lines) to data obtained where conversion ≤10%. (**C.**). Initial rate vs. initial concentration [**5b**]$_0$. See Tables S8 and S9 for tabulated data and fit parameters.

Table S10. Concentration [**9b**] vs. time data with varied [**5b**]$_0$. [a]

time (min)	[**9b**]$_t$ (M), where:							
	where [**5b**]$_0$ = 1.4 M			where [**5b**]$_0$ = 1.0 M			where [**5b**]$_0$ = 0.54 M	
	trial i	*trial ii*	*avg*	*trial i*	*trial ii*	*avg*	*trial i*	*trial ii*
10	1.126	1.123	1.124	1.112	1.137	1.125	1.085	1.108
20	1.114	1.099	1.106	1.103	1.121	1.112	1.076	1.088
30	1.089	1.093	1.091	1.067	1.098	1.082	1.030	1.073
45	1.078	1.067	1.072	1.051	1.076	1.063	1.042	1.069
60	1.047	1.049	1.048	1.044	1.067	1.055	1.025	1.058
80	1.020	1.038	1.029	1.019	1.032	1.025	0.996	1.038
100	0.988	0.992	0.990	0.999	1.005	1.002	0.987	1.011
120	0.963	0.967	0.965	0.970	0.980	0.975	0.975	1.012
150	0.923	0.935	0.929	0.933	0.949	0.941	0.958	0.972
180	0.896	0.889	0.892	0.898	0.920	0.909	0.935	0.965
240	0.826	0.823	0.825	0.841	0.859	0.850	0.905	0.921
300	0.768	0.771	0.769	0.791	0.813	0.802	0.871	0.891
360	0.704	0.711	0.708	0.755	0.757	0.756	0.836	0.861
420	0.652	0.657	0.655	0.709	0.712	0.711	0.808	0.835
480	0.591	0.599	0.595	0.660	0.669	0.665	0.773	0.806
540	0.537	0.539	0.538	0.610	0.605	0.607	0.739	0.771
600	0.479	0.490	0.485	0.564	0.571	0.568	0.707	0.737
720	0.396	0.403	0.399	0.496	0.499	0.498	0.674	0.700
1255	0.167	0.168	0.167	0.298	0.305	0.301	0.558	0.591
1440	0.130	0.139	0.135	0.277	0.281	0.279	0.551	0.584
1620	0.115	0.114	0.115	0.254	0.262	0.258	0.549	0.561
1800	0.100	0.108	0.104	0.237	0.249	0.243	0.528	0.531
1980	0.098	0.097	0.097	0.236	0.245	0.241	0.526	0.550
Initial Rate								
v_0 (10^{-3} M min^{-1})	1.53	1.22	1.37	1.32	1.46	1.39	1.18	0.93
[**9b**]$_0$ (M)	1.14	1.13	1.13	1.12	1.15	1.13	1.09	1.11
R^2	0.99	0.96	0.99	0.94	0.98	0.96	0.73	0.89
First-Order Fit								
k_{obs} (10^{-3} min^{-1})	1.41(2)	1.39(2)	1.40(2)	1.40(4)	1.47(4)	1.44(4)	1.58(6)	1.53(5)
[**9b**]$_0$ (M)	1.15(1)	1.14(1)	1.14(1)	1.12(1)	1.14(1)	1.13(1)	1.08(1)	1.11(1)
excess (M)	--	--	--	0.16(1)	0.17(1)	0.16(1)	0.49(1)	0.51(1)

[a] For all experiments, [**9b**]$_0$ = 1.2 M, [Fe]$_{tot}$ = 0.010 M. Reactions conducted in benzene at 25 °C. See Figures **S205**. Continued in Table S11.

Table S11. Concentration [**9b**] vs. time data with varied [**5b**]$_0$, continued. [a]

time (min)	[**9b**]$_t$ (M), where:								
	where [**5b**]$_0$ = 0.54 M, continued			where [**5b**]$_0$ = 0.39 M			where [**5b**]$_0$ = 0.22 M		
	trial iii	*trial iv*	*avg*	*trial i*	*trial ii*	*avg.*	*trial i*	*trial ii*	*avg.*
10	1.098	1.113	1.101	1.126	1.323	1.225	1.110	1.095	1.103
20	1.077	1.100	1.085	1.098	1.312	1.205	1.086	1.083	1.085
30	1.069	1.080	1.063	1.097	1.302	1.200	1.096	1.084	1.090
45	1.040	1.065	1.054	1.078	1.276	1.177	1.084	1.058	1.071
60	1.037	1.049	1.042	1.073	1.267	1.170	1.074	1.062	1.068
80	0.998	1.035	1.017	1.055	1.243	1.149	1.056	1.028	1.042
100	0.989	1.021	1.002	1.035	1.205	1.120	1.043	1.036	1.040
120	0.977	0.979	0.986	1.008	1.209	1.109	1.031	1.022	1.026
150	0.958	0.982	0.967	1.000	1.184	1.092	1.028	1.013	1.020
180	0.940	0.954	0.949	0.989	1.167	1.078	1.020	1.044	1.032
240	0.902	0.916	0.911	0.946	1.126	1.036	0.979	0.996	0.987
300	0.871	0.881	0.878	0.924	1.104	1.014	0.984	0.966	0.975
360	0.839	0.850	0.846	0.909	1.070	0.989	0.963	0.954	0.959
420	--	--	0.821	--	--	--	--	--	--
480	--	--	0.790	--	--	--	--	--	--
540	0.756	0.757	0.756	0.835	0.992	0.913	0.913	0.931	0.922
600	--	--	0.722	--	--	--	--	--	--
720	0.680	0.695	0.688	0.779	0.921	0.850	0.883	0.864	0.873
1255	0.588	0.587	0.581	0.705	0.842	0.773	0.829	0.826	0.828
1440	0.573	0.571	0.570	0.689	0.827	0.758	0.832	0.817	0.824
1620	--	--	0.555	--	--	--	--	--	--
1800	--	--	0.529	--	--	--	--	--	--
1980	--	--	0.538	--	--	--	--	--	--
Initial Rate									
v_0 (10^{-3} M min^{-1})	1.26	1.30	1.17	0.98	1.12	1.08	0.73	0.57	0.65
[**5b**]$_0$ (M)	1.11	1.12	1.11	1.13	1.33	1.23	1.11	1.10	1.11
R^2	0.94	0.98	0.94	0.87	0.98	0.95	0.36	0.68	0.48
First-Order Fit									
k_{obs} (10^{-3} min^{-1})	1.71(1)	1.68(7)	1.58(6)	1.9(1)	1.9(1)	1.9(1)	2.0(2)	1.6(2)	1.8(2)
[**5b**]$_0$ (M)	1.09(2)	1.11(1)	1.10(1)	1.12(1)	1.22(1)	1.22(1)	1.10(1)	1.09(2)	1.10(1)
excess (M)	0.52(1)	0.52(1)	0.51(1)	0.66(1)	0.79(1)	0.73(1)	0.81(1)	0.79(2)	0.80(1)

[a] For all experiments, [**9b**]$_0$ = 1.2 M, [Fe]$_{tot}$ = 0.010 M. Reactions conducted in benzene at 25 °C. See Figures **S205**. Continued from Table S10.

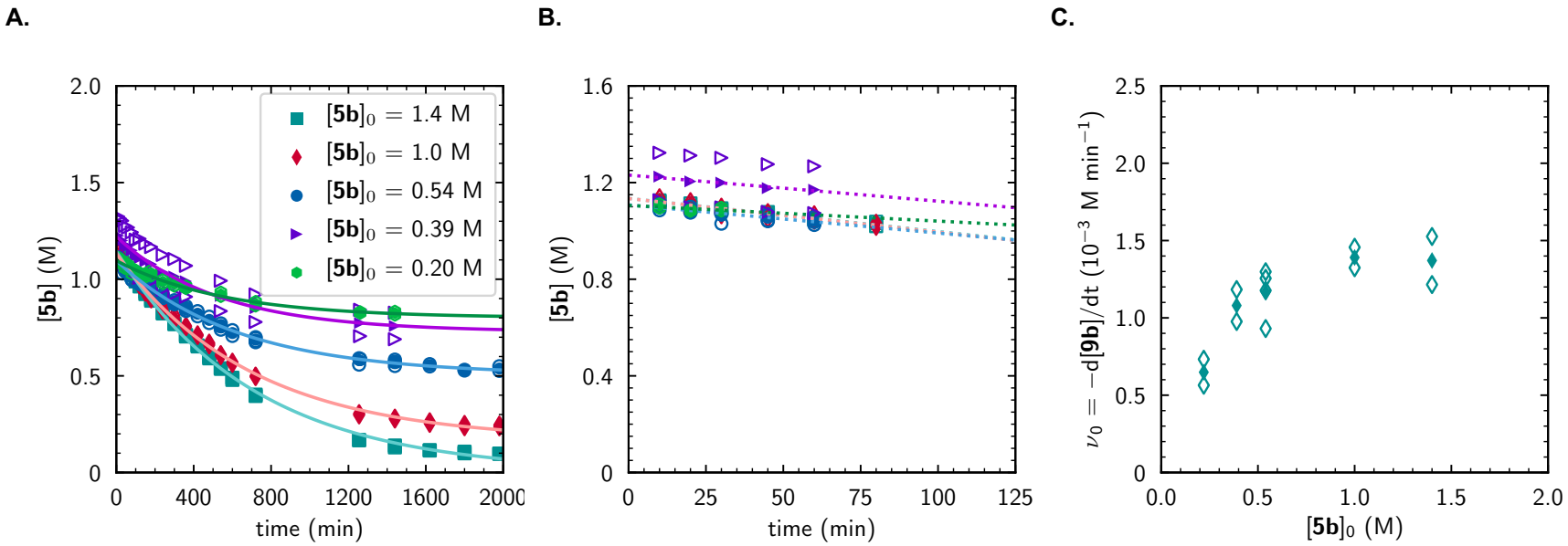

Figure S207. Concentration vs. time data, monitoring [**9b**]$_t$, for trials initiated with varied [**5b**]$_0$ where [**9b**]$_0$ = 1.2 M and [Fe]$_{tot}$ = 0.010 M. Open markers represent data points obtained from individual trials; closed markers represent average values obtained from duplicate trials. (**A.**) Full reaction time course fit to a first-order rate law (solid lines). (**B.**) Initial rate profiles obtained from linear regression (dotted lines) to data obtained where conversion ≤10%. (**C.**) Initial rate vs. initial concentration [**5b**]$_0$. See Table S9 for tabulated data and fit parameters.

Table S12. Concentration [**14bb**] vs. time data with varied [**5b**]$_0$. [a]

time (min)	[**14bb**]$_t$ (M), where:							
	where [**5b**]$_0$ = 1.4 M			where [**5b**]$_0$ = 1.0 M			where [**5b**]$_0$ = 0.5 M	
	trial i	*trial ii*	*avg*	*trial i*	*trial ii*	*avg.*	*trial i*	*trial ii*
10	0.009	0.010	0.009	0.006	0.009	0.008	0.006	0.006
20	0.028	0.028	0.028	0.023	0.025	0.024	0.018	0.018
30	0.048	0.047	0.047	0.039	0.045	0.042	0.030	0.031
45	0.072	0.071	0.071	0.061	0.062	0.061	0.046	0.044
60	0.094	0.089	0.091	0.078	0.080	0.079	0.055	0.056
80	0.121	0.123	0.122	0.100	0.104	0.102	0.073	0.071
100	0.148	0.148	0.148	0.124	0.130	0.127	0.088	0.088
120	0.172	0.170	0.171	0.144	0.143	0.143	0.100	0.100
150	0.212	0.205	0.209	0.174	0.178	0.176	0.120	0.119
180	0.247	0.244	0.246	0.203	0.207	0.205	0.138	0.137
240	0.318	0.323	0.320	0.256	0.268	0.262	0.176	0.175
300	0.396	0.385	0.391	0.322	0.333	0.328	0.220	0.210
360	0.453	0.447	0.450	0.377	0.391	0.384	0.249	0.252
420	0.526	0.529	0.527	0.429	0.435	0.432	0.283	0.281
480	0.608	0.589	0.599	0.476	0.491	0.483	0.318	0.309
540	0.653	0.640	0.647	0.537	0.537	0.537	0.349	0.339
600	0.715	0.731	0.723	0.575	0.608	0.592	0.372	0.365
720	0.831	0.823	0.827	0.662	0.667	0.664	0.426	0.422
1255	1.141	1.135	1.138	0.861	0.928	0.895	0.541	0.531
1440	1.180	1.198	1.189	0.931	0.950	0.941	0.552	0.560
1620	1.242	1.202	1.222	0.938	0.965	0.952	0.609	0.546
1800	1.226	1.243	1.234	0.965	0.948	0.956	0.553	0.559
1980	1.238	1.243	1.241	0.987	0.996	0.991	0.576	0.574
Initial Rate								
v_0 (10^{-3} M min^{-1})	1.60	1.58	1.59	1.34	1.34	1.34	1.00	0.99
[**14b**]$_0$ (M)	–0.003	–0.003	–0.003	–0.003	0.001	–0.002	–0.002	–0.002
R^2	0.99	0.99	0.99	0.99	0.99	0.99	0.98	0.99
First-Order Fit								
k_{obs} (10^{-3} min^{-1})	1.12(4)	1.10(4)	1.11(4)	1.20(3)	1.24(5)	1.22(3)	1.48(6)	1.49(4)
[**14b**]$_0$ (M)	1.45(3)	1.45(3)	1.45(3)	1.10(1)	1.11(2)	1.11(1)	0.63(1)	0.61(1)

[a] For all experiments, [**9b**]$_0$ = 1.2 M, [Fe]$_{tot}$ = 0.010 M. Reactions conducted in benzene at 25 °C. See Figure S206. Continued in Table S13.

Table S13. Concentration [**14bb**] vs. time data with varied [**5b**]$_0$. [a]

time (min)	[**14bb**]$_t$ (M), where:								
	where [**5b**]$_0$ = 0.54 M, continued			where [**5b**]$_0$ = 0.39 M			where [**5b**]$_0$ = 0.22 M		
	trial iii	*trial iv*	*avg*	*trial i*	*trial ii*	*avg.*	*trial i*	*trial ii*	*avg.*
10	0.004	0.004	0.005	0.004	0.006	0.005	0.001	0.001	0.001
20	0.017	0.016	0.017	0.013	0.017	0.015	0.008	0.008	0.008
30	0.026	0.028	0.029	0.023	0.028	0.025	0.016	0.014	0.015
45	0.042	0.042	0.044	0.035	0.042	0.038	0.021	0.021	0.021
60	0.053	0.054	0.054	0.043	0.054	0.048	0.027	0.026	0.027
80	0.069	0.068	0.070	0.054	0.063	0.058	0.035	0.031	0.033
100	0.081	0.083	0.085	0.062	0.076	0.069	0.039	0.037	0.038
120	0.085	0.092	0.094	0.069	0.083	0.076	0.043	0.040	0.042
150	0.102	0.110	0.113	0.083	0.102	0.093	0.056	0.051	0.054
180	0.127	0.130	0.133	0.101	0.118	0.109	0.063	0.064	0.064
240	0.159	0.164	0.169	0.124	0.151	0.138	0.075	0.077	0.076
300	0.189	0.196	0.203	0.150	0.187	0.169	0.094	0.090	0.092
360	0.224	0.231	0.239	0.179	0.216	0.197	0.110	0.109	0.109
420			0.282						
480			0.313						
540	0.309	0.326	0.331	0.255	0.301	0.278	0.157	0.153	0.155
600			0.369						
720	0.384	0.403	0.409	0.298	0.351	0.324	0.177	0.164	0.170
1255	0.505	0.534	0.528	0.390	0.458	0.424	0.218	0.211	0.214
1440	0.515	0.549	0.544	0.398	0.465	0.431	0.232	0.213	0.222
1620			0.578						
1800			0.556						
1980			0.575						
Initial Rate									
v_0 (10^{-3} M min^{-1})	0.97	1.00	0.99	0.78	0.96	0.87	0.72	0.65	0.68
[**14b**]$_0$ (M)	–0.004	–0.004	–0.003	–0.002	–0.002	–0.002	–0.006	–0.006	–0.005
R^2	0.99	0.99	0.99	0.99	0.99	0.99	0.99	0.99	0.99
First-Order Fit									
k_{obs} (10^{-3} min^{-1})	1.27(5)	1.20(4)	1.42(4)	1.36(5)	1.45(5)	1.41(5)	1.61(7)	1.73(7)	1.67(6)
[**14b**]$_0$ (M)	0.62(1)	0.68(1)	0.62(1)	0.47(1)	0.54(1)	0.50(1)	0.25(1)	0.24(1)	0.25(1)

[a] For all experiments, [**9b**]$_0$ = 1.2 M, [Fe]$_{tot}$ = 0.010 M. Reactions conducted in benzene at 25 °C. See Figures **S206**. Continued from Table S12.

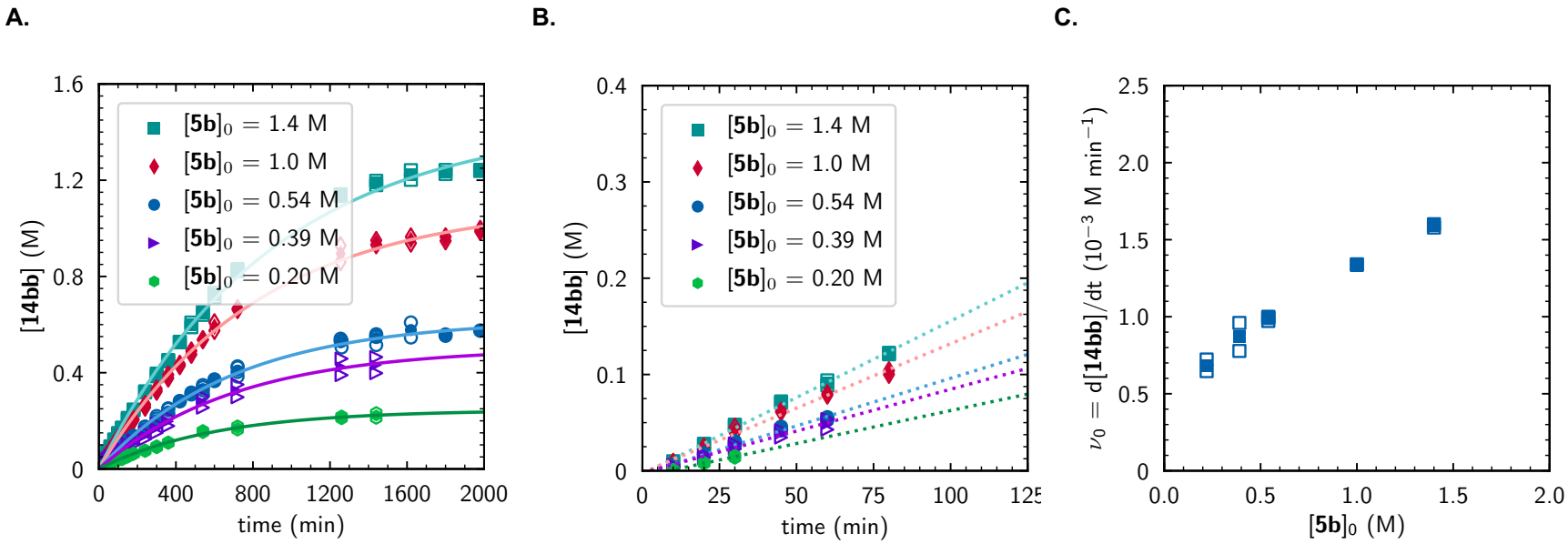

Figure S208. Concentration vs. time data, monitoring [**14bb**]$_t$, for trials initiated with varied [**5b**]$_0$ where [**9b**]$_0$ = 1.2 M and [Fe]$_{tot}$ = 0.010 M. Open markers represent data points obtained from individual trials; closed markers represent average values obtained from duplicate trials. (**A.**) Full reaction time course fit to a first-order rate law (solid lines). (**B.**) Initial rate profiles obtained from linear regression (dotted lines) to data obtained where conversion ≤10%. (**C.**) Initial rate vs. initial concentration [**5b**]$_0$. See Table S10 for tabulated data and fit parameters.

5.5 Determination of Order in $[Fe]_{tot}$

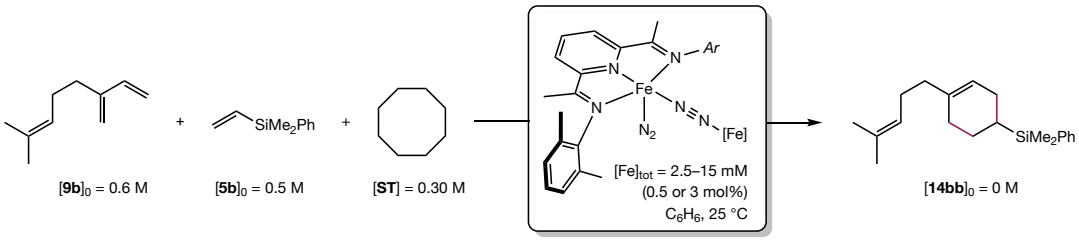

Figure S209. Determination of kinetic order in $[Fe]_{tot}$.

Experiments to determine the kinetic order in iron catalyst were performed by varying precatalyst concentration, ranging from $[Fe]_{tot}$ = 0.5 $[[(^{Me}PDI)Fe(N_2)]_2(\mu_2\text{-}N_2)]_0$ = 5 mM (0.5 mol%) to 30 mM (3.0 mol%), with constant $[\mathbf{5b}]_0$ = 1.0 M and $[\mathbf{9b}]_0$ = 1.2 M. Initial rates were determined from linear regression of the concentration vs. time data where conversion of the limiting substrate (**5b**) was ≤10%. The initial rate data were examined as a function of $[Fe]_{tot}$ where the linear dependence of reaction rate on $[Fe]_{tot}$ was indicative of a first-order dependence on $[Fe]_{tot}$ over the concentration range examined. While a slight deviation from linearity was observed, this was attributed to the high degree of sensitivity of the iron precatalyst to water or other trace impurities (e.g. chlorosilane) in the substrate. While attempts to minimize these effects were taken (*vida supra*), any trace remaining impurities that could result in immediate catalyst death would have a proportionally greater effect at low catalyst loading. The raw data and fit parameters are summarized in Tables S14–16 and plotted in Figures S208–S210.

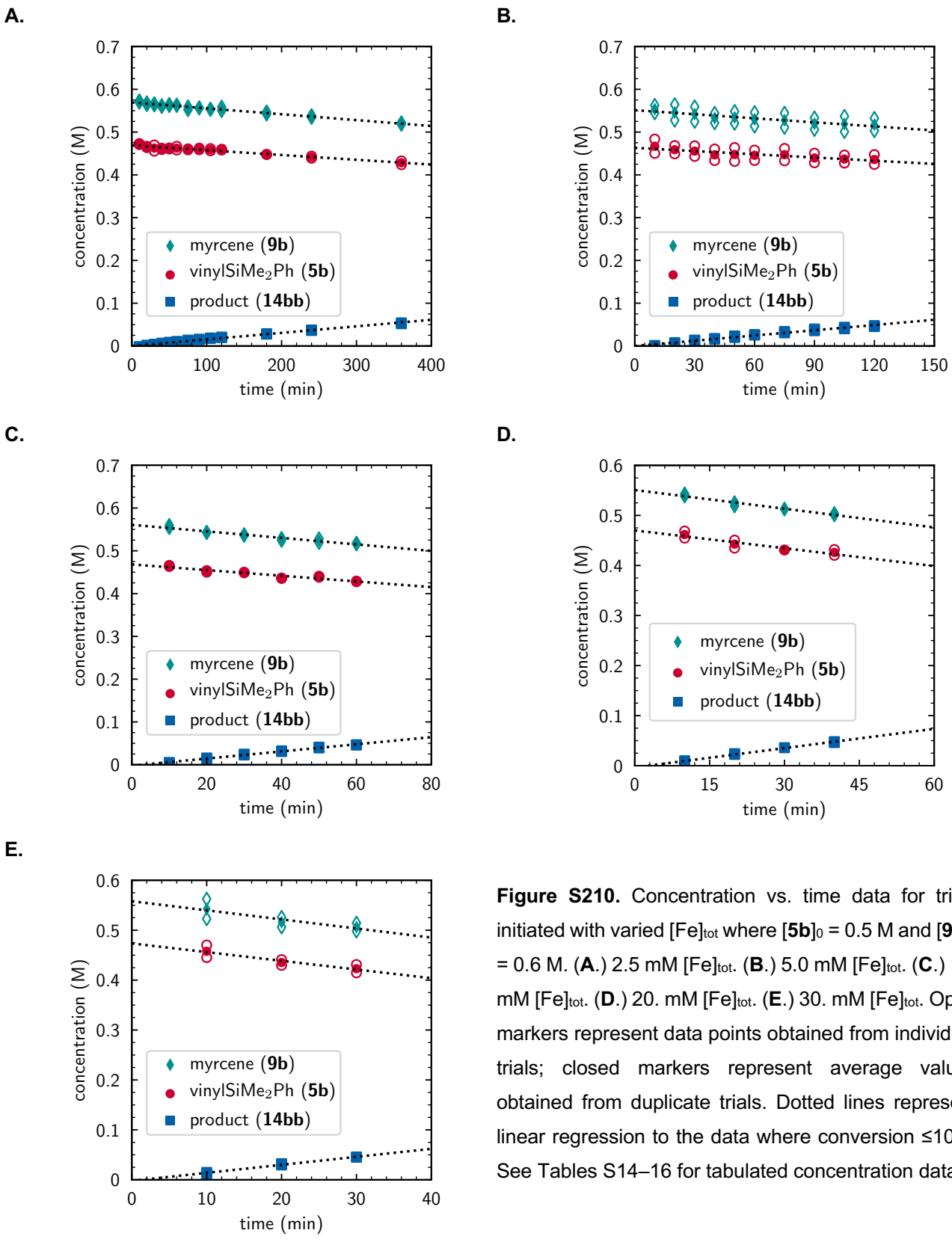

Figure S210. Concentration vs. time data for trials initiated with varied $[Fe]_{tot}$ where $[\mathbf{5b}]_0$ = 0.5 M and $[\mathbf{9b}]_0$ = 0.6 M. (**A**.) 2.5 mM $[Fe]_{tot}$. (**B**.) 5.0 mM $[Fe]_{tot}$. (**C**.) 10. mM $[Fe]_{tot}$. (**D**.) 20. mM $[Fe]_{tot}$. (**E**.) 30. mM $[Fe]_{tot}$. Open markers represent data points obtained from individual trials; closed markers represent average values obtained from duplicate trials. Dotted lines represent linear regression to the data where conversion ≤10%. See Tables S14–16 for tabulated concentration data.

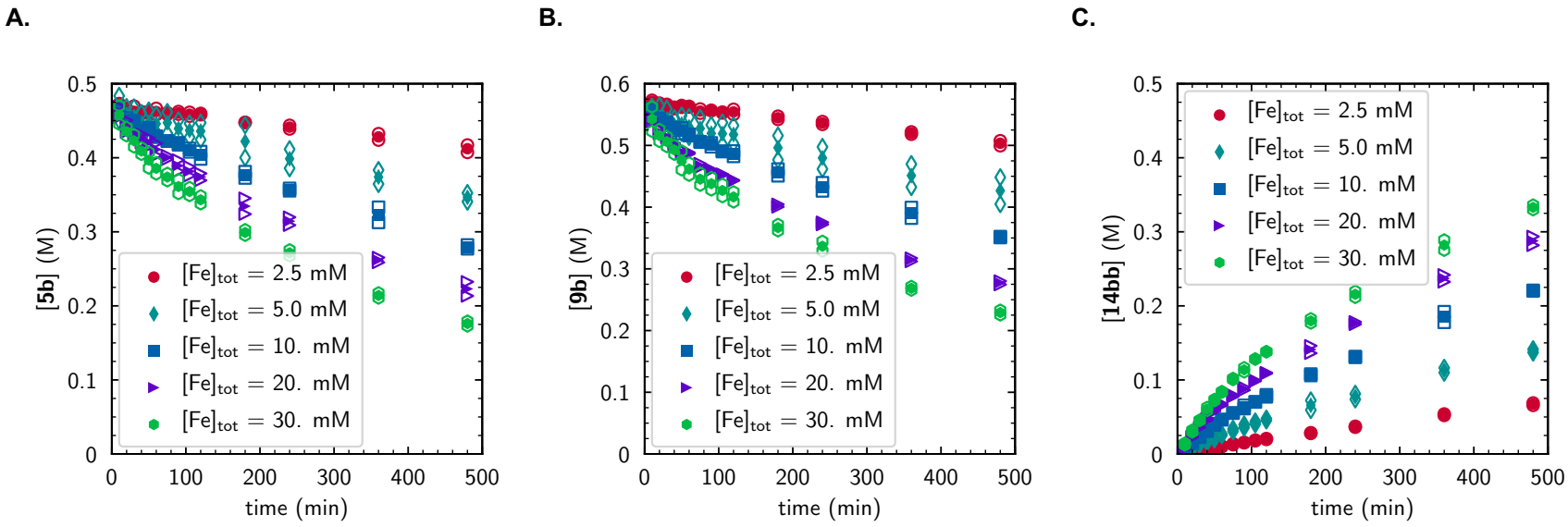

Figure S211. Concentration vs. time data for trials initiated with varied $[Fe]_{tot}$ where $[\mathbf{5b}]_0$ = 0.5 M and $[\mathbf{9b}]_0$ = 0.6 M monitored as (**A**.) $[\mathbf{5b}]_t$. (**B**.) $[\mathbf{9b}]_t$ (**C**.) $[\mathbf{14bb}]_t$ Open markers represent data points obtained from individual trials; closed markers represent average values obtained from duplicate trials. See Tables S14–16 for tabulated data and fit parameters.

Table S14. Concentration [**5b**] vs. time data with varied $[Fe]_{tot}$. [a]

time (min)	[**5b**]$_t$ (M) where:														
	$[Fe]_{tot}$ = 2.5 mM			$[Fe]_{tot}$ = 5.0 mM			$[Fe]_{tot}$ = 10. mM			$[Fe]_{tot}$ = 20. mM			$[Fe]_{tot}$ = 30. mM		
	trial i	*trial ii*	*avg*	*trial i*	*trial ii*	*avg*	*trial i*	*trial ii*	*avg*	*trial i*	*trial ii*	*avg*	*trial i*	*trial ii*	*avg*
10	0.473	0.471	0.472	0.450	0.484	0.467	0.464	0.466	0.465	0.469	0.455	0.462	0.470	0.445	0.458
20	0.464	0.467	0.465	0.449	0.468	0.459	0.450	0.454	0.452	0.451	0.435	0.443	0.441	0.430	0.435
30	0.470	0.456	0.463	0.443	0.468	0.456	0.449	0.450	0.449	--	0.431	0.450	0.431	0.415	0.423
40	0.462	0.459	0.461	0.433	0.460	0.447	0.436	0.435	0.436	0.432	0.420	0.426	0.414	0.405	0.409
50	0.463	0.461	0.462	0.432	0.464	0.448	0.438	0.441	0.439	0.427	0.415	0.421	0.407	0.386	0.397
60	0.467	0.458	0.462	0.434	0.458	0.446	0.429	0.428	0.428	0.419	0.403	0.411	0.393	0.378	0.386
75	0.459	0.461	0.460	0.433	0.462	0.447	0.423	0.422	0.423	0.403	0.398	0.400	0.379	0.369	0.374
90	0.462	0.459	0.461	0.428	0.451	0.439	0.420	0.418	0.419	0.397	0.382	0.389	0.371	0.352	0.361
105	0.461	0.456	0.459	0.428	0.446	0.437	0.413	0.408	0.410	0.388	0.376	0.382	0.360	0.349	0.354
120	0.460	0.458	0.459	0.424	0.447	0.436	0.408	0.398	0.403	0.379	0.369	0.374	0.349	0.338	0.343
180	0.448	0.448	0.448	0.400	0.444	0.422	0.381	0.373	0.377	0.345	0.324	0.335	0.303	0.295	0.299
240	0.444	0.439	0.441	0.386	0.412	0.399	0.359	0.355	0.357	0.320	0.309	0.314	0.276	0.268	0.272
360	0.433	0.424	0.428	0.365	0.383	0.374	0.333	0.313	0.323	0.265	0.259	0.262	0.218	0.211	0.214
480	0.417	0.407	0.412	0.341	0.352	0.347	0.277	0.282	0.280	0.232	0.213	0.223	0.179	0.173	0.176
Initial Rate															
v_0 (10^{-4} M min^{-1})	1.1	1.2	1.1	2.2	2.8	2.5	6.2	6.5	6.6	11.9	10.6	11.9	19.5	15.3	17.4
b (M)	0.47	0.47	0.47	0.45	0.48	0.46	0.47	0.47	0.47	0.48	0.46	0.47	0.47	0.46	0.47
R^2	0.93	0.92	0.96	0.82	0.84	0.87	0.92	0.93	0.91	0.97	0.92	0.93	0.92	0.99	0.97

[a] For all experiments, [**5b**]$_0$ = 0.5 M, [**9b**]$_0$ = 0.6 M. Reactions conducted in benzene at 25 °C. See Figure S209.

Table S15. Concentration [**9b**] vs. time data with varied $[Fe]_{tot}$. [a]

time (min)	[**9b**]$_t$ (M) where:														
	$[Fe]_{tot}$ = 2.5 mM			$[Fe]_{tot}$ = 5.0 mM			$[Fe]_{tot}$ = 10. mM			$[Fe]_{tot}$ = 20. mM			$[Fe]_{tot}$ = 30. mM		
	trial i	*trial ii*	*avg*	*trial i*	*trial ii*	*avg*	*trial i*	*trial ii*	*avg*	*trial i*	*trial ii*	*avg*	*trial i*	*trial ii*	*avg*
10	0.569	0.573	0.571	0.563	0.545	0.554	0.559	0.554	0.557	0.539	0.543	0.541	0.562	0.523	0.543
20	0.564	0.569	0.566	0.564	0.528	0.546	0.542	0.544	0.543	0.519	0.526	0.522	0.526	0.506	0.516
30	0.567	0.563	0.565	0.559	0.525	0.542	0.536	0.538	0.537	--	0.513	0.525	0.514	0.498	0.506
40	0.560	0.562	0.561	0.544	0.522	0.533	0.529	0.524	0.527	0.501	0.504	0.502	0.500	0.486	0.493
50	0.562	0.565	0.563	0.548	0.520	0.534	0.528	0.519	0.524	0.493	0.487	0.490	0.491	0.460	0.476
60	0.563	0.562	0.563	0.546	0.514	0.530	0.518	0.516	0.517	0.487	0.488	0.488	0.472	0.452	0.462
75	0.552	0.559	0.556	0.544	0.511	0.528	0.506	0.505	0.506	0.465	0.470	0.468	0.455	0.435	0.445
90	0.556	0.557	0.557	0.533	0.506	0.520	0.504	0.498	0.501	0.460	0.461	0.460	0.448	0.428	0.438
105	0.554	0.553	0.553	0.537	0.501	0.519	0.490	0.491	0.490	0.453	0.453	0.453	0.437	0.417	0.427
120	0.550	0.559	0.554	0.532	0.503	0.518	0.491	0.482	0.487	0.443	0.444	0.443	0.425	0.408	0.417
180	0.542	0.547	0.545	0.516	0.477	0.496	0.462	0.451	0.456	0.404	0.401	0.403	0.372	0.362	0.367
240	0.534	0.539	0.536	0.497	0.462	0.480	0.440	0.426	0.433	0.375	0.372	0.374	0.345	0.329	0.337
360	0.518	0.522	0.520	0.470	0.432	0.451	0.399	0.382	0.391	0.312	0.317	0.315	0.271	0.266	0.268
480	0.508	0.499	0.504	0.448	0.405	0.427	0.352	0.351	0.352	0.280	0.275	0.277	0.233	0.225	0.229
Initial Rate															
v_0 (10^{-4} M min^{-1})	1.4	1.3	1.4	2.9	3.4	3.2	7.3	7.4	7.6	12.0	13.0	12.5	24.0	12.4	18.2
b (M)	0.57	0.57	0.57	0.56	0.54	0.55	0.56	0.56	0.56	0.55	0.55	0.55	0.58	0.53	0.56
R^2	0.97	0.97	0.98	0.86	0.88	0.92	0.92	0.97	0.96	0.96	0.98	0.97	0.92	0.97	0.94

[a] For all experiments, [**5b**]$_0$ = 0.5 M, [**9b**]$_0$ = 0.6 M. Reactions conducted in benzene at 25 °C. See Figure **S209**.

Table S16. Concentration [**14bb**] vs. time data with varied $[Fe]_{tot}$. [a]

time (min)	[**14bb**]$_t$ (M) where:														
	$[Fe]_{tot}$ = 2.5 mM			$[Fe]_{tot}$ = 5.0 mM			$[Fe]_{tot}$ = 10. mM			$[Fe]_{tot}$ = 20. mM			$[Fe]_{tot}$ = 30. mM		
	trial i	*trial ii*	*avg*	*trial i*	*trial ii*	*avg*	*trial i*	*trial ii*	*avg*	*trial i*	*trial ii*	*avg*	*trial i*	*trial ii*	*avg*
-	-	-	-												
10	0.002	0.002	0.002	0.001	0.001	0.001	0.004	0.005	0.005	0.007	0.010	0.008	0.012	0.015	0.013
20	0.001	0.002	0.001	0.007	0.008	0.007	0.014	0.016	0.015	0.023	0.024	0.023	0.030	0.032	0.031
30	0.004	0.003	0.004	0.013	0.013	0.013	0.023	0.025	0.024		0.036	0.036	0.045	0.046	0.045
40	0.005	0.007	0.006	0.016	0.018	0.017	0.031	0.032	0.032	0.046	0.048	0.047	0.059	0.063	0.061
50	0.008	0.009	0.008	0.020	0.023	0.022	0.039	0.041	0.040	0.058	0.059	0.058	0.074	0.072	0.073
60	0.010	0.010	0.010	0.025	0.027	0.026	0.046	0.047	0.046	0.066	0.068	0.067	0.084	0.083	0.084
75	0.013	0.014	0.013	0.031	0.034	0.032	0.055	0.055	0.055	0.078	0.080	0.079	0.100	0.102	0.101
90	0.015	0.016	0.015	0.036	0.040	0.038	0.061	0.066	0.063	0.090	0.086	0.088	0.116	0.111	0.114
105	0.018	0.019	0.018	0.040	0.044	0.042	0.070	0.070	0.070	0.099	0.099	0.099	0.128	0.128	0.128
120	0.020	0.021	0.020	0.045	0.048	0.047	0.080	0.077	0.079	0.110	0.109	0.109	0.138	0.138	0.138
180	0.028	0.029	0.028	0.059	0.072	0.066	0.108	0.106	0.107	0.146	0.136	0.141	0.183	0.177	0.180
240	0.036	0.037	0.037	0.074	0.081	0.078	0.131	0.132	0.131	0.178	0.175	0.177	0.220	0.211	0.216
360	0.052	0.054	0.053	0.110	0.116	0.113	0.192	0.178	0.185	0.242	0.232	0.237	0.289	0.275	0.282
480	0.066	0.069	0.067	0.137	0.141	0.139	0.221	0.220	0.221	0.294	0.282	0.288	0.336	0.330	0.333
Initial Rate															
v_0 (10^{-4} M min^{-1})	1.5	1.5	1.5	3.9	4.2	4.1	8.4	7.7	8.3	12.8	12.7	12.8	16.6	15.5	16.0
b (10^{-4} M)	–0.3	3.0	1.3	–1.9	1.7	–0.1	–31	2.7	–23	–47	–22	–35	–42	–12	–21
R^2	0.99	0.99	0.99	0.99	0.98	0.99	0.99	0.99	0.99	0.99	0.99	0.99	0.99	0.99	0.99

[a] For all experiments, $[\mathbf{5b}]_0$ = 0.5 M, $[\mathbf{9b}]_0$ = 0.6 M. Reactions conducted in benzene at 25 °C. See Figure **S209**.

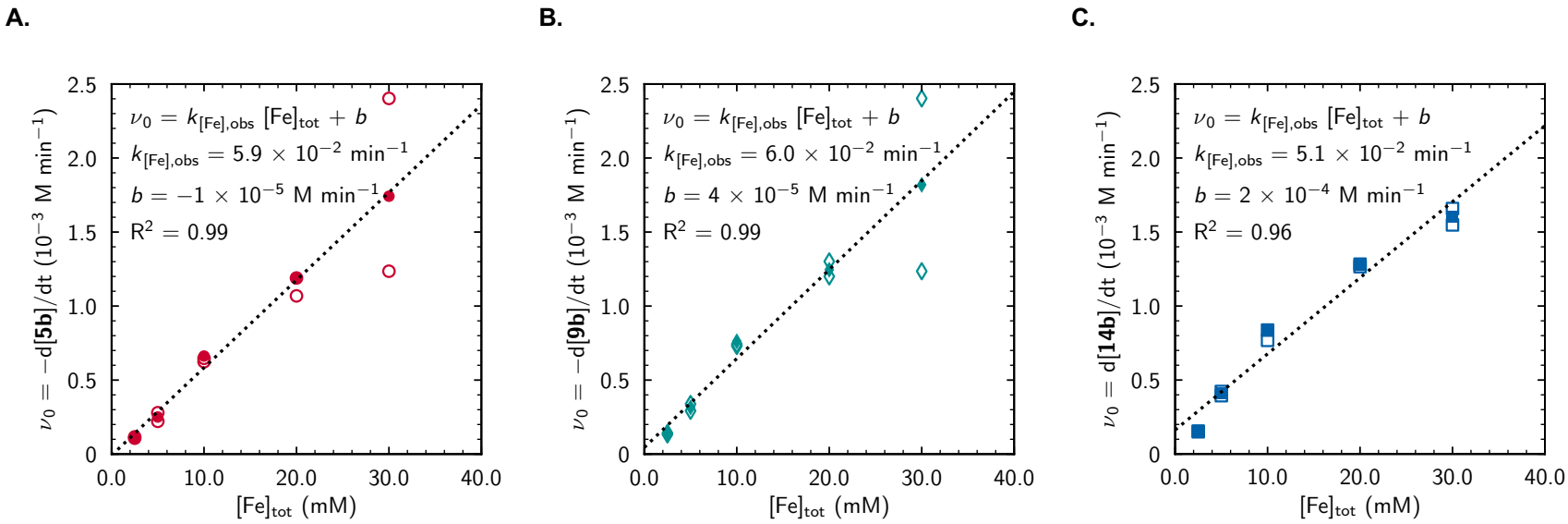

Figure S212. Initial rate as a function of catalyst concentration, $[Fe]_{tot}$, for trials initiated where $[\mathbf{5b}]_0$ = 0.5 M and $[\mathbf{9b}]_0$ = 0.6 M. Open markers represent data points obtained from individual trials; closed markers represent average values obtained from duplicate trials. See Table S17 for tabulated data and fit parameters.

Table S17. Initial rate, v_0, vs. $[Fe]_{tot}$. [a]

$[Fe]_{tot}$ (mM)		v_0 (10^{-4} M min^{-1}) =										
		–d[**5b**]/dt				–d[**9b**]/dt				d[**14bb**]/dt		
		trial i	*trial ii*	*avg*		*trial i*	*trial ii*	*avg*		*trial i*	*trial ii*	*avg*
2.5		1.1	1.2	1.1		1.4	1.3	1.4		1.5	1.5	1.5
5.0		2.2	2.8	2.5		3.9	4.2	4.1		3.9	4.2	4.1
10.		6.2	6.5	6.6		8.4	7.7	8.3		8.4	7.7	8.3
20.		11.9	10.6	11.9		12.0	13.0	12.5		12.8	12.7	12.8
30.		19.5	15.3	17.4		24.0	12.4	18.2		16.6	15.5	16.0

6. **Supplemental Figures**

6.1 The α-Silicon Effect

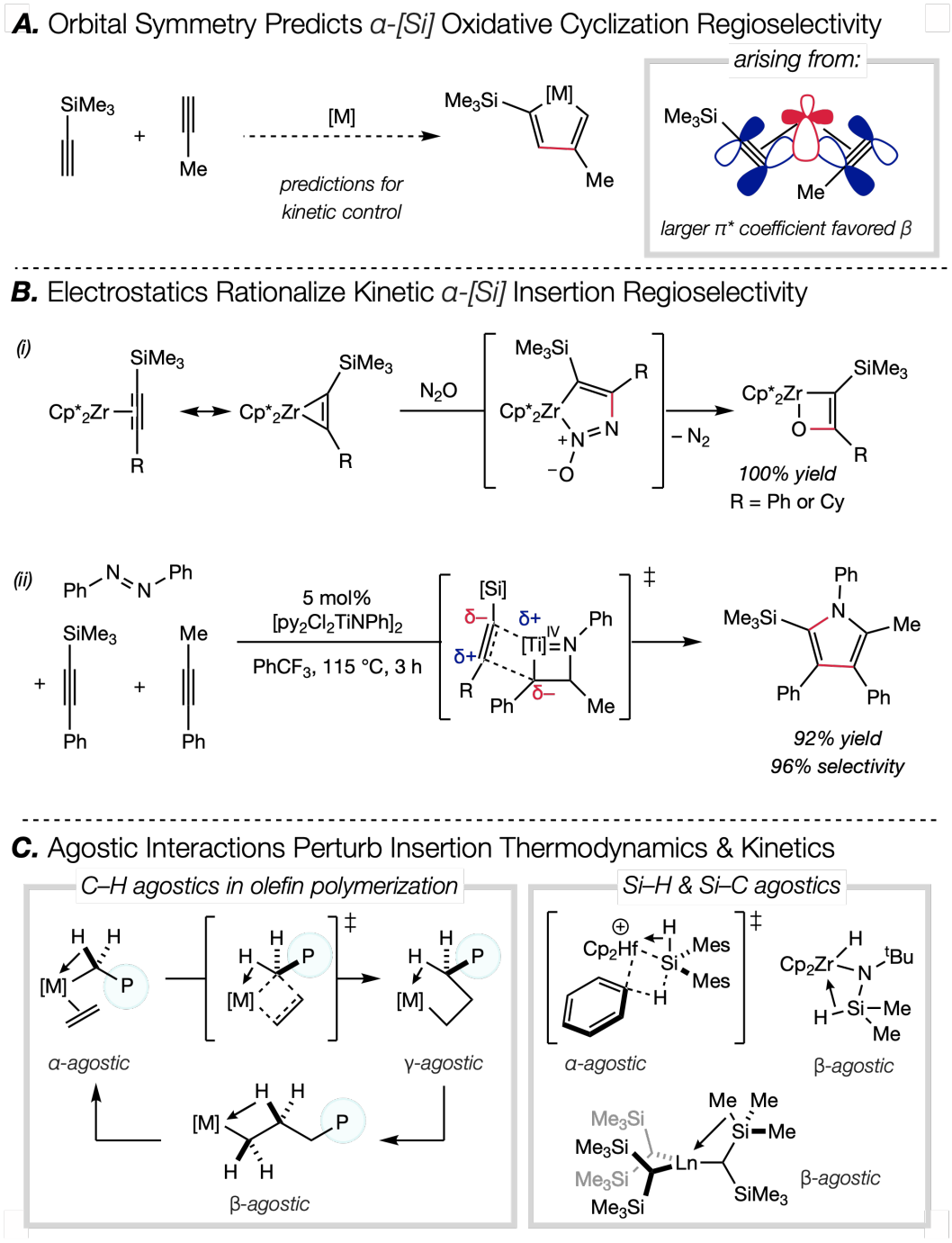

Scheme S1. The α-Silicon effect.[63-74]

6.2 Lewis Acid Screen

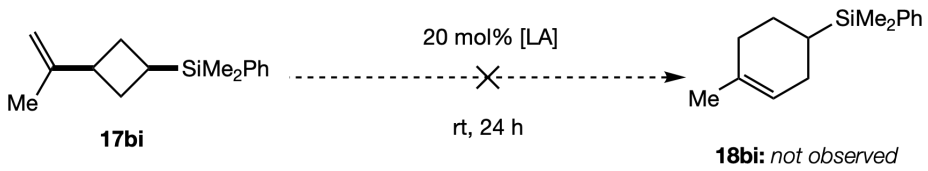

Lewis Acid	Conversion (GC)	Yield (GC)
$FeCl_3$	2%	trace
$AlCl_3$	100%[b]	0%
NaCl[a]	0%	0%
$MgCl_2$[a]	0%	0%
$BF_3{\bullet}Et_2O$	13%	0%

[a] Anhydrous salts were used. [b] Oligomer formation observed.

Figure 214: Summary of Lewis acids evaluated for the proposed rearrangement of **17bi**.

7. Computational Analyses

7.1 Sample Input File for Geometry Optimization & Mössbauer Parameter Calculation

(^{Me}PDI)Fe(myrcene)

```
#MePDIFemyrcene
! RKS B3LYP RIJCOSX def2-SVP def2/J Normalprint SlowConv TightSCF Opt Pal8 UCO

%basis  NewGTO 26 "def2-TZVP(-f)" end
       NewGTO 7 "def2-TZVP(-f)" end
       NewAuxGTO 26 "def2/J" end
       NewAuxGTO 7 "def2/J" end
      end

%SCF MaxIter 1000
     TolE 1e-7
     TolErr 1e-6
    end

* xyz 0 1
Fe        0.00000       0.00000       0.00000
N         0.38762      -1.89798      -0.51684
N         1.84117       0.00000      -0.00000
N         0.36924       1.93066       0.00001
C         2.23272      -3.58137      -0.86195
H         1.52450      -4.23922      -1.09273
H         2.80688      -3.54779      -1.61092
H         2.72977      -3.93812      -0.15622
C         1.67533      -2.23968      -0.50635
C         2.54519      -1.16363      -0.17899
```

C	3.93055	-1.19033	-0.07084
H	4.38464	-2.06492	-0.21127
C	4.61660	-0.02435	0.24684
H	5.57485	-0.01418	0.32299
C	3.91158	1.16082	0.39731
H	4.39731	1.97364	0.58197
C	2.52365	1.17146	0.23966
C	1.64845	2.28092	0.20755
C	2.14629	3.68583	0.34734
H	1.55606	4.27936	-0.06129
H	2.99160	3.78949	-0.05131
H	2.30143	3.95372	1.31669
C	-0.55822	-2.92615	-0.88269
C	-0.97744	-3.01972	-2.22346
C	-1.95411	-3.95805	-2.54654
H	-2.23678	-4.03054	-3.45671
C	-2.48256	-4.79649	-1.58848
H	-3.16838	-5.42186	-1.85051
C	-2.03466	-4.72668	-0.28892
H	-2.42824	-5.31512	0.37741
C	-1.07250	-3.79550	0.10042
C	-0.34645	-2.20208	-3.33328
C	-0.60442	-3.79760	1.54402
C	-0.55707	2.97393	-0.33710
C	-1.20974	3.73372	0.65244
C	-2.18025	4.65524	0.25204
H	-2.64012	5.18966	0.94477
C	-2.49625	4.83091	-1.06998

H -3.18821 5.44547 -1.27764

C -1.82821 4.10454 -2.03832

H -2.02840 4.25999 -2.96899

C -0.84173 3.17906 -1.70436

C -0.90337 3.60005 2.13176

C -0.06623 2.46033 -2.79579

C -0.56965 -0.21578 2.09163 NewGTO "def2-TZVP(-f)" end

H -0.50618 0.70229 2.39380

H -0.11883 -0.90169 2.63791

C -1.56302 -0.59135 1.19854 NewGTO "def2-TZVP(-f)" end

C -1.84594 -1.83204 0.94869

C -2.00120 0.37304 0.23873 NewGTO "def2-TZVP(-f)" end

H -2.14515 1.29870 0.55507

C -1.89325 0.05189 -1.11100 NewGTO "def2-TZVP(-f)" end

H -1.98858 -0.80584 -1.39216

H -2.10589 0.69614 -1.78558

H -0.14429 2.85933 2.27327

H -1.78975 3.30678 2.65448

H -0.55994 4.53972 2.51120

H -0.43985 2.75735 -3.75344

H -0.18340 1.40314 -2.67946

H 0.97061 2.71441 -2.72300

H -1.14163 -4.54322 2.09207

H -0.78438 -2.83659 1.97873

H 0.44279 -4.01448 1.57910

H -0.82173 -2.43590 -4.26297

H 0.69633 -2.43306 -3.39778

H -0.46860 -1.16021 -3.12237

C	-3.25209	-1.80459	0.84750
H	-1.40796	-2.17732	1.81272
H	-1.28441	-1.79441	0.08791
C	-4.29287	-3.21045	0.82135
H	-3.46549	-1.34337	-0.09428
H	-3.48970	-1.54879	1.85903
C	-6.15360	-3.76052	0.63307
C	-6.11693	-5.57545	0.76836
H	-5.47586	-5.97664	0.01140
H	-7.10609	-5.96273	0.64006
H	-5.74727	-5.85380	1.73312
C	-7.61996	-2.73142	0.37930
H	-8.48719	-3.35517	0.31802
H	-7.51399	-2.17759	-0.53006
H	-7.72588	-2.05292	1.19986
H	-3.71178	-4.05305	0.95325

*

%eprnmr nuclei = all Fe {rho, fgrad}

end

7.2 Sample Input File for Natural Bond Order (NBO) Analysis

Vinyl TMS

%chk=checkpoint.chk

%nprocshared=8

%mem=3GB

#p opt freq=noraman rb3lyp/6-31+g(d,p) pop=nbo geom=connectivity

vinylTMS.gjf

0 1

C	-4.08308936	0.12612518	0.51998710
C	-2.89153970	0.12167108	-0.12557978
H	-4.69396663	1.00454362	0.50949839
H	-4.41300123	-0.74877614	1.04018498
H	-2.56162695	0.99657304	-0.64577603
C	-2.08783650	-2.45033465	1.54028766
H	-3.11826891	-2.73172273	1.60297576
H	-1.47695960	-3.32875335	1.55077571
H	-1.83587830	-1.83068965	2.37542666
C	0.08429214	-0.96079564	-0.22022288
H	0.69516904	-1.83921434	-0.20973484
H	0.25188945	-0.42063386	-1.12853802
H	0.33625034	-0.34115065	0.61491612
C	-2.24078990	-2.59444440	-1.62074133
H	-2.07319259	-2.05428261	-2.52905647
H	-1.62991299	-3.47286310	-1.61025329
H	-3.27122231	-2.87583248	-1.55805323
Si	-1.78396849	-1.47097590	-0.10656408

1 2 2.0 3 1.0 4 1.0

2 5 1.0 18 1.0

3

4

5

6 7 1.0 8 1.0 9 1.0 18 1.0

7

8

9

10 11 1.0 12 1.0 13 1.0 18 1.0

11

12

13

14 15 1.0 16 1.0 17 1.0 18 1.0

15

16

17

18

8. References

1. Burger, B. J.; Bercaw, J. E. Vacuum Line Techniques for Handling Air-Sensitive Organometallic Compounds. In *Experimental Organometallic Chemistry*. ACS Symposium Series, Vol. 357; American Chemical Society, 1987; pp 79–115. DOI: 10.1021/bk-1987-0357.ch004

2.Pangborn, A. B.; Giardello, M. A.; Grubbs, R. H.; Rosen, R. K.; Timmers, F. J. Safe and Convenient Procedure for Solvent Purification. *Organometallics,* **1996**, *15*, 1518–1520. DOI: 10.1021/om9503712

3.Sargent, B. T.; Alexanian, E. J. Cobalt-Catalyzed Carbonylative Cross-Coupling of Alkyl Tosylates and Dienes: Stereospecific Synthesis of Dienones at Low Pressure. *J. Am. Chem. Soc.* **2017**, *139*, 12438–12440. DOI: 10.1021/jacs.7b07983

4. Adamson, N. J.; Hull, E.; Malcolmson, S. J. Enantioselective Intermolecular Addition of Aliphatic Amines to Acyclic Dienes with a Pd-PHOX Catalyst. *J. Am. Chem. Soc.* **2017**, *139*, 7180–7183. DOI: 10.1021/jacs.7b03480

5. Constantino, M. G.; de Oliveira, K. T.; Polo, E. C.; da Silva, G. V. J.; Brocksom, T. J. Core Structure of Eremophilanes and Bakkanes through Niobium Catalyzed Diels−Alder Reaction: Synthesis of (±)-Bakkenolide A. *J. Org. Chem.* **2006**, *71,* 9880–9883. DOI: 10.1021/jo061722x

6. Burks, H. E.; Kliman, L. T.; Morken, J. P. Asymmetric 1,4-Dihydroxylation of 1,3-Dienes by Catalytic Enantioselective Diboration. *J. Am. Chem. Soc.* **2009**, *131*, 9134–9135. DOI: 10.1021/ja809610h

7.Ueda, Y.; Damas, C. E.; Belleau, B. Nuclear analogs of (β-lactam antibiotics. XVIII. A short synthesis of 2-alkylthiocarbapen-2-em-3-carboxylate. *Can. J. Chem.* **1983**, *611*, 1996–2000. DOI: 10.1139/v83-334

8. Fiorito, D.; Folliet, S.; Liu, Y.; Mazet, C. A General Nickel-Catalyzed Kumada Vinylation for the Preparation of 2-Substituted 1,3-Dienes. *ACS Catal.* **2018**, *8*, 1392–1398. DOI: 10.1021/acscatal.7b04030

9. Wu, J. Y.; Moreau, B.; Ritter, T. Iron-Catalyzed 1,4-Hydroboration of 1,3-Dienes. *J. Am. Chem. Soc.* **2009**, *131*, 12915–12917. DOI: 10.1021/ja9048493

10. Kennedy, C. R.; Zhong, H.; Macaulay, R. L.; Chirik, P. J. Regio- and Diastereoselective Iron-Catalyzed [4+4]-Cycloaddition of 1,3-Dienes. *J. Am. Chem. Soc.* **2019**, *141*, 8557–8573. DOI: 10.1021/jacs.9b02443

11. Russell, S. K.; Darmon, J. M.; Lobkovsky, E.; Chirik, P. J. Synthesis of Aryl-Substituted Bis(imino)pyridine Iron Dinitrogen Complexes. *Inorg. Chem.* **2010**, *49*, 2782–2792. DOI: 10.1021/ic902162z

12. Russell, S. K.; Hoyt, J. M.; Bart, S. C.; Milsmann, C.; Stieber, S. C. E.; Semproni, S. P.; DeBeer, S.; Chirik, P. J. Synthesis, electronic structure and reactivity of bis(imino)pyridine iron carbene complexes: evidence for a carbene radical. *Chem. Sci.* **2014**, *5*, 1168–1174. DOI: 10.1039/C3SC52450G

13. Russell, S. K.; Lobkovsky, E.; Chirik. P. J. Iron-Catalyzed Intermolecular [2π + 2π] Cycloaddition. *J. Am. Chem. Soc.* **2011**, *133*, 8858–8861. DOI: 10.1021/ja202992p

14. Wreford, S. S.; Whitney, J. F. Magnesium butadiene as a reagent for the preparation of transition-metal butadiene complexes: molecular structure of bis(*η*-butadiene)[1,2-bis(dimethylphosphino)ethane]hafnium. *Inorg. Chem.* **1981**, *20*, 3918–3942. DOI: 10.1021/ic50225a063

15. Gottlieb, H. E.; Kotlyar, V.; Nudelman, A. NMR Chemical Shifts of Common Laboratory Solvents as Trace Impurities. *J. Org. Chem.* **1997**, 62, 7512–7515. DOI: 10.1021/jo971176v

16. Fulmer, G. R.; Miller, A. J. M.; Sherden, N. H.; Gottlieb, H. E.; Nudelman, A.; Stoltz, B. M.; Bercaw, J. E.; Goldberg, K. I. NMR Chemical Shifts of Trace Impurities: Common Laboratory Solvents, Organics, and Gases in Deuterated Solvents Relevant to the Organometallic Chemist. *Organometallics*, **2010**, *29*, 2176–2179. DOI: 10.1021/om100106e

17. *MestReNova Version 11.0.3-18688* Mestrelab Research S.L.: 2017. https://mestrelab.com

18. Prisecaru, I. *WMOSS4 Mössbauer Spectral Analysis Software*: 2009-2016. www.wmoss.org

19. Evans, D. F. 400. The determination of the paramagnetic susceptibility of substances in solution by nuclear magnetic resonance. *J. Chem. Soc.* **1959**, 2003–2005. DOI: 10.1039/JR9590002003

20. Sur, S. K. Measurement of magnetic susceptibility and magnetic moment of paramagnetic molecules in solution by high-field fourier transform NMR spectroscopy. *J. Magn. Reson.* **1989**, *82*, 169–173. DOI: 10.1016/0022-2364(89)90178-9

21. Hunter, J. D. Matplotlib: A 2D Graphics Environment. *Comput. Sci. Eng.* **2007**, *9*, 90–95. DOI: 10.1109/MCSE.2007.55

22. Pérez, F.; Granger, B. E. iPython: A System for Interactive Scientific Computing. *Comput. Sci. Eng.* **2007**, *9*, 21–29. DOI: 10.1109/MCSE.2007.53

23. Kluyver, T.; Ragan-Kelley, B.; Pèrez, F.; Granger, B.; Bussonnier, M.; Frederic, J.; Kelley, K.; Hamrick, J.; Grout, J.; Corlay, S.; Ivanov, P. Avila, D.; Abdalla, S.; Willing, C.; Jupyter Development Team. Jupyter Notebooks – a publishing format for reproducible computational workflows. In *Positioning and Powers in Academic Publishing: Players, Agents, and Agendas*; Loizides, F., Schmidt, B., Eds.; IOS Press: 2016; pp 87–90. DOI: 10.3233/978-1-61499-649-1-87

24. Hoops, S.; Sahle, S.; Gauges, R.; Lee, C.; Pahle, J.; Simus, N.; Singhal, M.; Xu, L.; Mendes, P.; Kummer, U. COPASI: a COmplex PAthway SImulator. *Bioinformatics*, **2006**, *22*, 3067–3074. DOI: 10.1093/bioinformatics/btl485

25. Frisch, M. J.; Trucks, G. W.; Schlegel, H. B.; Scuseria, G. E.; Robb, M. A.; Cheeseman, J. R.; Scalmani, G.; Barone, V.; Petersson, G. A.; Nakatsuji, H.; Li, X.; Caricato, M.; Marenich, A. V.; Bloino, J.; Janesko, B. G.; Gomperts, R.; Mennucci, B.; Hratchian, H. P.; Ortiz, J. V.; Izmaylov, A. F.; Sonnenberg, J. L.; Williams-Young, D.; Ding, F.; Lipparini, F.; Egidi, F.; Goings, J.; Peng, B.; Petrone, A.; Henderson, T.; Ranasinghe, D.; Zakrzewski, V. G.; Gao, J.; Rega, N.; Zheng, G.; Liang, W.; Hada, M.; Ehara, M.; Toyota, K.; Fukuda, R.; Hasegawa, J.; Ishida, M.; Nakajima, T.; Honda, Y.; Kitao, O.; Nakai, H.; Vreven, T.; Throssell, K.; Montgomery, J. A., Jr.; Peralta, J. E.; Ogliaro, F.; Bearpark, M. J.; Heyd, J. J.; Brothers, E. N.; Kudin, K. N.; Staroverov, V. N.; Keith, T. A.; Kobayashi, R.; Normand, J.; Raghavachari, K.; Rendell, A. P.; Burant, J. C.; Iyengar, S. S.; Tomasi, J.; Cossi, M.; Millam, J. M.; Klene, M.; Adamo, C.; Cammi, R.; Ochterski, J. W.; Martin, R. L.; Morokuma, K.; Farkas, O.; Foresman, J. B.; Fox, D. J. *Gaussian 16, Revision A.03*; Gaussian, Inc.: Wallingford CT, 2016. https://gaussian.com

26. Zhao, Y.; Truhlar, D. G. The M06 suite of density functionals for main group thermochemistry, thermochemical kinetics, noncovalent interactions, excited states, and transition elements: two new functionals and systematic testing of four M06-class functionals and 12 other functionals. *Theor. Chem. Acc.* **2008**, *120*, 215–241. DOI: 10.1007/s00214-007-0310-x

27. Raghavachari, K.; Binkley, J. S.; Seeger, R.; Pople, J. A. Self-Consistent Molecular Orbital Methods. 20. Basis set for correlated wave-functions. *J. Chem. Phys.* **1980**, *72*, 650-654. DOI: 10.1063/1.438955

28. McLean, A. D.; Chandler, G. S. Contracted Gaussian-basis sets for molecular calculations. 1. 2nd row atoms, Z=11-18. *J. Chem. Phys.* **1980**, *72*, 5639–5648. DOI: 10.1063/1.438980

29. Tomasi, J.; Mennucci, B.; Cammi, R. Quantum mechanical continuum solvation models. *Chem. Rev.* **2005**, *105*, 2999–3093. DOI: 10.1021/cr9904009

30. Barone, V.; Cossi, M. Quantum calculation of molecular energies and energy gradients in solution by a conductor solvent model. *J. Phys. Chem. A*, **1998**, *102*, 1995–2001. DOI: 10.1021/jp9716997

31. Cossi, M.; Rega, N.; Scalmani, G.; Barone, V. Energies, structures, and electronic properties of molecules in solution with the C-PCM solvation model. *J. Comp. Chem.* **2003**, *24*, 669–681. DOI: 10.1002/jcc.10189

32. Neese, F. The ORCA program system. *WIREs Comput. Mol. Sci.* **2012**, *2*, 73–78. DOI: 10.1002/wcms.81

33. Neese, F. *ORCA: An ab initio, DFT and semiempirical SCF-MO package, Version 4.0.1*; Max-Planck Institute for Chemical Energy Conversion: Müllheim, Germany, 2017. https://orcaforum.kofo.mpg.de/

34. Zhao, Y.; Truhlar, D. G. A new local density functional for main-group thermochemistry, transition metal bonding, thermochemical kinetics, and noncovalent interactions. *J. Chem. Phys.* **2006**, *125*, 1–18. DOI: 10.1063/1.2370993

35. Valeev, E. F. *Libint: A library for the evaluation of molecular integrals of many-body operators over Gaussian functions, Version 2.3.1*, http://libint.valeyev.net/

36. Perdew, J. P. Density-functional approximation for the correlation energy of the inhomogeneous electron gas. *Phys. Rev. B*, **1986**, *33*, 8822–8824. DOI: 10.1103/PhysRevB.33.8822

37. Perdew, J. P. Erratum: Density-functional approximation for the correlation energy of the inhomogeneous electron gas. *Phys. Rev. B*, **1986**, *34*, 7406. DOI: 10.1103/PhysRevB.34.7406

38. Lee, C. T.; Yang, W. T.; Parr, R. G. Development of the Colle-Salvetti correlation-energy formula into a functional of the electron density. *Phys. Rev. B*, **1988**, *37*, 785–789. DOI: 10.1103/PhysRevB.37.785

39. F. Neese, E. I. Solomon In *Magnetism: From Molecules to Materials*; J. S. Miller, M. Drillon, Eds.; Wiley: New York, 2002; Vol. *4*, p 345.

40. Schäfer, A.; Horn, H.; Ahlrichs, R. Fully optimized contracted Gaussian basis sets for atoms Li to Kr. *J. Chem. Phys.* **1992**, *97*, 2571–2577. DOI: 10.1063/1.463096

41. Schäfer, A.; Huber, C.; Ahlrichs, R. Fully optimized contracted Gaussian basis sets of triple zeta valence quality for atoms Li to Kr. *J. Chem. Phys.* **1994**, *100*, 5829–5835. DOI: 10.1063/1.467146

42. Weigend, F.; Ahlrichs, R. Balanced basis sets of split valence, triple zeta valence and quadruple zeta valence quality for H to Rn: Design and assessment of accuracy. *Phys. Chem. Chem. Phys.* **2005**, *7*, 3297–3305. DOI: 10.1039/B508541A

43. Eichkorn, K.; Weigend, F.; Treutler, O.; Ahlrichs, R. *Theor. Chem. Acc.* **1997**, *97*, 119–124. DOI: 10.1007/s002140050244

44. Weigend, F. Accurate Coulomb-fitting basis sets for H to Rn. *Phys. Chem. Chem. Phys.* **2006**, *8*, 1057–1065. DOI: 10.1039/B515623H

45. Neese, F.; Wennmohs, F.; Hansen, A.; Becker, U. Efficient, approximate and parallel Hartree–Fock and hybrid DFT calculations. A 'chain-of-spheres' algorithm for the Hartree–Fock exchange. *Chem. Phys.* **2009**, *356*, 98–109. DOI: 10.1016/j.chemphys.2008.10.036

46. Kossmann, S.; Neese, F. Comparison of two efficient approximate Hartee–Fock approaches. *Chem. Phys. Lett.* **2009**, *481*, 240–243. DOI: 10.1016/j.cplett.2009.09.073

47. Ekstrom, U.; Visscher, L.; Bast, R.; Thorvaldsen, A. J.; Ruud, K. Arbitrary-Order Density Functional Response Theory from Automatic Differentiation. *J. Chem. Theory Comput.* **2010**, *6*, 1971–1980. DOI: 10.1021/ct100117s

48. Neese, F. An improvement of the resolution of the identity approximation for the formation of the Coulomb matrix. *J. Comput. Chem.* **2003**, *24*, 1740–1747. DOI: 10.1002/jcc.10318

49. van Wüllen, C. Molecular Density Functional Calculations in the Regular Relativistic Approximation: Method, Application to Coinage Metal Diatomics, Hydrides, Fluorides and Chlorides, and Comparison with First-Order Relativistic Calculations. *J. Chem. Phys.* **1998**, *109*, 392–399. DOI: 10.1063/1.476576

50. Pantazis, D. A.; Chen, X.-Y.; Landis, C. R.; Neese, F. All-Electron Scalar Relativistic Basis Sets for Third-Row Transition Metal Atoms. *J. Chem. Theory Comput.* **2008**, *4*, 908–919. DOI: 10.1021/ct800047t

51. McWilliams, S. F.; Brennan-Wydra, E.; MacLeod, K. C.; Holland, P. L. Density Functional Calculations for Prediction of ^{57}Fe Mössbauer Isomer Shifts and Quadrupole Splittings in β-Diketiminate Complexes. *ACS Omega* **2017**, *2*, 2594–2606, DOI: 10.1021/acsomega.7b00595

52. Ginsberg, A. P. Magnetic exchange in transition metal complexes. 12. Calculation of cluster exchange coupling constants with the Xα-scattered wave method *J. Am. Chem. Soc.* **1980**, 102, 111–117. DOI: 10.1021/ja00521a020

53. Noodleman, L.; Peng, C. Y.; Case, D. A.; Mouesca, J. M. Orbital interactions, electron delocalization and spin coupling in iron-sulfur clusters. *Coord. Chem. Rev.* **1995**, *144*, 199–244. DOI: 10.1016/0010-8545(95)07011-L

54. Kirchner, B.; Wennmohs, F.; Ye, S.; Neese, F. Theoretical bioinorganic chemistry: the electronic structure makes a difference. *Curr. Opin. Chem. Biol.* **2007**, *11*, 134–141. DOI: 10.1016/j.cbpa.2007.02.026

55. Neese, F. Definition of corresponding orbitals and the diradical character in broken symmetry DFT calculations on spin coupled systems. *J. Phys. Chem. Solids,* **2004**, *65*, 781–785. DOI: 10.1016/j.jpcs.2003.11.015

56. Legault, C. Y. *CYLview 1.0b*; Université de Sherbrooke: Sherbrooke, QC, 2009. http://www.cylview.org

57. Pettersen, E. F.; Goddard, T. D.; Huang, C. C.; Couch, G. S.; Greenblatt, D. M.; Meng, E. C.; Ferrin, T. E. UCSF Chimera—A visualization system for exploratory research and analysis. *J. Comput. Chem.* **2004**, *25*, 1605–1612. DOI: 10.1002/jcc.20084

58. Kennedy, C. R.; Zhong, H.; Joannou, M. V.; Chirik, P. J. Pyridine(diimine) Iron Diene Complexes Relevant to Catalytic [2+2]-Cycloaddition Reactions. *Adv. Synth. Catal.* **2019**, *362*, 404–416. DOI: 10.1002/adsc.2019011289

59. Hoyt, J. M.; Schmidt, V. A.; Tondreau, A. M.; Chirik, P. J. Iron-catalyzed intermolecular [2+2] cycloadditions of unactivated alkenes. *Science*, **2015**, *349*, 960–963. DOI: 10.1126/science.aac7440

60. Fleming, I.; Terrett, N. K. Stereospecific syntheses and reactions of allyl- and allenyl-silanes. *J. Organomet. Chem.* **1984**, *264*, 99–118. DOI: 10.1016/0022-328X(84)85136-0

61. Chen; T.-G.; Barton, L. M.; Lin, Y.; Tsien, J.; Kossler, D.; Bastida, I.; Asai, S.; Bi, C.; Chen, J. S.; Shan, M.; Fang, H.; Fang, F. G.; Choi, H.-w.; Hawkins, L.; Qin, T.; Baran, P.S. Building C(sp^3)-rich complexity by combining cycloaddition and C–C cross-coupling reactions. *Nature*, **2018**, *560*, 350–354. DOI: 10.1038/s41586-018-0391-9

62. Blackmond, D. G. Reaction progress kinetic analysis: a powerful methodology for mechanistic studies of complex catalytic reactions. *Angew. Chem. Int. Ed.* **2005**, *44*, 4302–4320. DOI: 10.1002/anie.200462544

63. Sadow, D. A.; Tilley, D. T. Activation of Arene C−H Bonds by a Cationic Hafnium Silyl Complex Possessing an α-Agostic Si−H Interaction. *J. Am. Chem. Soc.* **2002**, 124, 24, 6814–6815. DOI: 10.1021/ja025940t

64. Sadow, D. A.; Tilley, D. T. Enhanced Reactivity of Cationic Hafnocene Complexes toward σ-Bond Metathesis Reactions. Si−H and Si−C Bond Activations in Stoichiometric and Catalytic Organosilane Conversions. *Organometallics* **2003**, *22*, 3577-3585. DOI: 10.1021/om0210107

65. Sadow, D. A.; Tilley, D. T. Cationic Hafnium Silyl Complexes and Their Enhanced Reactivity in σ-Bond Metathesis Processes with Si−H and C−H Bonds. *J. Am. Chem. Soc.* **2003**, *125*, 9462-9475. DOI: 10.1021/ja030024g

66. Lamač, M.; Spannenberg, A.; Baumann, W.; Jiao, H.; Fischer, C.; Hansen, S.; Arndt, P.; Rosenthal, U. Si−H Bond Activation of Alkynylsilanes by Group 4 Metallocene Complexes. *J. Am. Chem. Soc.* **2010**, *132*, 4369-4380. DOI: 10.1021/ja910527w

67. Peulecke, N.; Ohff, A.l; Kosse, P.; Tillack, A.; Spannenberg, A.; Kempe, R.; Baumann, W.; Burlakov, V. V; Rosenthal, U. Si–H Activation in Titanocene and Zirconocene Complexes of Alkynylsilanes RC≡CSiMe2H (R=tBu, Ph, SiMe3, SiMe2H): A Model To Understand Catalytic Reactions of Hydrosilanes.

Chem. Eur. J. **1998**, *4*, 1852-1861. DOI:10.1002/(SICI)1521-3765(19980904)4:9<1852::AID-CHEM1852>3.0.CO;2-E

68. Ohff, A.; Kosse, P.; Baumann, W.; Tillack, A.; Kempe, R.; Goerls, H., Burlakov, V.V.; Rosenthal, U. Novel trans-. eta. 2-Alkyne Complexes of Titanocene with Strong Si-H-Ti Interactions. Synthesis, Spectral Characteristics, and x-ray Crystal Structure. *J. Am. Chem. Soc.* **1995**, *117*, 10399-10400. DOI: 10.1021/ja00146a032

69. Procopio, L.J.; Carroll, P.J.; Berry, D.H. Agostic. beta.-silicon-hydrogen interactions in silylamido complexes of zirconocene. *J. Am. Chem. Soc.* **1994**, *116*, 177-185. DOI: 10.1021/ja00080a020

70. Herrmann, W.A.; Eppinger, J.; Spiegler, M.; Runte, O.; Anwander, R., β-Si− H Agostic Rigidity in a Solvent-Free Indenyl-Derived ansa-Yttrocene Silylamide. *Organometallics*, **1997**, *16*, 1813-1815. DOI: 10.1021/ja00080a020

71. Hieringer, W., Eppinger, J., Anwander, R. and Herrmann, W.A., C2-Symmetric Ansa-Lanthanidocene Complexes. Theoretical Evidence for a Symmetric Ln···(SiH) β-Diagostic Interaction. *J. Am. Chem. Soc.* **2000**, *122*, 11983-11994. DOI: 10.1021/ja993421t

72. Andersen, R.A.; Faegri Jr, K.; Green, J.C.; Haaland, A.; Lappert, M.F.; Leung, W.P.; Rypdal, K. Synthesis of bis [bis (trimethylsilyl) amido] iron (II). Structure and bonding in M [N (SiMe3) 2] 2 (M= manganese, iron, cobalt): two-coordinate transition-metal amides. *Inorg. Chem.* **1998**, *27*, 1782-1786. DOI: 10.1021/ic00283a022

73. Perrin, L., Maron, L.; Eisenstein, O.; Lappert, M.F. γ Agostic C–H or β agostic Si–C bonds in La{CH $(SiMe_3)_2\}_3$? A DFT study of the role of the ligand. *New J. Chem*. **2003**, *27*, 121-127. DOI: 10.1039/B206120C

74. Clark, D.L.; Gordon, J.C.; Hay, P.J;, Martin; R.L.; Poli, R. DFT Study of Tris (bis (trimethylsilyl) methyl) lanthanum and-samarium. *Organometallics* **2002**, *21*, 5000-5006. DOI: 10.1021/om020506l